

A STUDY OF COMMINUTION IN A VERTICAL STIRRED BALL MILL

by

Mustafa Asim Tüzün

Submitted in partial fulfillment of the
requirements for the degree of
Doctor of Philosophy,
in the
Department of Chemical Engineering,
University of Natal
1993

PREFACE

I hereby declare that the material incorporated in this thesis is my own original and unaided work, except where specific acknowledgement is made. It has not been submitted for a degree at any other university or institution.

M. A. Tüzün

Department of Chemical Engineering

University of Natal

Durban

August 1993

ACKNOWLEDGEMENTS

I wish to express my sincere appreciation to:

Mr M.F. Dawson and Prof. R.I. Edwards for their guidance, consistent encouragement and stimulating discussions during this project.

Dr B.K. Loveday for his valuable advice and assistance.

Dr L.A. Vermulen, Dr A.L. Hinde and Dr M. Mulholland for their helpful suggestions and guidance during the final stages of the project.

Mr D.W. Penn and the workshop staff of the Chemical Engineering Department for setting up the apparatus and making numerous modifications.

The Council for Mineral Technology for providing funds to finance this project. I extend my thanks to Dr W.A.M. Te Riele who has given me the opportunity to complete this thesis.

My wife, Hazel, for her invaluable encouragement and support throughout the project.

SYNOPSIS

A 20 litre experimental batch and continuous test rig and 5 litre batch and 50 litre continuous test rigs for stirred ball milling were built at the University of Natal and Mintek respectively. All the mills featured a grinding vessel with a central shaft equipped with pins and a torque measurement system. A washed chrome sand from the Bushveld Igneous Complex was used for the grinding experiments. Particle size analysis of products was performed using standard sieves and a Malvern Particle Sizer.

Batch tests were run in the 20 litre stirred ball mill to achieve efficient grinding conditions. The effects of grinding conditions such as pulp density, media size, media density and shaft rotation speed and mill design parameters such as ball load, pin spacing and pin diameter on product size, power consumption and media wear were studied. It has been shown that the median size of the product can be calculated by the Charles' Energy-Size Equation.

The stirred ball mill has been found to be more energy efficient than the tumbling ball mill. An energy reduction of 50% was possible for a product size of 6 microns when the stirred ball mill was employed instead of the tumbling ball mill. The energy input per ton of grinding media in the stirred ball mill could be 10 times higher than for the tumbling ball mill. Although during coarse grinds the media wear was higher in the stirred ball mill than in the tumbling mill, it became less so as grinding proceeded and for a product median size of 4.8 microns it was the same.

Using a 5 litre batch mill, an experimental programme was designed to study the comminution characteristics of the stirred mill. A factorial design was prepared with the following parameters, which influence grinding in the stirred ball mill: pulp density, pin tip velocity and ball density and size. The energy required for grinding the chromite sand in the stirred ball mill was determined by the use of Charles' Equation. The findings were in agreement with the results predicted by this equation. It was shown that the Rosin-Rammler size distribution equation was a suitable procedure for presenting and comparing grinding data obtained from the stirred ball mill. The factors that had the greatest effect on grindability were, in order of importance: ball size, pin tip velocity and ball density. Interactions

between the grinding parameters were negligible. The results implied that accurate predictions can be made to determine the grinding conditions required to achieve a desired product specification.

An attempt was made to study the grinding kinetics of the chromite ore using the mass population-balance model. Grinding tests were performed with two monosize fractions -53+38 and -38+25 microns and natural feed size -100 microns using various pin tip velocities, ball densities and sizes within the normal stirred ball milling operating range. The relationship between the ball diameter and the particle size was explained by the "angle of nip" theory which is applied for roller crushers. It was shown that the particle size giving the maximum breakage rate was directly proportional to the ball diameter. Estimated grinding kinetic parameters from monosize tests provided a good basis for accurate predictions of natural size feed. However, the breakage rate obtained from monosize tests appeared to be lower than those from the natural feed size. It was found that if the selection and breakage functions were determined by monosize tests, it was possible to modify selection function parameters by back-calculation which gave the best fit to the natural feed size. A good correlation was obtained between the experimental and calculated product size distributions using a population-balance model. The links between the empirical model combining Charles' and Rosin-Rammler equations and the first-order batch grinding equation were also shown.

The stirred ball mills were operated in batch and continuous mode. The median size of the products from the batch stirred ball mill experiments closely matched those of the continuous grinding experiments under similar grinding conditions. Using a salt solution as a tracer material, an attempt was made to estimate the residence time distribution based on a simplified analysis of the motion of the water in the mill.

The current scale-up methods for the stirred ball mill are discussed. A torque model was developed for given shaft geometry and ball size relating the power requirements of the stirred ball mill to the following prime design and operating parameters : mill diameter, mill height, pin tip velocity and effective density of the mill load. The basic assumptions underlying the model were that the mill content behaved as a fluidised bed, consequently a $\rho_{eff} g h$ type model for the pressure was applied throughout the grinding media bed and the effective charge

velocity was proportional to the pin tip velocity. It was found that pin spacing, pin diameter and ball diameter significantly affected the mill torque. A semi-empirical torque model was derived to include these parameters. The relationships formulated from these models were shown to be in excellent agreement with experimental results.

CONTENTS

	<u>Page</u>
ACKNOWLEDGEMENTS	ii
SYNOPSIS	iii
CONTENTS	vi
LIST OF FIGURES	x
LIST OF TABLES	xv
CHAPTER 1 : INTRODUCTION	1
CHAPTER 2 : LITERATURE SURVEY	6
2.1. REVIEW OF PREVIOUS WORK	6
2.2. CONCLUDING COMMENTS	23
CHAPTER 3 : EXPERIMENTAL TECHNIQUE	24
3.1. TEST MATERIAL	24
3.2. GRINDING APPARATUS	25
3.2.1. Stirred ball mill	25
3.2.2. Tumbling ball mill	33
3.3. GRINDING MEDIA	33
3.4. EXPERIMENTAL PROCEDURE	35
3.4.1. Batch grinding in stirred and tumbling ball mill	35
3.4.2. Continuous grinding in stirred ball mill	36
3.4.3. Media wear test	37
3.5. PARTICLE SIZE ANALYSIS	37
3.5.1. Sieve analysis	37
3.5.2. Sub-sieve size analysis	37
3.6. PRESENTATION OF RESULTS	38
CHAPTER 4 : BATCH GRINDING EXPERIMENTS IN A 20 LITRE MILL	39

	<u>Page</u>
4.1. PULP DENSITY	43
4.2. GRINDING MEDIA SIZE	48
4.3. GRINDING MEDIA DENSITY	56
4.4. LOAD DEPTH	58
4.5. SHAFT ROTATION SPEED	59
4.6. PIN SPACING AND DIAMETER	68
CHAPTER 5 : COMPARISON BETWEEN STIRRED AND TUMBLING BALL MILLS	73
5.1. INTRODUCTION	73
5.2. PRODUCT SIZE DISTRIBUTION	74
5.3. ENERGY EFFICIENCIES	76
5.4. VARIATION OF MILL TORQUE	81
5.5. POWER DENSITY	81
5.5. MEDIA WEAR	84
CHAPTER 6 : BATCH GRINDING EXPERIMENTS IN A 5 LITRE MILL	87
6.1. INTRODUCTION	87
6.2. EXPERIMENTAL PROGRAMME	88
6.3. RESULTS AND DISCUSSIONS	91
CHAPTER 7 : SIMULATION OF BATCH GRINDING IN A 5 LITRE STIRRED BALL MILL	105
7.1. INTRODUCTION	105
7.2. THEORETICAL BACKGROUND	105
7.3. EXPERIMENTAL METHOD	107
7.4. RESULTS AND DISCUSSIONS	109
7.4.1. Estimation of the monosize specific selection function	109
7.4.2. Estimation of the monosize breakage function	109
7.4.3. Estimation of the natural size kinetics parameters	113

	<u>Page</u>
7.4.4	Effect of ball size on the specific selection function 116
7.4.5	Prediction of monosize and natural size distribution by simulation 122
7.4.6	Links between the empirical model in Chapter 6 and the linear population balance model 122
CHAPTER 8 :	CONTINUOUS GRINDING EXPERIMENTS 127
8.1.	TESTWORK 127
8.2.	RESIDENCE TIME DISTRIBUTION 130
8.2.1.	Experimental Methods 130
8.2.2	Results and discussions 132
CHAPTER 9 :	MILL POWER 137
9.1.	INTRODUCTION 137
9.2.	LITERATURE SURVEY 137
9.3.	POWER EQUATIONS 138
9.3.1.	Dimensional Analysis 139
9.3.2.	Fluid dynamics 142
9.3.3.	Theory of mill power 144
9.4.	DISCUSSIONS 154
CHAPTER 10:	CONCLUSIONS 163
REFERENCES 166
APPENDIX	
1	SIEVING TESTS TO DETERMINE THE OPTIMUM SIEVING TIME 172
2	ENERGY CONSUMPTION CALCULATIONS FOR THE STIRRED BALL MILL 173

	<u>Page</u>
3	CALCULATIONS FOR THE WEIGHT OF CHARGE MATERIAL 174
4	DRAWING OF 20 LITRE STIRRED BALL MILL 175
4	BATCH GRINDING RESULTS FROM A 20 LITRE STIRRED BALL MILL 179
5	OPTIMUM BATCH GRINDING CONDITIONS IN TUMBLING BALL MILL 185
5	COMPARISON BETWEEN STIRRED AND TUMBLING BALL MILLS 189
6	EXPERIMENTAL AND CALCULATED PRODUCT SIZE DISTRIBUTIONS AT VARIOUS GRINDING CONDITIONS IN A 5 LITRE STIRRED BALL MILL 192
6	PRESENTATION OF SIZE DISTRIBUTIONS 209
6	CALCULATIONS OF STANDARD ERRORS FOR EFFECTS USING HIGHER-ORDER INTERACTIONS 213
6	STATISTICAL DATA FOR NONLINEAR REGRESSION ANALYSIS 214
7	SIMULATION OF BATCH GRINDING IN A 5 LITRE STIRRED BALL MILL 215
7	STATISTICAL DATA FOR A LINEAR REGRESSION ANALYSIS 232
8	CONTINUOUS GRINDING RESULTS 233
9	MILL POWER 238
10	BATCH TEST DATA AT TWO DIFFERENT LEVELS OF ENERGY INPUT AND SOME STATISTICAL PROPERTIES OF DATA DISTRIBUTIONS 244

NOMENCLATURE

LIST OF FIGURES

<u>Figure</u>		<u>Page</u>
2.1	Schematic drawing of the Klein continuous stirred ball mill with centrifugal separation.	8
2.2	Schematic representation of the Szegvari attritor.	9
2.3	Schematic drawing of the operating principle of the Westerlund vertical mill.	11
2.4	Schematic drawing of the Union Process attritor.	13
2.5	Schematic drawing of the U.S.B.M. 5 inch attrition mill.	15
2.6	Schematic drawing of the Pokorny agitated ball mill.	17
2.7	Schematic drawings of three different versions of the Drais stirred ball mills.	19
2.8	Schematic drawing of the NRZK wet grinding system.	20
2.9	Schematic drawing of a typical tower mill wet grinding system.	22
3.1	Photograph of 5 litre stirred ball mill.	26
3.2	Schematic drawing of 5 litre stirred ball mill.	27
3.3	Photograph of 20 litre stirred ball mill.	29
3.4	Schematic drawing of 20 litre continuous stirred ball mill.	30
3.5	Photograph of 50 litre stirred ball mill.	31
3.6	Schematic drawing of 50 litre continuous stirred ball mill. ..	32
3.7	Schematic drawing of the batch grinding tumbling mill.	34
4.1	Effect of pulp density on median size.	44
4.2	Median size of product as a function of energy input for various pulp densities.	45
4.3	Variation of mill torque as a function energy input at various pulp densities.	47

	<u>Page</u>
4.4 Media wear as a function of energy input at various pulp densities.	49
4.5 Effect of pulp density on media wear.	50
4.6 Median size of chromite ore as a function of energy input for various ball sizes at 72 r.p.m.	51
4.7 Median size of chromite ore as a function of energy input for various ball sizes at 164 r.p.m.	52
4.8 Effect of ball diameter on torque.	55
4.9 Effect of ball diameter on media wear.	57
4.10 Effect of load depth on median size.	60
4.11 Torque as function of load depth.	61
4.12 Effect of load depth on media wear.	62
4.13 Effect of shaft rotation speed on median size using grinding media of varying sizes and densities.	64
4.14 Effect of shaft rotation speed on torque using grinding media of varying sizes and densities.	65
4.15 Effect of shaft rotation speed on media wear using grinding media of varying sizes.	67
4.16 Effect of pin spacing on median size.	69
4.17 Effect of pin spacing on torque.	70
4.18 Effect of pin spacing on media wear.	71
5.1 Comparison between size distribution of ground products from stirred and tumbling ball mills at two different energy input levels	75
5.2 Comparison between grinding efficiency of stirred and tumbling ball mills for the median size of chromite ore.	77
5.3 Energy reduction in percent for the median size of chromite ore when stirred ball mill is used instead of tumbling ball mill.	78

	<u>Page</u>
5.4 Median size of chromite ore as a function of grinding energy input for stirred and tumbling ball mills.	80
5.5 Variation of mill torque for stirred and tumbling ball mills.	82
5.6 Comparison between the energy input per ton grinding media as a function of mill speed for stirred and tumbling ball mills.	83
5.7 Comparison between media wear in stirred and tumbling ball mills.	85
5.8 Media wear as a function of median size for stirred and tumbling ball mills.	86
6.1 A typical example of product size distribution at various levels of energy input using grinding conditions in Table 6.1, test no: 14.	93
6.2 A typical example of size modulus of product size distribution at various levels of energy input using grinding conditions in Table 6.1, test no: 14.	98
6.3 Plot of residuals versus predicted values.	102
6.4 Comparison between the observed and predicted results.	103
7.1 First-order plot for grinding -53+38 and -38+25 microns monosize feeds.	110
7.2 A typical example of fine size production plot for -53+38 microns monosize feed.	111
7.3 Cumulative breakage distribution parameters for -53+38 and -38+25 microns monosize feeds.	112
7.4 Specific breakage rate as a function of particle size using balls of various diameters.	118
7.5 Particle size at which maximum breakage rate occurs as a function of ball diameter.	119
7.6 Forces exerted on the particles by two rotating balls according to the angle of nip theory.	120

	<u>Page</u>
7.7 Comparison between experimental and predicted product size distributions for -53+38 microns monosize feed using grinding conditions in Table 7.1, test no: 8.	123
7.8 Comparison between experimental and predicted product size distributions for natural size feed using grinding conditions in Table 7.1, test no: 8.	124
8.1 Median size of product from the continuous and batch grinding of stirred ball mill as a function of specific energy input.	129
8.2 Comparison between size distribution of batch and continuous grinding products at 75 kWh/t.	131
8.3 Comparison of experimental and model dimensionless R.T.D functions.	134
8.4 Comparison between size distribution of batch and continuous grinding and calculated products at 75 kWh/t energy input.	136
9.1 Typical power characteristics of a mixing impeller.	141
9.2 Illustration for derivation of power equation based on fluid dynamics.	143
9.3 Typical torque curve as a function of pin tip velocity for stirred ball mill.	145
9.4 Effect of effective density on the mill torque at a pin velocity of 0.37 m/s.	148
9.5 Effect of effective density at various pin tip velocities on the mill torque.	148
9.6 Illustration for derivation of torque equation for the bottom of the vessel	149
9.7 Illustration for derivation of torque equation for vessel wall	151
9.8 Plot of residuals versus torque values calculated by a torque model.	157

	<u>Page</u>
9.9 Plot of residuals versus torque values calculated by a semi-empirical torque model.	158
9.10 Plot of observed torque values versus torque values calculated by a torque model.	160
9.11 Plot of observed torque values versus torque values calculated by a semi-empirical torque model.	161

LIST OF TABLES

<u>Table</u>	<u>Page</u>
3.1	Size analysis of feed materials. 25
3.2	Properties of different types of grinding media used for grinding experiments. 33
4.1	"One-variable-at-a-time" experimental programme and grinding conditions. 40
4.2	Additional grinding test conditions. 41
4.3	Effect of grinding media density on median size and torque at various feed sizes and shaft rotation speeds. 58
4.4	Effect of pin diameter with 6 mm and 10 mm balls. 72
5.1	Optimum grinding conditions used in stirred and tumbling ball mills. 74
6.1	2^4 factorial design matrix. 89
6.2	Distribution of ball size. 90
6.3	Effect of variables in factorial design. 94
6.4	Estimated effects from factorial design experiments. 99
7.1	2^3 factorial design matrix. 108
7.2	Cumulative breakage functions for various grinding conditions and size fractions. 113
7.3	Parameters of grinding kinetics in the stirred ball mill. 115
8.1	Experimental conditions and results for continuous and batch tests at equivalent conditions. 128
8.2	The mean residence times of calculated solids and water and of tracer curves. 133
9.1	Model fitting results for torque and semi-empirical torque models. 156
9.2	Analysis of variance for the full regression of torque and semi-empirical models. 159

CHAPTER 1

INTRODUCTION

Due to the growing demand for ultrafine minerals in several industries, the ever increasing cost of energy and the depletion of the sources of high grade ores, the development of improved methods for grinding fine particles has become essential.

The wide use and importance of grinding as a unit operation, coupled with the rather low energy efficiency of the conventional mill for fine grinding, provide a challenging incentive to investigate novel methods of comminution. Most present day development work however is taking place in mill performance, modelling and optimization or with various detailed improvements of existing technology rather than in the field of new equipment development.

Using the somewhat arbitrary definition, "very fine grinding" and "superfine grinding" (ultrafine) refer to the processes from which the product sizes fall below 100 microns and 10 microns respectively as proposed by Hukki (1). As the grinding process proceeds into the fine and ultrafine region, particles resist fracture and tend to aggregate. As a result, more energy is consumed to achieve the desired liberation of valuable minerals (2). Because of the escalation in cost, considerable work has been done in the past in an attempt to find possible ways to improve the efficiency of this operation. In this regard, several different types of wet and dry size reduction devices have been developed to meet the needs of industry for fine and ultrafine grinding. Each device has particular advantages and disadvantages for any given application as illustrated by the following examples:

Vibratory Mill: This is usually constructed from twin tubes mounted in parallel on an eccentric which gyrates them around the cylinder axis, thus causing the grinding media to vibrate and produce fast rotary movements transverse to the tube axis. This mill uses balls of a relatively small size, pebbles, porcelain balls, rods or cylpebs as grinding media which may occupy from 60 to 80% of the mill volume. Breakage is chiefly achieved by impact crushing. It is possible to operate the mill either wet or dry with underpressure or overpressure and in a gaseous atmosphere. The mechanical stresses on the drive are very high, the mill is not

conveniently scaled to large continuous capacity, acceptance of oversize in the feed is limited and the grinding efficiency is lower than in the tumbling ball mill (3-5).

High Speed Hammer Mill: Size reduction of products down to 10 microns or less can be achieved by the hammer mill. This mill has small rotors to which are attached hammers of various shapes enabling a very high rotor velocity. This provides sufficient energy for the fracture of small particles by the impact of the hammers. Particularly with abrasive rocks, wear on the hammers could be severe (6-8).

The Fluid Energy Mill: This has no moving parts and consists of a shallow cylindrical grinding chamber with input fluid jets and a raw material inlet and outlet for the high velocity fluid which contains the product. Grinding is achieved by multiple particle to particle collisions. Although the energy requirement is high compared with mechanical mills, it is capable of producing very fine material (e.g., finer than 5 microns) (9,10).

Szego Mill: This is a relatively new concept. The mill consists of a stationary, cylindrical grinding surface inside which are a number of helically grooved rotating rollers suspended vertically by a flexible wire rope. It may be operated wet or dry. It has a high capacity and modest power consumption. It can grind the material down to ultrafine size (11).

Stirred Ball Mill: The use of a stirred ball mill first started in 1934 (12) and operating and design characteristics of the stirred ball mill were first patented in 1956 (13). It was used for grinding pigments or solids, suspending fine solid particles in a liquid and the mixing of two different solids. This mill consisted of a water jacketed vessel and a central shaft fitted with opposing pairs of pins at angles to each other to fluidize the grinding media.

Attritor: In the early 1960's the U.S. Bureau of Mines developed an attrition mill which was adapted from an attrition scrubber constructed earlier (14-21). This type of milling is characterised by the intense agitation of a slurry consisting of a coarse grinding medium and a fine material to be ground in a baffled vessel by a concentrically mounted impeller.

In recent years, stirred ball milling has found a more prominent place in the fine grinding industry. Reasons for this can be attributed to improved mechanical design, more effective pulp temperature control, the availability of less costly small grinding media and the invention of the media retention systems.

There are several types of stirred ball mill available on the market. They are based on the same grinding principle of stirring the small grinding media with agitators of various designs in a stationary vessel. They can be operated either horizontally or vertically. Open top vertical mills are somewhat less energy intensive than the closed horizontal mills. Preference for a mill orientation depends on the grinding conditions required (22).

The cylindrical vessel usually has a water jacket to control the pulp temperature of the charge during grinding. A central rotating shaft is equipped with several types of impeller, mainly either pins or discs. Pins are radially fastened in rows to the surface of the shaft. Plain or perforated discs are mounted onto the shaft eccentrically or concentrically. The feed pulp is pumped into the bottom of the grinding chamber and flows upwards through a bed of grinding media. In the case of the horizontal mill, there is a system which prevents the grinding media exiting (23).

During the stirred ball milling process, solid particles are subjected to intense compressive and shear forces. Stirred ball mills use grinding media in the 10 to 1 mm range. In this mill, mineral grinding can be accomplished with media of various densities such as steel, zircon, alumina, or steatite. The preferable feed size is below 100 microns, due to the increase in efficiency of the stirred ball mill in this size range.

This size reduction technique has been successfully used in the paint and ceramic industries for several years (24,25). The fine grinding of pigments has attracted considerable interest as a result of changes in surface chemistry, optical properties, reaction kinetics and magnetism. The grinding of pigments for disperse dyes in a stirred ball mill has a considerable economic significance to the manufacturers because they require a milling step in order to produce a dye paste exhibiting the proper quality characteristics. In order to produce a saleable dye, crystals must be dispersed in water and ground to between 1 and 2 microns. Applications of the stirred ball mills for the chemical and metallurgical industries are becoming more common. Stirred ball milling is being used in the following:

Foodstuffs	Chocolate products, sesame, peanuts.
Ink	Printing inks, textile inks
Chemicals	Insecticides, pesticides, herbicides, fungicides, bitumen, acids and vulcanising agents.
Metallurgy	Rare earth metal alloys, metallic oxides, ferrites hard metallic powders.
Minerals	Transparent oxides, fine ceramic slurries, delamination of clays, paper coatings and fillers.

In recent years, stirred ball milling has found a new application in the area of coal-water slurries. Increases in oil prices and the uncertain availability of oil have necessitated a search for alternative forms of fossil fuels to meet energy needs. Coal-water slurries have the potential to be an immediate substitute for premium liquid and gaseous fossil fuels in process heaters and industrial and utility boilers, the evolution of this technology having taken place during the last few years. Very fine coal particle sizes are required (such as 5 microns or smaller) for coal-water slurry applications. Stirred ball milling may be the only viable method of achieving minimum energy requirements for the preparation of these suspensions (26).

The papers published on stirred ball milling appear to be very limited in number and they do not cover many aspects in detail, therefore indicating a need to obtain more data relating to this subject. In this thesis, comminution in the stirred ball mill is studied together with the problems involved therein.

The objectives of this study are as follows:

1) To show the influence of various grinding parameters defining the characteristics of the stirred ball mill and grinding media and to establish the optimum operating and design parameters in order to find conditions under which the stirred ball mill would be effective.

2) To carry out experiments in order to make a comparison between tumbling ball milling and stirred ball milling as far as energy requirements and ball wear are concerned.

3) To determine the effect of grinding variables and of interaction between them and to correlate the product size distribution with energy input.

4) To develop a breakage model in order to determine the product size distribution and examine the influence of various grinding conditions on model parameters.

5) To develop a model for the convective transport of particles in the stirred ball mill based on a simplified analysis of the physical process.

6) To calculate the power required to drive the mill by means of a mechanical law relating the power, the configuration and the operating conditions of the mill to establish scale-up parameters.

CHAPTER 2

LITERATURE SURVEY

2.1. REVIEW OF PREVIOUS WORK

Mineral grinding is well known for being an energy inefficient and energy intensive process. In mineral processing, the decrease in ore grades and an increase in the need for metal values of fine degree dictate a need for increased fineness of grind. Because of the low energy efficiency of crushing and grinding, a great deal of effort has been made in the past to improve the existing comminution process and to develop a new grinding machine with the ever increasing possibility of a breakthrough which could revolutionize the grinding process.

The advantages of micro fine wet grinding has been widely known for many years. Recently, an upsurge in popularity has been noted by manufacturers in Europe since there has been an increase in demand for products such as plastics and ceramics. This in turn has created more demand at basic processing levels resulting in an increase in the need for fine grinding equipment, especially the stirred ball mill. The stirred ball mills belong to broad categories - low speed and high speed which can be subdivided into vertical, horizontal, open, closed, batch and continuous.

Wet low speed stirred ball mill (tip velocity < 4 m/s): The idea of using a stirred ball mill goes back to 1934. It was originally developed by P. Klein, et. al. (12) to disperse substances in liquids, the fine material to be dispersed being subjected to the action of round grinding elements induced by means of a stirrer. Quartz stones or flint stones, sized preferably between 1 mm and 8 mm could be employed as grinding media. It was found that mixing small grinding media with hard balls of a large diameter resulted in an increase in efficiency.

In the patent, apparatus of several designs suitable for carrying out the dispersion process were illustrated. In general these mills consisted of upright stationary vessels having non metallic coatings and equipped with stirrer arms.

For continuous grinding, the material was introduced through a hollow shaft and subjected to the grinding action in the mill, ground material being removed through the discharge opening. The fine dispersed particles, prior to their discharge, could be continuously separated by means of conventional methods such as sedimentation and centrifuging to increase the efficiency of the grinding device and coarse particles were returned to the mill while the fine particles were discharged.

One of these, a continuous mill with centrifugal separation, is illustrated (Figure 2.1). The material was admitted through the hollow shaft and after the particles were ground, they passed through the perforated bottom of the rotating double cone. The patent claims that coarse particles were separated at the greatest diameter of the cones by a centrifugal force which was created by the rotation of the latter and then returned to the mill, while fine particles were discharged from the mill through the overflow.

One of the first grinding attritors was patented by A.Szegvari in 1956 (13). He claimed that the process of breakage in his attritor had particular value in fine grinding. The patent described the operating and design characteristics of the attritor. Schematic representation of the Szegvari attritor is shown in Figure 2.2. The apparatus was an upright cylindrical vessel having a central rotating shaft equipped with agitating arms. The bottom arm was somewhat shorter than those above it. The upper arms were arranged in pairs at slight angles to each other and spaced wide enough apart to permit the slurry to pass between them. This arrangement provided adequate agitation with minimum hydrodynamic resistance. The attrition was produced by the movements of the arms through the bulk of the attritive elements which might be flint pebbles, steel balls etc. The circulation of the slurry was facilitated by a pump which drew off the slurry from the top and returned it to the vessel at the bottom. The details of the grinding process in the attritor were given in his patent which included the optimum operating characteristics of the latter, such as: the speed of the agitator, the clearance between the agitator arms and the side of the vessel, the size of the grinding media and the specific gravity of the grinding media and the liquid. Three examples were given to illustrate the application of the attritor.

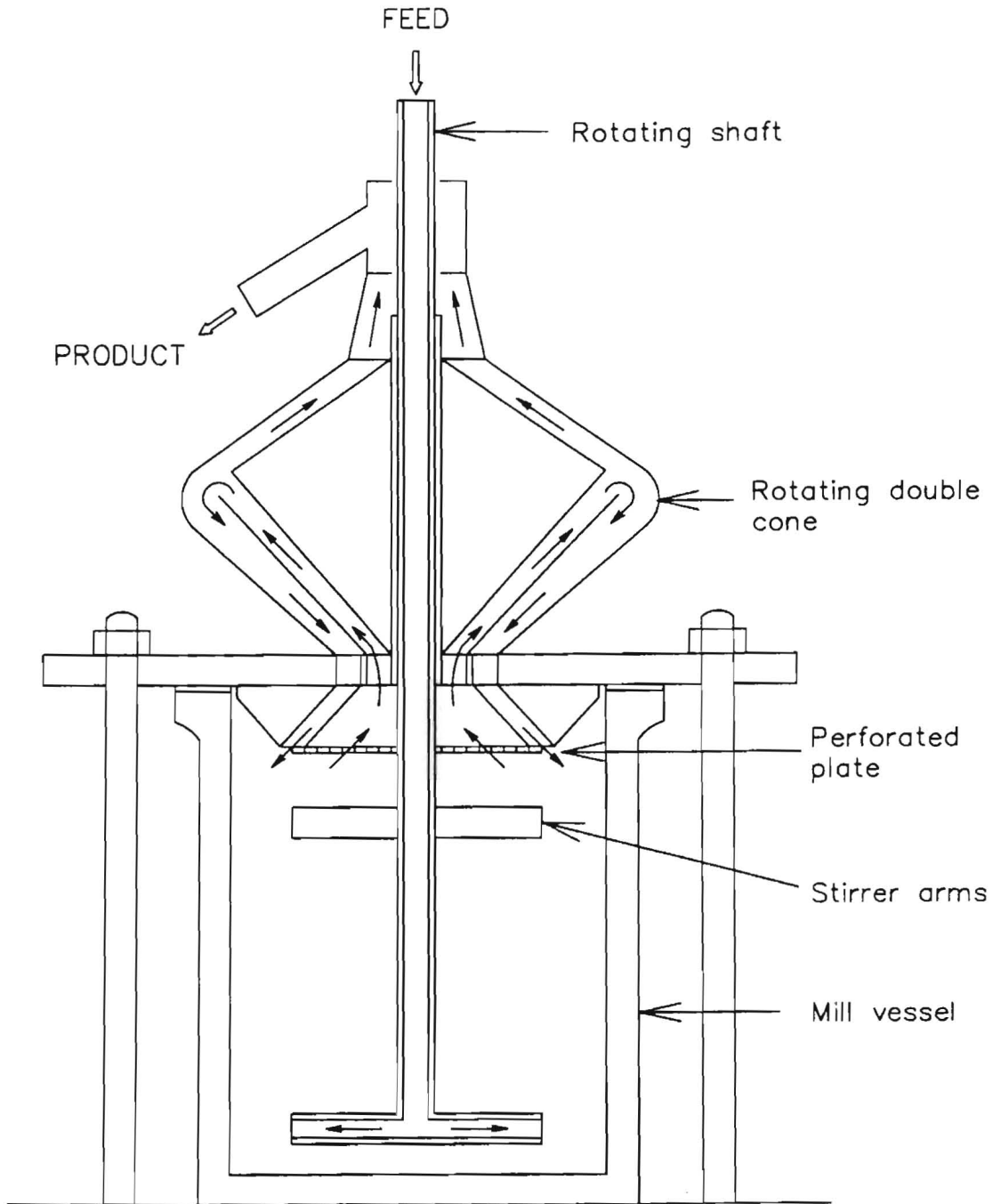


Figure 2.1. Schematic drawing of the Klein continuous stirred ball mill with centrifugal separation

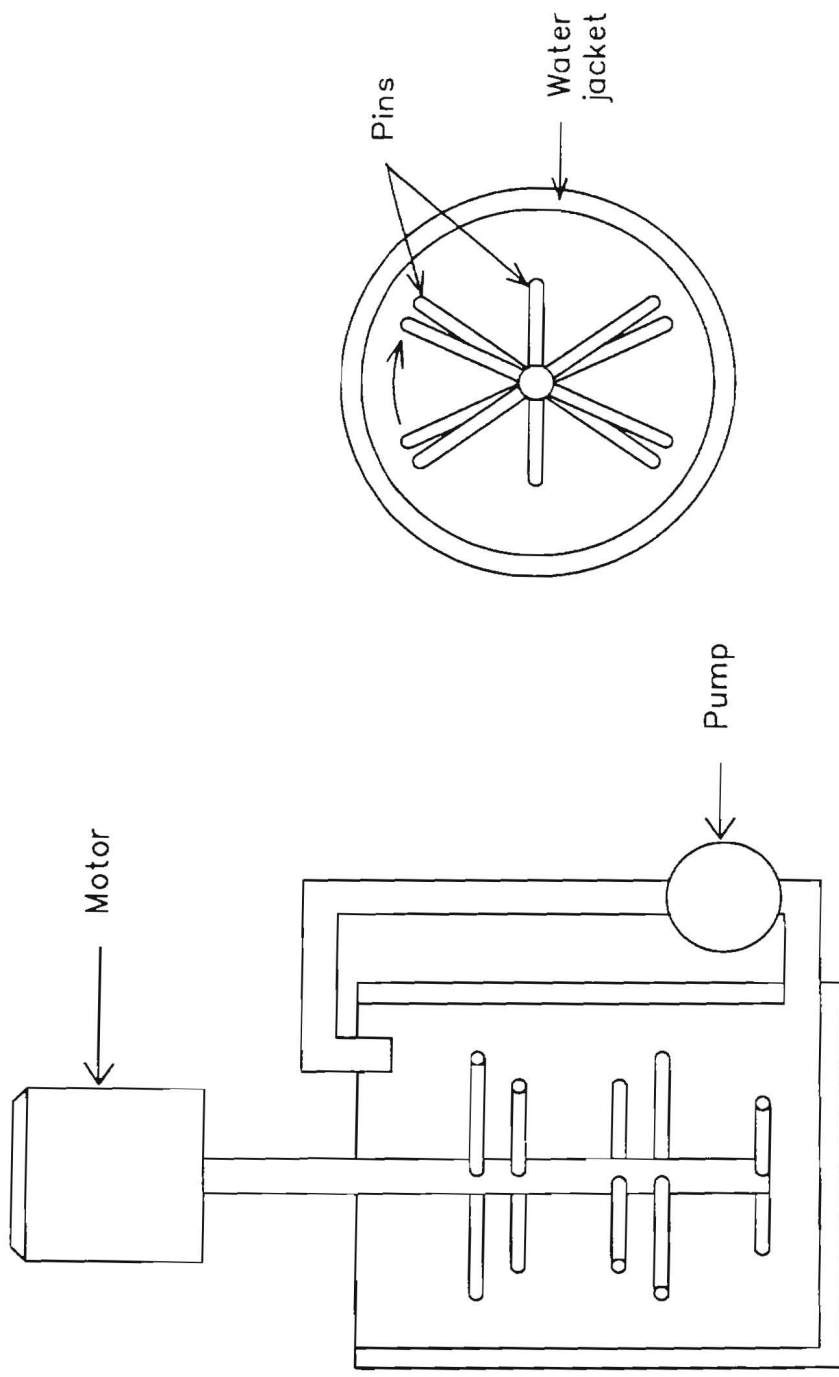


Figure 2.2. Schematic representation of the Szegvari attritor

Example 1: Particle sizes below 60 microns of processed ultramarine blue pigment were ground down to 4 microns or smaller particles in 2 to 4 hours. The conventional pebble mill required 24 to 48 hours grinding time to obtain the same product size.

Example 2: The preparation of dispersions of compounding ingredients to be used in latex for the production of foamed rubber products or dipped goods was achieved successfully in five to six hours grinding. It would take 90 hours to produce the same product size in the conventional pebble mill.

Example 3: A titanium dioxide alkyd paste containing 50% titanium was reduced to a particle size of approximately 6.24 microns in 20 to 30 minutes. For the same fineness, the conventional pebble mill required 24 to 48 hours.

For all three examples, the dimensions of the attritor and the grinding conditions were given in the patent.

Westerlund, P. (27) made an attempt to demonstrate the advantage of using the vertical mill. After a series of preliminary tests in a prototype vertical mill, he constructed a modified vertical mill consisting of two cylinders, one inside the other. It is portrayed in Figure 2.3. The outer cylinder was stationary while the inner cylinder rotated. The shell surfaces were equipped with vertical ribbing. Comparative grinding tests run in a vertical mill and in a conventional horizontal mill of equal size, showed that, for the same fineness of product, the vertical mill has a capacity 6 to 8 times greater, although the net energy consumption was the same in both mills. Some other series of comparative tests were run with grinding media of steel balls (10 mm) and of ore pebbles (-12+8 mm) which demonstrated that the mill capacity increased with the increasing feed rate when the steel balls were used and it was nearly independent of the feed rate with use of ore pebbles. The grinding capacities in a vertical mill with a steel medium and with ore pebbles could hardly be compared because of the high rate of wear on the steel balls. The experiments which were done to show the proper ratio between the cylinder diameters, indicated that the motion in crushed ore was transferred to an average distance of five times the maximum particle size diameter from the rotor.

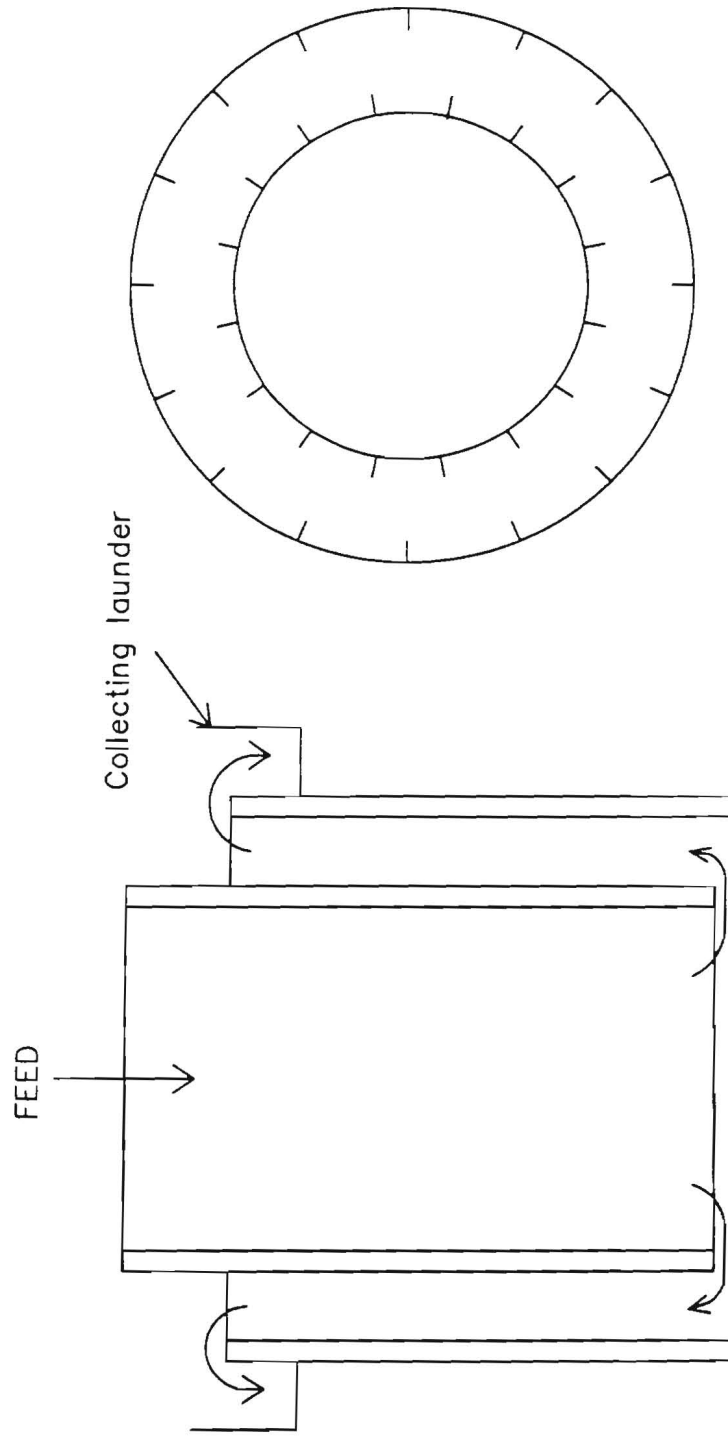


Figure 2.3. Schematic drawing of the operating principle of the Westerlund vertical mill

Recent studies have indicated that it is possible to achieve fine and ultrafine grinding of ores effectively using stirred ball mills. Sepulveda, J.A. and Herbst, J.A. (29,32) stated that stirred ball mills are effective devices for grinding ores into the fine (<10 microns) and ultrafine (<1 micron) size range. All the experimental data were obtained from Union Process Attritors. A schematic drawing of the Union Process attritor is shown in Figure 2.4. Capacities were 1, 3 and 10 gallons. The agitator rotation speed varied between 100 and 500 r.p.m. The grinding media consisted of stainless steel balls of 1/4, 1/8, 3/32 inch and ceramic balls of 1/4 inch in diameter. The solid percent of slurry ranged from 20 to 40% by volume. Various minerals were used for grinding including chalcopyrite, limestone, quartz, pyrite, sphalerite and coal. The size distribution of the products were determined by using the Micromeretic's SediGraph 5000 D or the Coulter Electronic's Coulter Counter Model TA. The product size for a given energy input was predicted by using a Charles' energy-size reduction relationship. The power characteristics of the mill were presented by the same type of model as used for turbine mixers. It was shown that when the energy input equation was used in conjunction with the energy size reduction relationship, it was possible to predict a reasonably accurate median size of product.

A mathematical model based on the Microscopic Population Balance Model provided more accurate predictions of complete size distribution. Working under this framework, models based either on fragmentation or attrition breakage mechanism or a combination of both were developed. Experimental data indicated that attrition breakage does not play an important role in the grinding mechanism of the stirred ball mill. A model, based on the fragmentation breakage mechanism and accounting for the distribution of strength for the products being ground, was formulated and solved analytically. It was demonstrated that different grinding mechanisms become more effective in the stirred ball mill as the grinding proceeds. Good predictions of product size distribution were obtained with the single strength model at low levels of energy input. Later the kinetics of the grinding became non linear, often at high energy input. In this case, the distributed strength model allowed for a more accurate product size distribution to be predicted.

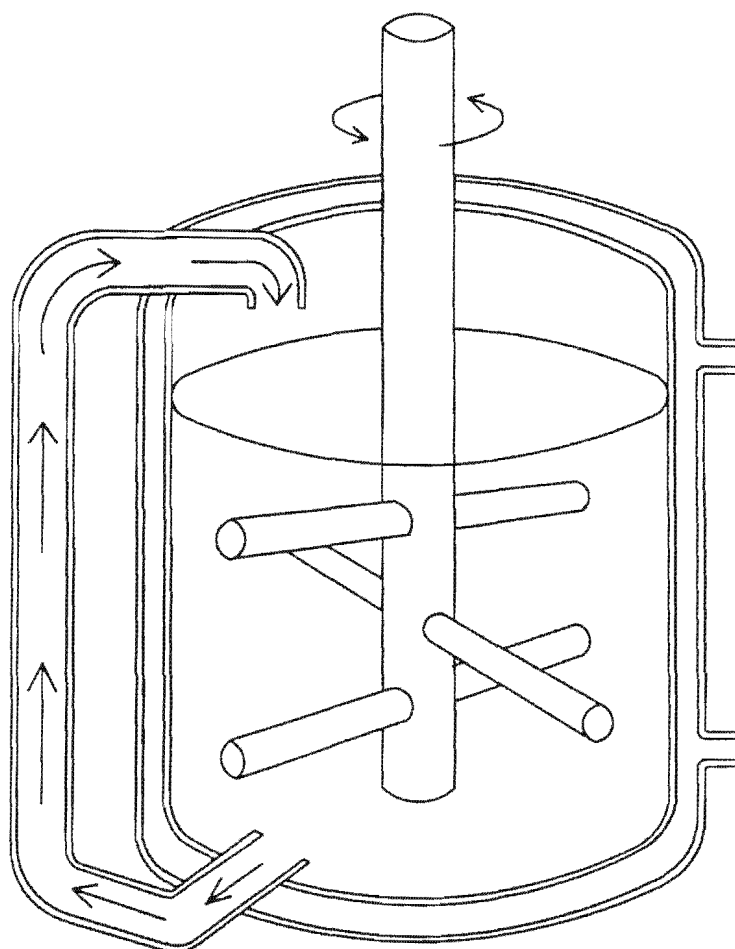


Figure 2.4. Schematic drawing of the Union Process attritor

Wet high speed stirred ball mill (tip velocity > 4 m/s): The commercial breakthrough of the high speed stirred ball mill occurred in 1948 with the introduction of the DuPont "sand mill" which has been primarily used as a pigment grinder in the paint and coatings industry (30). The essential operating principle of the sand mill was the use of small grinding media and high stirrer speed. The sand mill consisted of a vertical grinding chamber and had a comparatively small diameter. The slurry was pumped into the chamber at the bottom and the ground product was overflowed at the top and passed through a screen arrangement. The grinding action of the mill was supplied by concentric discs on a central rotating shaft. The grinding media size ranged from 0.5 to 1.0 mm diameter.

A modified sand mill was patented by the U.S. Bureau of Mines and referred to as an "attrition grinder". They investigated the feasibility of producing subsieve-size material by an attrition grinding method. The original grinding unit was adapted from the scrubbing device developed for attrition or scrubbing glass sand to remove iron oxide stain (14). This technique, patented by the Bureau of Mines, employed intense agitation of a slurry composed of a granular grinding media, the material to be ground and the suspending liquid (15). The 5 inch attrition mill is illustrated in Figure 2.5. It was basically a device for the intense agitation of a slurry consisting of a coarse rounded medium. Agitation was provided by the shearing action of the cage-like rotor turning inside a cage-like stator, both of which were mounted in a cylindrical water-jacketed container. A qualitative study of the basic operating variables on particle size reduction and energy consumption was performed (16) and also quantitative studies were made to obtain the necessary information for scale-up and design. The effect of rotor velocity, medium concentration and slurry density on the grinding efficiency and power consumption were determined (17). Power characteristics of the attrition mill were essentially the same as those of a radial flow turbine mixer. Studies were made to determine the efficiency of the attrition methods in grinding industrial minerals to minus 2 microns (18) and ceramic powders to an average particle size ranging from 0.1 to 0.01 microns (19,20). The comminution of silicon carbide (SiC) was also studied using the attrition grinding process. During the prolonged attrition, iron and silica contamination occurred due to wear from the mill and mill

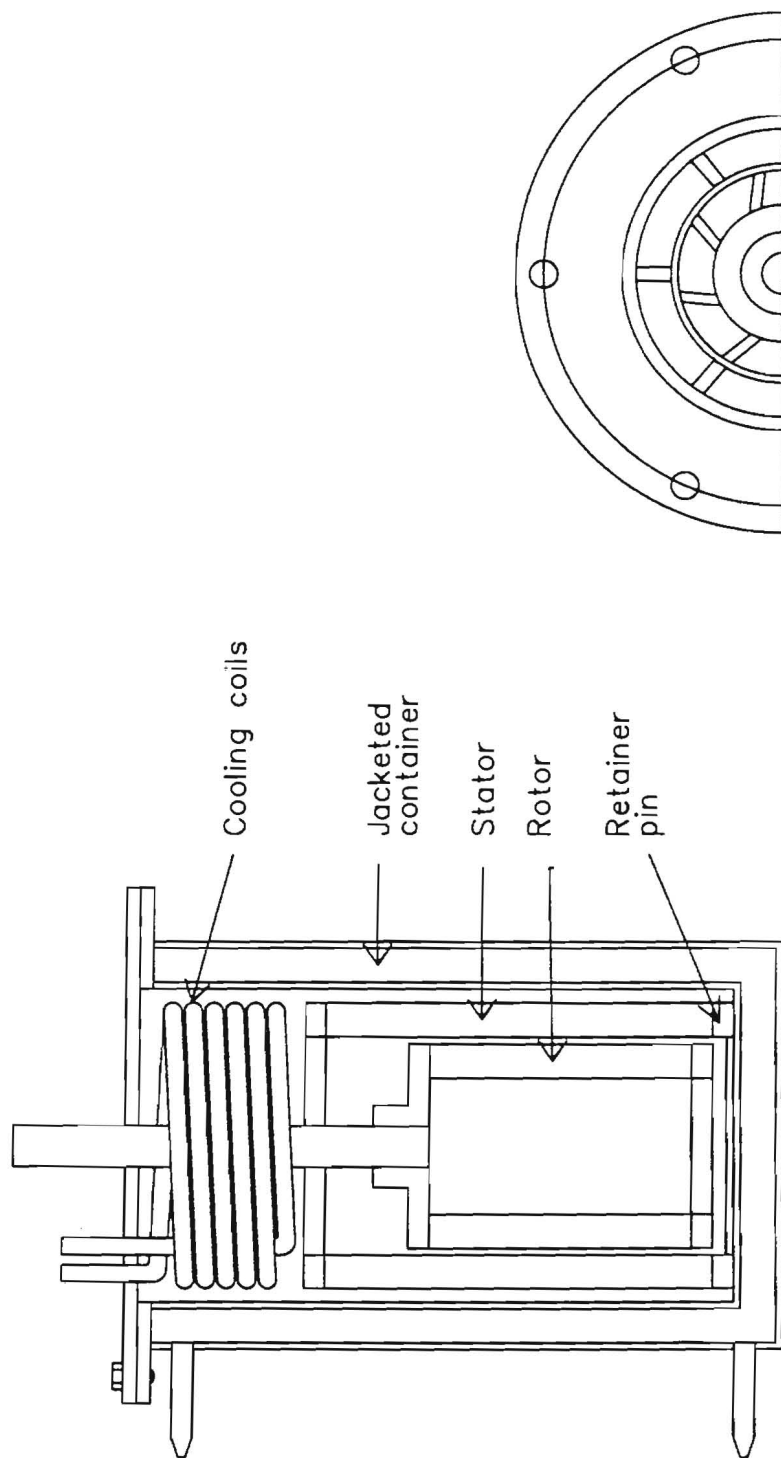


Figure 2.5. Schematic drawing of the U.S.B.M. 5 inch attrition mill

media. However, iron can be eliminated by polymer mill construction materials. Contamination from the milling medium can be avoided by using a material having an identical or similar composition to the material being ground (21).

Since the early high speed stirred ball mills such as the sand mill, were open at the top, there were practical operating limitations on the maximum stirrer speed. Centrifugal force created a vortex and the grinding media bed tended to rise therefore their performance deteriorated. This limitation was overcome with the development of the closed stirred ball mills. The grinding media remained in the mill and the grinding media bed expansion was restricted regardless of the stirrer speed (figure 2.7).

Dry stirred ball mill: During the last two decades, research was conducted on the mechanical activation of minerals and ceramics. It was found that materials formed by hot consolidation of powders posed considerably better properties than conventionally prepared ones. There has been success in the dry grinding of some metal oxides (Fe,Cr). Such results have led to more interest in fine dry grinding in energy intensive grinding mills. Besides that, dry grinding is sometimes necessary with some materials due to the physical or chemical changes which occur if water is added.

Pokorny, J. (31) demonstrated applications of the agitated ball mill, originally designed for wet grinding, for dry grinding. A schematic drawing of the agitated mill is represented in Figure 2.6. The mill consisted of a vertical mill vessel and coaxial shaft with impellers (disc) perpendicular to it. Balls of 0.6 to 8.0 mm in diameter were used as a milling charge. The peripheral velocity of the impellers ranged from 6 to 12 m/s. Power consumption, temperature and heat transfer in the mill were investigated using 20 and 100 litre commercial full scale mills. During the dry grinding problems arose, mostly due to the absence of liquid inside the mill. These included: an inhomogeneous distribution of solid particles, an increase in the abrasion wear on all parts of the mill, a greater difficulty in discharging solid particles and a decrease in the thermal conductivity of the mill charge.

Sepulveda, J.L. (32) carried out wet and dry grinding experiments to compare energy utilization in both these grinding environments. The results indicated that dry and wet grinding proceeded very similarly with respect to the efficiency of one over the other. However, it was observed that agglomeration of

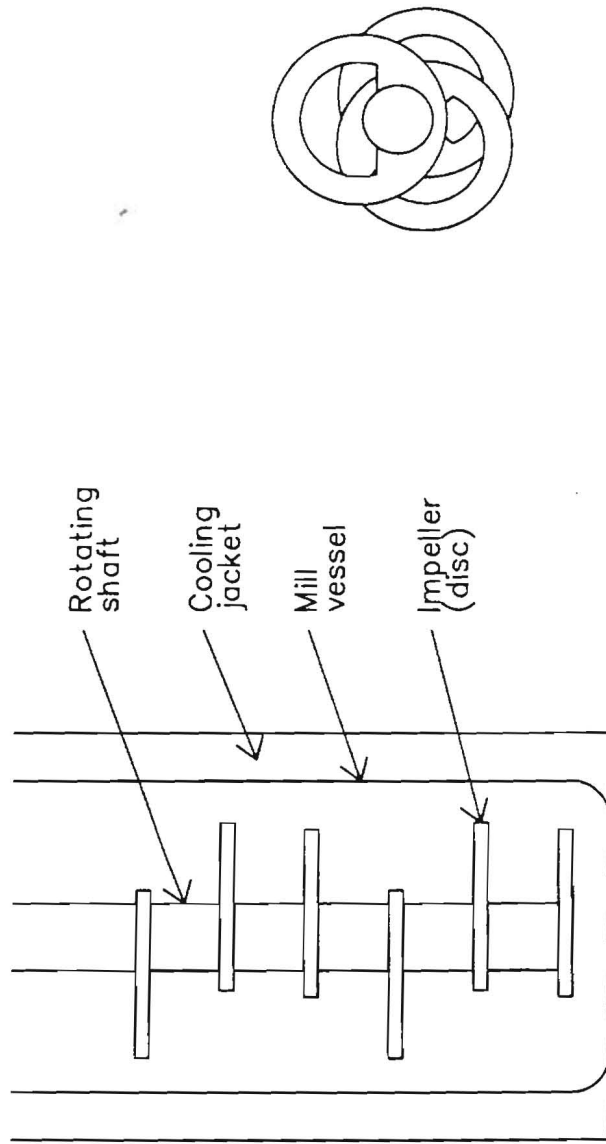


Figure 2.6. Schematic drawing of the Pokorny agitated ball mill

solid particles and in some cases, compaction of solids with the grinding media occurred at high levels of energy input, especially within less intense areas of activity in the grinding vessel.

Some examples of commercially available stirred ball mills: There are several types of stirred ball mill available on the market. One of the bigger producers of the stirred ball mill is Netzsch-Feinmahitechnik Gmb H of Selb, West Germany (Figure 2.7). The mill has a cylindrical grinding chamber which can be operated either horizontally or vertically and the agitator is located in the centre of the chamber. The agitator is furnished with either perforated discs or pins. The pinned agitator works particularly well when counter pins are attached to the vessel. The grinding chamber is filled with grinding media generally in the range 60 to 90%. The circumferential speed of the agitator ranges from 4-20 m/s. The slurry is continuously fed to the mill and at the discharge end of the mill, the ground product is allowed to leave the mill while the grinding media is retained by means of either a screen cartridge or a frictional gap separator.

Another producer is Matter & Partner Ltd of Switzerland, who have mills for both wet (NRZK) and dry grinding (TRZK). The latter has a double step air classifier (33). A schematic drawing of the NRZK wet grinding system is shown in Figure 2.8. The primary features of these mills are that the feed enters from the top and the product, along with the grinding media, leaves from the bottom. Small steel or ceramic balls are used as grinding media. It is possible to wet grind minerals at high solid concentration (lime up to 78%). The grinding media and slurry are agitated with stirring arms. Depending upon the feed, an end product with the fineness of 99.5% < 5 - 6 microns can be produced. The mill is equipped with a cooling jacket to increase the grinding efficiency. In certain cases, it is necessary to add grinding aids. The small media grinding consumes about 50% less energy than other conventional grinding methods.

Another means of energy-efficient fine grinding in commercial use is the " Tower Mill " (34-40). It was originally developed in Japan during the 1950's where it has been used to grind a wide variety of minerals. The Tower mill is basically a vertical stirred ball mill. It consists of a vertical cylindrical grinding chamber and a screw flight agitator driven by a motor through a gear box. The screw rotates within the body, with a significant clearance between the bottom and side walls of the unit. The interior of the body is protected from abrasion by sheet

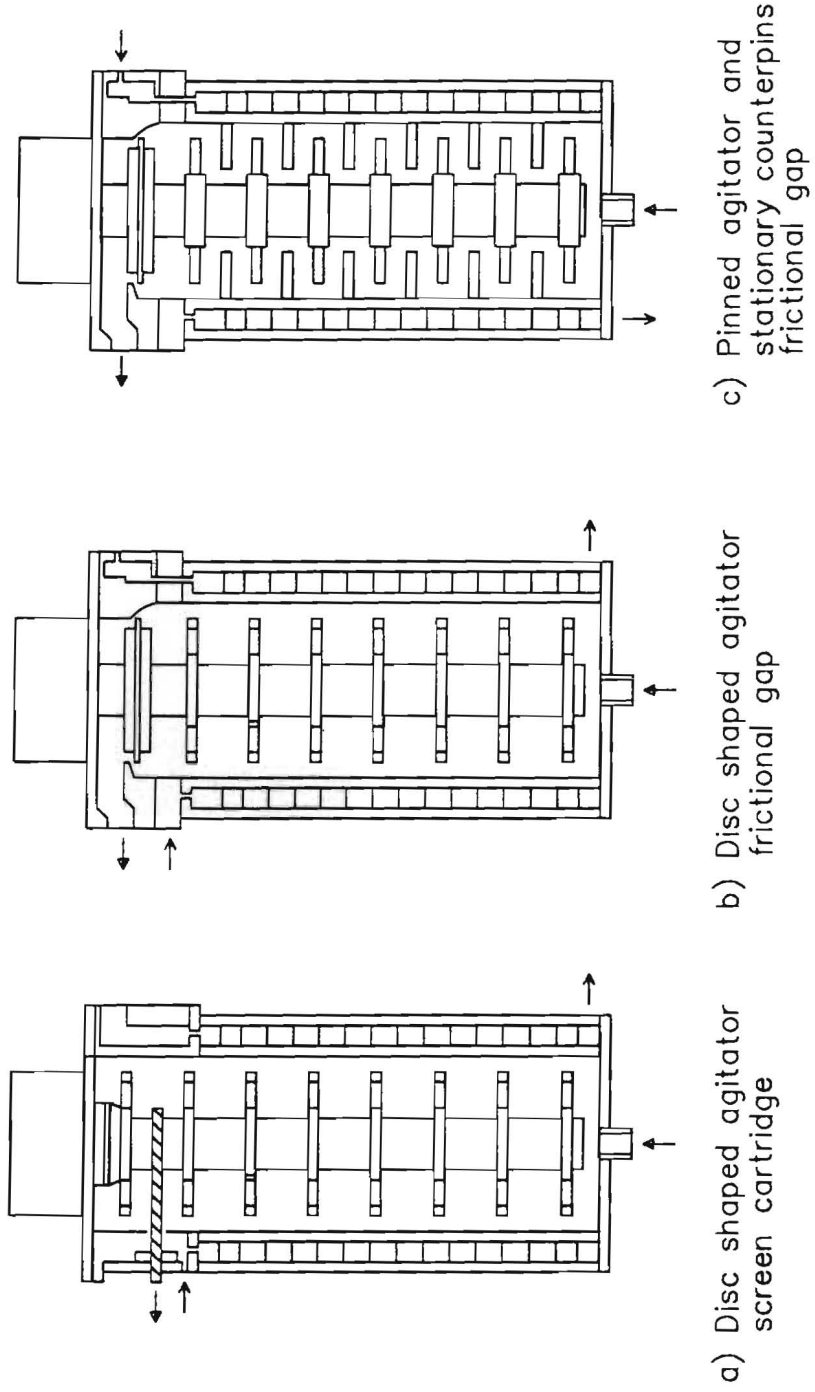


Figure 2.7. Schematic drawings of three different versions of Drais stirred ball mills

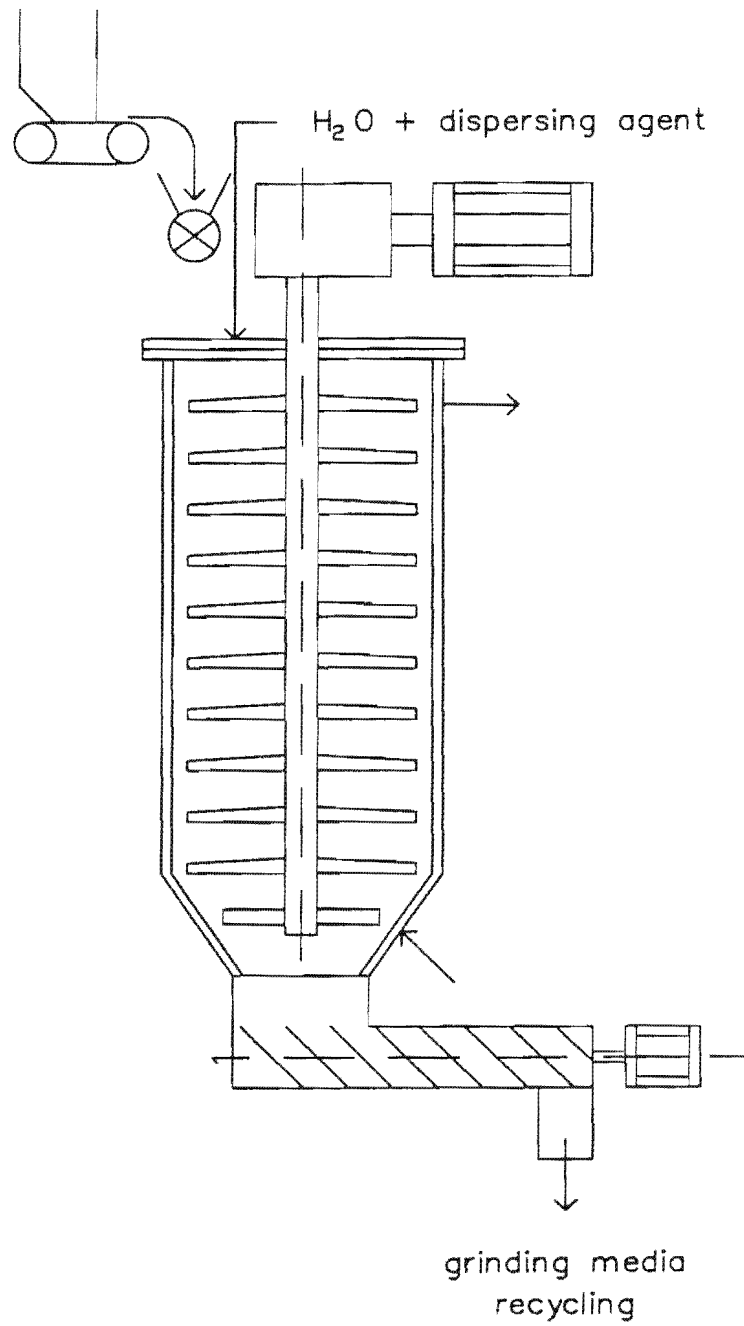
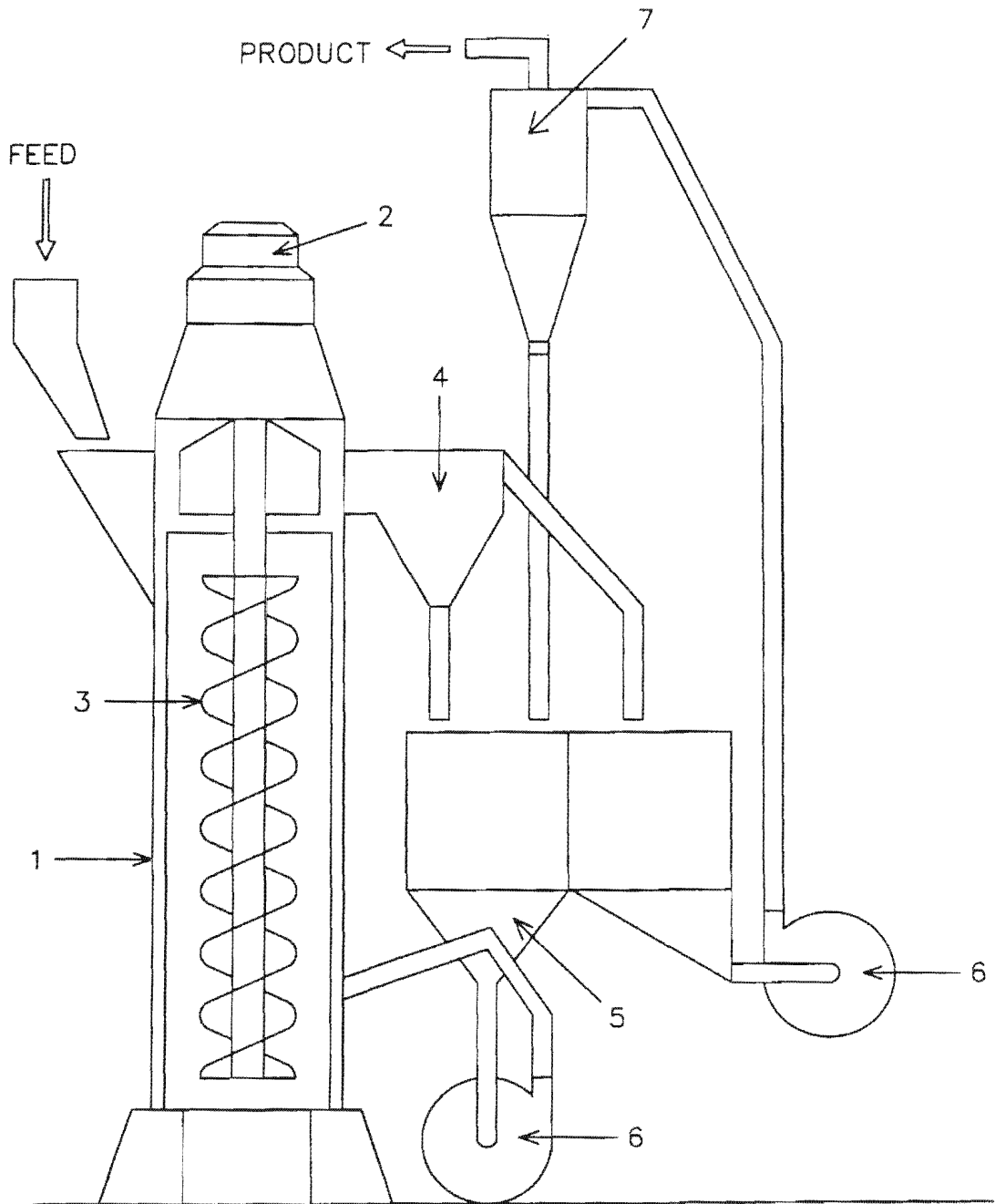


Figure 2.8. Schematic drawing of the NRZK wet grinding system

or spray elastomer. In addition, the interior walls are further protected by a grid bar system which traps the grinding media and acts as a regenerating wear lining. The grinding chamber contains steel or ceramic balls or pebbles. The ball sizes in the Tower Mill are limited to a maximum of 30 mm. For very fine grinding, balls as small as 5 mm are used.

Figure 2.9 shows the most common arrangement of a Tower Mill for closed circuit operation. Material is fed from the top of the Tower Mill, entering approximately 180 degrees from the mill overflow behind a buffer plate to minimize short-circuiting of coarse material. As coarse material settles, the ground material and fine material in the feed rise in an upward flow of slurry and overflow into a coarse classifier where the large particles are removed and returned to the bottom of the grinding chamber via a mill pump. The fine product of the coarse classifier can be further classified if needed into a final product with an external classification system such as the hydrocyclone. Given the proper feed and the requirement for a fine grind, the Tower Mill shows a power saving of up to 50% over a conventional tumbling mill. At the Butte Molybdenum Plant of the Anaconda Minerals Company, experimental results obtained on the regrind of moly concentrates indicate that an energy saving of approximately 40% can be realized by using a Tower Mill instead of a ball mill (39) and the results of an experimental study on a Tower Mill at Mintek have given the same confirmatory evidence (40). The Tower Mill grinds efficiently up to a maximum slurry density of 50 to 55% solids by weight (for 2.7 specific gravity solid). The following advantages are claimed for the Tower Mill. Grinding media consumption in the Tower Mill is no higher than in a tumbling ball mill and in many installations it has proven to be less, due to better utilization of energy for grinding. The rubber covering inside the mill sees very little wear because there is virtually no motion due the fact that the grid bar protection system traps the grinding media, creating a renewable wear surface. The installation cost of a Tower Mill could be 30% of that for a comparable ball mill due to less foundation cost and space requirements.

There are more commercially available stirred ball mills on the market which are described and some technical information given by Sepulveda, J. L. (28).



- | | |
|--|----------------------|
| 1. Grinding chamber – mill body | 4. Coarse classifier |
| 2. Motor | 5. Slurry sump |
| 3. Screw flight – grinding charge agitator | 6. Recycle pump |
| | 7. Hydrocyclone |

Figure 2.9. Schematic drawing of a typical tower mill wet grinding system.

2.2. CONCLUDING COMMENTS

Very little information about attrition grinding and the study of stirred ball milling fundamentals is available in the literature, indicating that the subject has not yet been well explored.

Some valuable work which has made a contribution to the understanding of attrition milling has been done by the U.S. Bureau of Mines (14-21). In the literature, only the work which has been reported by Sepulveda and Herbst covers the study of operating variables, empirical scale-up and the development of a mathematical model to present the grinding behaviour of the low speed vertical stirred ball mill (29,32).

Basically there are two major cost items in stirred ball mill grinding operations: mill energy consumption and media wear (balls, liners, rotating shaft). In early studies, the measurements of the power drawn by the mill were crude (27) and in some papers the power data was not even available (12,13). However, recent studies claimed to show that the energy consumption in the stirred ball mill can be predicted using a well established scale-up procedure for turbine mixers (29,32). So far, no data has been published concerning media wear which accounts for a substantial fraction of the total cost of grinding.

All the stirred ball mills have a stationary cylindrical grinding vessel, many equipped with a water jacket. The only major differences are the design features of the stirring mechanism for the grinding media. Regarding the comparison between the different types of stirring mechanism, no paper has yet been published to establish which design feature is more effective under comparable grinding conditions.

Generally speaking, Stirred ball mills are used for wet grinding applications only although some attempts have been made to use the stirred ball mill for dry grinding. More problems were observed in dry grinding as compared to wet grinding (31,32)

CHAPTER 3

EXPERIMENTAL TECHNIQUE

3.1. TEST MATERIAL

Due to its ready availability and homogeneous nature, a washed export chrome sand from the Bushveld Igneous Complex was used for the grinding tests. The chemical and physical properties of the material were as follows:

Mineralogical formula	=	$(\text{Mg}, \text{Fe}^{+2})(\text{Cr}, \text{Fe}^{+3}, \text{Al})_2\text{O}_4$
Approximate chemical analysis	=	Al_2O_3 : 15
		Fe_2O_3 : 8
		FeO : 19
		Cr_2O_3 : 48
		MgO : 10
Specific gravity ¹	=	4.5 g/cm ³
Moh's hardness	=	5.5
Natural particle size	=	-600 microns

The as-received chromite was sieved on a 600 micron sieve to remove a small portion of oversize material. The undersize material (-600 microns) is referred to as coarse feed sample.

After the removal of the +600 micron portion from the 4 tons of chromite ore received, the chromite ore was well mixed and a representative sampling procedure (ie repeated riffing or coning or quartering) was used to prepare the representative feed samples. Some of the material was wet ground to produce an approximately 100% passing 100 microns sample. The ground material which was referred to a fine feed material was dried and then thoroughly mixed. Particle size analyses were performed on several coarse and fine feed samples using standard sieving technique and Malvern Particle Sizer respectively. The results given in Table 3.1 show that the variations in the both coarse and fine feed size distributions were negligible.

¹ determined by liquid pycnometer

Table 3.1. Size analysis of feed materials.

Particle size microns	Cumulative weight percent passing					
	Coarse feed			Fine feed		
600.0	100.0	100.0	100.0	100.0	100.0	100.0
425.0	63.1	63.9	62.4	100.0	100.0	100.0
300.0	35.1	35.5	35.3	100.0	100.0	100.0
212.0	9.0	9.8	8.9	100.0	100.0	100.0
150.0	2.3	2.6	2.3	100.0	100.0	100.0
106.0	0.6	0.7	0.7	100.0	100.0	100.0
75.0	0.0	0.0	0.0	91.2	90.7	91.2
47.1	0.0	0.0	0.0	77.6	77.2	78.2
30.8	0.0	0.0	0.0	62.4	61.7	63.0
20.1	0.0	0.0	0.0	47.3	46.3	47.7
13.2	0.0	0.0	0.0	34.2	33.2	34.5
8.6	0.0	0.0	0.0	23.8	22.9	24.0
5.6	0.0	0.0	0.0	16.2	15.5	16.3
3.7	0.0	0.0	0.0	10.8	10.2	10.8
Ave. Median size microns	370.0			22.0		

3.2. GRINDING APPARATUS

3.2.1. Stirred ball mills.

Grinding experiments were carried out in stirred ball mills of three different sizes. Preliminary batch tests were conducted in a 20 litre mill and specific breakage rate measurements and further batch tests were carried out in a 5 litre mill. The scale up experiments were performed in 5 litre and 50 litre stirred ball mills and continuous experiments were conducted in 20 litre and 50 litre stirred ball mills. The clearance between the tip of the pins and the wall of the vessel was kept constant at 3 cm for all the vessels used for the experiments, except in the 20 litre mill when it was 4 cm. All the units had variable speed and torque measuring systems.

5 litre stirred ball mill: The machine essentially consisted of a vessel and an impeller. The vessel had a 1:1 diameter to height ratio (20 cm in diameter and 20 cm high). A photograph and sketch of the mill are shown in Figures 3.1 and 3.2. The impeller was composed of vertical pins attached to the drive shaft. Each pair of pins was offset by 90° and spaced at 2.5 cm apart. A variable speed 1.5 kW



Figure 3.1. Photograph of 5 litre stirred ball mill

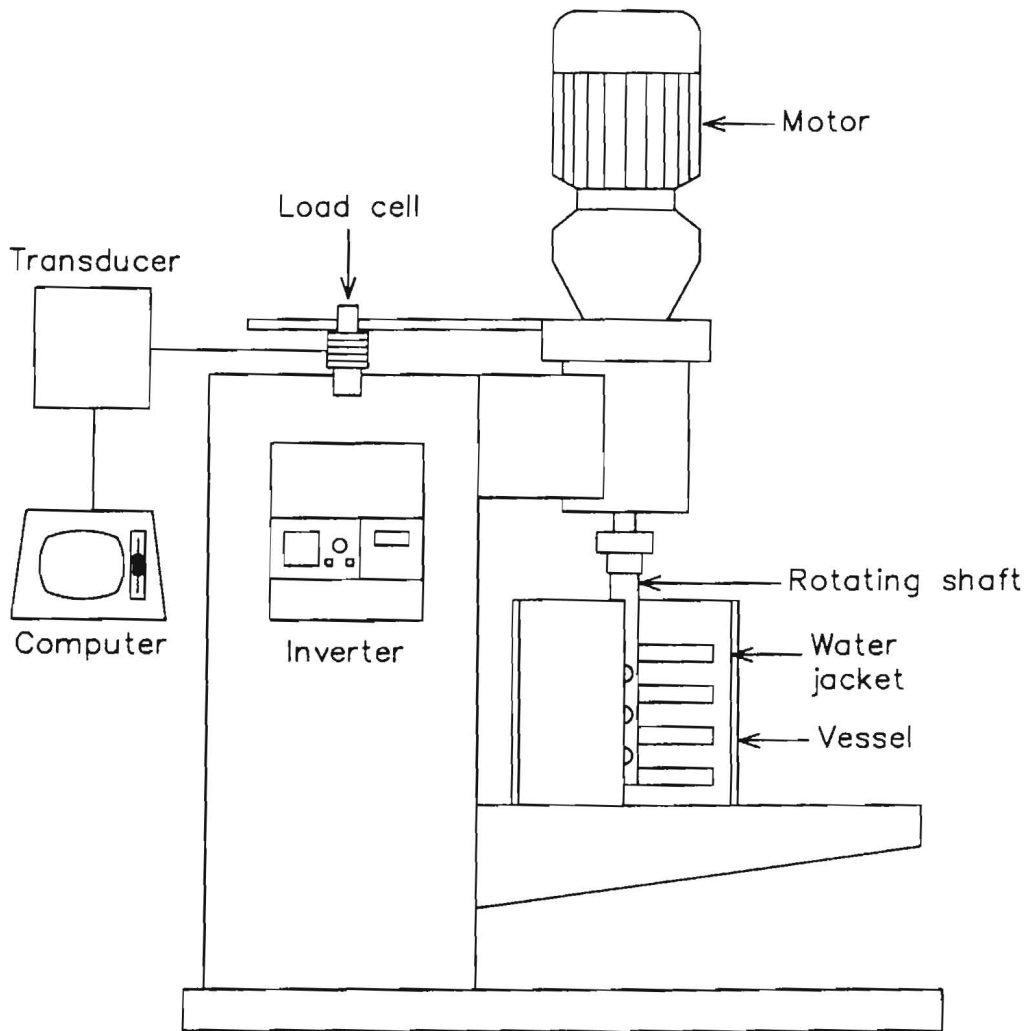


Figure 3.2. Schematic drawing of 5 litre stirred ball mill

A.C. motor and a gearbox system were used to drive the shaft and permit the variations of the shaft speed. This ranged from 50 to 650 r.p.m. and was measured with an inductive sensor and pin arrangement mounted on a collar attached to the shaft. The shaft and the drive system rested on a large ball bearing. The force exerted onto the shaft by the stirred mill content was measured by holding an extension arm, attached to the drive assembly, with a load cell (the light flexible aluminium tubing that was used to cover the power cable only weighed 177 grams and was supported at both ends, thus having no effect on the torque measurement). The torque was monitored and recorded continuously by a computer.

20 litre stirred ball mill: The mill, which was constructed at the University of Natal, is shown in Figures 3.3, 3.4, A4.1, A4.2, and A4.3. It consisted of a stationary grinding vessel (26 cm in diameter, 40 cm deep) and a central hollow shaft equipped with pins 18 cm long from tip to tip, which rotated in a bed of grinding media. The shaft rotation speed was set by means of a D.C. motor, belt, gear and sprocket system and measured continuously by using a photoelectric diode system and a toothed disc attached to the shaft. The grinding shaft torque was obtained by measuring the torque exerted on the grinding vessel which was firmly mounted on a turn-table. The force at a chosen radius needed to hold the table was measured by a load cell, the torque being recorded continually by a computer and chart recorder.

50 litre stirred ball mill: A test rig was constructed for studying performance characteristics and power requirements of larger units (Figure 3.5 and 3.6). It accommodated vessels which were 20 cm, 25 cm and 30 cm in diameter and 90 cm long and 50 cm in diameter and 50 cm long. Like the other 5 and 20 litre units the central shaft was furnished with pins. The test rig was designed to permit an adjustment for clearance between the bottom of the shaft and the grinding chamber and the diameter and spacing of the pins on the shaft were adjustable to investigate the effect of shaft geometry on the grinding performance and the power requirements of the mill. Shaft rotation speed was varied from 30 to 370 r.p.m. The shaft speed and the torque measuring systems were the same as for the 5 litre stirred ball mill.

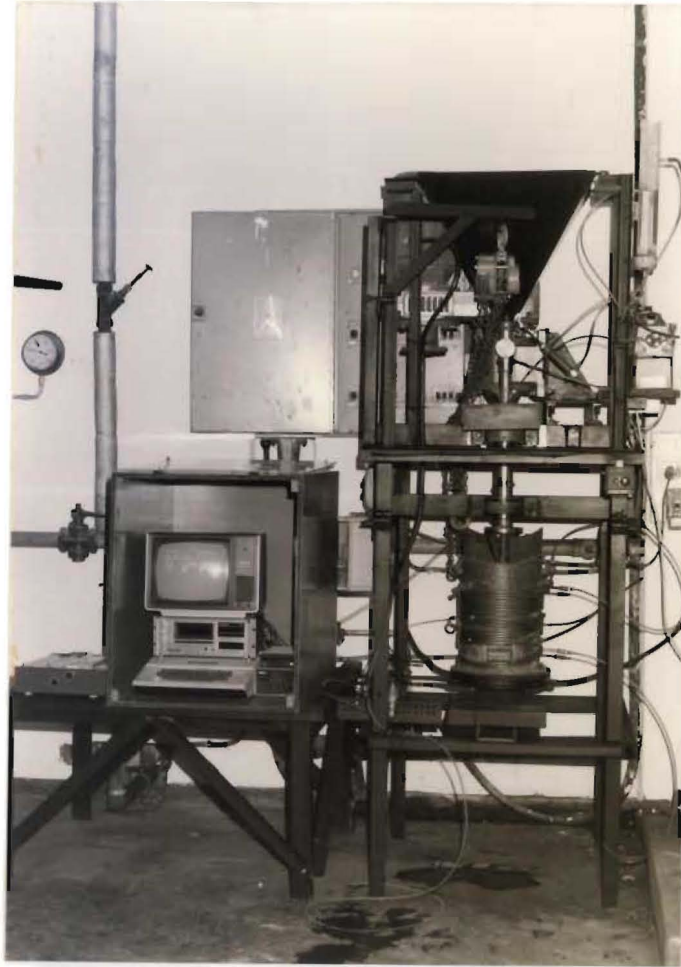


Figure 3.3. Photograph of 20 litre stirred ball mill

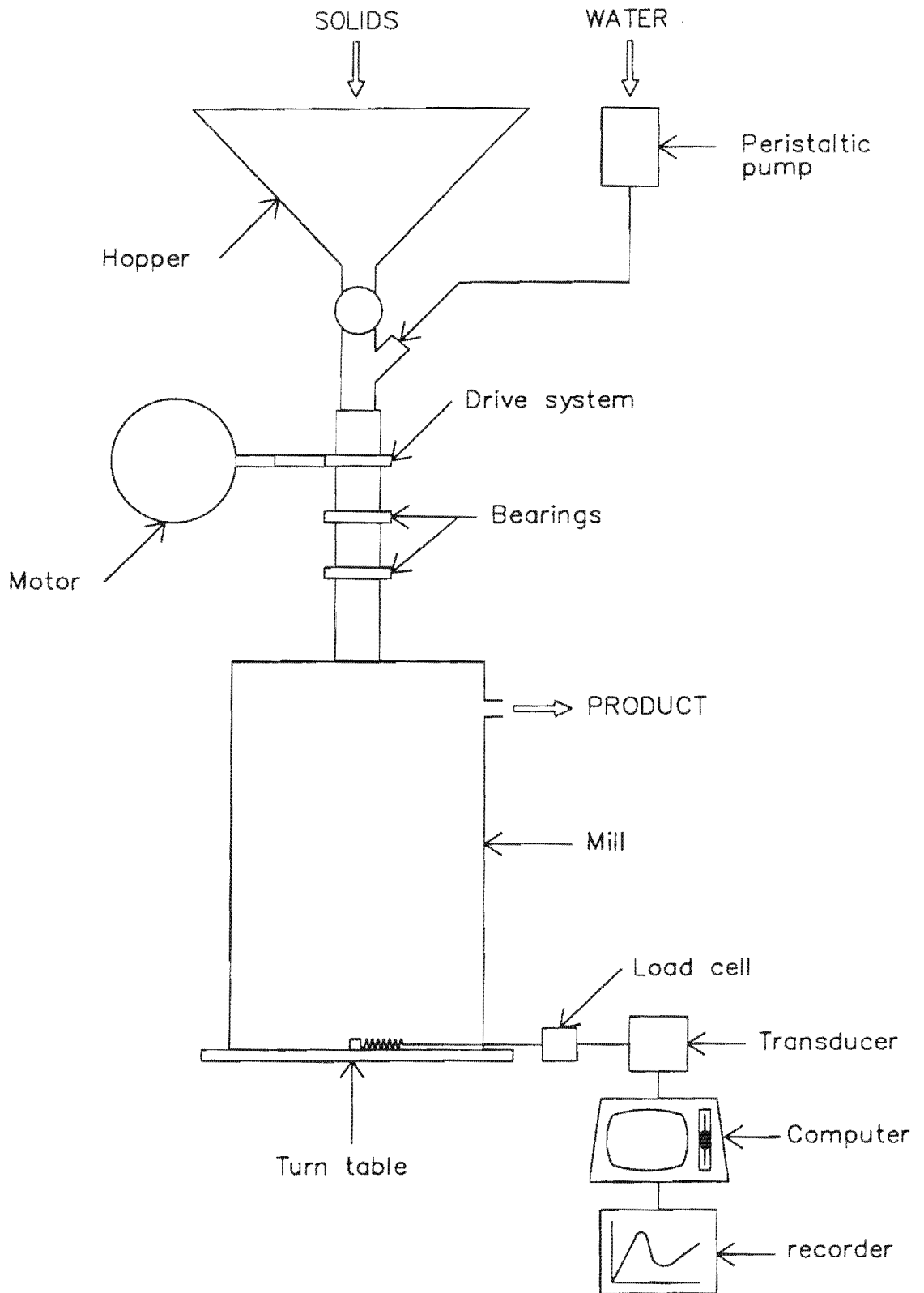


Figure 3.4. Schematic drawing of 20 litre continuous stirred ball mill



Figure 3.5. Photograph of 50 litre stirred ball mill

3.2.2. Tumbling ball mill

The mill used was a 31.5 cm diameter X 29.5 cm length steel batch ball mill with 6 lifters of rectangular shape, 20 mm wide X 4 mm high fitted symmetrically around the shell. It was equipped with a variable speed D.C. motor and the torque was measured by a load cell restraining the rotation of the drive assembly which was induced by the torque on the shaft (Figure 3.7). The torque was recorded continually by a computer and the mill revolutions were recorded by a counter attached to the mill shaft.

3.3. GRINDING MEDIA

Type, size and density of grinding media used in the stirred and the tumbling ball mills are given in Table 3.2.

Table 3.2. Properties of different types of grinding media used for the grinding experiments

Types of grinding machine	Type of grinding media	Grinding media	
		Diameter mm	Density g/cm ³
Stirred ball mill	Steel	15	7.85
	Steel	10	7.85
	Steel	6	7.85
	Steel	4	7.85
	Steel	3	7.85
	Steel	2	7.85
	Zirconia	6	5.50
	Alumina	6	3.45
	Alumina	4	3.45
	Alumina	3	3.45
	Steatite	6	2.65
Tumbling ball mill	Steel	² 40 & 30	7.85
		23	7.85

² 38.2% of 40 mm & 61.8% of 30 mm balls by weight

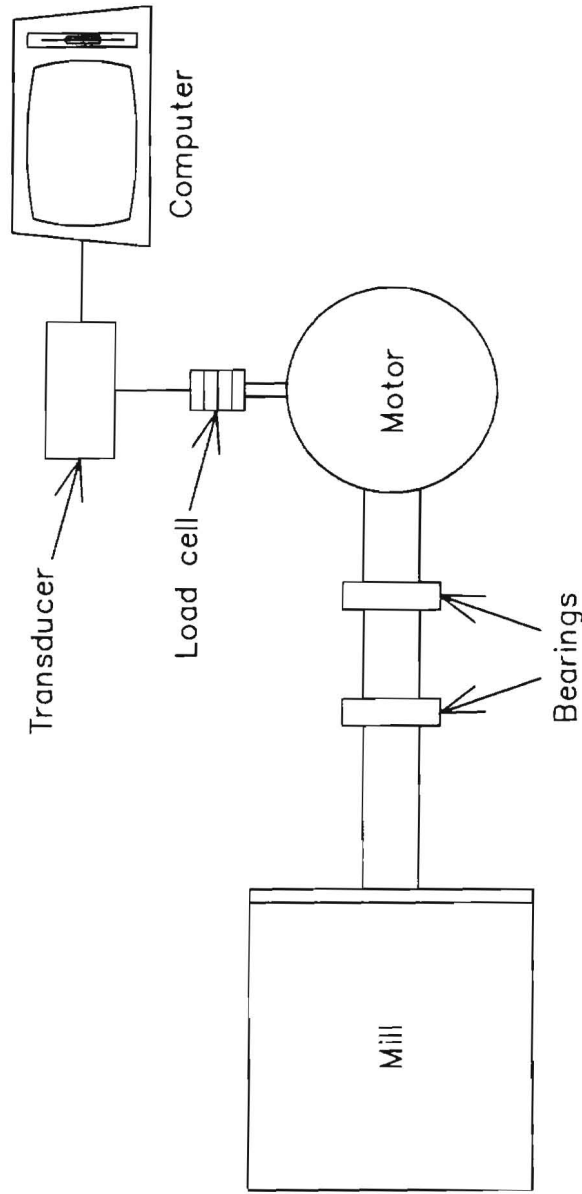


Figure 3.7. Schematic drawing of the batch grinding tumbling ball mill

3.4. EXPERIMENTAL PROCEDURE

3.4.1. Batch grinding in stirred and tumbling ball mill

The following experimental procedures were used for both the stirred and the tumbling ball mills. All batch grinding tests were done on a wet basis.

3.4.1.1. Batch grinding tests in the stirred ball mill

Complete size distribution method: The feed for the grinding experiments had a complete distribution of sizes. A representative sample was taken from the starting material. The mill was layer loaded (ie. a layer of balls, a layer of sample, a layer of balls etc.) to ensure that the charge would be well mixed in the initial stage of the grinding. Variations in ore solids were achieved by changing the solids to water ratio to give a total slurry volume which was 44% of the steel plus porosity volume (Appendix 3). At the completion of the grinding, the total mill contents were tipped through a coarse screen to retain the balls. The slurry was filtered and oven dried. The dry cake was broken up on a 600 micron sieve and well mixed. The product was reduced by coning and quartering to a suitable size to perform the particle size analysis. Fresh material was used for each experiment.

The one-size fraction method: One size material which was in a $\sqrt{2}$ interval was sieved out from the starting material. 540 mm diameter Rhologon sieves and 300 mm diameter laboratory sieves were used for preparing the sample. A representative sample of the above starting material was taken and subjected to a "blank sieving test evaluation" using the two standard sieves describing the size interval (69). The sieve loading and sieving times used for this head sample evaluation were also used for the subsequent milling test evaluations. The percentage of the material passed through the lower screen was determined. The passing percentage of the material should not be greater than 5% to obtain accurate results. When a suitable amount of material of the desired test size was prepared and blank size analysis performed, the mill was filled with the desired filling of balls, material and water. They were spread in the mill uniformly. The material was then ground in the mill for varying times which were chosen to enable specific breakage rate values to be calculated. The mill content was

sampled and size analysis performed by the Malvern Particle Sizer or standard sieves. A fractional weight disappearance from the original size per unit kWh/t was determined. The mill discharge was returned to the mill together with the sample taken for particle sizing, for further grinding.

3.4.1.2. Batch grinding tests in the tumbling ball mill

The complete size distribution method was used for the tumbling ball mill experiments. The mill discharge was returned to the mill together with the sample taken for particle sizing for further grinding.

3.4.2. Continuous grinding in stirred ball mill

20 litre stirred ball mill: For continuous mode operation, the hollow in the shaft allowed the material to be fed in at the top with the slurry flowing down through the shaft and up the annular grinding zone between the shaft and the vessel. The material was fed with an adjustable pneumatically driven star feeder from the feed hopper (Figure 3.4). The addition of water to the mill feed was controlled by a peristaltic pump from the overhead tank. The experiments were carried out by allowing the mill to reach a steady state, as determined by a constant discharge rate and pulp density. The mill overflow was collected in buckets at 10 minute intervals. At the end of each continuous run, the material remaining in the mill was weighed to provide the instantaneous value of the final hold-up and the pulp density. The samples collected were analysed for the percent solids and the particle size distribution.

50 litre stirred ball mill: The continuous grinding experiments were also performed in the 50 litre stirred ball mill. The solids and water were fed into the small pump sump simultaneously. The solid feed rate was controlled by a vibratory feeder while the water flow was set using a rotameter. The slurry was pumped into the grinding vessel at the bottom by means of the peristaltic pump and flowed up through the grinding media bed. The continuous experiments were carried out using the same procedure as that for the 20 litre stirred ball mill except that the mill discharge slurry was collected in buckets at successive 1 minute intervals.

3.4.3. Media wear test.

Media wear tests were carried out using the 15, 10 and 6 mm steel balls in the stirred ball mill and 23 mm steel balls in the tumbling ball mill. All balls were conditioned before grinding tests by removing the outer rusted layer. The total grinding media was oven dried, cooled and accurately weighed before and after each grinding experiment. The weight loss is reported as kg per ton of ore ground and as kg per ton of minus 10 micron product.

3.5. PARTICLE SIZE ANALYSIS

3.5.1. Sieve analysis

The representative sample was wet sieved at 38 microns. The -38 micron material was recovered by a pressure filter followed by the drying of retained and passing material. The oversize material was dry screened on a nest of sieves with an Endecott test sieve shaker for 30 minutes. The sieve sizes were chosen in $\sqrt{2}$ intervals. The experimental results for the determination of the optimum sieving time are given in Appendix 1.

3.5.2. Sub-sieve size analysis

Sieving as a standard method of size analysis gives no information on the distribution sizes of material below 38 microns. Since the research on high level energy input products requires rapid and accurate sub-sieve size analysis, the Malvern MasterSizer was used on the analysis of ground products. It can analyse particle size distribution in the range of 0.1 to 600 microns (41). The principle of the system used by the instrument is based on the measurement of diffraction from the particles. A low power visible laser transmitter produces a parallel monochromatic beam of light which is arranged to illuminate the particles to give a stationary diffraction pattern regardless of particle movement. Integration over a suitable period with a continuous flux of particles through the sample cell, gives the measured diffraction pattern of a representative bulk sample.

The MasterSizer employs two forms of optical configuration. The first is optical method, called "Conventional Fourier optics". The second is a new optical configuration, called "Reverse Fourier optics", used in order to allow the measurement size range to be extended down to 0.1 microns. The Fourier Transform Lens focuses the diffraction pattern onto a multi-element photo-electric detector which produces an analogue signal proportional to the light received. The detector is interfaced directly to a desk computer, allowing it to read the diffraction pattern and perform the necessary integration digitally. The computer uses the method of non-linear least squares analysis to find the size distribution giving the closest fitting diffraction pattern.

3.6. PRESENTATION OF RESULTS

Where possible in this thesis, a graphic approach has been used to present the results. Some figures and tables of experimental results will be found in the Appendices under the prefix A. Experimental conditions are given in the figures as well as in the tables and relevant figures and tables are referred to each other.

Although it is customary to plot the dependent variable on a Y axis against the independent variable on an X axis, it has been found a more useful basis for evaluating Charles' Equation if the data is plotted in reverse i.e. which takes the characteristics of the equation into account. This type of graphical analysis was applied by other investigators (1,32,43).

In order to obtain the correlation between the models, the same units used for the torque models (Chapter 9) were employed for the energy-size model (Chapter 6) and the linear population model (Chapter 7).

CHAPTER 4

BATCH GRINDING EXPERIMENTS IN A 20 LITRE MILL

In stirred ball milling, several variables simultaneously influence particle size reduction, power consumption and media wear. Efficient grinding can only be achieved when the right set of operating conditions is used. Therefore, this required a detailed investigation to determine the effect of changes in design and operating variables such as pulp density, ball size, ball density, load depth, shaft speed, pin spacing and pin diameter.

In the first stage of the preliminary experiments, the smallest grinding media at our disposal were 23 mm and 15 mm diameter steel balls. Very few experimental investigations were available in the literature which related to the variable operating parameters, in fact, the effect of ball size was unknown especially in the use of large balls. The shaft speed was therefore set at 72 r.p.m. (similar to the tower mill which uses 23 mm and 15 mm ball size) by means of a chain and sprocket system and then the shaft speed was doubled to accommodate 10 mm and 6 mm steel balls. At a later stage of this phase, the mill drive system was changed to a variable speed drive system as the investigation progressed. In this phase of the investigation only 6 mm steatite balls were available to investigate the effect of the ball density. A general combination of variables and the range studied were selected within the limitations of the prototype mill and scarcity of available grinding media of small size and density.

The "one-variable-at-a-time" approach was used to determine the effect of each one by changing it while holding all other variables as constant as possible. Experimental programme and grinding conditions are given in Table 4.1. Due to the lack of data in the available literature, additional testwork, given in Table 4.2, were carried out to develop a greater understanding regarding the effect of milling variables and to verify the conclusions drawn from the one-variable-at-a-time experimental programme as to whether they can be applied under the other grinding conditions. Data from "one-variable-at-a-time" testwork and additional experiments were considered and discussed together.

Table 4.1. "One-variable-at-a-time" experimental programme and grinding conditions

Variable parameters		Constant parameters							
		Pulp density % solids by weight	Ball size mm	Ball density g/cm ³	Load depth cm	Shaft speed r.p.m.	Pin spacing cm	Pin diameter cm	Energy Input kWh/t
Pulp density, % solids by weight	62.5 70.0 75.0 80.0	-	6	7.85	32	164	8.6	1.6	66.0
Ball size, mm	6 10 15	75	-	7.85	32	164	8.6	1.6	66.0
Ball density, g/cm ³	2.65 7.85	75	6	-	32	164	8.6	1.6	66.0
Load depth, cm	13.7 22.9 32.0	75	6	7.85	-	164	8.6	1.6	66.0
Shaft speed, r.p.m.	164 300 400	75	6	7.85	32	-	8.6	1.6	66.0
Pin spacing, cm	3.6 5.6 8.6 13.1	75	6	7.85	32	164	-	1.6	66.0
Pin diameter, cm	1.6 3.2	75	6	7.85	32	164	8.6	-	66.0

Mill diameter (26 cm) and pin length (18 cm from tip to tip) were kept constant. The coarse feed size ($d_{50} = 370$ microns) was used for the experiments.

Table 4.2. Additional grinding test conditions

Variable parameters	Constant parameters								
	Pulp density % solids by weight	Ball size mm	Ball density g/cm ³	Load depth cm	Shaft speed r.p.m.	Pin spacing cm	Pin diameter cm	Energy Input kWh/t	Feed size mic. d50
Pulp density, % solids by weight	62.5	6	7.85	32.0	300	8.6	1.6	66.0	370
	70.0	6	7.85	32.0	300	8.6	1.6	66.0	370
	75.0	6	7.85	32.0	300	8.6	1.6	66.0	370
	80.0	6	7.85	32.0	300	8.6	1.6	66.0	370
	62.5	6	2.65	32.0	300	8.6	1.6	66.0	370
	70.0	6	2.65	32.0	300	8.6	1.6	66.0	370
	75.0	6	2.65	32.0	300	8.6	1.6	66.0	370
	62.5	15	7.85	32.0	72	8.6	1.6	66.0	370
	70.0	15	7.85	32.0	72	8.6	1.6	66.0	370
	75.0	15	7.85	32.0	72	8.6	1.6	66.0	370
80.0	15	7.85	32.0	72	8.6	1.6	66.0	370	
Ball size, mm	75.0	6	7.85	32.0	72	8.6	1.6	66.0	370
	75.0	10	7.85	32.0	72	8.6	1.6	66.0	370
	75.0	15	7.85	32.0	72	8.6	1.6	66.0	370
Ball density, g/cm ³	75.0	6	7.85	32.0	400	8.6	1.6	66.0	370
	75.0	6	2.65	32.0	400	8.6	1.6	66.0	370
	75.0	6	7.85	32.0	164	8.6	1.6	36.0	9.3
	75.0	6	2.65	32.0	164	8.6	1.6	36.0	9.3
	75.0	6	2.65	32.0	300	8.6	1.6	36.0	9.3
	75.0	6	2.65	32.0	400	8.6	1.6	36.0	9.3
Load depth, cm	75.0	15	7.85	32.0	72	8.6	1.6	66.0	370
	75.0	15	7.85	22.9	72	8.6	1.6	66.0	370
	75.0	15	7.85	13.7	72	8.6	1.6	66.0	370
Shaft speed, r.p.m.	75.0	6	2.65	32.0	164	8.6	1.6	66.0	370
	75.0	6	2.65	32.0	300	8.6	1.6	66.0	370
	75.0	6	2.65	32.0	400	8.6	1.6	66.0	370
	75.0	10	7.85	32.0	72	8.6	1.6	66.0	370
	75.0	10	7.85	32.0	164	8.6	1.6	66.0	370
	75.0	10	7.85	32.0	300	8.6	1.6	66.0	370
	75.0	15	7.85	32.0	50	8.6	1.6	66.0	370
	75.0	15	7.85	32.0	72	8.6	1.6	66.0	370
	75.0	15	7.85	32.0	164	8.6	1.6	66.0	370
	Pin spacing, cm	75.0	10	7.85	32.0	164	5.6	1.6	66.0
75.0		10	7.85	32.0	164	8.6	1.6	66.0	370
75.0		10	7.85	32.0	164	13.1	1.6	66.0	370
75.0		10	7.85	32.0	164	20.8	1.6	66.0	370

Variable parameters	Constant parameters								
	Pulp density % solids by weight	Ball size mm	Ball density g/cm ³	Load depth cm	Shaft speed r.p.m.	Pin spacing cm	Pin diameter cm	Energy Input kWh/t	Feed size mic. d50
Pin diameter, cm	75.0	10	7.85	32.0	164	8.6	1.6	66.0	370
	75.0	10	7.85	32.0	164	8.6	3.2	66.0	370
Energy input, kWh/t	62.5	6	7.85	32.0	164	8.6	1.6	36.0	370
	62.5	6	7.85	32.0	164	8.6	1.6	66.0	370
	62.5	6	7.85	32.0	164	8.6	1.6	90.0	370
	62.5	6	7.85	32.0	164	8.6	1.6	150.0	370
	62.5	6	7.85	32.0	164	8.6	1.6	200.0	370
	75.0	6	7.85	32.0	164	8.6	1.6	28.0	370
	75.0	6	7.85	32.0	164	8.6	1.6	36.0	370
	75.0	6	7.85	32.0	164	8.6	1.6	52.5	370
	75.0	6	7.85	32.0	164	8.6	1.6	66.0	370
	75.0	6	7.85	32.0	164	8.6	1.6	90.0	370
	75.0	6	7.85	32.0	164	8.6	1.6	150.0	370
	75.0	6	7.85	32.0	164	8.6	1.6	200.0	370
	75.0	10	7.85	32.0	164	8.6	1.6	20.0	370
	75.0	10	7.85	32.0	164	8.6	1.6	36.0	370
	75.0	10	7.85	32.0	164	8.6	1.6	49.5	370
	75.0	10	7.85	32.0	164	8.6	1.6	66.0	370
	75.0	10	7.85	32.0	164	8.6	1.6	90.0	370
	75.0	10	7.85	32.0	164	8.6	1.6	150.0	370
	75.0	10	7.85	32.0	164	8.6	1.6	200.0	370
	75.0	10	7.85	32.0	72	8.6	1.6	20.0	370
	75.0	10	7.85	32.0	72	8.6	1.6	36.0	370
	75.0	10	7.85	32.0	72	8.6	1.6	52.5	370
	75.0	10	7.85	32.0	72	8.6	1.6	66.0	370
	75.0	15	7.85	32.0	72	8.6	1.6	20.0	370
75.0	15	7.85	32.0	72	8.6	1.6	36.0	370	
75.0	15	7.85	32.0	72	8.6	1.6	52.5	370	
75.0	15	7.85	32.0	72	8.6	1.6	66.0	370	

4.1. PULP DENSITY

Figure 4.1 and Table A4.1 show the effect of pulp density on the median size of the product in various grinding conditions for a fixed energy input at a constant pulp volume which fills the interstitial ball voids. When 15 mm balls were used at a shaft rotation speed of 72 r.p.m., the median size decreased steadily with an increase in solids content of up to 80% solids by weight. At a pulp density of 85% the mill jammed.

The effect of pulp density on the median size was investigated using 6 mm steel balls at shaft rotation speeds of 164 r.p.m and 300 r.p.m. At a shaft rotation speed of 164 r.p.m., the median size decreased slightly with increasing pulp density from 62.5% to 70%. After reaching a minimum value at a pulp density of 70%, it increased at 75% pulp density to a value similar to that at 62.5%. A further increase in pulp density resulted in an increase in the median size. At a shaft rotation speed of 300 r.p.m, the median size at a pulp density of 62.5% was somewhat high and then decreased to a minimum and remained constant in the pulp density range of 70% to 75%. Beyond a pulp density of 75%, the median size increased significantly and at a pulp density of 80% it reached a similar value to that at 164 r.p.m. In addition to these test results, the experiments with the 6 mm steel balls at a shaft rotation speed of 164 r.p.m. gave somewhat smaller median sizes than those at 300 r.p.m at pulp densities lower than 75%. However, statistical analysis of the data given in Table A4.1 using the Student t-test indicated that the difference between the means of the median sizes of the products obtained at shaft rotation speeds of 164 r.p.m. and 300 r.p.m. using steel balls was not significant at 95 percent confidence level.

Another series of tests was made to study the effect of varying the pulp density while using 6 mm steatite balls at a shaft speed of 300 r.p.m. Between 62.5% to 70% solids, the median size increased only slightly but at a pulp density of 75% there was a considerable increase.

Further experiments were run over a range of energy input levels to study the effect of pulp densities of 62.5% and 75% on the median size of the product using 6 mm steel balls (Figure 4.2 and Table A4.2). Pulp densities of 62.5% and 75% gave the same median size product within the range of energy input levels studied.

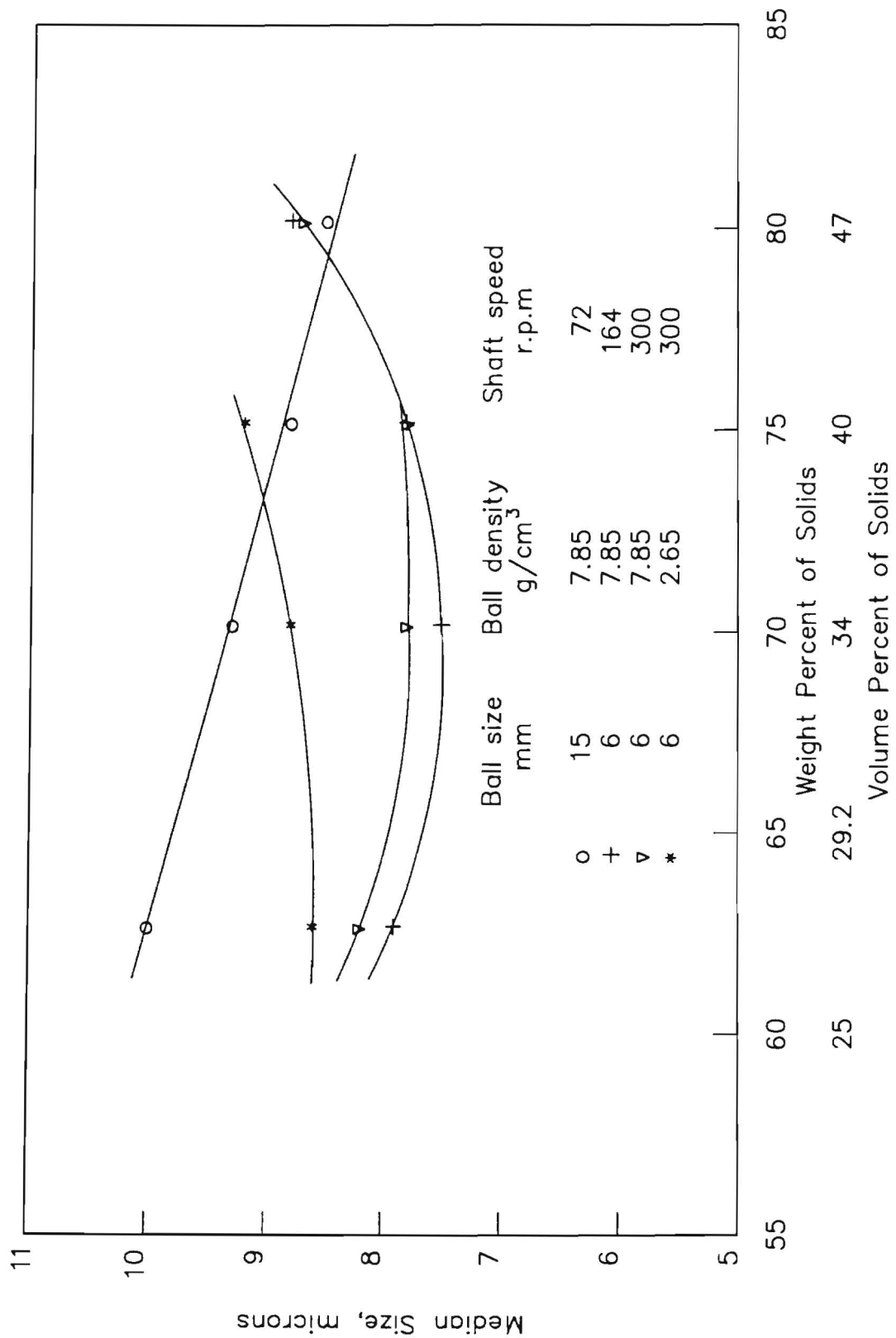


Figure 4.1. Effect of pulp density on median size : load depth = 32 cm, pin spacing = 8.6 cm, pin diameter = 1.6 cm, energy input = 66 kWh/t (data given in Table A4.1).

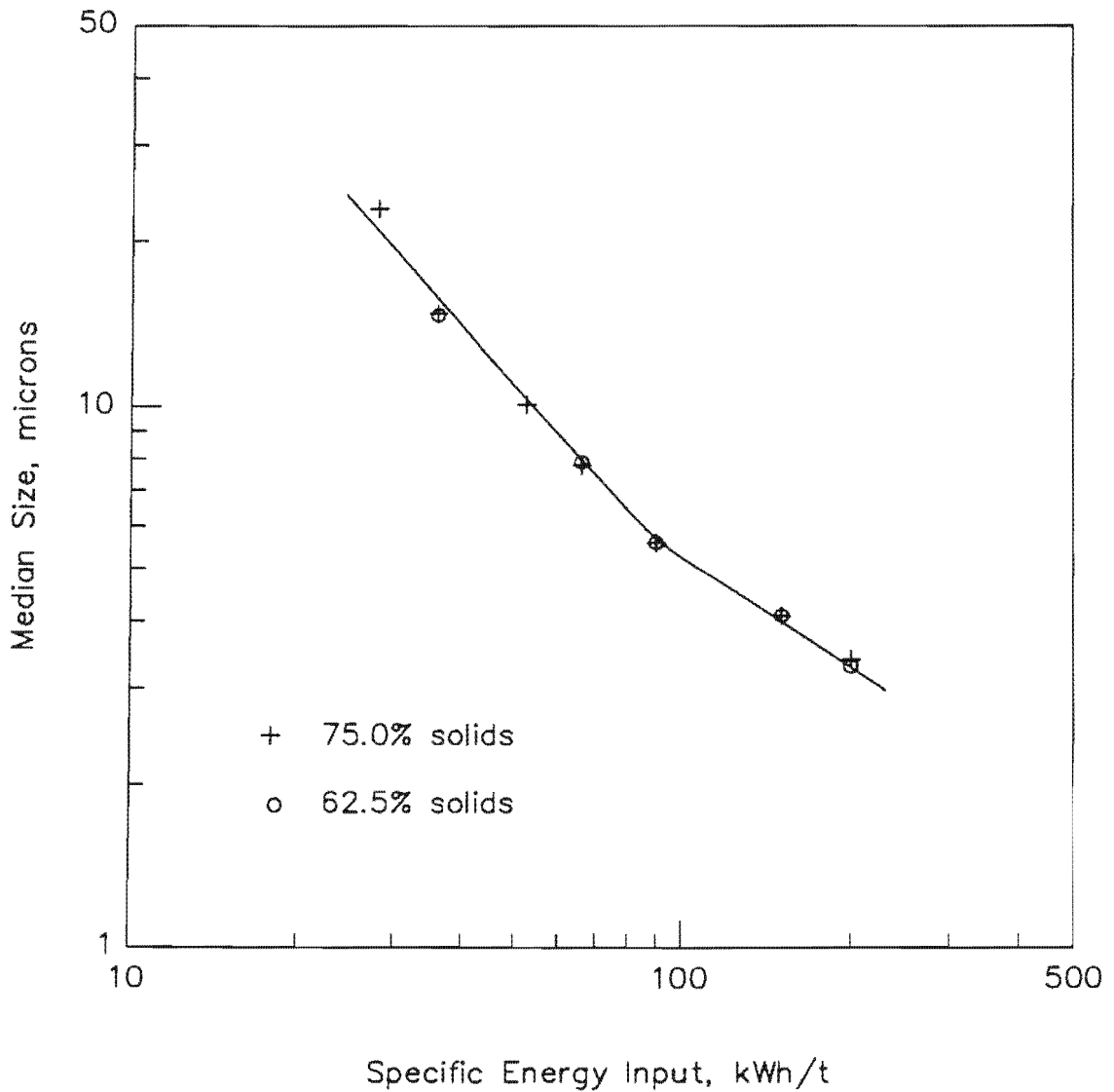


Figure 4.2. Median size of product as a function of energy input for various pulp densities : 6 mm steel balls, load depth = 32 cm, shaft speed = 164 r.p.m., pin spacing = 8.6 cm, pin diameter = 1.6 cm (data given in Table A4.2).

When 15 mm steel balls were used, the increased rate of breakage observed with a high slurry density was probably due to the higher solid packing with a greater mass of particles effectively dispersed within a given volume of slurry. Although for the very dense slurry (above 75% solids by weight or 40% by volume) the viscosity increased rapidly, the production of fines from the stirred ball mill continued to increase at a pulp density of 80%. This can be attributed to the mechanical stirring of balls of a large diameter which enhances the break up of viscous aggregates and the low shaft rotation speed which results in a less pronounced viscosity effect.

When 6 mm steel balls were used, the product median size was almost independent of pulp density in the region of 62.5% to 75% at shaft rotation speeds of 164 r.p.m. and 300 r.p.m.. This is probably due to a greater number of contact points between the smaller balls and greater frequency of collisions that capture and fracture the particles, even at low pulp densities. In addition to this, more impacts compensate for increased viscosity. When the pulp density increases above 75%, the grinding rate decreases sharply as the viscosity builds up.

Investigation also demonstrated that the difference between the ball and pulp densities had a significant effect on particle size reduction. The steatite ball density of 2.65 g/cm^3 was near the grinding pulp density of 2.4 g/cm^3 (40% solids by volume) which was used for the grinding tests. It can therefore be concluded that a high pulp density hindered the grinding efficiency of small density balls rather than enhanced it. This might result from the movement of the light balls in the mill being impeded by the high pulp density, decreasing the probability of particle fracture. It could be somewhat overcome by an increase in the shaft rotation speed.

The torque as a function of slurry density and energy input is shown in Figure 4.3 and Table A4.3. The initial torque was very high in the stirred ball mill which was probably due to the high friction caused by the narrow size of a relatively coarse feed. Higher pulp densities gave higher torque readings due to the initial mixing of the higher solid content of the pulps. The mill torque decreased gradually and fell to an almost constant value after an energy input of about 30 kWh/t. The torque decreased somewhat as the pulp density increased because of changes in slurry rheology. High density and fine fluid pulp would lower the friction coefficient between the grinding media ball surfaces and reduce the power

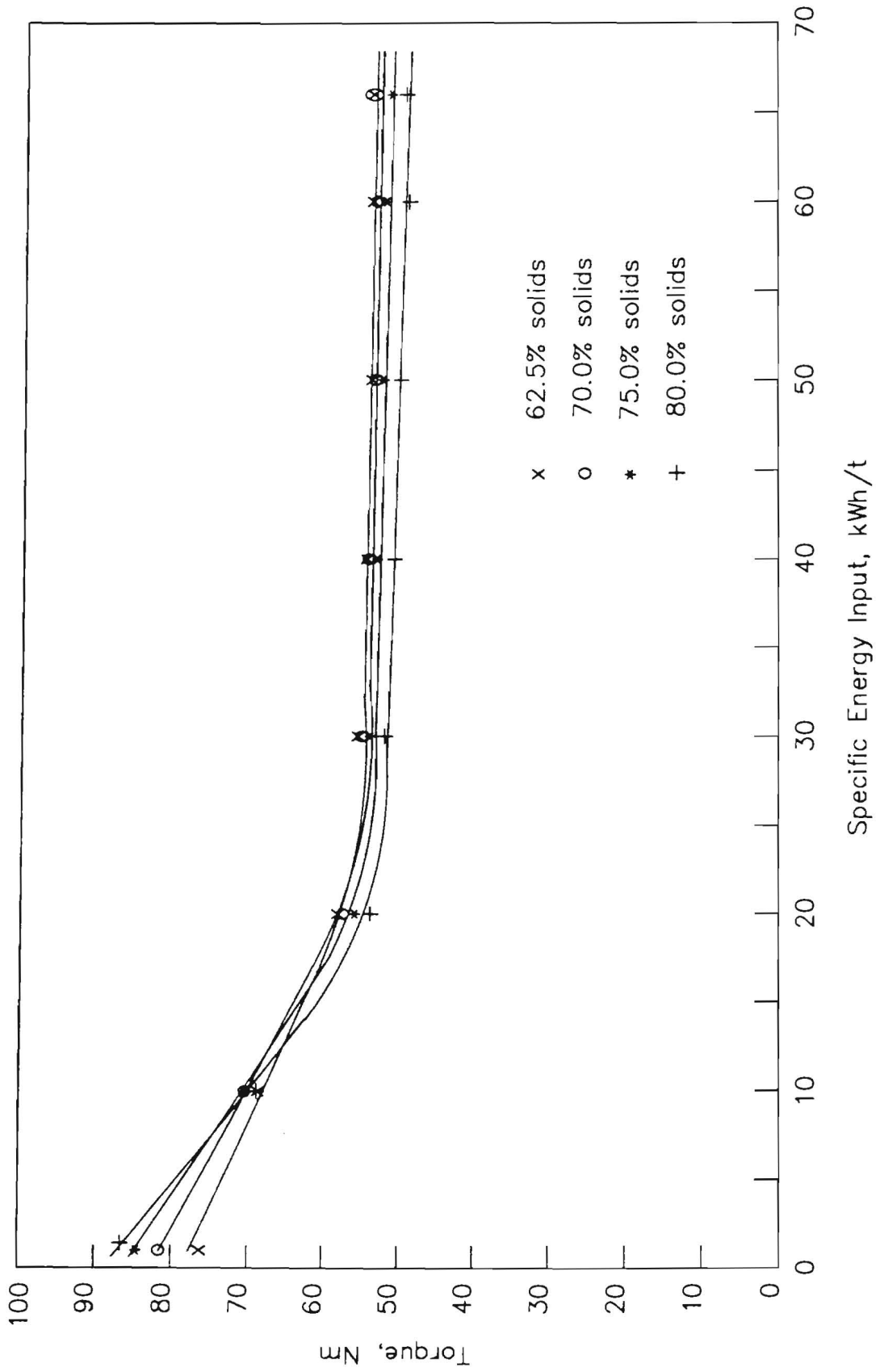


Figure 4.3. Variation of mill torque as a function of energy input at various densities : 6 mm steel balls, load depth = 32 cm, shaft speed = 164 r.p.m., pin spacing = 8.6 cm, pin diameter = 1.6 cm (data given in Table A4.3).

consumption since such a pulp acts as a lubricant. On the other hand very high pulp viscosity would impede the displacement of the grinding media and lead to increased power consumption (32).

Figure 4.4 and Table A4.4 show the ball wear per ton of ore ground and minus 10 micron material produced as a function of energy input for various percent solids. The wear per ton of ore ground initially shows a linear relationship with a decrease in the rate of ball wear as the grinding becomes finer. The ball wear was similar at a pulp density of 62.5% and 70% however it decreased significantly at a pulp density of 75%. The wear values for the production of minus 10 micron material increase with increasing energy input up to a maximum then decrease with a further increase in the energy input, in addition to which the media wear clearly differs depending on the pulp density. Figure 4.5 and Table A4.5 show the effect of pulp density on the media wear for various grinding conditions. The experimental results demonstrated that the higher the pulp density, the less the media wear, regardless of grinding conditions used.

The pulp density should be as high as possible, consistent with the ease of flow through the stirred mill. It is essential that the balls are coated with a layer of ore since a dilute pulp increases metal contact, giving increased steel consumption and reduced efficiency.

4.2. GRINDING MEDIA SIZE

The effect of ball size on the grinding efficiency of the stirred ball mill was studied by determining the median size as a function of energy input. Experimental results are presented as specific energy input against median size on log-log paper (Figure 4.6 and 4.7 and Table A4.6 and A4.7).

Plots of this type can be described by the Charles' Equation as previously shown by other researchers (43,44).

$$E = A(k_p^{-\beta} - k_f^{-\beta}) \quad (4.1)$$

E = The energy input, kWh/t.

A = A constant that is characteristic of the grinding device.

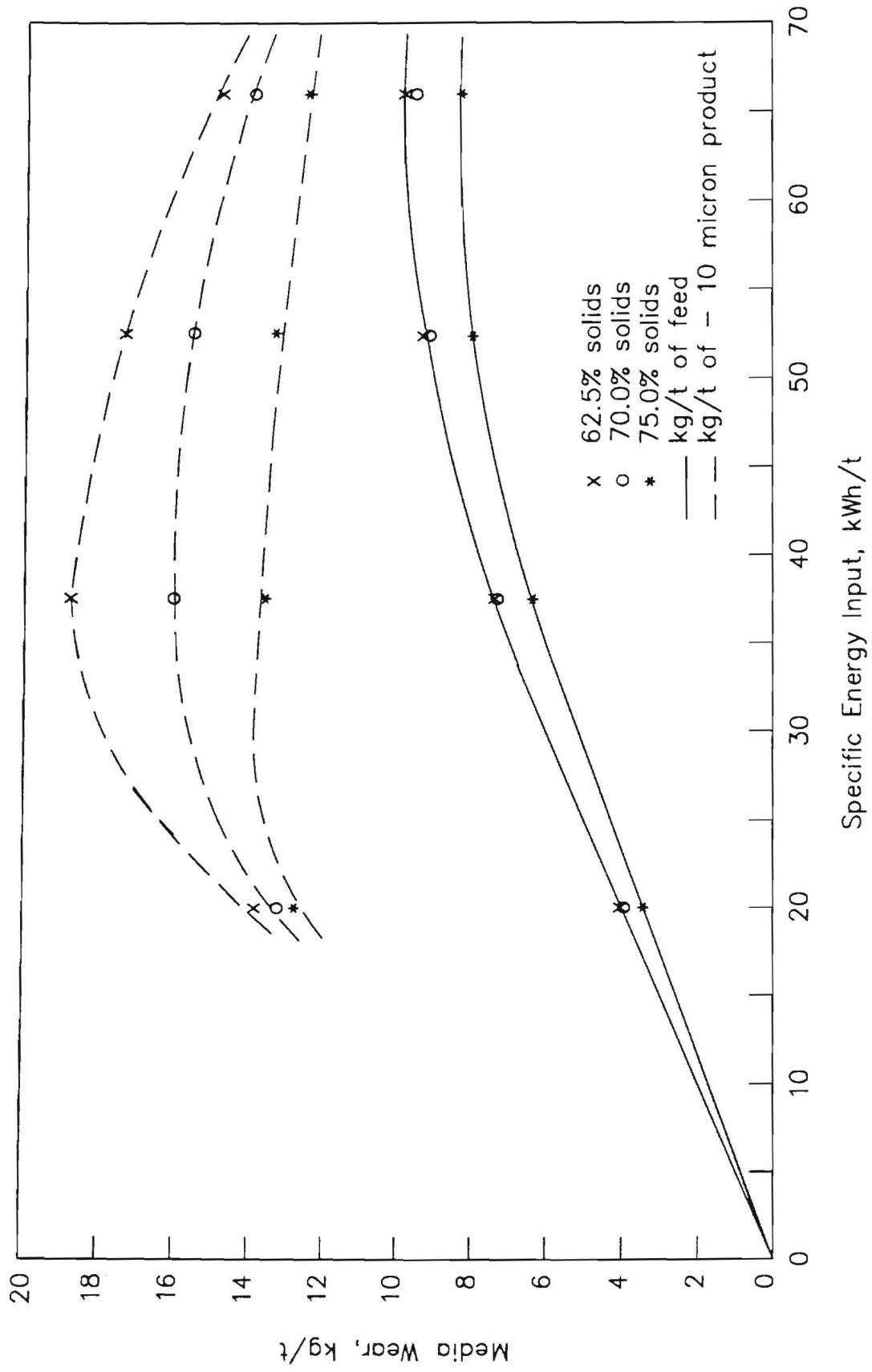


Figure 4.4. Media wear as a function of energy input at various pulp densities: 6 mm steel balls, load depth = 32 cm, shaft speed = 164 r.p.m., pin spacing = 8.6 cm, pin diameter = 1.6 cm (data given in Table A4.4).

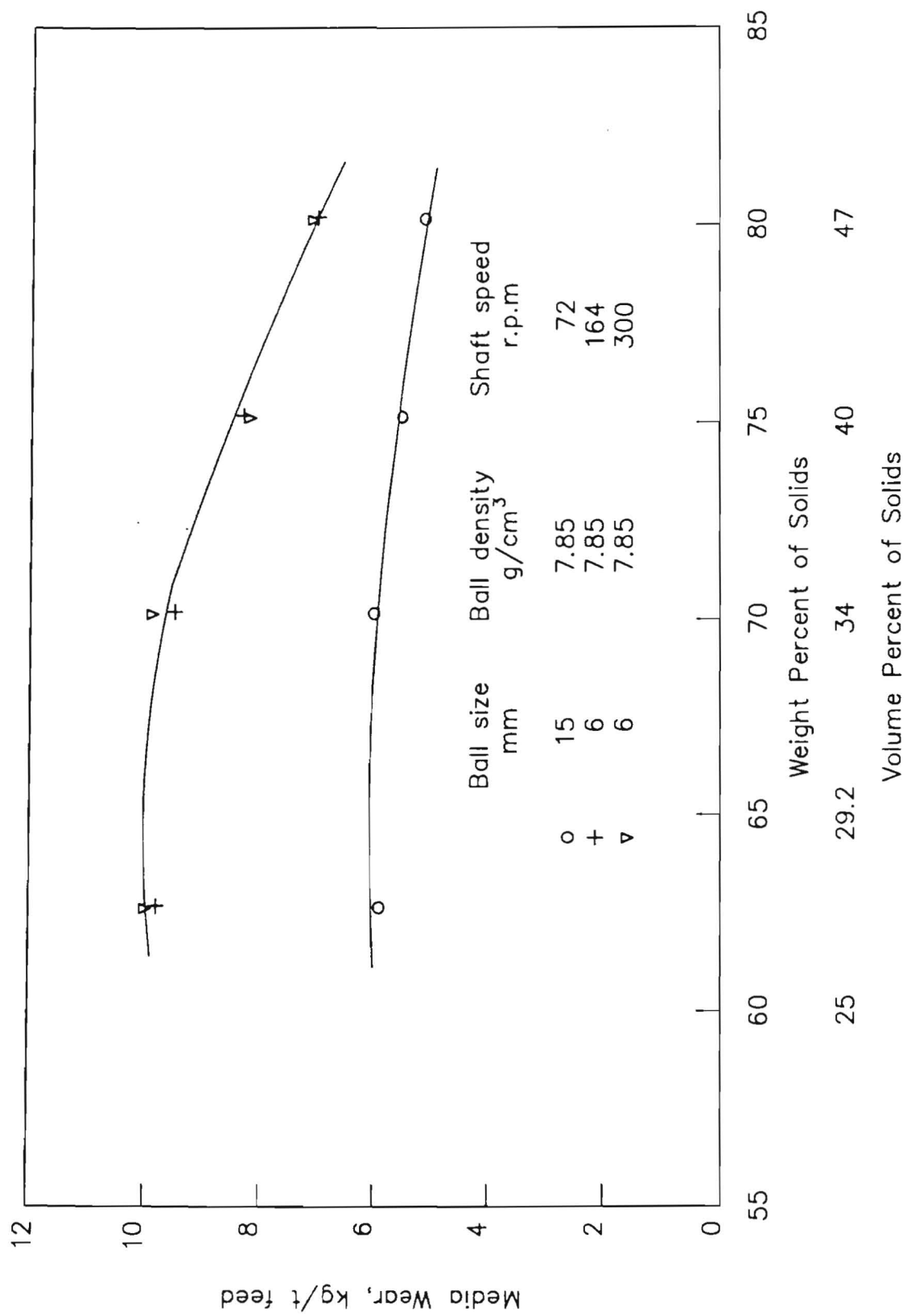


Figure 4.5. Effect of pulp density on media wear: load depth = 32 cm, pin spacing = 8.6 cm, pin diameter = 1.6 cm, energy input = 66 kWh/t (data given in Table A4.5).

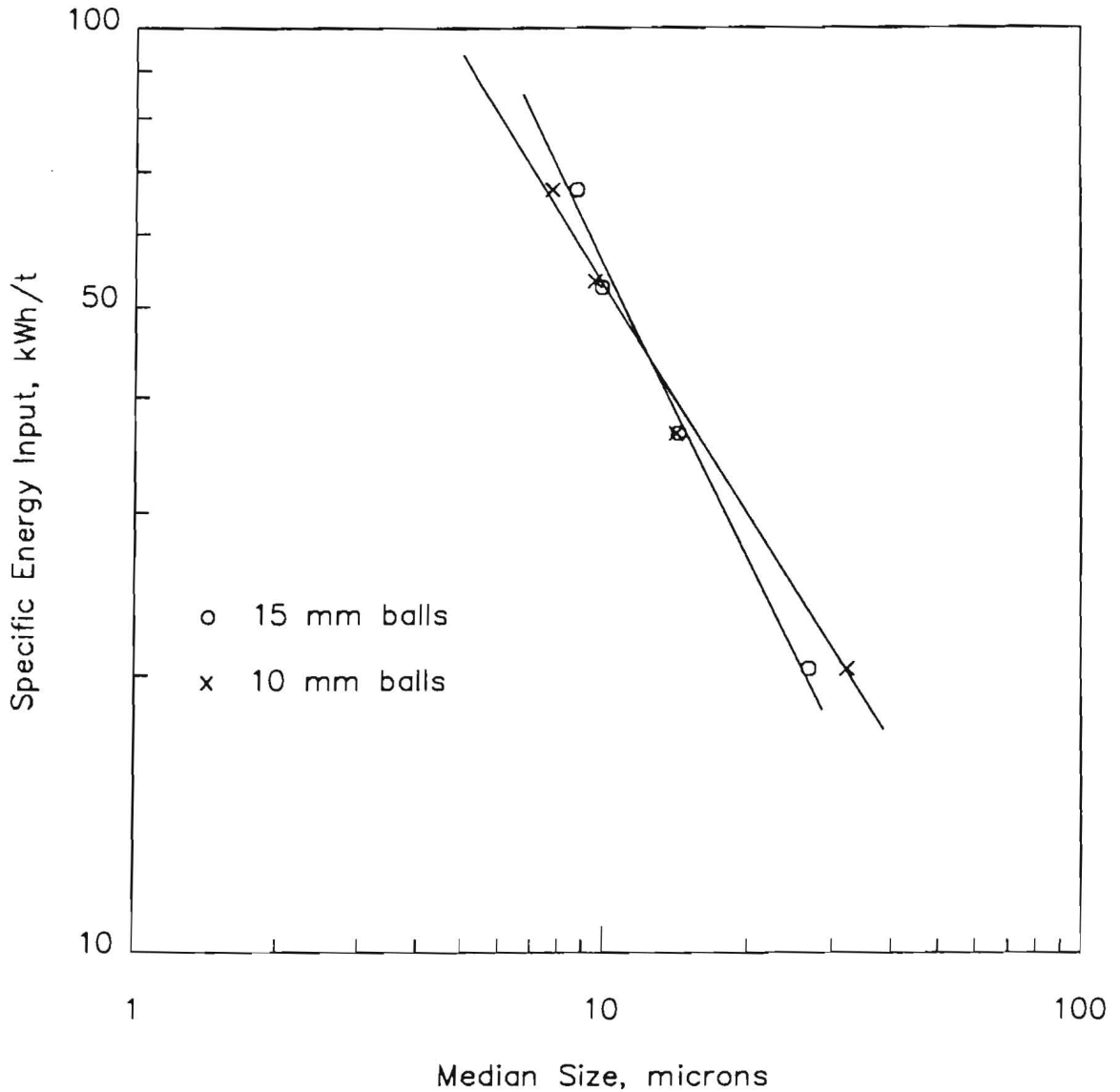


Figure 4.6. Median size of chromite ore as a function of energy input for various ball sizes at 72 r.p.m.: pulp density = 75% solids by weight, media type = steel, load depth = 32 cm, pin spacing = 8.6 cm, pin diameter = 1.6 cm (data given in Table A4.6).

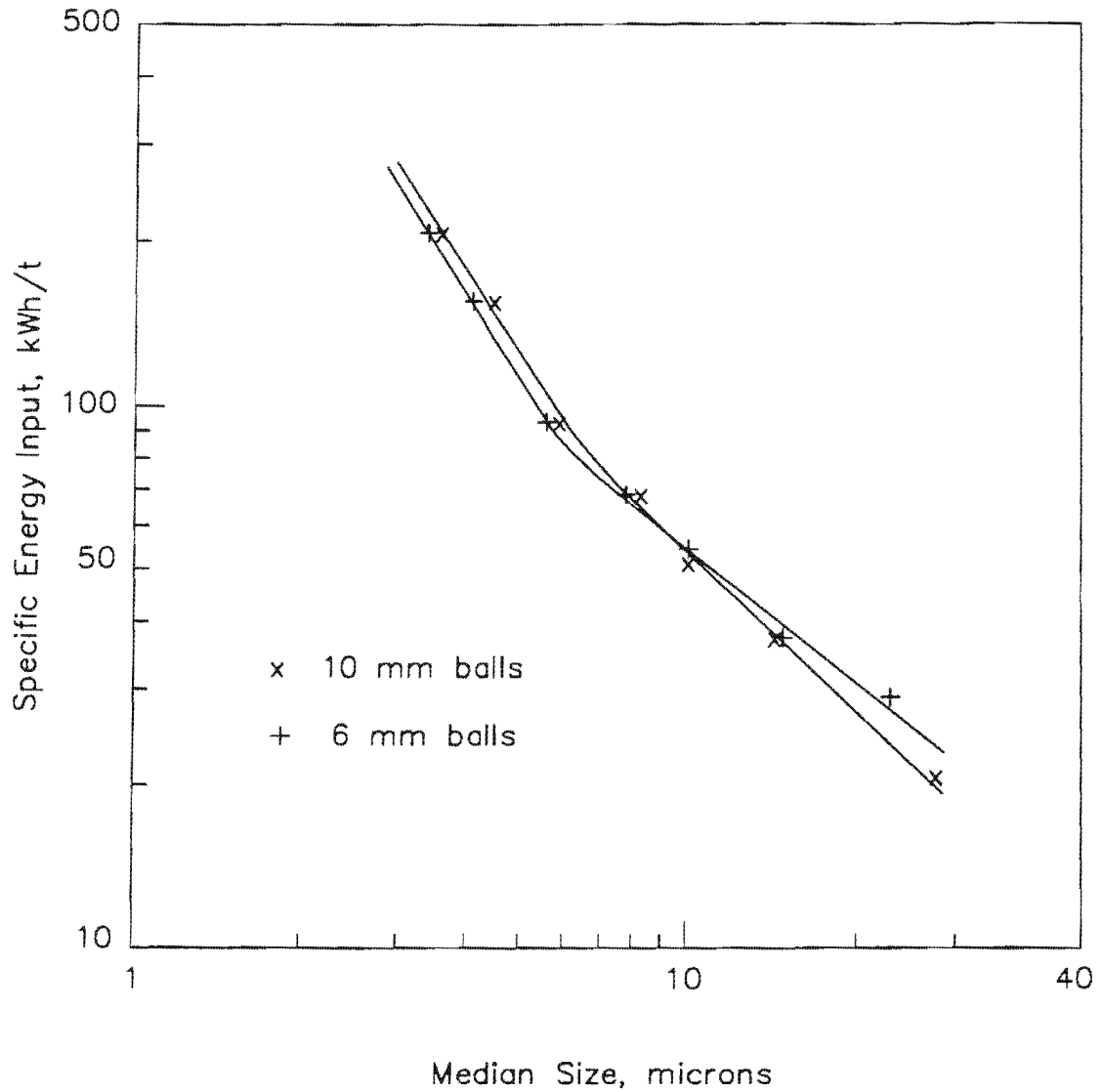


Figure 4.7. Median size of chromite ore as a function of energy input for various ball sizes at 164 r.p.m.: pulp density = 75% solids by weight, media type = steel, load depth = 32 cm, pin spacing = 8.6 cm, pin diameter = 1.6 cm (data given in Table A4.7).

β = An exponent that depends on the material and method of comminution.

k = Size modulus that is the extrapolation of the straight lines of size distribution on a Schuhmann plot to the cumulative weight fraction at 100% intercept.

If the product size modulus is taken as the d_{50} (median size), the Charles' Equation takes the form of

$$E = A(d_{median,P}^{-\beta} - d_{median,F}^{-\beta}) \quad (4.2)$$

When the product is much finer than the feed, the above equation can be simplified as

$$E = A d_{median,P}^{-\beta} \quad (4.3)$$

Experiments conducted at a shaft rotation speed of 72 r.p.m revealed the following results. With 15 mm balls, the rate of grinding was higher for a comparatively short grinding time because big balls had sufficient kinetic energy to break the largest particles in the feed sample. When the grinding time was longer, this gain was in part offset by a reduced number of balls and consequently a reduced number of contact points.

Balls of 10 mm were too small to nip the particles and break them. As the grinding proceeded, large particles were gradually broken down by the progressive breakage of corners and edges. As soon as the particles were fine enough to be broken efficiently, the 10 mm balls became more effective.

When using the 6 mm balls, the pins were not long enough to stir the grinding media completely. A visual observation of the media bed at the top showed the balls on the periphery of top layer were motionless and it could therefore be assumed that this applied to the complete vessel depth. As a result, some particles were trapped between the motionless balls and the product contained unground coarse particles.

Experimental results at an energy input level of up to 66.0 kWh/t at a shaft rotation speed of 164 r.p.m using 10 mm and 6 mm balls clearly demonstrated that the correlation was the same as that which existed between 15 mm and 10 mm at 72 r.p.m. It is clear from the results that the energy requirements for size reduction can be described by the Charles' Equation.

However, there is a deviation in the exponent of the energy-size reduction equation when different size balls and high energy input levels are used. Up to an energy input of 66.0 kWh/t, the exponent values were -1.06 and -0.83 for 15 mm and 10 mm balls at a shaft rotation speed of 72 r.p.m and -0.96 and -0.81 for 10 mm and 6 mm balls at the shaft rotation speed of 164 r.p.m respectively. The values of the exponent decreased with increased ball size. A further increase in the energy input level resulted in a decrease in the grinding rate of 10 mm and 6 mm balls and the exponents did not remain constant. Experimental results showed that the plot actually consisted of a series of straight lines joined together. The slope of the lines varied for different ranges of product size and increased as size distribution became finer. A possible reason for this might be a production of fines giving increased viscosity. The grinding rate for both sizes was virtually the same. The exponents of the straight lines were -1.62 and -1.60 for 10 mm and 6 mm balls.

These findings are in agreement with Sepulveda's conclusions. He stated that the energy-size reduction relationship was well described by a single straight line, regardless of the grinding conditions employed. However he pointed out that a decrease in the size of grinding media seemed to have a beneficial effect on the grinding efficiency. This investigation clearly demonstrated the use of the Charles' Equation as a scale-up criteria for the stirred ball mill. However, the effect of ball size and long grinding times on the value of the exponent should not be overlooked. Experiments must be made to obtain the proper value of an exponent for a desired product size range rather than extrapolating the energy versus median size plot to estimate the energy requirements.

Figure 4.8 (Table A4.8) shows the relationship between the torque and ball diameter at two different shaft rotation speeds. The torque increases with the ball diameter. The torque as a function of ball diameter could be shown by the following empirical formulas 4.4 and 4.5.

$$\text{At } 72 \text{ r.p.m} \quad T = 7.69d^{0.71} \quad (4.4)$$

$$\text{At } 164 \text{ r.p.m} \quad T = 7.13d^{0.83} \quad (4.5)$$

Where T is the torque, Nm; d is the ball diameter, mm.

The effect of ball diameter on the torque was slightly greater at 164 r.p.m than 72 r.p.m.

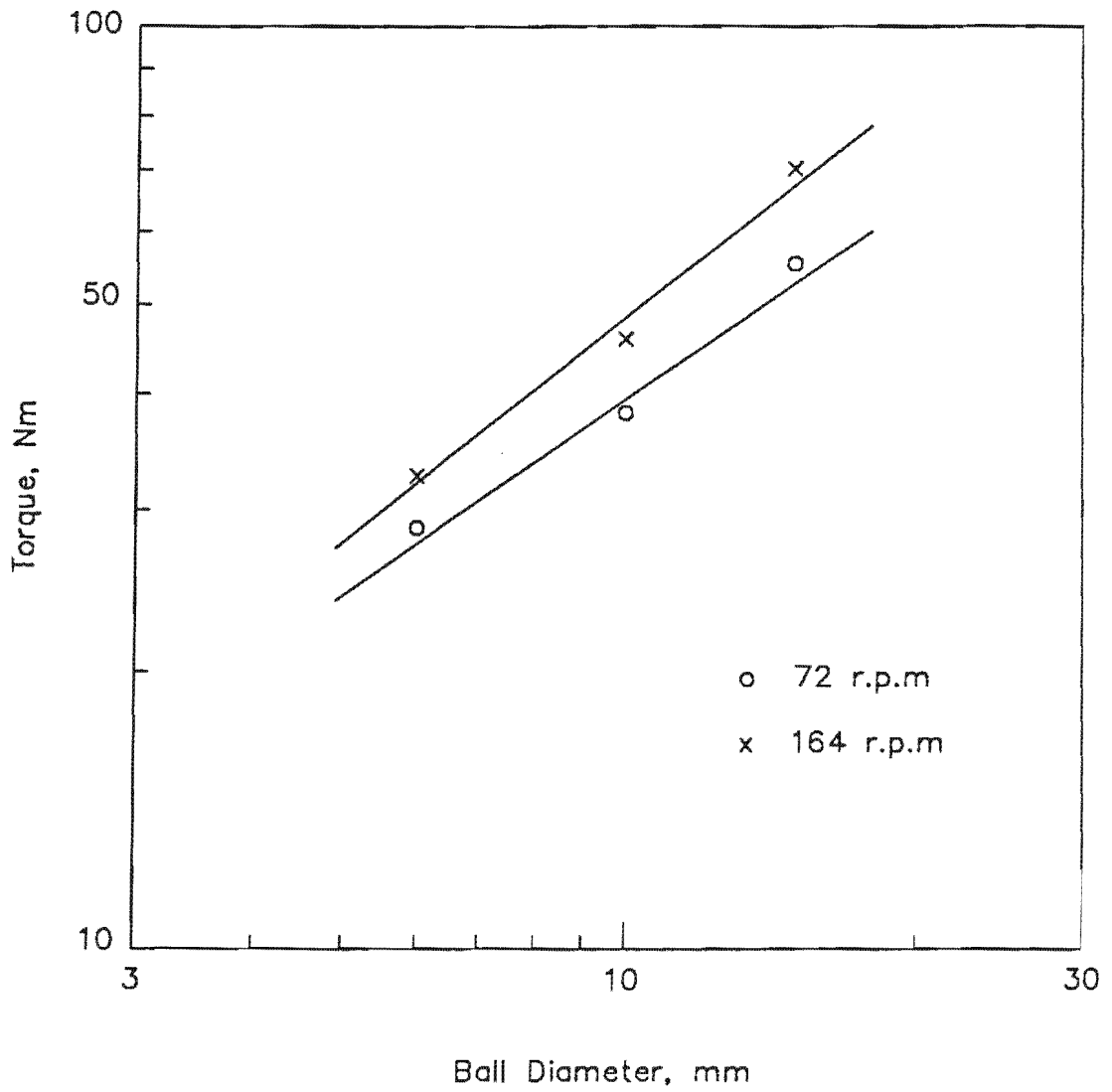


Figure 4.8. Effect of ball diameter on torque: pulp density = 75% solids by weight, media type = steel, load depth = 32 cm, pin spacing = 8.6 cm, pin diameter = 1.6 cm, energy input = 66 kWh/t (data given in Table A4.8).

Figure 4.9 and Table A4.8 show the effect of ball diameter on media wear at two different shaft rotation speeds. The ball wear per ton of ore ground and minus 10 micron material produced are both inversely proportional to the ball size. Media wear values per ton of ore ground give a steeper slope than that of per ton minus 10 micron material produced. It can be concluded that, although an improved grinding efficiency at a high levels of energy input is attained when small diameter balls are used, this improvement is obtained only at the expense of increased ball wear.

4.3. GRINDING MEDIA DENSITY

Several tests were performed to determine the effect of grinding media density on the median size and torque at various feed sizes and shaft rotation speeds. The results are given in Table 4.3.

The data shows that steatite balls gave a less efficient size reduction than steel balls, particularly at a low rotation speed with a coarse feed size. This finding was in agreement with the work of M.J. Monkosa et.al. (42). Since breakage of particles is achieved by the relative motion of rotating grinding balls in the stirred ball mill, one might have expected that it would require less energy to move less dense balls in the grinding vessel without reducing the energy efficiency, that this does not hold true must be due to the fact that compressive stresses play as big a role as torsional stress, indicating that the density of balls is important in grinding in the stirred ball mill.

As shown in Table 4.3, the power consumption of the stirred ball mill increases with the density of the grinding media. Under the same grinding conditions, the ratio of torque values for steel balls (7.85 g/cm^3) to steatite balls (2.65 g/cm^3) ranged from 7.1 to 3.4 which is higher than the ball density ratio. This is caused by the pulp density and viscosity which minimises the movement of low density balls at a low shaft rotation speed.

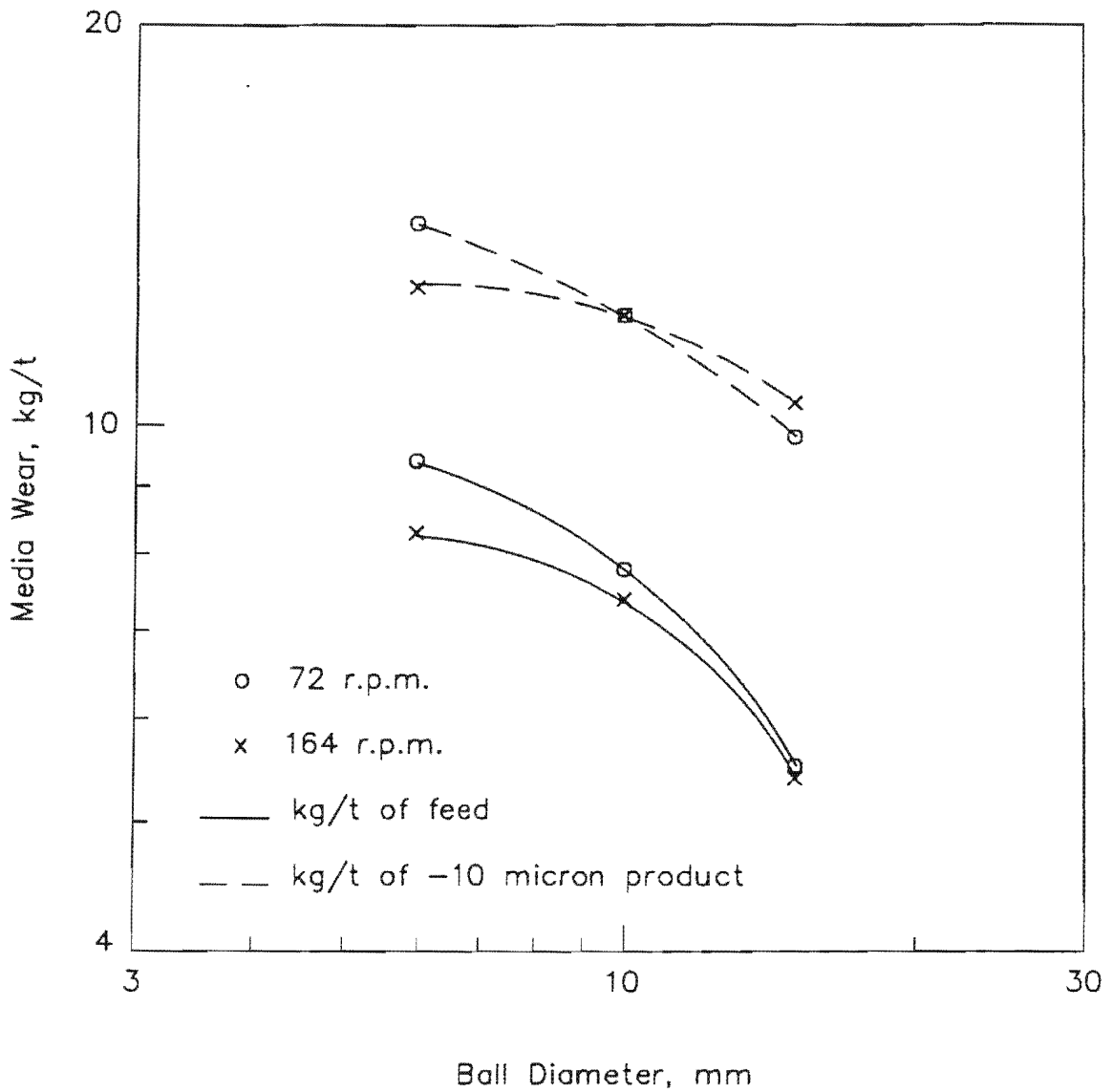


Figure 4.9. Effect of ball diameter on media wear: pulp density = 75% solids by weight, media type = steel, load depth = 32 cm, pin spacing = 8.6 cm, pin diameter = 1.6 cm, energy input = 66 kWh/t (data given in Table A4.8).

Table 4.3. Effect of grinding media density on median size and torque at various feed sizes and shaft rotation speeds: pulp density = 75% solids by weight, ball size = 6 mm, load depth = 32 cm, pin spacing = 8.6 cm, pin diameter = 1.6 cm.

Energy Input kWh/t	Ball density g/cm ³	Grinding time minutes	Shaft rotation speed r.p.m.	Median size, mic.		Torque Nm
				Feed	Product	
66.0	7.85	79.6	164	370.0	7.8	33.0
		25.5	400	370.0	7.8	49.3
	200.1	164	370.0	107.6	7.4	
			90.2	400	370.0	9.1
36.0	7.85	45.3	164	9.3	5.5	32.1
	2.65	336.8	164	9.3	6.3	4.5
		-	300	-	-	10.2
		44.5	400	9.3	6.0	16.3

A comparison between steel balls and steatite balls favours steel balls, since their greater density produces a higher grinding efficiency and capacity for a given mill size than steatite balls. However, where iron contamination in the ground ore is objectionable, steatite balls or a different type of grinding media can still be used in preference to steel balls.

4.4. LOAD DEPTH

An experimental study on the effect of the stirred ball mill load depth was carried out. The mill was charged with 30, 50 and 70 kg steel balls which corresponded to load depths of 13.7, 22.9 and 32.0 cm respectively.

¹ The shaft rotation speed of 164 r.p.m. was not high enough to give sufficient kinetic energy to the steatite balls. As a result of this, the product size was coarse.

Size analyses of the ground products produced using various heights of ball load showed that for the same energy input, the median size remained the same with 15 mm steel balls at 72 r.p.m and increased slightly (0.1 microns increments) with increasing load depth with 6 mm steel balls at 164 r.p.m. (Figure 4.10 and Table A4.9), it was thus evident that the median size was not dependent on the load depth over the range of mill load depths investigated.

The relationship between power consumption and load depth was also determined. The torque versus load depth is plotted in Figure 4.11. The load depth had a pronounced effect on the power draft and the rate of energy input to the mill increased with the load depth. Torque is related to load depth by the following empirical functions 4.6 and 4.7.

$$T = 0.20H^{1.61} \quad (4.6)$$

For ball size: 15 mm; shaft rotation speed: 72 r.p.m

$$T = 0.19H^{1.49} \quad (4.7)$$

For ball size: 6 mm; shaft rotation speed: 164 r.p.m.

where T is the torque in Newton-meter and H is the load depth in cm.

The results of the media wear tests shown in Figure 4.12 demonstrated that the media wear per ton feed and per ton minus 10 micron material produced decreases with increasing load depth. A possible explanation of this relationship might be the shorter grinding time required to obtain the same energy input level as the load depth increases. This would apply to any contributory factor such as chemical corrosion, that was dependent on the time rather than energy input.

These results suggest that larger (taller) stirred mills give not only an increased grinding capacity per unit volume but also lower media wear.

4.5. SHAFT ROTATION SPEED

Figure 4.13 and Table A4.10 show the influence of shaft rotation speed on particle size. The shaft speed ranged from 50 to 400 r.p.m. depending on the ball diameter and density.

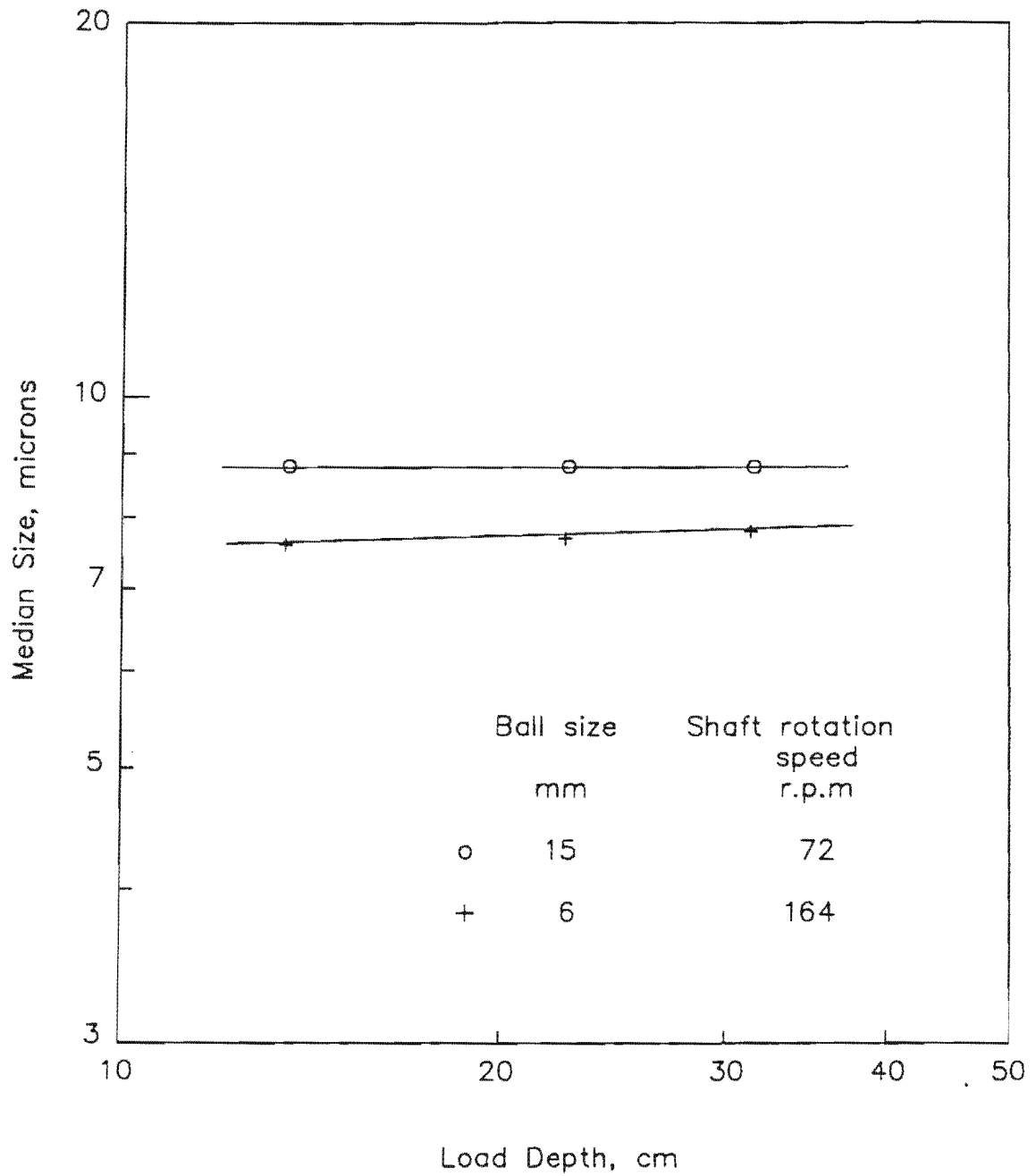


Figure 4.10. Effect of load depth on median size: pulp density = 75% solids by weight, media type = steel, pin spacing = 8.6 cm, pin diameter = 1.6 cm, energy input = 66 kWh/t (data given in Table A4.9).

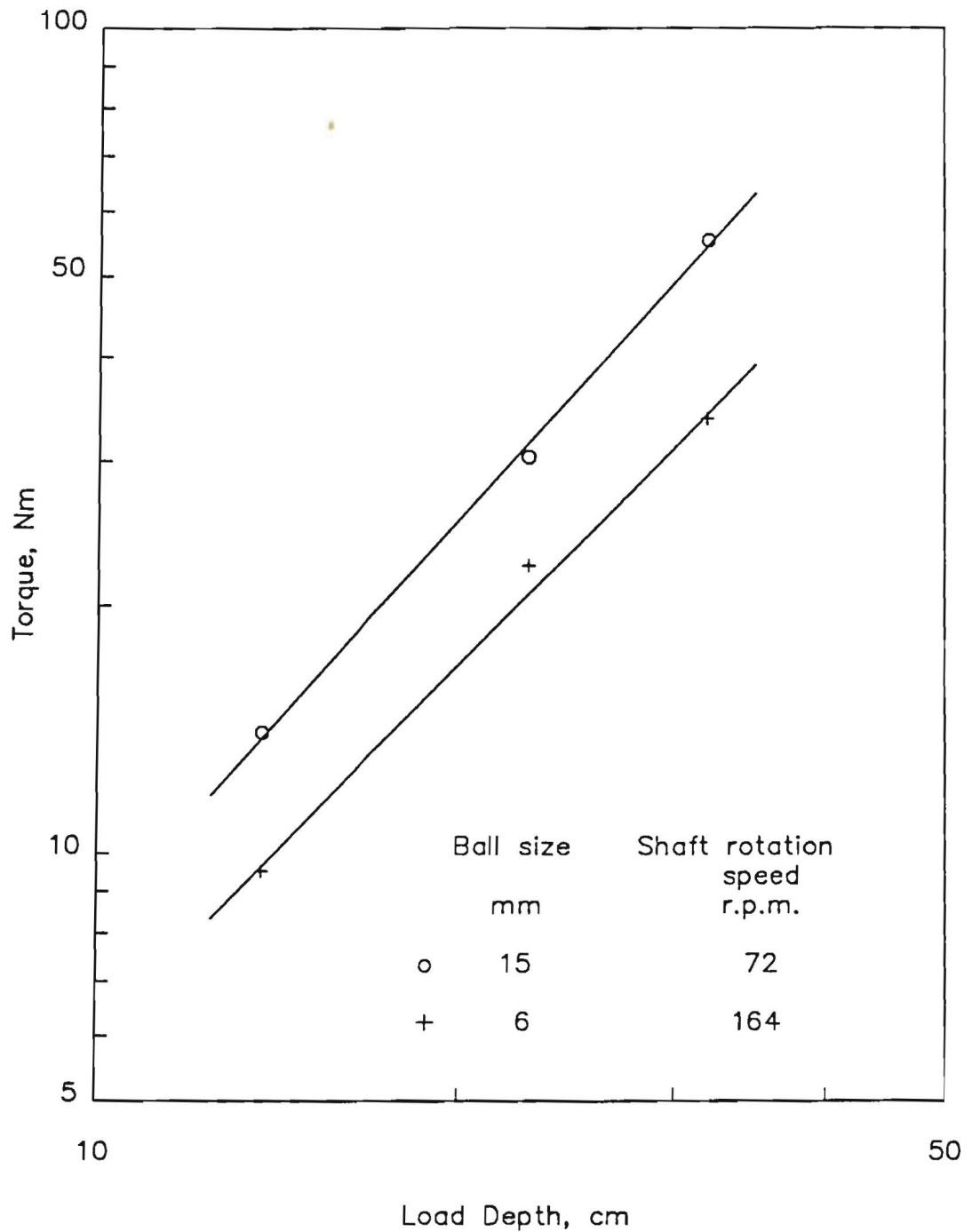


Figure 4.11. Torque as a function of load depth: pulp density = 75% solids by weight, media type = steel, pin spacing = 8.6 cm, pin diameter = 1.6 cm, energy input = 66 kWh/t (data given in Table A4.9).

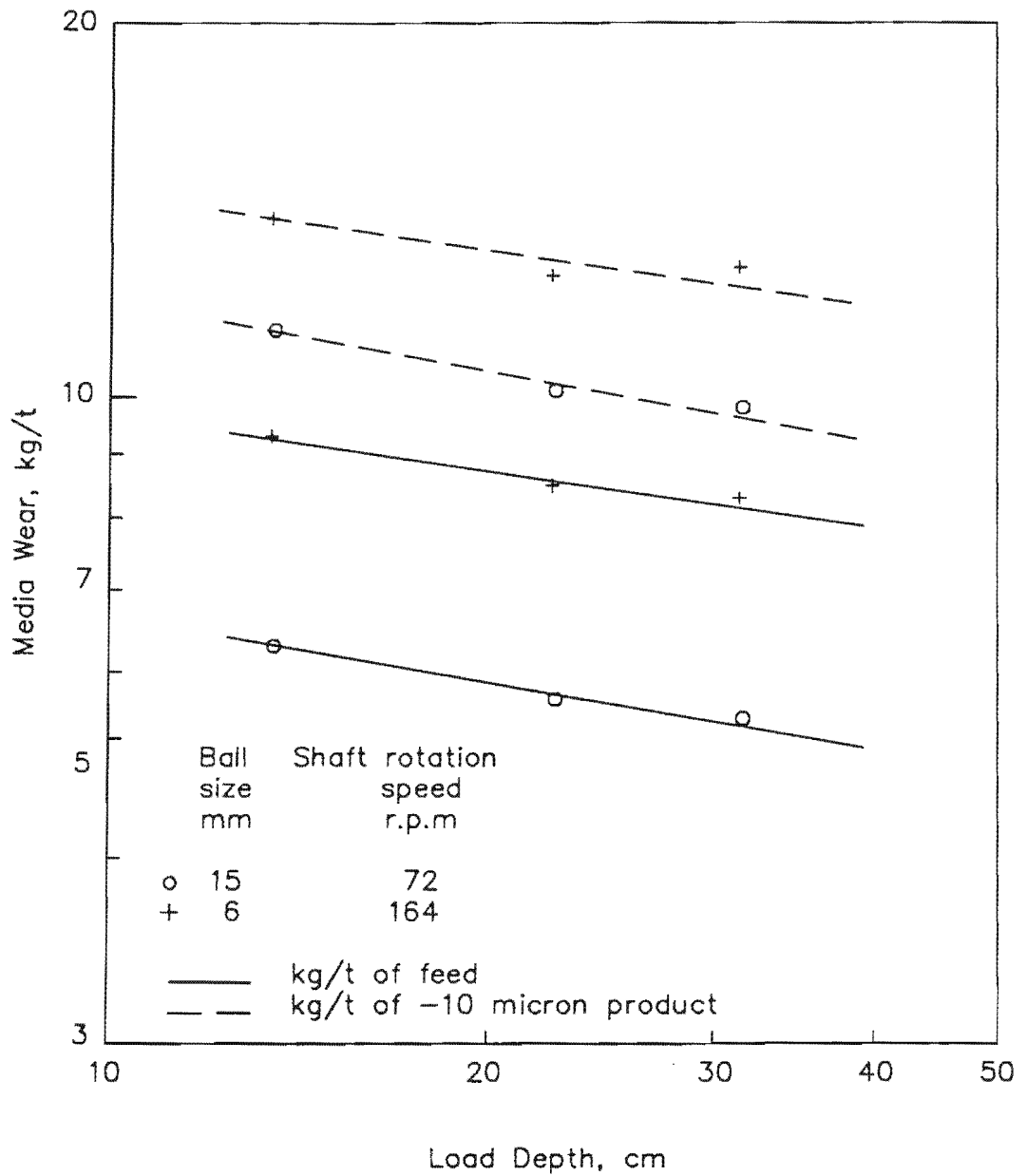


Figure 4.12. Effect of load depth on media wear: pulp density = 75% solids by weight, media type = steel, pin spacing = 8.6 cm, pin diameter = 1.6 cm, energy input = 66 kWh/t (data given in Table A4.9).

Using 15 and 10 mm steel balls, the greatest size reduction was obtained with lower shaft rotation speeds. The median size of the product increased with increasing shaft speeds. Above 164 and 300 r.p.m for 15 and 10 mm steel balls respectively, the movements of the balls in the grinding vessel were not smooth. This caused the vessel to jerk and as a result of this the torque reading fluctuated erratically. The experiments at high speed were therefore abandoned. When 6 mm steel balls were used, the median size of the products was the same at shaft speeds of between 164 and 400 r.p.m. At 72 r.p.m. the product contained coarse particles. The pins did not impart enough kinetic energy to the 6 mm balls to achieve particle breakage.

At 164 r.p.m the grinding efficiency of the steatite balls was too low. As the shaft speed increased, the median size of the product decreased and a higher percentage of fines was produced.

The results showed that there was a minimum shaft rotation speed limit for each ball size and density. Below this limit the product contained unground coarse particles. This was more evident at 72 r.p.m and 164 r.p.m with 6 mm steel and steatite balls respectively. The grinding media should have enough kinetic energy exerted by the pins to break the particles efficiently. This can be obtained by an increase in shaft rotation speed.

However, there is a limiting speed depending on the ball size, above which the grinding efficiency drops due to the vessel wall effect which gives violent shaft torque fluctuations. In addition to this, the effective energy transfer is curtailed at high shaft rotation speeds because of high centrifugal limitations such as grinding media rejection and vortex development.

The stirred ball mill should therefore be run at the highest possible pin speed providing minimum energy consumption and media wear for the required product size. The energy input per unit volume of the mill increases with increasing shaft speeds, therefore a high pin velocity should substantially decrease milling time requirements. This results in a higher mill capacity or a smaller mill size being needed for the same capacity, i.e., capital cost.

To investigate the effect of shaft rotation speed on the power draft of the mill, a set of tests was run under the grinding conditions in which the torque was measured for a range of speeds with varying ball sizes and densities. Test results presented in Figure 4.14 show that the torque at low speeds is dependent on the

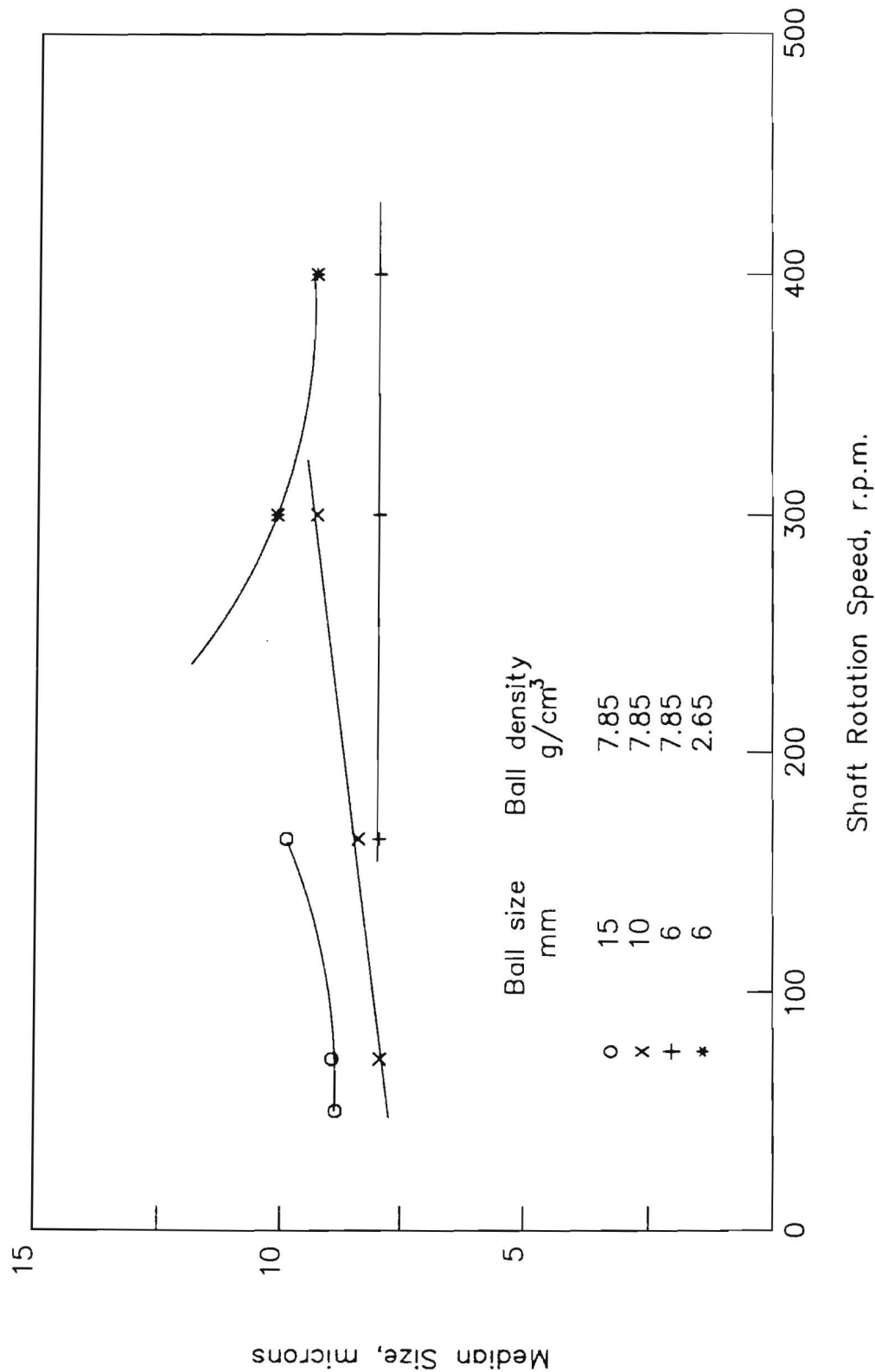


Figure 4.13. Effect of shaft rotation speed on median size using grinding media of varying sizes and densities: pulp density = 75% solids by weight, load depth = 32 cm, pin spacing = 8.6 cm, pin diameter = 1.6 cm, energy input = 66 kWh/t (data given in Table A4.10).

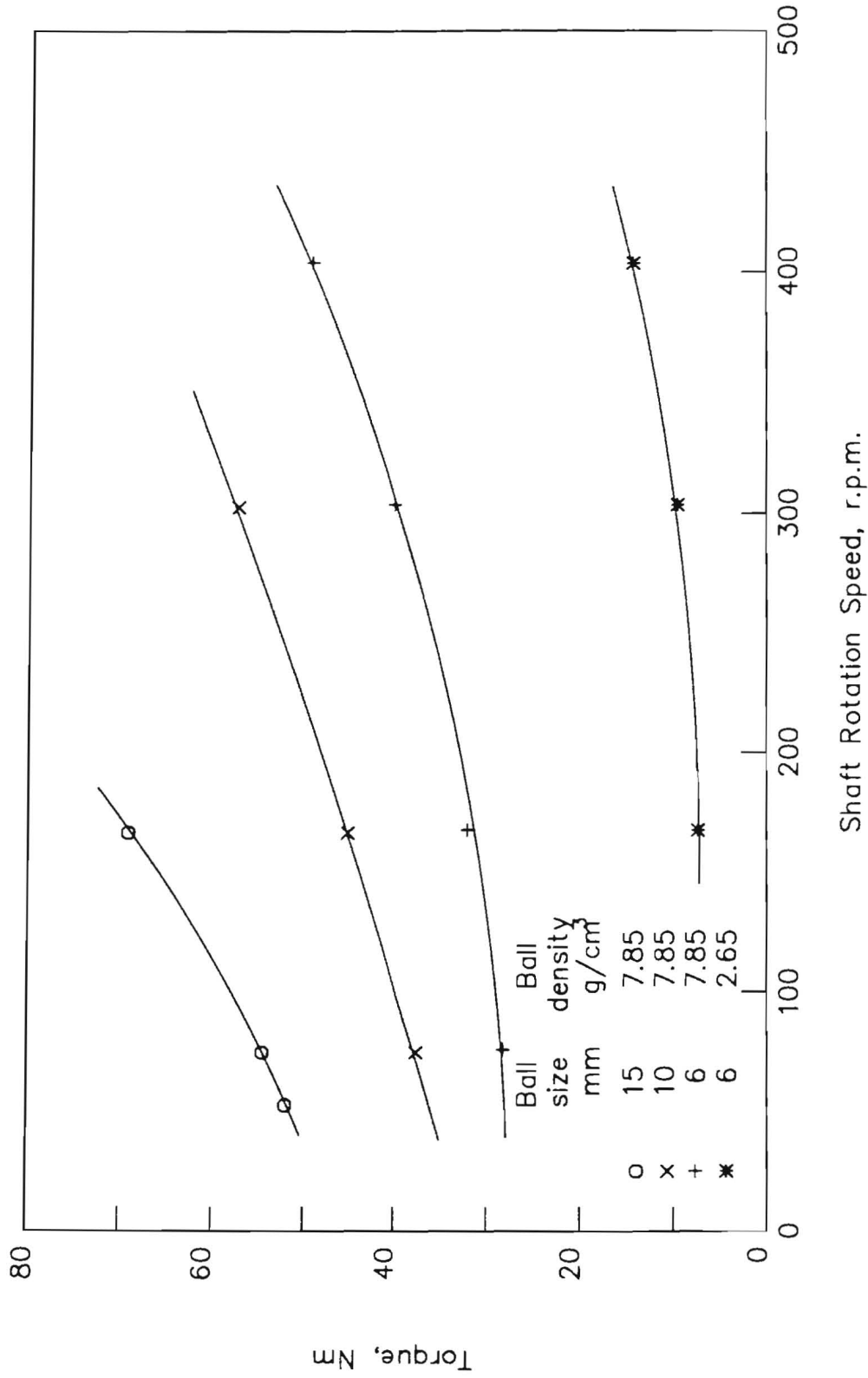


Figure 4.14. Effect of shaft rotation speed on torque using grinding media of varying sizes and densities: pulp density = 75% solids by weight, load depth = 32 cm, pin spacing = 8.6 cm, pin diameter = 1.6 cm, energy input = 66 kWh/t (data given in Table A4.10).

ball diameter and density. The greater the ball diameter and density, the higher the torque. This must be due to an increase in friction forces between the balls as a function of ball size and mass.

The torque then increases with stirring speed and a linear least squares fit to data gives the following equations for the various ball sizes and densities.

$$T = 48.0 + 0.016N^{1.40} \quad (4.8)$$

For ball size: 15 mm; Ball density: 7.85 g/cm³

$$T = 35.0 + 0.004N^{1.52} \quad (4.9)$$

For ball size: 10 mm; Ball density: 7.85 g/cm³

$$T = 27.0 + 8.8 \cdot 10^{-4}N^{1.69} \quad (4.10)$$

For ball size: 6 mm; Ball density: 7.85 g/cm³

$$T = 6.0 + 6.6 \cdot 10^{-5}N^{1.94} \quad (4.11)$$

For ball size: 6 mm; Ball density: 2.65 g/cm³

where T is torque in Newton-meter and N is shaft rotation speed r.p.m.

It can be concluded that the effect of the shaft rotation speed on the power consumption is complex and cannot be explained in terms of a simple model. However an attempt was made to determine the scale-up relationship and the power requirements of the stirred ball mill in Chapter 9.

The effect of shaft rotation speed on media wear is shown in Figure 4.15. The rotation speed versus media wear per ton of ore ground curves, clearly show the same trend for all ball sizes. The media wear dropped rapidly when the shaft rotation speed was increased to 72 r.p.m with 15 mm balls and 164 r.p.m with 6 mm and 10 mm balls, then remained virtually the same with a further increase in the speed. An increase in the shaft rotation speed giving the same energy input has little effect on the grinding media wear. This may be attributed to the shorter grinding time which compensates for the media wear which might be increased by the larger number of contact points per unit time at a higher shaft rotation speed. It was also found that at a low shaft rotation speed the media wear per ton of minus 10 micron material produced, with the exception of 10 mm balls,

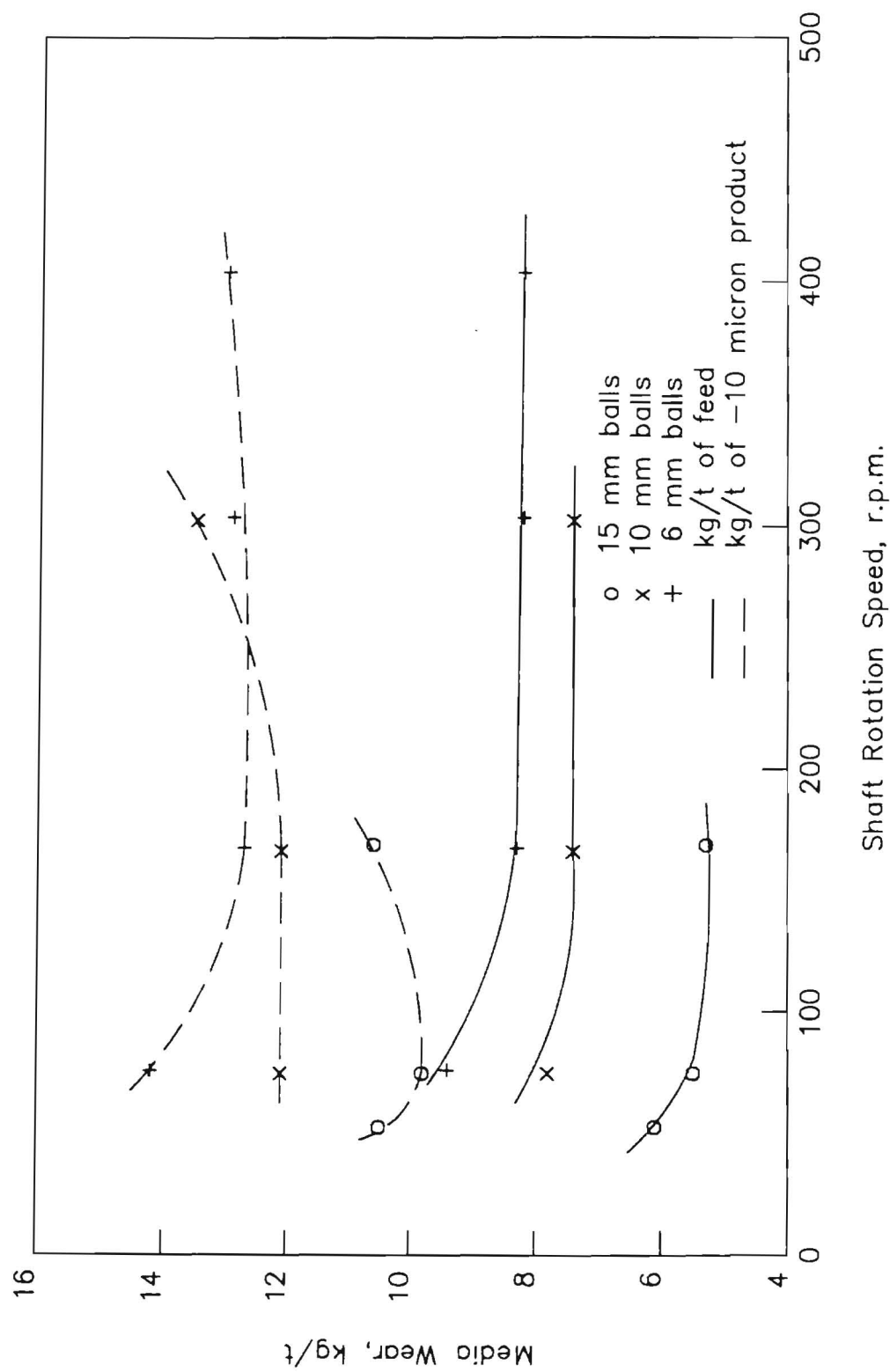


Figure 4.15. Effect of shaft rotation speed on media wear using grinding media of varying sizes: pulp density = 75% solids by weight, load depth = 32 cm, pin spacing = 8.6 cm, pin diameter = 1.6 cm, energy input = 66 kWh/t (data given in Table A4.10).

was high for both 15 mm and 6 mm balls. After a minimum value, the media wear increased with increasing shaft speed for all the ball sizes employed, since the production of minus 10 micron material decreased as the shaft speed increased.

4.6. PIN SPACING AND DIAMETER

The shaft of the stirred ball mill was designed to allow for changes to be made in pin spacing and pin diameters.

A series of tests was made to determine the effect of changing the distance between two pins on the median size using 10 mm and 6 mm grinding media (Figure 4.16 and Table A4.11). The results were obtained with pin spacing between 3.6 cm and 20.8 mm. The data in general reveals that the smallest median size achieved and the most efficient energy utilization occurred when the pins were closely spaced and the least efficient grinding with regard to particle size reduction and energy consumption was observed when the mill operated with the pins widely spaced.

Figure 4.17 shows the effect on the torque of changing the spacing between the pins. The torque increased with decreasing pin spacing for 10 mm and 6 mm steel balls, thus, grinding with a smaller pin spacing resulted in an increase in the energy input per unit volume of the mill. The torque as a function of pin spacing can be fitted by the empirical functions 4.12 and 4.13.

$$T = 114.6s^{-0.44} \quad \text{for ball size: 10 mm} \quad (4.12)$$

$$T = 91.7s^{-0.44} \quad \text{for ball size: 6 mm} \quad (4.13)$$

where T is torque in Newton-meter and s is pin spacing in cm.

The study of the effect of pin spacing on media wear demonstrated that media wear decreased progressively when the pin spacing was changed from 3.6 cm to 20.8 cm (Figure 4.18). On the other hand, with respect to a media weight loss per ton of minus 10 micron material produced, the media wear decreased slightly by increasing the pin spacing when 6 mm balls were used whereas the media wear was virtually the same with 10 mm grinding media.

A series of grinding tests were carried out to establish the relationship between the pin diameter and median size, torque and media wear. The results were shown in Table 4.4.

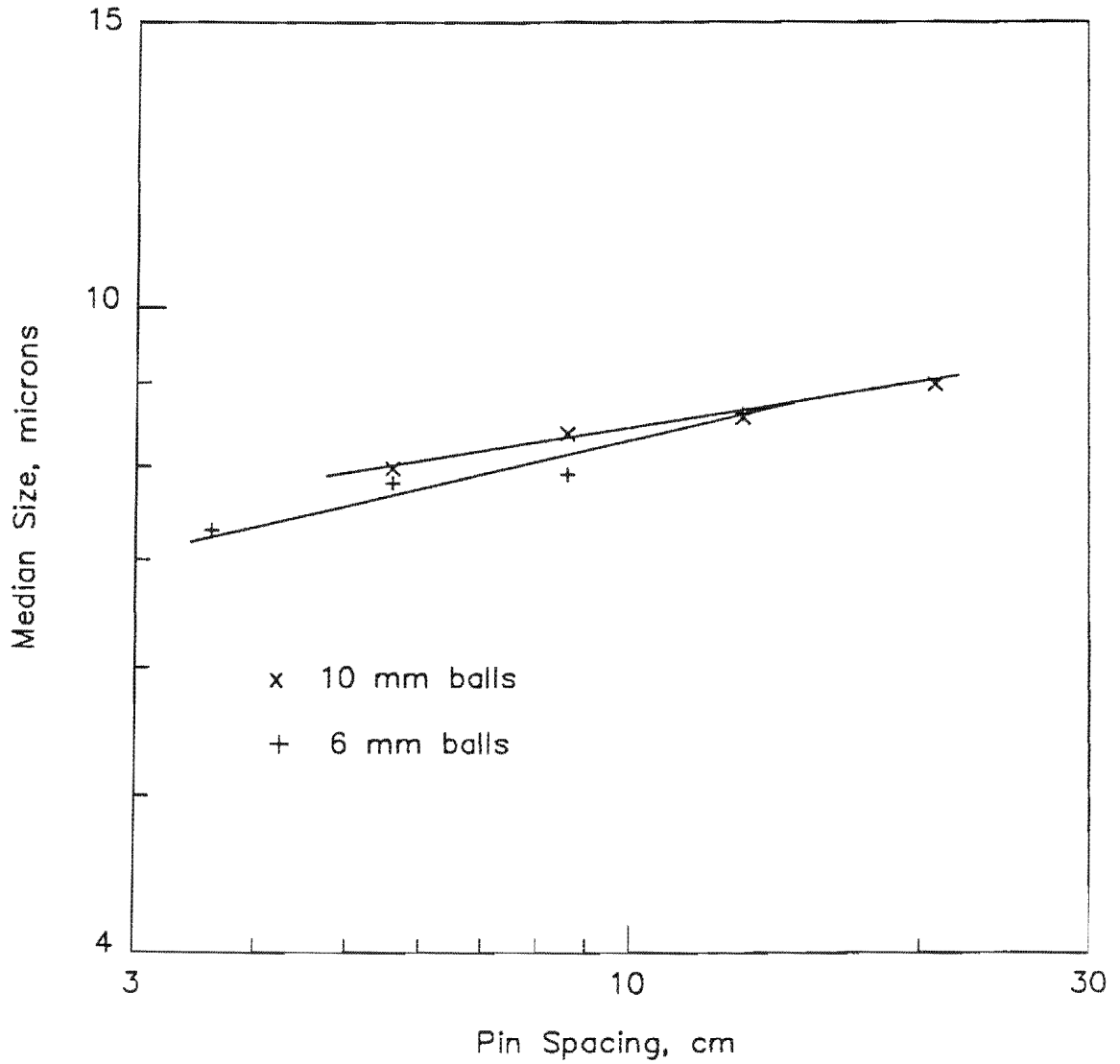


Figure 4.16. Effect of pin spacing on median size: pulp density = 75% solids by weight, media type = steel, load depth = 32 cm, shaft speed = 164 r.p.m., pin diameter = 1.6 cm, energy input = 66 kWh/t (data given in Table A4.11).

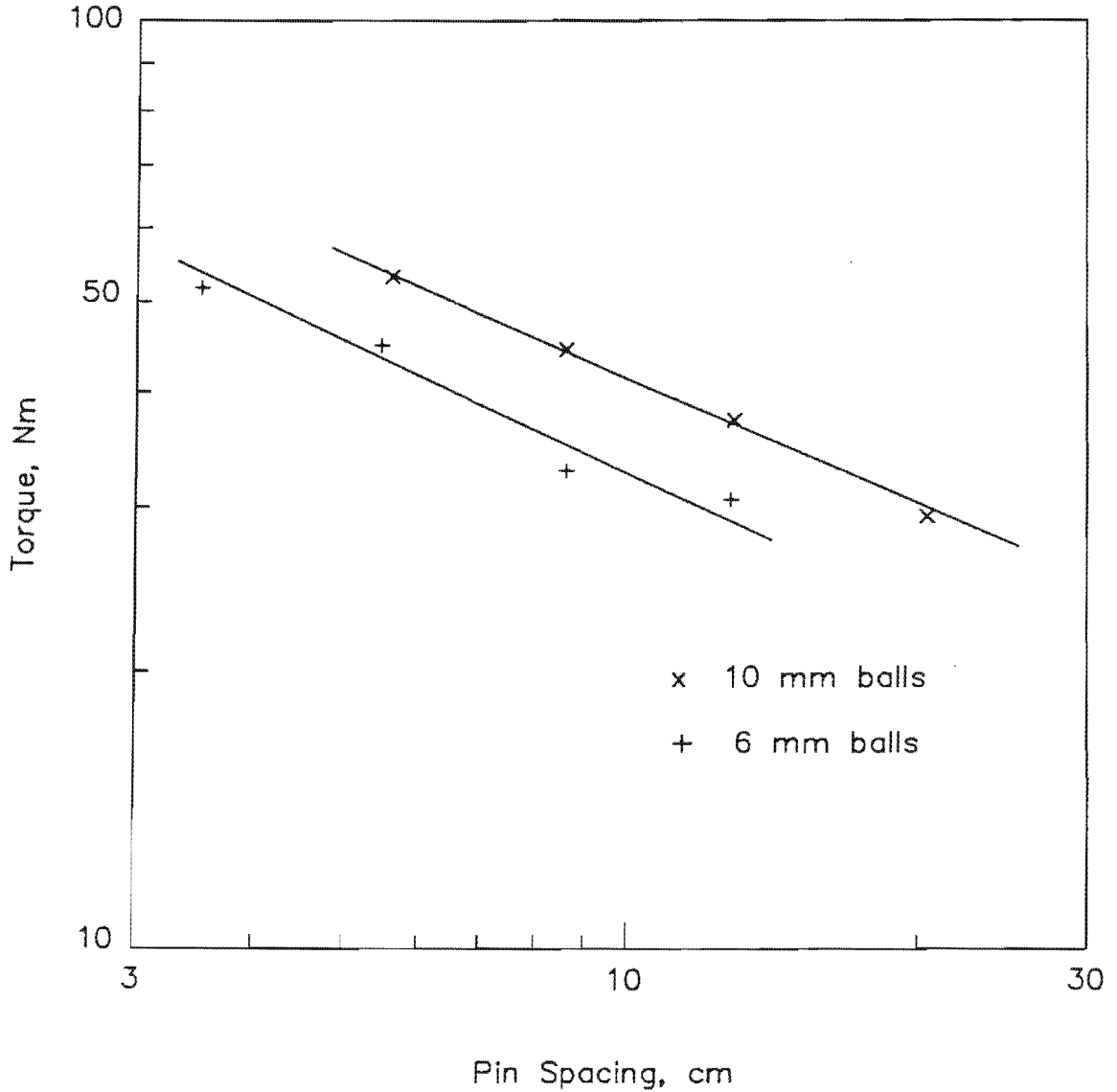


Figure 4.17. Effect of pin spacing on torque: pulp density = 75% solids by weight, media type = steel, load depth = 32 cm, shaft speed = 164 r.p.m., pin diameter = 1.6 cm, energy input = 66 kWh/t (data given in Table A4.11).

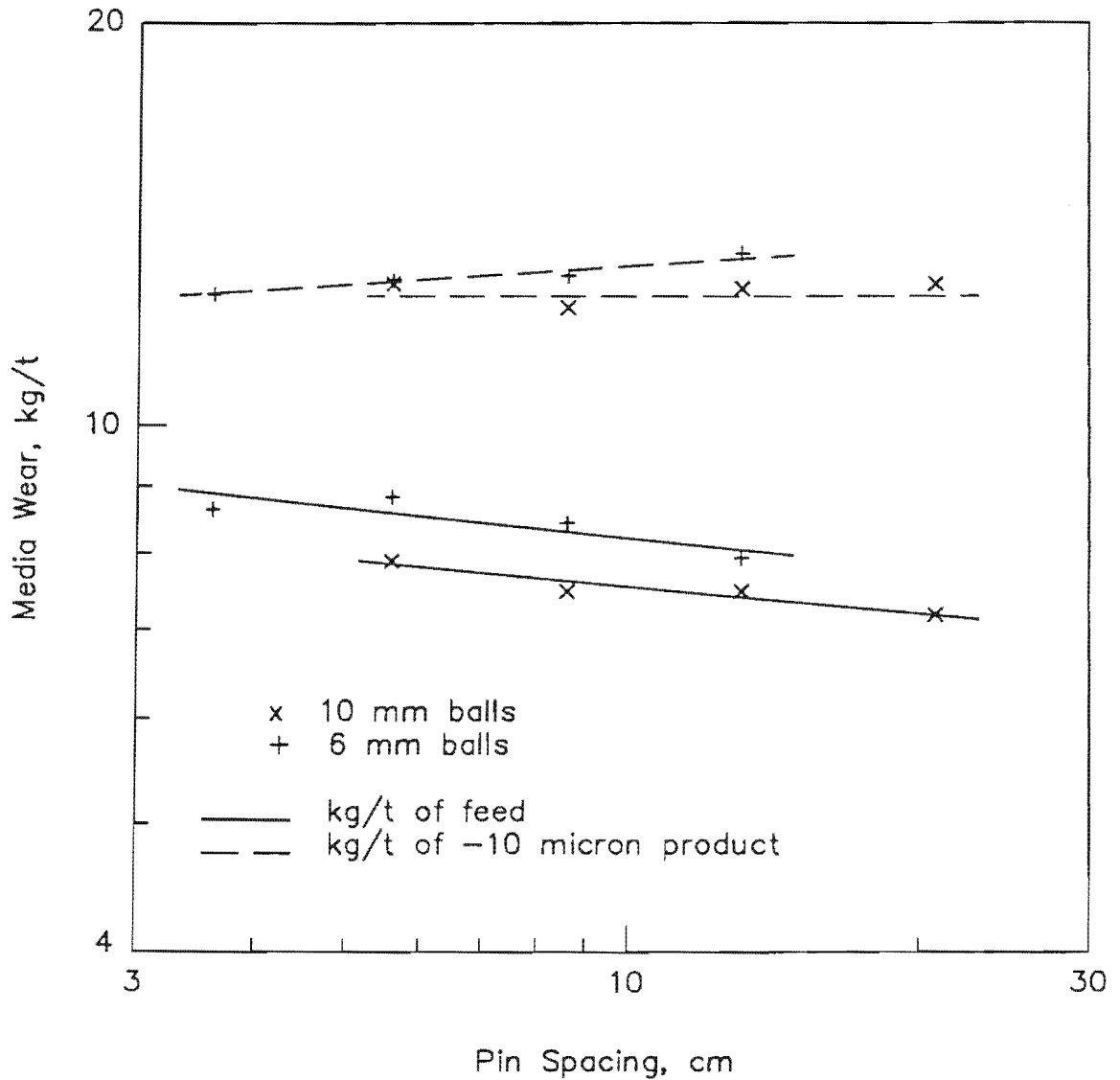


Figure 4.18. Effect of pin spacing on media wear: pulp density = 75% solids by weight, media type = steel, load depth = 32 cm, shaft speed = 164 r.p.m., pin diameter = 1.6 cm, energy input = 66 kWh/t (data given in Table A4.11).

Table 4.4. Effect of pin diameter with 6 mm and 10 mm balls: pulp density = 75% solids by weight, media type = steel, load depth = 32 cm, shaft speed = 164 r.p.m., energy input = 66 kWh/t.

Ball size mm	Pin diameter cm	Pin ² spacing cm	Median size mic.	Torque Nm	Media wear kg/t	Media wear - 10 mic.
6	1.6	8.6	7.8	32.1	8.3	12.7
6	3.2	8.6	7.2	43.5	8.7	12.8
10	1.6	8.6	8.3	45.2	7.4	12.1
10	3.2	8.6	7.9	52.7	7.9	12.3

The data demonstrated that the grinding efficiency and energy input per unit volume of the mill increased as the pins of a bigger diameter were used. The results also indicated that the least media wear occurred when using pins of a smaller diameter. However, no significant difference was evident in media wear when minus 10 micron material was produced using pins of 1.6 cm and 3.2 cm in diameter.

The results show that using a greater number of pins with a bigger diameter contributed more to the grinding efficiency and capacity of the mill than when fewer pins with a smaller diameter were used. This may be due to the fact that when more pins are used and the diameter is greater, the displacement and relative motion of the grinding media is increased.

2 The distance between the centre lines of the nearest two pins.

CHAPTER 5

COMPARISON BETWEEN STIRRED AND TUMBLING BALL MILLS

5.1. INTRODUCTION

The most widely used machine for dry and wet grinding is a tumbling mill. Some important points with regard to the limitations of the tumbling mill can be made.

Firstly, it is known that in conventional tumbling mills, the grind limit is determined by the size of the grinding medium; the smaller the medium the finer the product. There is a lower limit to the size of balls or other media because as the balls become smaller the cohesive forces between the grinding media and the mill charge become greater, until eventually the contents of the mill cease to have a relative motion.

Secondly, the grinding charge of the conventional mill only occupies at most, one half of the entire volume available.

Thirdly, the grinding capacity of the tumbling mill is also limited by a maximum rotational speed, above which centrifuging occurs.

For obvious reasons, none of these limitations applies to the vertical stirred ball mill. The use of a more efficient type of mill is required to overcome these limitations of the tumbling mill. In general terms, the resulting mill can be called a Stirred Type Vertical Ball Mill.

In order to evaluate the capabilities of the vertical stirred ball mill and to justify continuing research on stirred ball milling, a comparison between the stirred ball mill and the tumbling ball mill was made under the following optimum grinding conditions determined experimentally for each mill (Chapter 4 and Appendix 5) and given in Table 5.1.

Table 5.1. Optimum grinding conditions used in stirred and tumbling ball mills

Grinding conditions	Stirred ball mill	Tumbling ball mill
Feed size (d ₅₀), microns	370	370
Pulp density, % solids by weight	75.0	75.0
Ball density, g/cm ³	7.85	7.85
Ball diameter, mm	6.0	23.0
Ball charge, kg	70.0	42.7
Mill speed, r.p.m.	¹ 164.0	54.8
Mill length, cm	35.5	29.5
Mill diameter, cm	26	31.5
Pin length, cm	18	-
Pin spacing, cm	² 3.6	-
Pin diameter, cm	1.6	-

5.2. PRODUCT SIZE DISTRIBUTION

Figure 5.1 and Table A5.3 show a comparison between the product size distributions obtained from the stirred and tumbling ball mills at two energy levels of 28 kWh/t and 66,0 kWh/t.

The size distributions from these tests can be described by the Schuhmann Equation characterised by the distribution moduli (slopes) m . The finer portion of the size distribution in this graph fits well into the straight lines which have constant slopes of $m = 0,97$ at 28,0 kWh/t for both mills and $m = 0,80$ and $0,87$ at 66,0 kWh/t for the stirred and the tumbling ball mills respectively. The similar size distribution slope of the finer portion of the products from both mills suggests that they have the same size distribution characteristics, however as can

¹ Product median size for a given energy input remained constant at shaft rotation speeds of between 164 r.p.m. and 400 r.p.m. A shaft rotation speed of 164 r.p.m. was chosen because of convenience. The speed was only varied for some comparisons (ref. Figure 5.6).

² The distance between the centre lines of the two nearest pins.

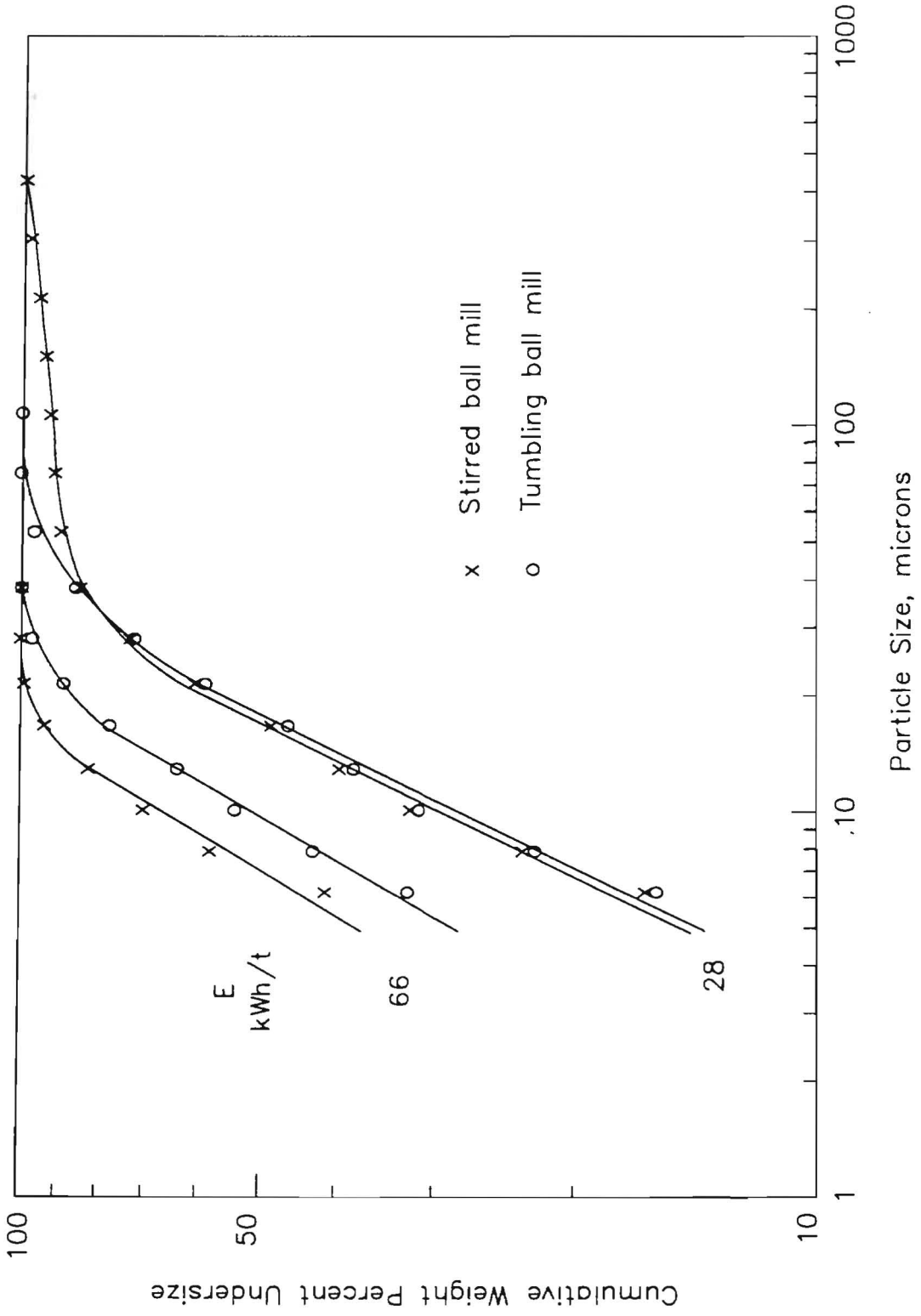


Figure 5.1. Comparison between size distribution of ground products from stirred and tumbling ball mills at two different energy input levels (experimental conditions given in Table 5.1 and data given in Table A5.3).

be seen from the graph, the stirred ball mill product has a higher percentage of coarse size fractions than that from the tumbling mill at the comparatively low energy input of 28,0 kWh/t. At an energy input level of 66,0 kWh/t, the difference in the coarse size range disappeared and the grinding efficiency of the stirred ball mill over the tumbling ball mill became obvious. The minus 10 micron fraction is 16,1% larger at an energy input level of 66,0 kWh/t, compared with 0,8% for an energy input level of 28,0 kWh/t.

5.3. ENERGY EFFICIENCIES

A comparison between the grinding efficiency of the stirred and tumbling ball mills is demonstrated in Figure 5.2 and Table A5.4. The product size of ³d50 is plotted versus specific energy input. In the tumbling ball mill, the rate of fines production is fairly constant up to a certain energy input level and then decreases slowly as grinding proceeds. In the stirred ball mill, at a low energy input, the grinding efficiency is less than in the tumbling ball mill. However at inputs of energy higher than 30 kWh/t, the median size of the product from the stirred ball mill becomes increasingly finer than that obtained from the tumbling ball mill at the same energy input level.

The energy utilisation of the stirred ball mill is clearly far superior to that of the tumbling mill when a high percentage of fine material is produced.

Figure 5.3 (Table A5.5) shows a plot of the energy reduction obtained when the stirred ball mill is used instead of the tumbling ball mill. The d50 is plotted as a function of the energy reduction percent, defined as:

$$\text{Energy reduction} = \frac{E_T - E_S}{E_T} \times 100 \quad (5.1)$$

E_T = Energy input level for tumbling ball mill for the same median size

E_S = Energy input level for stirred ball mill for the same median size

³ d50 is 50% weight passing size (median size)

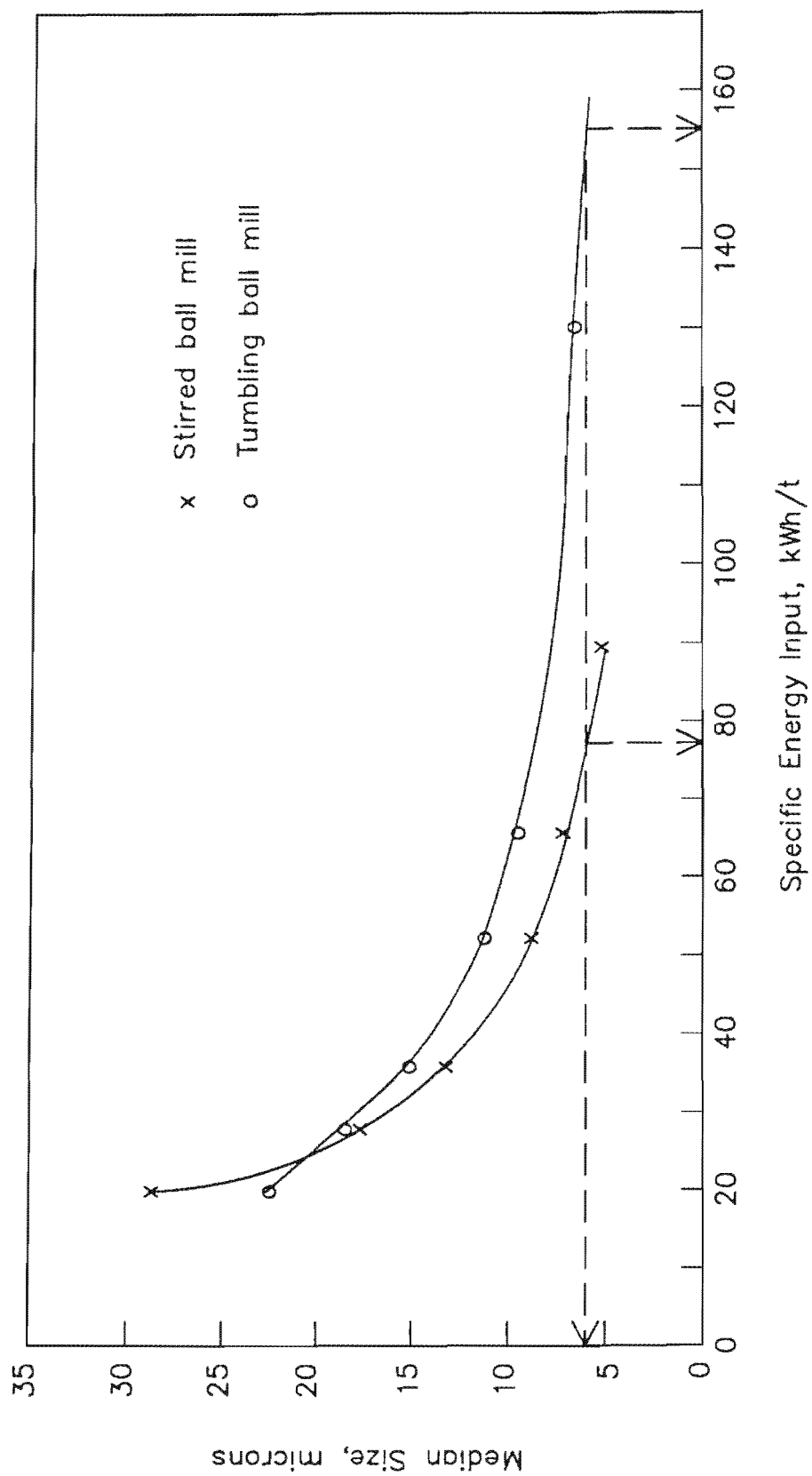


Figure 5.2. Comparison between grinding efficiency of stirred and tumbling ball mills for the median size of chromite ore (experimental conditions given in Table 5.1 and data given in Table A5.4).

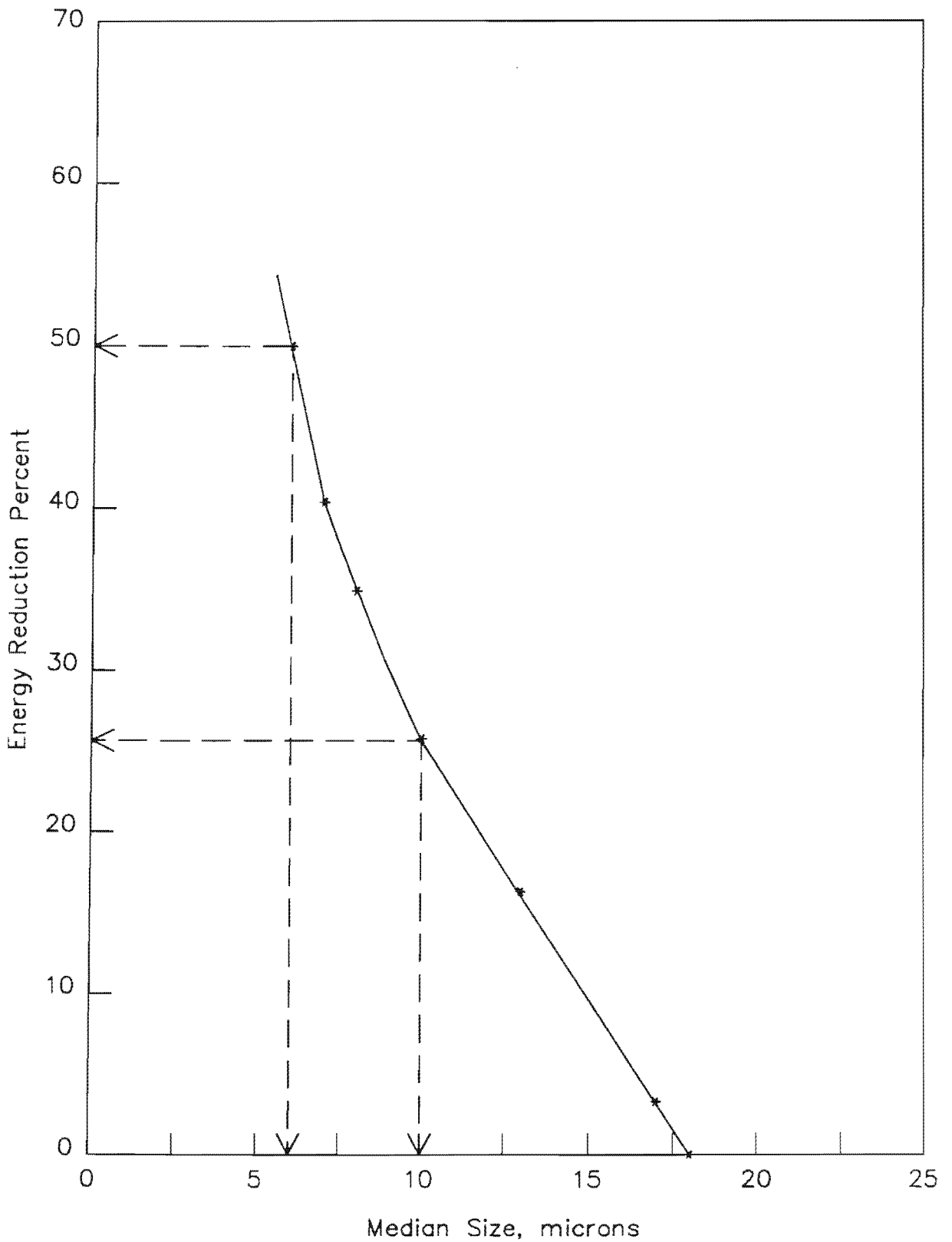


Figure 5.3. Energy reduction in percent for the median size of chromite ore when stirred ball mill is used instead of tumbling ball mill (data given in Table A5.5).

The reduction of energy increases linearly from zero for a product d50 of 18 microns to 25 percent for a d50 of 10 microns. Beyond this value, the energy reduction continues to increase but at a slower rate. At a median size of 6 microns, the energy input can be reduced by 50% when the stirred mill is used instead of the tumbling mill.

These results are in line with the findings of Stehr, N., et.al. (47). When grinding coal samples, they found that the use of the stirred ball mill could reduce energy input by up to 60% at grinds of 98% passing 45 microns.

The grinding performances of the stirred and tumbling mills can be characterised and compared by an empirical relationship in the form of the Charles' Equation. In Figure 5.4 (Table A5.4), the median size of the milled chromite ore is plotted on log-log paper as a function of energy input. The log E versus log d50 relationship results in a straight line for both the stirred and tumbling ball mills. However, for an energy input level of below 28.0 kWh/t, there is a slight deviation from the straight line for the stirred ball mill. This is due to the presence of particles too large to be broken by the grinding media in the mill.

The equations of the energy - size reduction relationships for the stirred ball mill (energy input levels of between 28.0 kWh/t and 90.0 kWh/t) and the tumbling ball mill are:

$$E_{SBM} = 433.5 d_{50}^{-0.96} \quad \text{Corr. coef. } -0.999 \quad (5.2)$$

$$E_{TBM} = 1963.4 d_{50}^{-1.47} \quad \text{Corr. coef. } -0.996 \quad (5.3)$$

The fact that all data is well described by the straight line makes it possible to predict the median size of the product within the energy input levels studied. These two energy - median size plots have an intersection at 18.0 microns particle size. This could be interpreted that when the median size product is finer than 18 microns, the stirred ball mill consumes less energy than the tumbling ball mill. However, the stirred ball mill used more energy than the tumbling mill on grinds having a median size coarser than 18.0 microns. The high energy consumption above 18.0 microns was partly due to the fact that the stirred ball mill was not operating at maximum efficiency in that region. It can be improved to a certain extent by changing grinding conditions such as using larger balls.

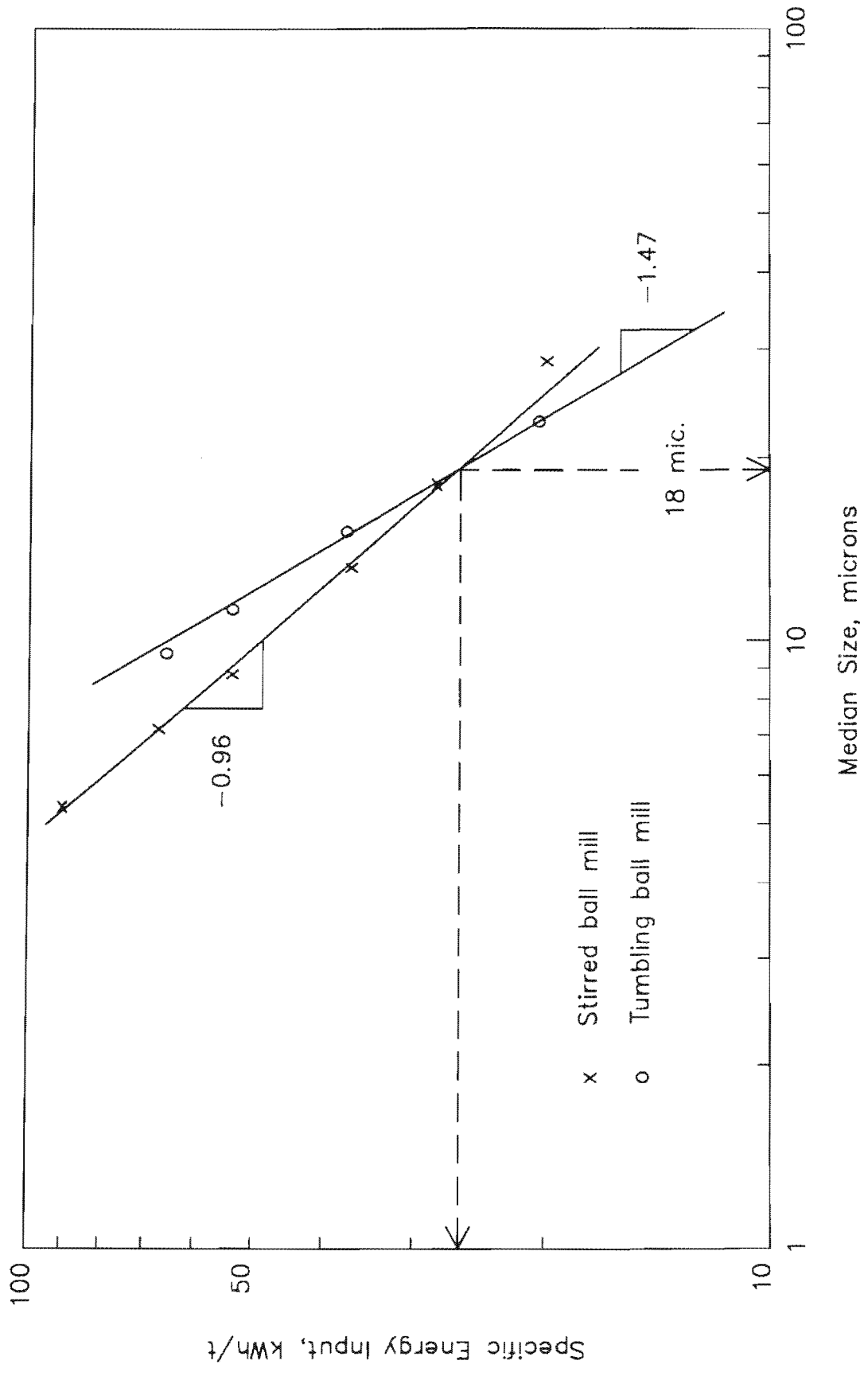


Figure 5.4. Median size of chromite ore as a function of grinding energy input for stirred and tumbling ball mills (experimental conditions given in Table 5.1 and data given in Table A5.4).

5.4. VARIATION IN MILL TORQUE

The variation in the torque for the stirred ball mill and the tumbling ball mill as a function of specific energy input is shown in Figure 5.5 and Table A5.4. The effect of feed size (-600+100 microns) on the torque for the tumbling mill was not significant and it was approximately constant at 23 Nm. For the stirred ball mill, the initial torque was high, due to the friction between feed particles and the grinding balls. The high torque represented an inefficient use of energy in that the ball to particle ratio was too small for the optimal breakage and thus decreased the grinding efficiency of the stirred ball mill. As the grinding proceeded, the torque decreased gradually until the particles were ground to a fine size range (below median size of 20 microns), reaching a constant value of 54Nm after an energy input of about 30 kWh/t. The constant torque region corresponds to the straight line portion of the Charles' Equation.

5.5. POWER DENSITY

The term power density is defined as "the rate of energy input per ton of grinding media". The power density as a function of mill speed for both mills is shown in Figure 5.6 and Table A5.6. In the tumbling ball mill, the maximum mill speed was limited by the critical speed, above which centrifuging occurred. The tumbling mill speed is usually expressed as a percentage of the critical speed with a range from 60 to 90% of critical being used in practice. The power density is directly proportional to the tumbling ball mill speed. In the stirred ball mill, power density increases with rotation speed at an exponent value of approximately 1.30.

During the experiments in the tumbling ball mill the maximum energy input per ton of grinding media was found to be 4.1 kW which is 10 times less than in the stirred ball mill. Consequently, the volume is 10 times smaller and it is therefore possible to obtain a very high product output from a small mill when the stirred ball mill is employed.

The exponent of the power density versus mill speed relationship in the stirred ball mill is slightly higher than in the tumbling ball mill and also during the experiments, the maximum power density in the stirred ball mill was found to be 40 kW/t. However, the exponent of the power density versus mill speed relationship and the maximum power density can be increased considerably by

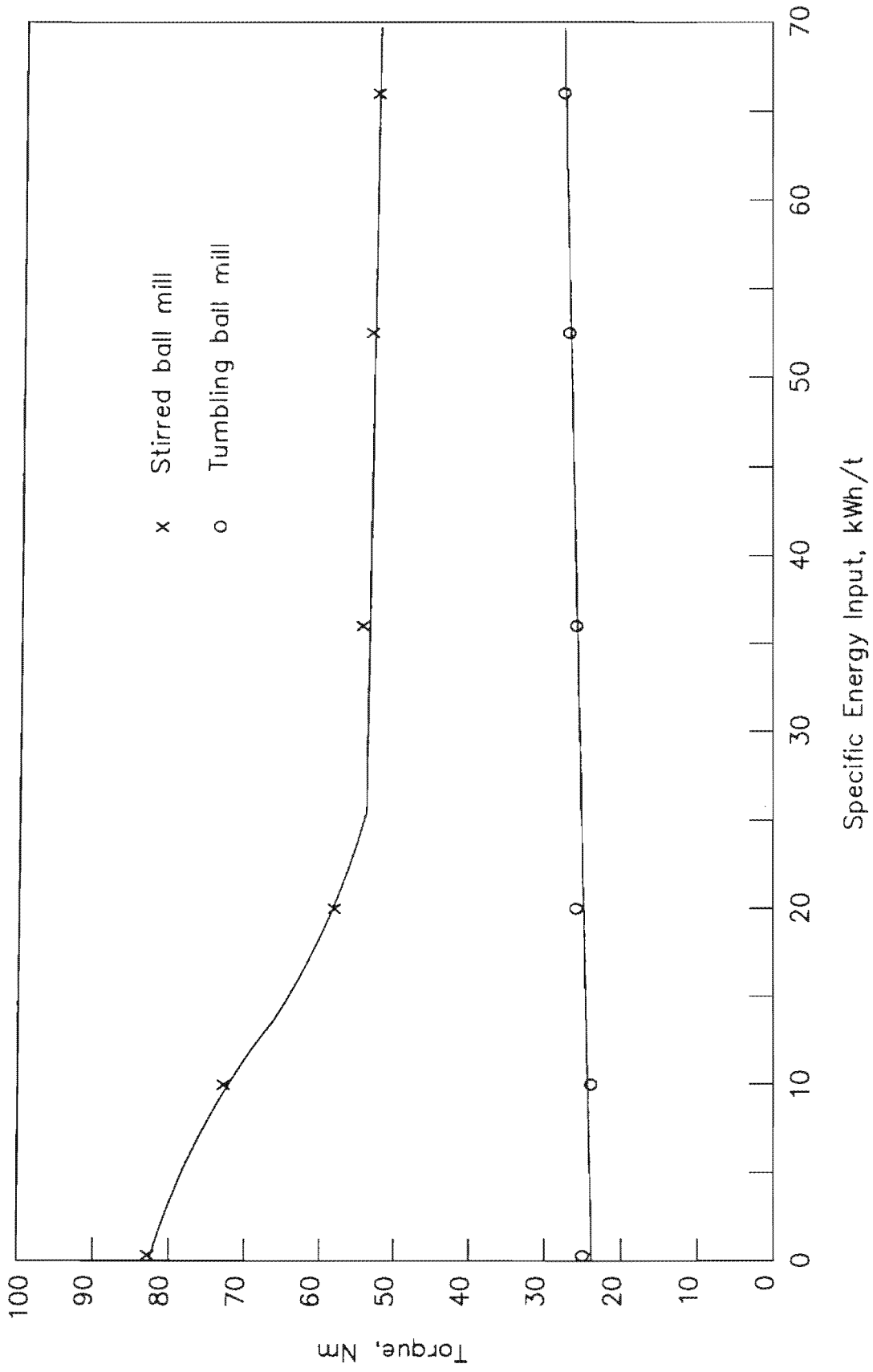


Figure 5.5. Variation of mill torque for stirred and tumbling ball mills (experimental conditions given in Table 5.1 and data given in Table A5.4).

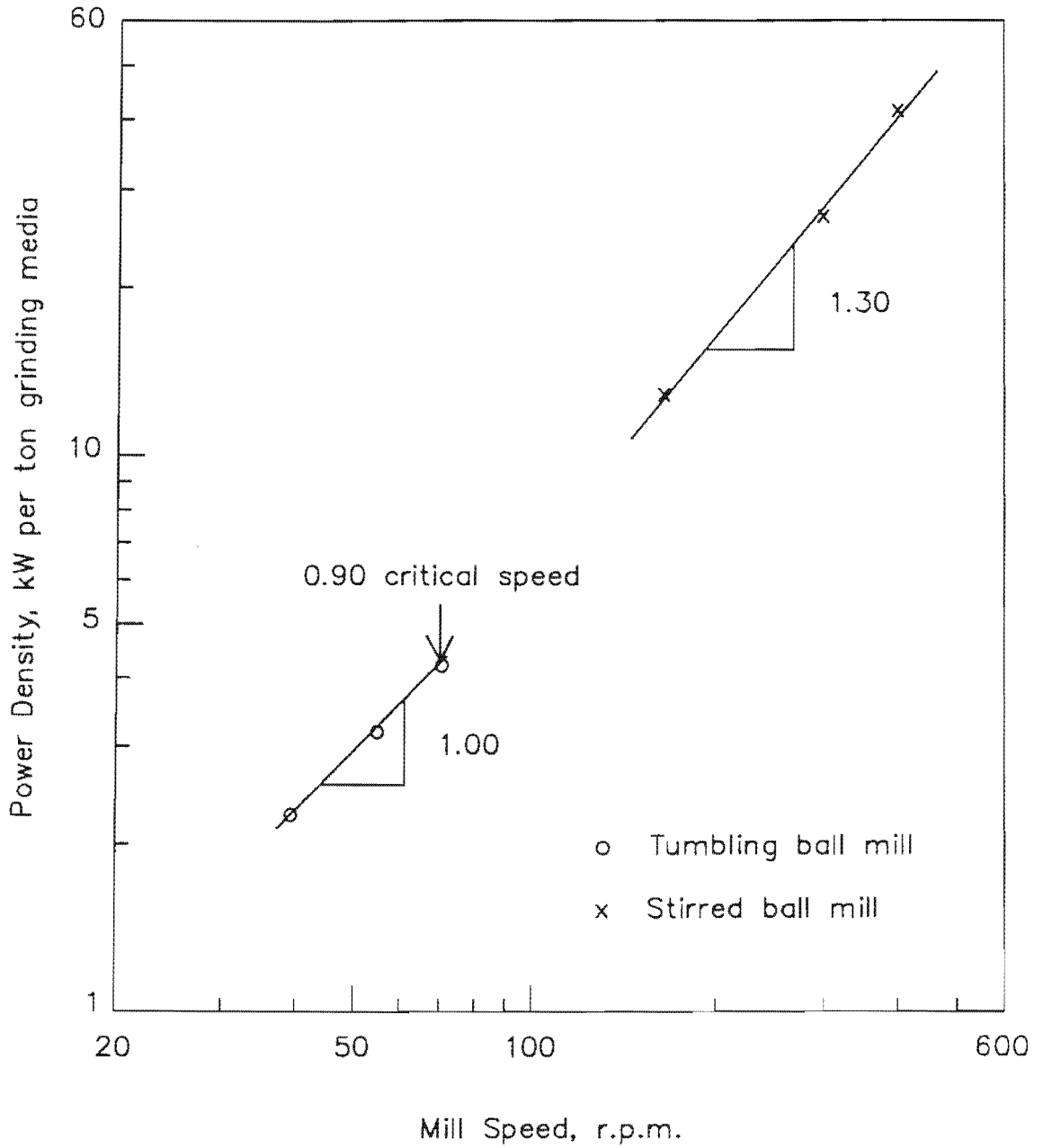


Figure 5.6. Comparison between the energy input per ton grinding media as a function of mill speed for stirred and tumbling ball mills (experimental conditions given in Table 5.1 and data given in Table A5.6)

increasing the shaft rotation speed and modifying the mill configurations. Although there is no critical speed for the stirred ball mill, at high shaft rotation speeds the effect of centrifugal force on the grinding media increases and the grinding media level rises which prevents an efficient energy transfer. This problem can be partially solved by using enclosed vessels and stationary pins fixed on to the vessel which increases the power density in the stirred ball mill. For example, the experiments conducted by Stehr, N., et.al. in the horizontal, enclosed, high speed stirred ball mill which has a vessel equipped with stationary pins, exhibited an exponent of 2.82 and a power density of 200 kW/t (47).

5.5. MEDIA WEAR

A comparison between the media wear of the stirred and tumbling ball mills as a function of energy input level is plotted in Figure 5.7 (Table A5.4). When the ball wear was measured in kg per ton of feed, the media wear rate showed a linear increase initially with increasing energy input level and then slowed down for both mills. If the media wear was taken as kg per ton of minus 10 micron product, the media wear was high at comparatively low energy input levels. As grinding proceeded, the media wear decreased and reached an almost constant value. Ball wear in the stirred ball mill is somewhat higher than in the tumbling ball mill. This correlation exists for both methods of media wear comparison. The media wear in the stirred and the tumbling ball mills as a function of the median size is shown in Figure 5.8. The media wear-median size relationship gave fairly good straight lines which had the slope values of -0.64 and -0.83 for the stirred and tumbling balls mills respectively. The stirred ball mill had higher media wear than the tumbling ball mill at the same median size in the coarse product size range. However, this disadvantage with regard to the media wear in the stirred ball mill disappeared gradually as the product median size became smaller. The media wear was the same for both mills when a product median size of 4.8 microns was obtained. The higher values of slope for the stirred ball mill as opposed to the tumbling ball mill is a result of the increasing grinding efficiency of the stirred ball mill over the tumbling ball mill as a higher percentage of fines is produced.

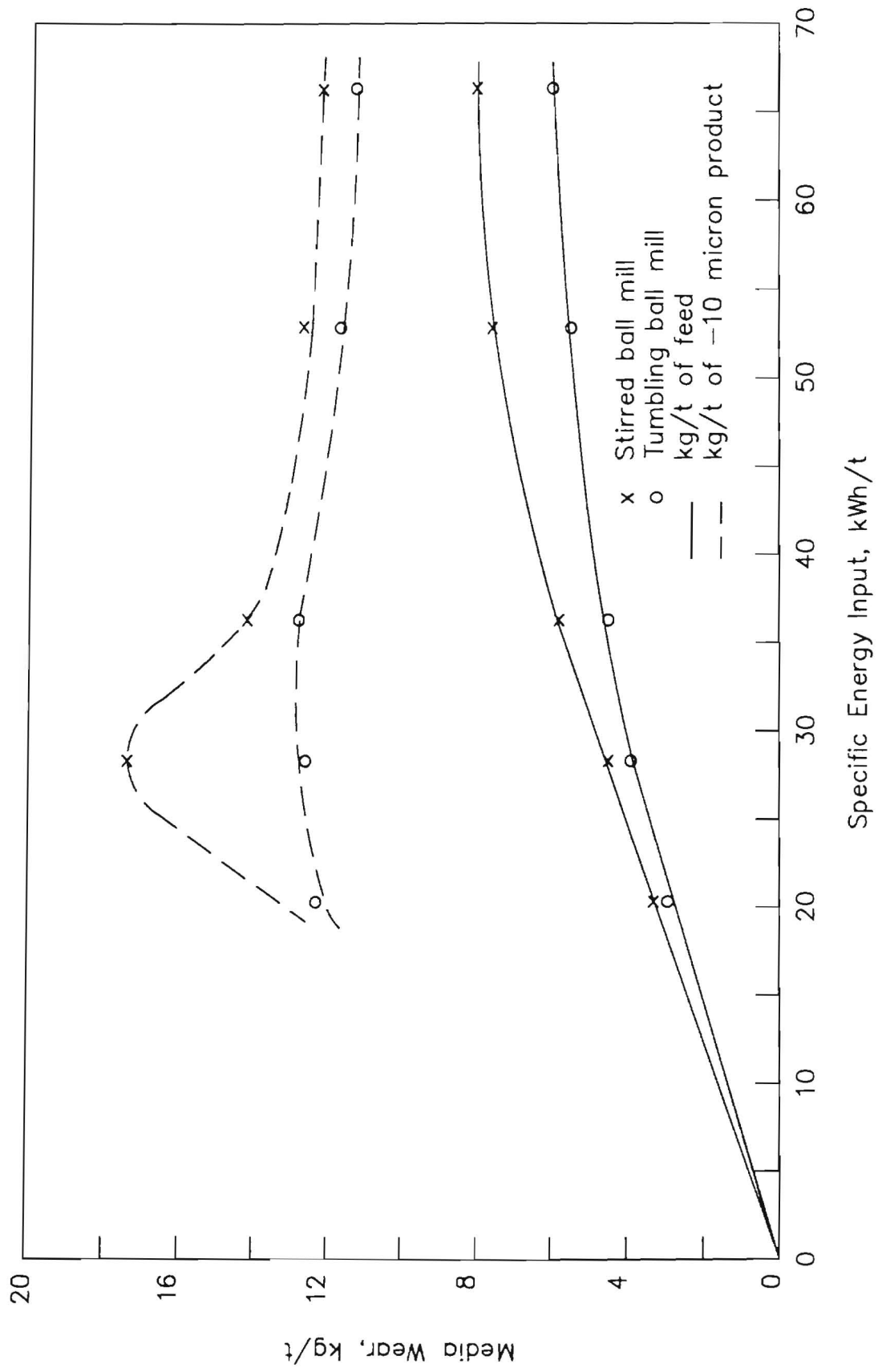


Figure 5.7. Comparison between media wear in stirred and tumbling ball mills (experimental conditions given in Table 5.1 and data given in Table A5.4).

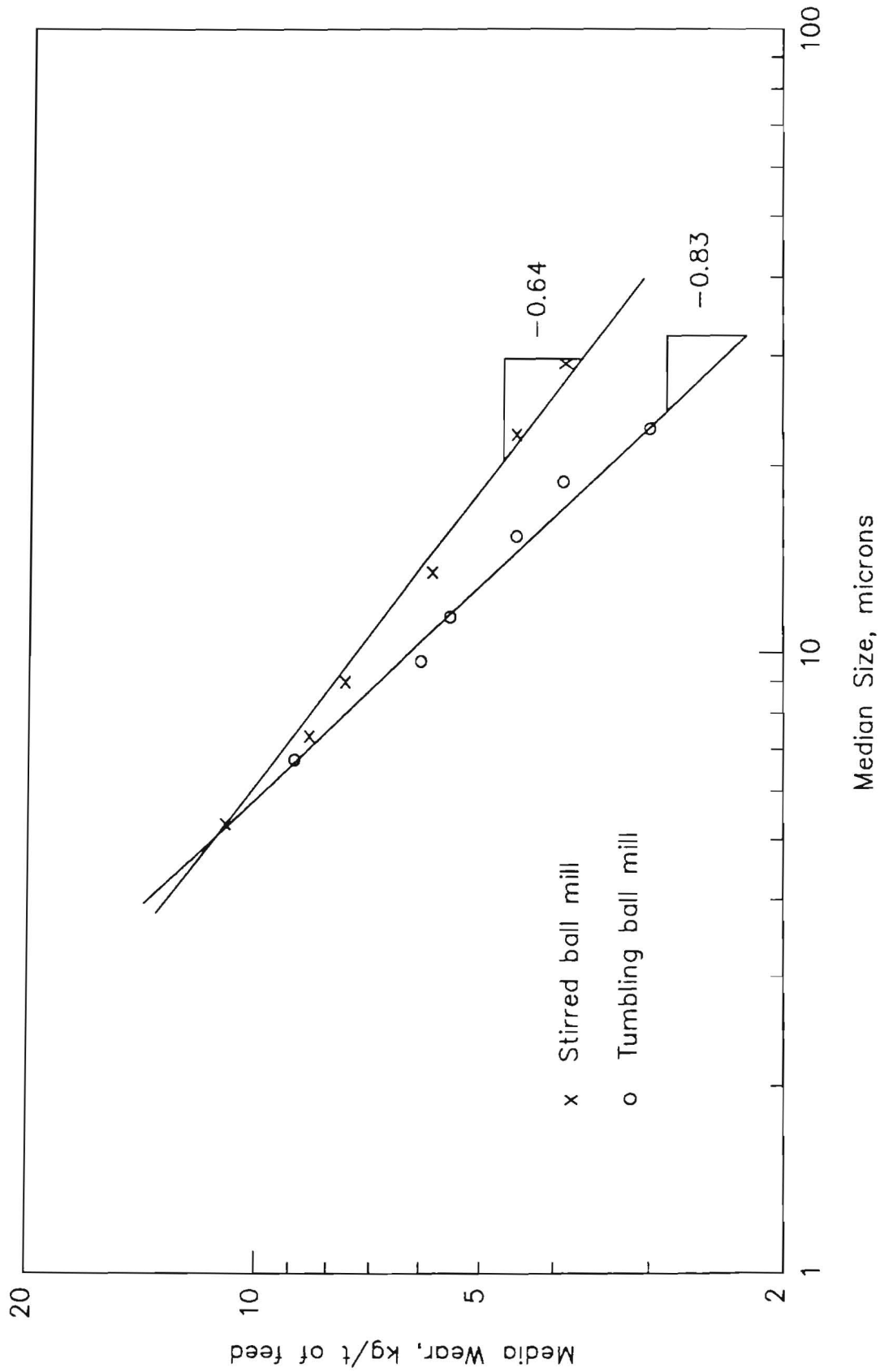


Figure 5.8. Media wear as a function of median size for stirred and tumbling ball mills (experimental conditions given in Table 5.1 and data given in Table A5.4).

CHAPTER 6

BATCH GRINDING EXPERIMENTS IN A 5 LITRE MILL

6.1. INTRODUCTION

Size reduction in a stirred ball mill subjects ore particles to a relatively constant fracture-producing environment. The intensity of the forces is determined by such factors as the mass of the grinding elements (balls), the pin tip velocity, the configuration of the shaft and dimensions of the vessel. For a particular ore, the extent of the size reduction will depend on both the intensity of grinding and the residence time of the ore in the mill.

Size reduction can therefore be regarded as a rate process in which the weight of material in various size intervals varies as a function of energy input. It has been shown that it is possible to predict the median size of the product for a given energy input with Charles' energy-size relationship (Chapter 4). However, there is usually a relationship between the size distribution obtained from the grinding operation and the subsequent metallurgical processes. If the efficiency of these processes does not depend only on a passing percentage of a single point of the grind, e.g., the one 50 % passing size, it is important to find a system that can be used to determine and compare the various product size distributions.

The objective of this chapter is to present experimental data that have been obtained in order to compare the various grinding conditions in a 5 litre batch test unit using a factorial design experimental procedure and to analyse the data using an energy-size reduction relationship in the form of Charles' Equation. The product size distribution was also correlated with the energy input.

6.2. EXPERIMENTAL PROGRAMME

The grinding process is complex, influenced by many independent and yet interacting variables, the extent of which is often difficult to isolate. This problem can be overcome by employing a statistical procedure in experimentation designing. Factorial design provides an efficient method of achieving this objective since 1) it is possible to maximise the information obtained for a given set of variables, 2) there are no subjective guesses as to the conclusions, 3) interaction between the variables can be discerned.

Table 6.1 shows the design matrix for a full factorial design which means that all combinations of the levels of the variables are tested in the sixteen runs. Designated as 2^4 four variables were tested at two levels (+ and -). Each run was carried out with the levels as allocated in Table 6.1. Signs for the main effects were determined by associating plus signs (+) with high levels and minus signs (-) with low levels.

In this study, a full factorial design was used to screen four variables: pulp density, pin tip velocity, ball density and size. Care was taken in the choice of variable range. Preliminary experiments presented in Chapter 4 influenced the choice of variable range in this experimental programme.

Mill size : The prototype 20 litre mill was redesigned to meet the simple batch testwork requirements. As a result of this, a smaller 5 litre batch unit was used for the experiments. This size mill was also used by other investigators as a standard test unit (32,42).

Pin tip velocity : Stirring must have enough intensity to give sufficient kinetic energy to the grinding media to break the particles but it should not be so high as to cause a vortex. The pin tip velocity ranged from 2.56 m/s to 3.66 m/s.

Energy input level : The energy input level was varied from 25 kWh/t to 200 kWh/t at which point an ultrafine product which had a median size of approximately 2 microns was obtained.

Table 6.1. 2^4 factorial design matrix

Test no	Variable level			
	ρ_p Pulp density kg/m ³	V Pin tip velocity m/s	ρ_b Ball density kg/m ³	d Ball size m
1	-	-	-	-
2	+	-	-	-
3	-	+	-	-
4	+	+	-	-
5	-	-	+	-
6	+	-	+	-
7	-	+	+	-
8	+	+	+	-
9	-	-	-	+
10	+	-	-	+
11	-	+	-	+
12	+	+	-	+
13	-	-	+	+
14	+	-	+	+
15	-	+	+	+
16	+	+	+	+

Pulp density		Tip velocity		Ball density		Ave. ball size	
-	+	-	+	-	+	-	+
1880	2200	2.56	3.66	3450	7850	0.0036	0.005

Feed size : Since the stirred ball mill is relatively energy inefficient in grinding coarse particles, the maximum particle size in the feed sample should not exceed 100 microns (Chapter 5) therefore a fine feed sample was used for the experiments (Table 3.1).

Ball size : For practical purposes, it was assumed that the balls lose diameter at a constant rate, so that the ball size distribution approximated that of an "equilibrium charge distribution" containing an equal number of balls in each size interval. In this testwork, two different types of ball size distributions were used to establish ball size effect on grinding. The top ball size varied from 6 mm to 4 mm. Distribution of ball sizes are listed in Table 6.2.

Table 6.2. Distribution of ball size

Ball diameter d (m)	Percent by weight (X)	
	d _{max} = 0.006	d _{max} = 0.004
0.006	70.6	-
0.004	20.6	70.6
0.003	8.8	29.4
Average ball ¹ diameter d _{ave} (m)	0.005	0.0036

Ball density : For some samples, especially industrial minerals, it was undesirable to have iron contamination. Consequently different types of grinding media such as zirconia or alumina, in other words grinding media of different densities have to be employed for grinding purposes. Steel balls (7850 kg/m³) and alumina balls (3450 kg/m³) were chosen as variables.

1 Average ball diameter can be calculated according to the following equation

$$d_{ave} = \frac{1}{\sum \frac{X}{d}}$$

Pulp density : As a matter of economics, grinding experiments were carried out in as dense a pulp as possible, consistent with good grinding efficiency. The more dense the pulp, the less the mill volume required and the less the media wear. Preliminary experiments indicated that the pulp density might be as high as 75 % (2400 kg/m³) for steel balls and 70 % (2200 kg/m³) for steatite balls (Chapter 4). Therefore, the pulp density varied between 60% (1880 kg/m³) and 70% (2200 kg/m³).

6.3. RESULTS AND DISCUSSIONS

The comminution-work laws of Rittinger, Bond and Kick can be combined in the following differential equation.

$$dE = -Cx^{-n} dx \quad (6.1)$$

Where dE energy differential required to reduce particle size x by an infinitesimal amount dx and C and n are constants, the exponent n is 2 in the Rittinger, 1.5 in the Bond and 1 in the Kick equation. In reality, C as well as n may be continuously changing variables (1). Constant C depends on the material and the manner in which it is broken and n is not restricted to 1, 1.5 and 2. The formula can be made to fit experimental data best by varying n over a range, rather than keeping it fixed.

The Charles energy-size reduction relationship gives a method for analyzing the correlation between different grinding conditions (43). According to Charles, the energy E expended for size reduction is

$$E = K \left(\frac{1}{k^\beta} - \frac{1}{k_0^\beta} \right) \quad (6.2)$$

Where K is a constant, k is the size modulus of the product, k₀ is the size modulus of the feed and β is the exponent.

Size distributions of grinds in the stirred ball mill can be presented by making use of empirical relationships. Such relationships provide a compact mathematical representation of size distribution data and allow subsequent mathematical and

statistical analyses to be carried out in a convenient fashion. Among the most commonly used forms of empirical distribution, the following Rosin-Rammler-Bennett equation was employed to describe the product size distributions obtained from the stirred ball mill (Appendix 6.2):

$$Y = 1 - e^{-\left(\frac{x}{k}\right)^\delta} \quad (6.3)$$

As an illustration of typical size distribution data, Figure 6.1 presents the size distributions of ground chromite products at various levels of energy input from test no:14 in Tables 6.1 and 6.3. All the products obtained in these experiments are characterized by a size modulus which is 63.2% passing size and a size distribution modulus (slopes), δ , of about 1.09. The size analysis of the product of the tests given in Figure 6.1 are parallel lines on these Rosin-Rammler plots and fit the experimental points very well.

This phenomenon was observed for all the tests; the slope (δ) was relatively insensitive to the test conditions, and varied between 1.05 and 1.22. The phenomenon of constant slope in any individual test implies that the progress of grinding can be measured in terms of the size modulus only. The size distribution at the start can have any slope, but once the critical slope has been attained, the size distribution is characterized by the size modulus alone.

Equation 6.2 can also be expressed as:

$$(E + E_0) = K/k^\beta \quad (6.4)$$

where E_0 is the theoretical energy needed to prepare the feed and is equal to K/k_0^β .

Given the size modulus of the feed (30.5 microns), the parameters K and β may be estimated by progressive substitution as follows:

1) Estimate E_0 and from values of E and k calculate K and β by regression to Equation 6.4.

2) Calculate E_0 using k_0 , K and β and repeat the process until the value of E_0 converges.

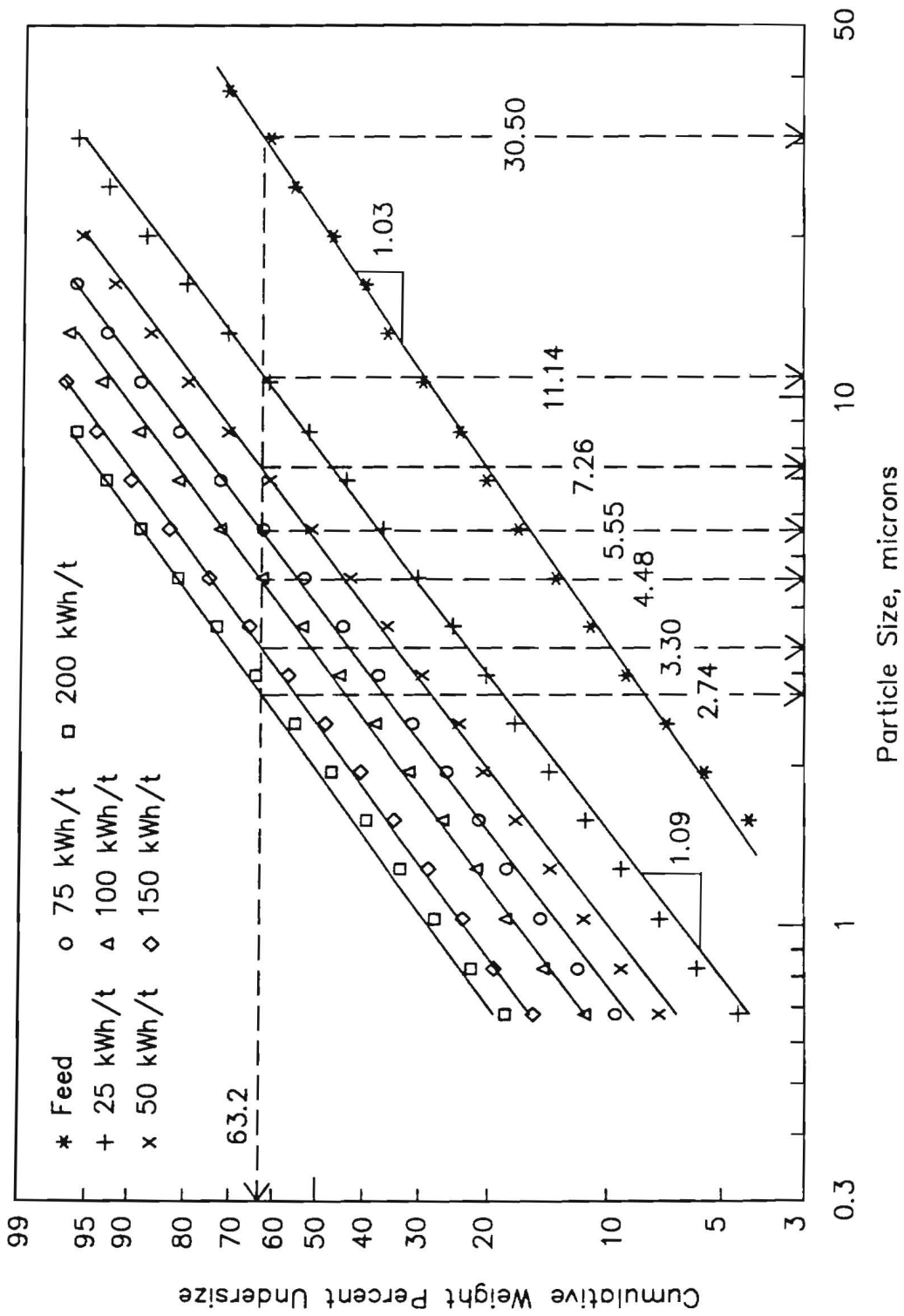


Figure 6.1. A typical example of product size distribution at various levels of energy input using grinding conditions in Table 6.1, test no:14: pulp density = 2200 kg/m³, pin tip velocity = 2.56 m/s, ball density = 7850 kg/m³, ave. ball size = 0.005 m, mill size = 5 litres.

Figure 6.2 shows a plot of Equation 6.4 for the data shown in Figure 6.1 (test No:14). The points in the graph fit well onto a straight line which has a correlation coefficient of 0.999 and a calculated size modulus value of -1.30.

The summary of the data from factorial design experiments is presented in Table 6.3. The results recorded for each run were size and distribution modulus, the Charles' Equation constant K and grindability $1/K$ as the responses of the factorial design.

The values of size modulus $k_{63.2}$ and size distribution modulus δ were generated by the Malvern soft-wear programme, which calculates the parameters of the Rosin-Rammler Equation, fitting it to the size distribution obtained by model independent analysis.

Table 6.3. Effect of variables in factorial design

Test no	Energy input kWh/t	Distribution modulus δ	Size modulus mic.	Charles' Law		
				Exponent β	Constant K	Grindability $1/K$
1	25	1.16	9.15	-1.25	508.2	1.97×10^{-3}
	50	1.19	5.63			
	75	1.20	4.10			
	100	1.21	3.33			
	150	1.22	2.50			
	200	1.22	2.05			
2	25	1.14	9.52	-1.23	516.1	1.94×10^{-3}
	50	1.18	5.90			
	75	1.18	4.32			
	100	1.18	3.49			
	150	1.17	2.67			
	200	1.16	2.10			
3	25	1.12	9.44	-1.27	548.9	1.82×10^{-3}
	50	1.16	6.03			
	75	1.16	4.52			
	100	1.17	3.64			
	150	1.16	2.76			
	200	1.15	2.16			

Test no	Energy input kWh/t	Distribution modulus δ	Size modulus mic.	Charles' Law		
				Exponent β	Constant K	Grindability 1/K
4	25	1.12	9.83	-1.28	607.7	1.65×10^{-3}
	50	1.15	6.12			
	75	1.15	4.56			
	100	1.14	3.71			
	150	1.12	2.82			
	200	1.12	2.31			
5	25	1.14	9.92	-1.23	555.6	1.80×10^{-3}
	50	1.18	6.41			
	75	1.20	4.76			
	100	1.22	3.89			
	150	1.21	2.76			
	200	1.22	2.22			
6	25	1.14	9.85	-1.26	574.5	1.74×10^{-3}
	50	1.18	6.13			
	75	1.20	4.55			
	100	1.20	3.61			
	150	1.21	2.67			
	200	1.22	2.25			
7	25	1.10	10.72	-1.22	609.8	1.64×10^{-3}
	50	1.14	6.87			
	75	1.15	5.09			
	100	1.14	4.13			
	150	1.17	2.98			
	200	1.19	2.41			
8	25	1.10	10.47	-1.21	582.7	1.72×10^{-3}
	50	1.15	6.64			
	75	1.18	4.97			
	100	1.19	4.06			
	150	1.19	2.91			
	200	1.22	2.33			
9	25	1.14	10.35	-1.30	677.9	1.48×10^{-3}
	50	1.15	6.40			
	75	1.17	4.80			
	100	1.17	3.96			
	150	1.18	3.06			
	200	1.18	2.49			
10	25	1.13	10.55	-1.29	687.6	1.45×10^{-3}
	50	1.16	6.40			
	75	1.18	4.83			
	100	1.19	4.02			
	150	1.19	3.08			
	200	1.17	2.53			

Test no	Energy input kWh/t	Distribution modulus δ	Size modulus mic.	Charles' Law		
				Exponent β	Constant K	Grindability 1/K
11	25	1.09	12.95	-1.23	873.9	1.14×10^{-3}
	50	1.10	7.48			
	75	1.10	5.96			
	100	1.09	4.88			
	150	1.10	3.76			
	200	1.11	3.15			
12	25	1.07	11.75	-1.26	777.2	1.29×10^{-3}
	50	1.09	7.23			
	75	1.10	5.68			
	100	1.12	4.76			
	150	1.09	3.55			
	200	1.09	2.83			
13	25	1.07	11.52	-1.25	740.7	1.35×10^{-3}
	50	1.08	7.65			
	75	1.08	5.74			
	100	1.07	4.64			
	150	1.09	3.48			
	200	1.07	2.74			
14	25	1.10	11.14	-1.30	777.9	1.29×10^{-3}
	50	1.11	7.26			
	75	1.11	5.55			
	100	1.09	4.48			
	150	1.07	3.30			
	200	1.07	2.74			
15	25	1.04	13.50	-1.21	888.2	1.13×10^{-3}
	50	1.05	8.83			
	75	1.05	6.76			
	100	1.05	5.74			
	150	1.05	4.21			
	200	1.05	3.26			
16	25	1.05	11.75	-1.28	810.2	1.23×10^{-3}
	50	1.06	7.95			
	75	1.05	6.10			
	100	1.05	4.87			
	150	1.05	3.57			
	200	1.05	2.88			
Average		1.14	-	-1.25		

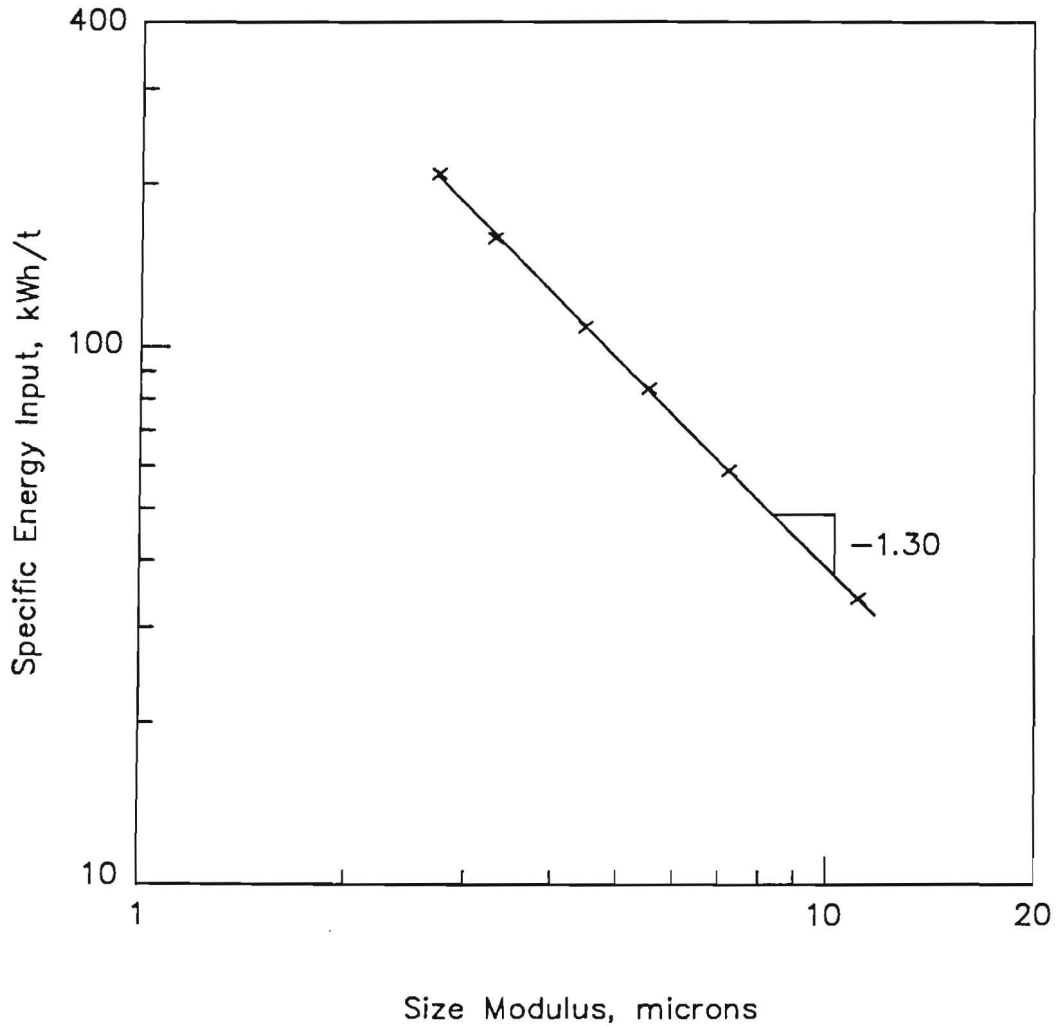


Figure 6.2. A typical example of size modulus of product size distribution at various levels of energy input using grinding conditions in Table 6.1, test no: 14.

Pulp density : 2200 kg/m³
 Pin tip velocity : 2.56 m/s
 Ball density : 7850 kg/m³
 Ave. ball size : 0.005 m
 Mill size : 5 litre

Magnitude of the distribution modulus (δ): The value of δ (the Rosin-Rammler slope) remains almost the same at different levels of energy input for given grinding conditions, with the exception of δ values at an energy input level of 25 kWh/t using 4&3 mm grinding media. This might be due to the effect of the feed size distribution, which has an δ value of 1.03, on the ground product at a low level energy input. The magnitude of the difference between feed size and the δ values of the product sizes obtained when the energy input levels were 50 kWh/t and higher determined the effect on the δ value of the product size obtained when the energy input level was 25 kWh/t.

The grinding conditions in the mill affect the size distribution of the product, consequently the value of δ . Data from the series of experiments, in which various grinding conditions were used, illustrated that the size distribution modulus δ of products decreased slightly as the pin tip velocity, ball diameter and density increased.

The differences in δ values can be attributed to a change in the efficiency of energy transfer from the grinding media to the material. The size distribution of the product from the stirred ball mill depends on the relative proportion of impact and attrition events. Altering the grinding conditions may change these proportions and consequently alter the size distribution of the product.

Magnitude of the exponent of Charles' Equation (β): According to Equation 6.4 a straight line should be obtained if the size modulus is plotted as a function of expended energy on log-log paper. It was observed that the data for each series of grinding tests on the chromite sample, which had been ground in an identical manner, were distributed in a straight line (Figure 6.2).

This allowed calculations of β values for the basic energy-size reduction equation (Equation 6.4). Table 6.3 shows that the slopes of each series of tests closely follow the overall trends and the values of β varied over a narrow range from 1.21 to 1.30 for all the tests using Charles' Law. The correlation coefficient of these lines varied between 0.999 and 0.994.

Magnitude of grindability ($1/K$): Grindability may be conveniently defined as a reciprocal of K for comparing various grinding conditions. Equation 6.2

therefore provides a simple measure of grindability ($1/K$) as the weight of material ground to pass unit size per unit energy consumption. The values of $1/K$ are given in Table 6.3 and the unit size was chosen as 1 micron.

When Charles' Equation was applied to the data from Table 6.3, the constant of the equation and the position of the data points along the straight lines changed with the grinding conditions. Under all conditions, the highest grindability was obtained with a pulp density of 1880 kg/m^3 , $4\&3 \text{ mm}$ alumina balls and a pin tip velocity of 2.56 m/s . The lowest grindability was obtained with a pulp density of 1880 kg/m^3 , $6\&4\&3 \text{ mm}$ steel balls and a pin tip velocity of 3.66 m/s .

The results in Table 6.3 were used to analyse the main effects of changing levels of variables and the interaction between the variables. Table 6.4 shows, within the range of levels used, the effect of factorial design experiments on grindability using Yates' algorithm. The standard deviation was calculated to be 0.338×10^{-4} (Appendix 6.3).

Table 6.4. Estimated effects from factorial design experiments

Parameter	Estimated effects \pm standard error
average	15.400×10^{-4}
ρ_p	$-0.025 \times 10^{-4} \pm 0.388 \times 10^{-4}$
V	$-1.750 \times 10^{-4} \pm 0.338 \times 10^{-4}$
ρ_b	$-1.050 \times 10^{-4} \pm 0.338 \times 10^{-4}$
d	$-4.900 \times 10^{-4} \pm 0.338 \times 10^{-4}$
$\rho_p V$	$0.425 \times 10^{-4} \pm 0.338 \times 10^{-4}$
$\rho_p \rho_b$	$0.175 \times 10^{-4} \pm 0.338 \times 10^{-4}$
$\rho_p d$	$0.425 \times 10^{-4} \pm 0.338 \times 10^{-4}$
$V \rho_b$	$0.600 \times 10^{-4} \pm 0.338 \times 10^{-4}$
$V d$	$-0.200 \times 10^{-4} \pm 0.338 \times 10^{-4}$
$\rho_b d$	$0.150 \times 10^{-4} \pm 0.338 \times 10^{-4}$
$\rho_p V \rho_b$	$0.325 \times 10^{-4} \pm 0.338 \times 10^{-4}$
$\rho_p V d$	$0.425 \times 10^{-4} \pm 0.338 \times 10^{-4}$
$\rho_p \rho_b d$	$-0.375 \times 10^{-4} \pm 0.338 \times 10^{-4}$
$V \rho_b d$	$0.050 \times 10^{-4} \pm 0.338 \times 10^{-4}$
$\rho_p V \rho_b d$	$-0.375 \times 10^{-4} \pm 0.338 \times 10^{-4}$

The reference t-value given in Appendix 6.3 was 0.869×10^{-4} . A comparison between the estimated effect of the parameters from Table 6.4 and the reference t-value showed that the media size, pin tip velocity and ball density all had greater estimated effects than the reference t-value and it can be concluded, at 95% confidence level, that they affected the grindability of the chromite ore significantly.

The size of the grinding media had the greatest effect on the grindability. As was expected, the smaller grinding media have a smaller size modulus for the same energy input level (Chapter 4).

The pin tip velocity appeared to have the second largest effect on the grindability of the chromite ore which decreased with an increase in pin tip velocity.

The grindability of the ore was significantly affected by the density of the grinding media. Lighter balls produced finer products than heavier balls.

The grindability of the chromite sample was not affected by the pulp densities between 1880 and 2200 kg/m³. The interactions between the variables were negligible.

Overall, the results suggest that the stirred ball mill should be operated at a slower speed with smaller and lighter grinding media so that the mill energy can be used efficiently. However, a decrease in pin tip velocity, ball size and density relate to power decreases; consequently, these grinding conditions reduce the capacity of the mill considerably. When the grinding results are evaluated, the capital and running costs of the grinding operation should be taken into consideration.

Equations 6.2 and 6.3 have parameters, β , k and δ , often called exponent, size modulus and distribution modulus, respectively. Whenever a product size distribution is known to agree with these functions, the entire distribution can be specified at various energy input levels and grinding conditions.

Equations 6.2 and 6.3 can be combined and re-arranged in the following general form

$$Y = 1 - e^{-\left(\frac{x}{k}\right)^\delta} \quad (6.5)$$

where k for the Charles' Equation is,

$$k = \left(\frac{1}{E/K + (1/k_0)^\beta} \right)^{1/\beta} \quad (6.6)$$

The constant K in Charles' Equation for chromite ground in the stirred ball mill varied according to some function of the pin tip velocity, ball size and density.

$$K \propto V^a \rho_b^b d^c \quad (6.7)$$

In order to describe these relationships between the product size distribution and the energy input under the various grinding conditions mathematically, a nonlinear regression equation was computed, relating the constant K in Charles' Equation with the pin tip velocity, ball density and size, using average β and δ values from Table 6.3 and combining Equation 6.6 with Equation 6.7, yielding

$$Y = 1 - e^{-\left(\frac{x}{\left(\frac{1}{\left(\frac{E}{13302V^{0.437} \rho_b^{0.148} d^{0.868}} \right) + \left(\frac{1}{k_0} \right)^{1.25}} \right)^{0.8}} \right)^{1.14}} \quad (6.8)$$

Statistical data for the nonlinear regression analysis is given in Appendix 6.4.

The square of the multiple correlation coefficient R^2 was calculated to be 0.998. The large values of R^2 indicates that Equation 6.8 can be used to explain the variations in the data.

Figure 6.3 shows the overall plot of residuals versus predicted values. The residuals revealed no apparent trend or abnormality. The empirical model would not appear to be invalidated.

Figure 6.4 is a graph of the observed values and the predicted values. The graph indicates that the empirical model is a good predictor of the particle size distribution.

The student t-test was used to compare observed and predicted values. The null hypothesis that there was no difference between the means of the observed and predicted values was tested. The calculated t statistic ranged from 0.022 with a 236 degree of freedom to 0.390 with a 260 degree of freedom. These values were lower than the critical t value = 1.960 at 95% confidence level from the

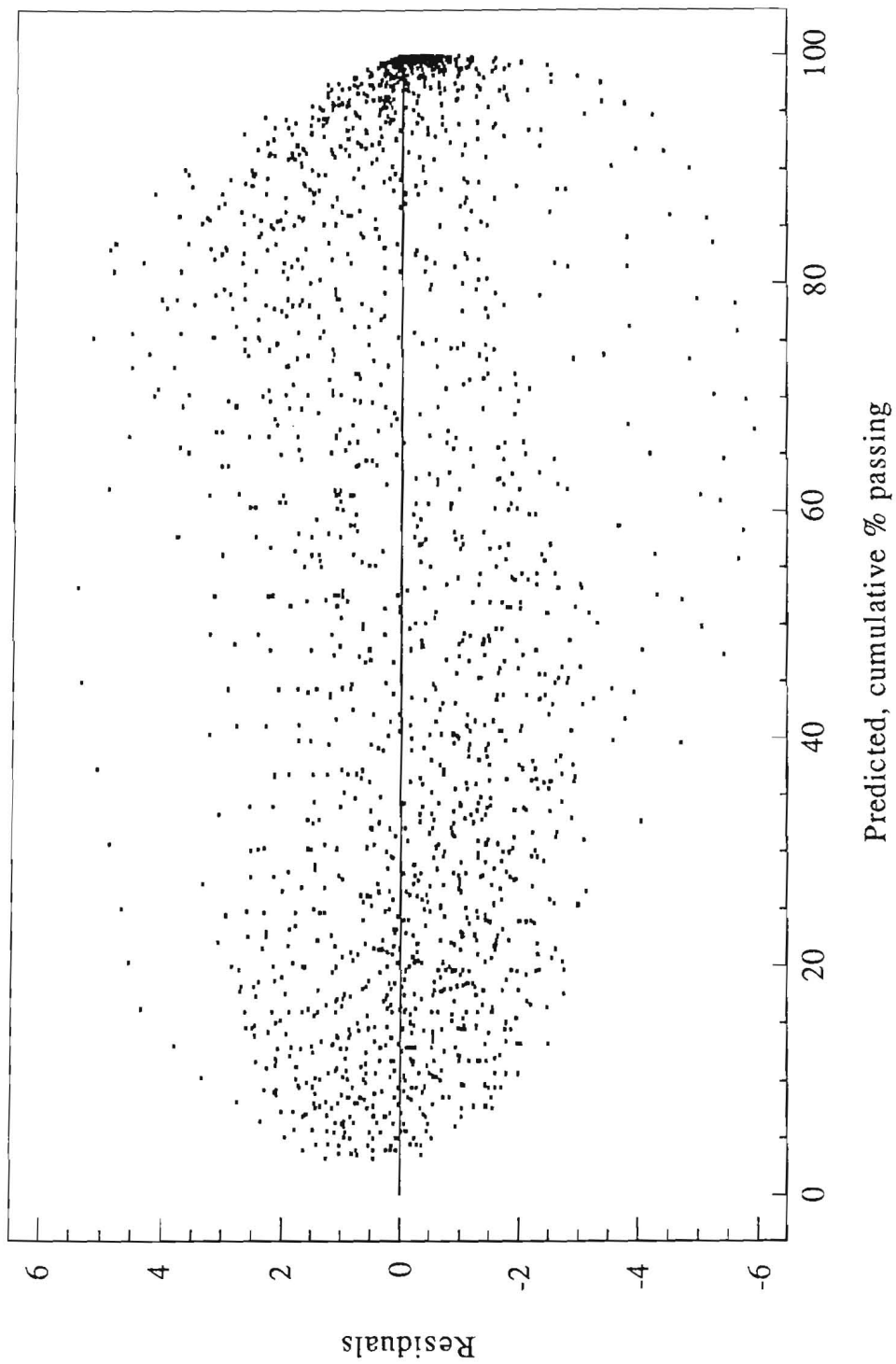


Figure 6.3. Plot of residuals versus predicted values (Eq.6.8).

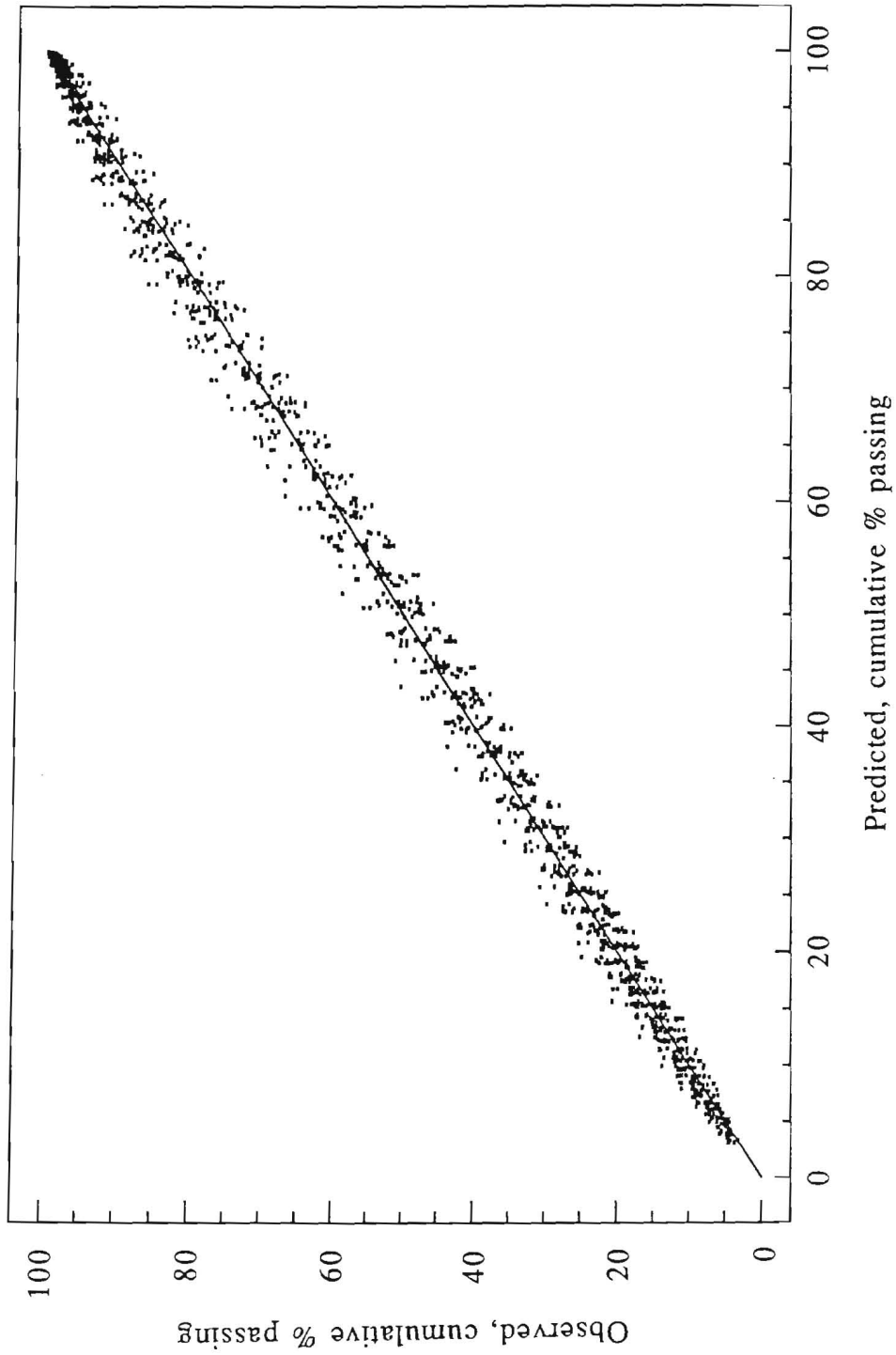


Figure 6.4. Comparison between the observed and predicted results (Eq.6.8).

student's t distribution table (64). The low computed value of t suggested that there was no difference between the means of the observed and expected values so that null hypothesis could not be rejected.

Although grinding investigations based on population balance models are closer to reality and more fundamental than methods based on the Charles' and Rosin-Rammmler-Bennet equations, the latter may still lead to a useful and simple procedure to predict the product size distributions of the chromite ore at any energy input and grinding conditions within the range of variables used for the tests. This approach does not require the use of a digital computer.

CHAPTER 7

SIMULATION OF BATCH GRINDING IN A 5 LITRE STIRRED BALL MILL

7.1. INTRODUCTION

The linear, size-discretized population-balance model was first proposed more than 20 years ago. A considerable effort has been devoted to developing a form of grinding model for tumbling ball mills (69-71). However, it has not been well extended to other comminution devices. Although, an empirical model was successfully applied to the batch grinding tests in the 5 litre stirred ball mill (Chapter 6), in this chapter a detailed analysis of the basic grinding pattern was analysed using the concepts of the specific rates of breakage and primary breakage distributions in a complete size-mass balance to assist in the understanding of the grinding system in the stirred ball mill.

7.2. THEORETICAL BACKGROUND

The breakage process is characterised by two physically interpretable quantities: a selection function that gives the fractional rate of breakage of particles in each size interval and a breakage function that gives the average size distribution of daughter fragments resulting from primary breakage events. The development of these equations is discussed briefly below.

In the population balance approach for modelling the grinding processes, the mass of material in the mill is divided into n narrow size intervals. A mass balance for the material in the size interval i th at time t may be written as

$$\frac{dm_i(t)}{dt} = -S_i m_i(t) + \sum_{j=1, i>1}^{i-1} b_{ij} S_j m_j(t), \quad n \geq i \geq j \geq 1 \quad (7.1)$$

where $m_i(t)$ is the mass fraction of material in the mill in the i th size interval, t is the grinding time, S_i is the size-discretized selection function which gives the fraction broken out of the i th size interval per unit time, and b_{ij} is the size-discretized breakage function from the j th size interval which appears in the i th size interval.

If first-order disappearance was assumed for the top size in the mill feed. The solution to the set of n differential Equations 7.1 yields for the first size interval, assuming $S_i \neq S_i(t)$:

$$m_1(t) = m_1(0) \exp(-S_1 t) \quad (7.2)$$

A plot of $m_1(t)$ on a log scale versus t on a linear scale should then be a straight line with a slope of $S_1/2.3$.

Previous batch and continuous experiments showed that specific energy input was the most important scale-up criteria and correlated well with the product size distributions as a function of various grinding conditions and mill sizes. Therefore, it was assumed that for various grinding conditions the selection function S_i was proportional to the specific power input to the mill.

$$S_i = S_i^E \left(\frac{P}{H_{mill}} \right) \quad (7.3)$$

where S_i^E referred to a specific selection function. P is the net power and H_{mill} is the hold-up of the material to be broken in the mill. Incorporating Equation 7.3 into Equation 7.1 yields:

$$\frac{dm_i(\bar{E})}{d\bar{E}} = -S_i^E m_i(\bar{E}) + \sum_{j=1, i > j}^{i-1} b_{ij} S_j^E m_j(\bar{E}), \quad n \geq i \geq j \geq 1 \quad (7.4)$$

where \bar{E} is the specific energy input to the mill and is equal to the product of specific power, P/H and grinding time t .

Equation 7.2 can also be rewritten

$$m_1(\bar{E}) = m_1(0) \exp(-S_1^E \bar{E}) \quad (7.5)$$

The cumulative breakage function can be determined by a graphical method from the monosize grinding tests using the following Equation 7.6 (72).

$$B_{i1} = \frac{F_i^E}{S_1^E} \quad (7.6)$$

where F_i^E is the initial slope of the cumulative mass fraction finer than the size interval i against the specific energy input \bar{E} .

7.3. EXPERIMENTAL METHOD

In this study, a factorial design experimental programme was employed to investigate the grinding kinetics of the chromite sample. Table 7.1 shows the design matrix for 2^3 factorial design experiments. On the basis of the analysis of the data in Chapter 6, three operating parameters were chosen for the grinding tests to determine the effect of pin tip velocity, ball size and ball density on the kinetics of fine grinding in the stirred ball mill. The range of variable parameters was kept the same as those used in Chapter 6. The feed samples used were natural size - 100 microns and monosize -53+38 microns and -38+25 microns. Eight monosize grinding tests were run using four different grinding conditions. Factorial design was arranged in two blocks, thus reducing the need for major amounts of work and sample preparation. Monosize feed runs were marked and numbered test 2, 3, 5 and 8 in Table 7.1. They were prepared by using a procedure as explained in Chapter 3.

There were some drawbacks when applying the monosize feed technique to fine grinding. Firstly, It took a long time to prepare the monosize feed sample and it was not possible to use sieves to prepare monosize samples below 25 microns. Secondly, there was a difference between the size measurements obtained by the sieves and the Malvern Particle Sizer. Monosize feed samples measured with the Malvern Particle Sizer tended to contain a higher percentage of coarse fractions. Therefore, the preferable coarsest monosize feed was below 53 microns due to the decrease in efficiency of the stirred ball mill above the 100 microns size range. As a result of this, -53+38 microns and -38+25 microns monosize feed samples were chosen to study the grinding kinetics of the chromite in the stirred ball mill and the same sizing technique was employed to characterize the size distribution of the feed and product samples.

Additionally, the effect of ball size on the specific selection function was examined using a monosize feed from 425 to 38 microns in $\sqrt{2}$ interval. Grinding results from the factorial design programme using natural feed size -100 microns were compared with those of monosize test results under the same grinding conditions.

Table 7.1. 2^3 factorial design matrix

Test no	Variable level		
	V Pin tip velocity m/s	ρ_b Ball density kg/m ³	d Ball size m
1	-	-	-
*2	+	-	-
*3	-	+	-
4	+	+	-
*5	-	-	+
6	+	-	+
7	-	+	+
*8	+	+	+

Tip velocity		Ball density		Ave. ball size	
-	+	-	+	-	+
2.56	3.66	3450	7850	0.0036	0.005

7.4. RESULTS AND DISCUSSIONS

7.4.1. Estimation of the monosize specific selection function

According to Equation 7.5 a semilog plot of the fraction of feed material remaining in the top size interval versus specific energy input will result in a straight line with a slope proportional to the specific selection function S_i^E . A typical example of disappearance plots from the grinding experiments are shown in Figure 7.1. Data for -53+38 and -38+25 micron size fractions exhibits a linear disappearance. The values of S^E determined from the plot for -53+38 microns and -38+25 microns size fractions are 0.069 and 0.046 kWh/t⁻¹ respectively. Specific breakage rates determined from monosize feed tests are given in Table 7.3. The results indicated that all the monosize grinding tests exhibited a first order breakage. Therefore the first order model appears to be suitable for the treatment of grinding kinetics in the stirred ball mill.

7.4.2. Estimation of the monosize breakage function

A complete description of the kinetics of size reduction in the stirred ball mill requires knowledge of the breakage function. It can be estimated by plotting the cumulative fraction finer than size x_i versus specific energy input. An example of such a fine size production plot for -53+38 microns monosize feed is shown in Figure 7.2. From the slope, F_i^E measured at low energy input intervals, the cumulative breakage function can be calculated according to Equation 7.6. Data determined in this manner for all monosize grinding experiments are given in Table 7.2.

Figure 7.3 shows a plot of the cumulative breakage function for various operating conditions and size fractions given in Table 7.2. B values do not seem to be sensitive to the milling conditions such as pin tip velocity, ball size and density. It is apparent from the graph that the breakage functions are normalizable and the range of values observed from various grinding conditions and sizes appear to be small.

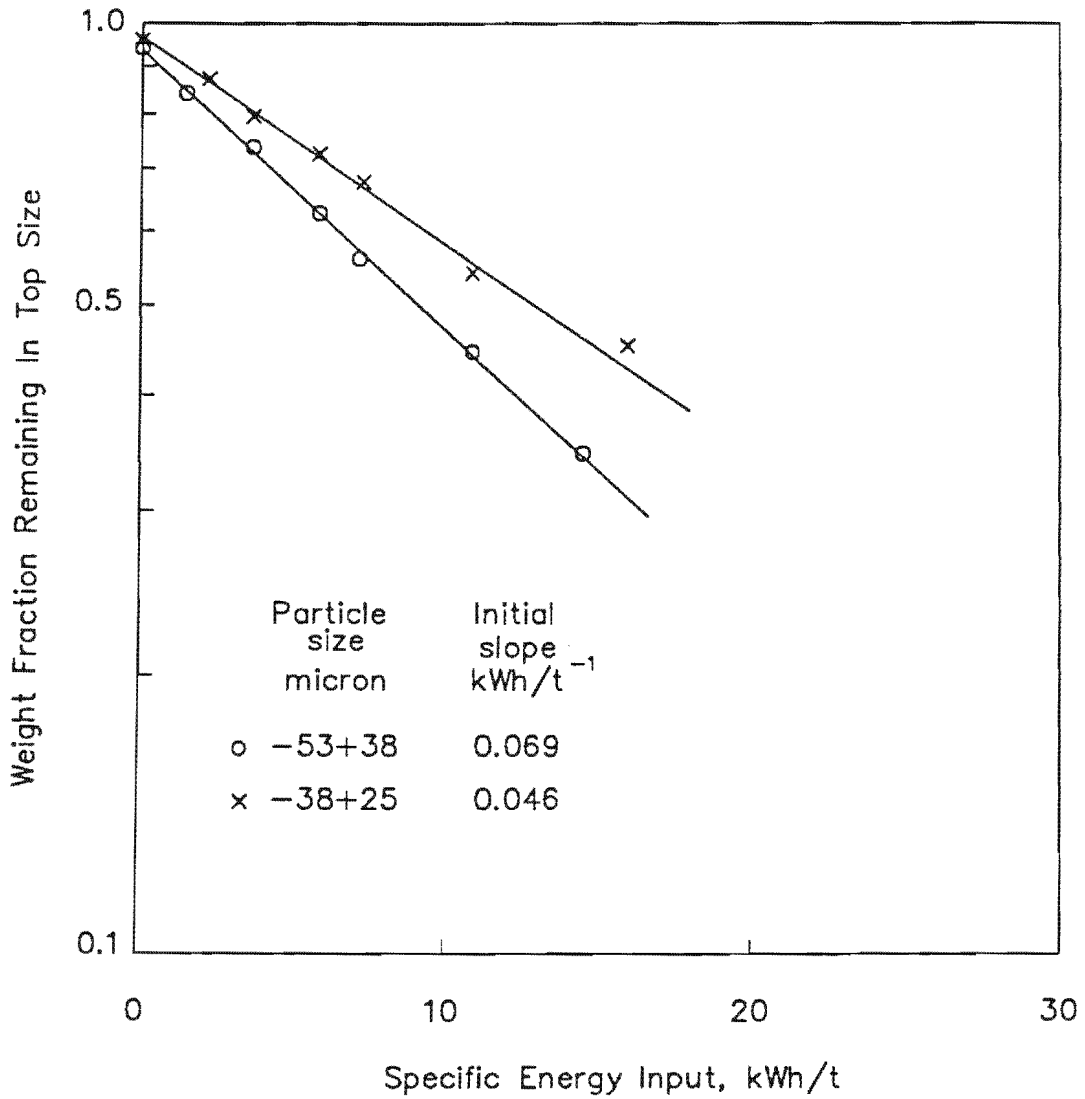


Figure 7.1. First-order plot for grinding -53+38 and -38+25 microns monosize feeds: ave. 0.005 m steel balls pulp density = 1880 kg/m³, pin tip velocity = 3.66 m/s (data given in Tables A7.1.8.2 and A7.1.8.3).

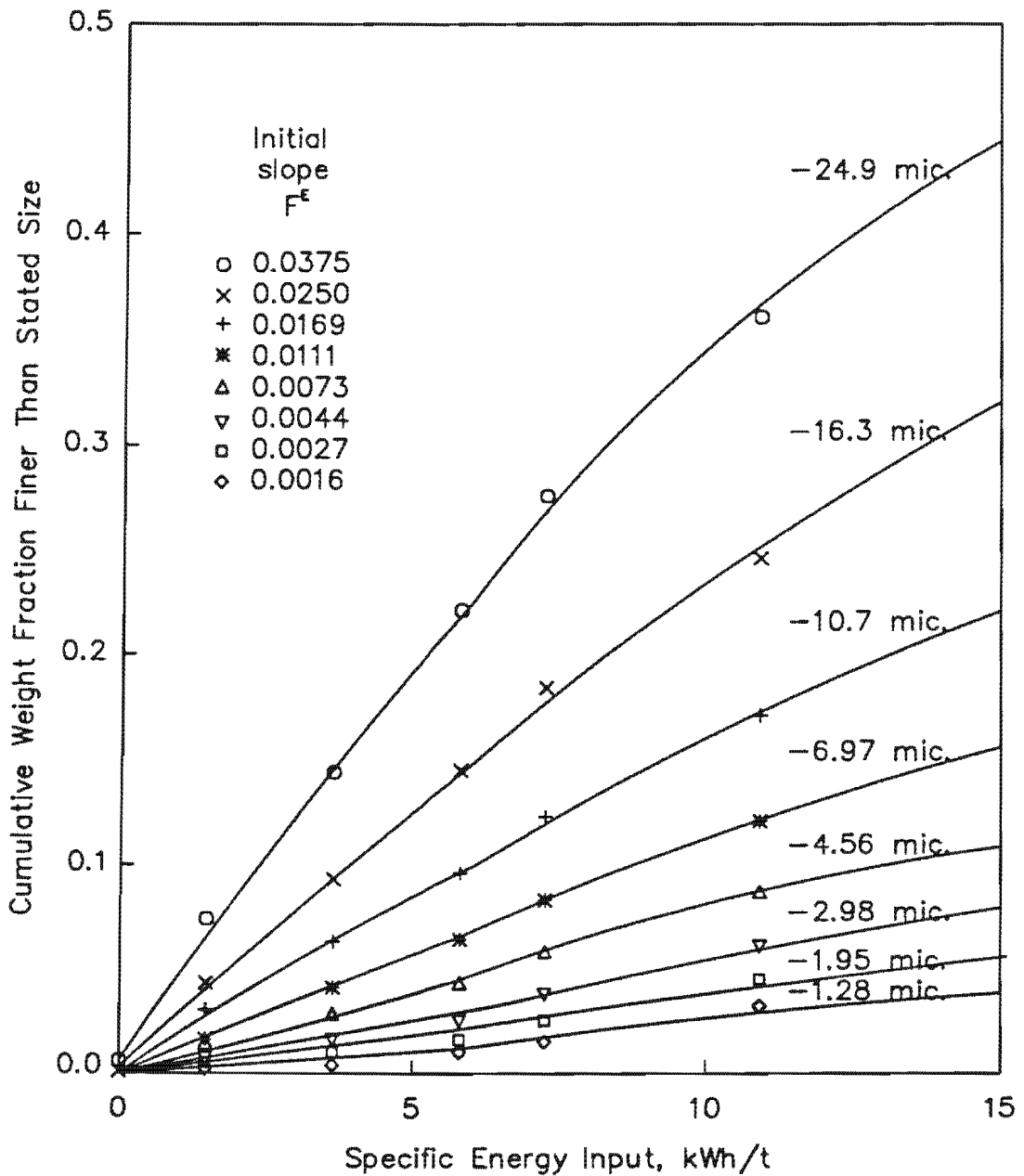


Figure 7.2. A typical example of fine size production plot for $-53+38$ microns monosize feed: ave. 0.005 m steel balls, pulp density = 1880 kg/m^3 , pin tip velocity = 3.66 m/s (data given in Table A7.1.8.2).

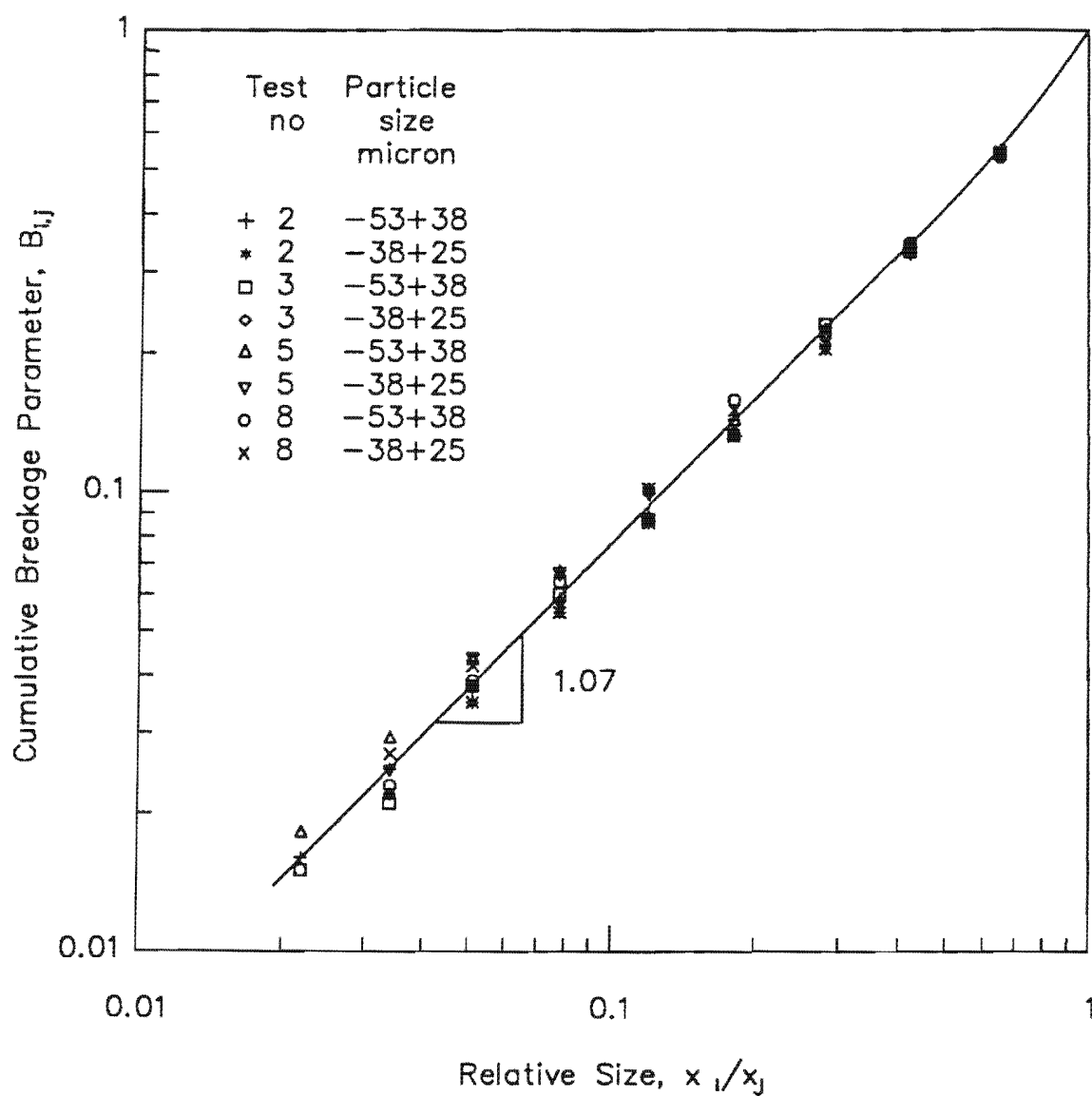


Figure 7.3. Cumulative breakage distribution parameters for -53+38 and -38+25 microns monosize feeds (experimental conditions given in Table 7.1 and data given in Table 7.2).

The breakage function for all the grinding conditions used in this study can be represented by the value of $\gamma=1.07$. The values of the cumulative breakage parameter B_{ij} can be fitted by the following empirical function

$$B_{ij} = \left(\frac{x_i}{x_{j+1}} \right)^\gamma \quad (7.7)$$

Table 7.2. Cumulative breakage function for various grinding conditions and size fractions.

Particle size	Test 2		Test 3		Test 5		Test 8	
	-53+38	-38+25	-53+38	-38+25	-53+38	-38+25	-53+38	-38+25
38.10	1.000	-	1.000	-	1.000	-	1.000	-
24.90	0.540	1.000	0.549	1.000	0.569	1.000	0.543	1.000
16.30	0.329	0.542	0.339	0.565	0.344	0.573	0.362	0.556
10.70	0.208	0.326	0.214	0.345	0.220	0.361	0.245	0.356
6.97	0.133	0.205	0.136	0.217	0.145	0.254	0.161	0.238
4.56	0.090	0.133	0.086	0.138	0.101	0.170	0.106	0.159
2.98	0.059	0.086	0.061	0.088	0.067	0.111	0.064	0.106
1.95	0.037	0.055	0.039	0.053	0.043	0.066	0.039	0.066
1.28	0.025	0.035	0.021	0.037	0.029	0.044	0.025	0.043
0.83	0.016	0.022	0.015	0.020	0.018	0.025	0.015	0.028

7.4.3. Estimation of the natural size kinetics parameters

In Chapter 6, it was shown that the results of batch grinding tests fitted to Charles' law and product size distribution was characterized very well by the Rosin-Rammler equation. This provides that the specific selection function has the following form (67,68):

$$S_i^E = AX_i^\alpha \quad (7.8)$$

where X_i is the upper limit of the interval i (microns) and A , α are the descriptive parameters that depend on the grinding conditions and properties of the material being ground.

This form of specific selection function implies that the grinding is performed on particles that are significantly finer than the size at which the selection function passes through a maximum value.

Specific selection and breakage functions can be determined from experimental data using monosize fractions for different grinding conditions. The average values of α_m and γ were calculated from the monosize tests as 1.25 and 1.07 respectively. Fixing the value of $\gamma=1.07$, the initial estimate of α_m was improved and values of A were determined by fitting the product size distributions measured in natural feed size grinding tests. The computer algorithm was used to obtain values of these parameters which resulted in the "best least squares" of the linear model to the natural size feed data. The objective function used was to minimize sum of squares = $\sum_{i=1}^n (Y_i \text{observed} - Y_i \text{calculated})^2$ where Y is the passing percent for given size.

The value of α_n , determined by the computer programme based on the Reid solution (70), was 1.23.

Variations in the estimated values of A , with changes in operating conditions, can be expressed using linear regression analysis by the following equation.

$$A = CV^{-0.473} \rho_b^{-0.146} d^{-0.832} \quad (7.9)$$

where C is 0.0139

Statistical data for the linear regression analysis is given in Appendix 7.2.

Final estimates of the specific selection and breakage functions were:

$$S_i^E = 0.0139V^{-0.473} \rho_b^{-0.146} d^{-0.832} \left(\frac{X_i}{100} \right)^{1.23} \quad (7.10)$$

$$B_{ij} = \left(\frac{X_i}{X_{j+1}} \right)^{1.07} \quad (7.11)$$

Table 7.3. Parameters of grinding kinetics in the stirred ball mill.

Test no	Monosize			Natural			
	γ	S_i^E (kWh/t) ⁻¹	α_m	Cal. S_i^E (kWh/t) ⁻¹	α_n	¹ A _b	² A _c
1	-	-	-	-	1.23	0.288	0.292
2	-	-	-	-	1.23	0.258	0.247
2(53+38)	1.06	0.104	1.28	0.118	-	-	-
2(38+25)	1.10	0.068		0.075	-	-	-
3	-	-	-	-	1.23	0.243	0.258
3(53+38)	1.08	0.110	1.24	0.118	-	-	-
3(38+25)	1.09	0.073		0.078	-	-	-
4	-	-	-	-	1.23	0.226	0.218
5	-	-	-	-	1.23	0.231	0.222
5(53+38)	1.02	0.101	1.28	0.102	-	-	-
5(38+25)	1.04	0.066		0.068	-	-	-
6	-	-	-	-	1.23	0.175	0.188
7	-	-	-	-	1.23	0.205	0.197
8	-	-	-	-	1.23	0.165	0.166
8(53+38)	1.08	0.069	1.22	0.076	-	-	-
8(38+25)	1.05	0.046		0.050	-	-	-
Average	1.07	-	1.25	-	1.23	-	-

When the values of specific selection function parameters obtained from the two monosize tests and the calculated specific selection function parameters from the natural feed size are compared in Table 7.3, it is apparent that monosize grinding processes are satisfactory. This is accurate when the upper size -53+38 microns and

1 back-calculated by the computer programme

2 calculated using Equation 7.9

-38+25 microns monosize feed samples which were 53 and 38 microns were used for the calculations. However, different sizing techniques will produce different results when analysing the same product. It was evident that there was a difference in the size measurement obtained for narrow size fractions of the material by sieving and the Malvern Particle Sizer due to the shape of the particles. It appears that the sieve diameter of the particle is less than its Malvern Particle Sizer diameter. This indicates a somewhat reduced grinding efficiency for the monosize grinding tests. In other words, the ratio of the specific breakage rate values, that is the parameter A obtained from monosize experiments, are lower than those of the natural feed size. This may be partly attributed to the initial mechanical mixing of the particles in short grinding monosize tests, although the sample was placed into the mill layer by layer and partly to the absence of fine particles, resulting in poor fluidity of the pulp at the preliminary stages of the monosize experiments. These factors may lead to lower rates of breakage but yet give the same type of breakage, and consequently the same primary progeny fragment distribution.

In conclusion, since the determination of the specific selection and breakage function from monosize tests provide the correct value of parameters, the monosize tests are essential to determine the pertinent breakage functions. Final and more reliable parameters of the specific selection functions should be determined from natural feed size by back-calculation giving optimal values α_n and A to accommodate the real system.

7.4.4. Effect of ball size on the specific selection function

It is shown in Chapter 4 that in the stirred ball mill grinding system, there is a strong relationship between the ball diameter and particle size. In this section, in the early stages of kinetic grinding studies in the stirred ball mill, the effect of ball size on the specific selection rate is investigated using balls of a single size and the "angle of nip" theory is proposed to explain the relationship between the ball diameter and particle size.

The influence of ball size on particle size can be measured most conveniently by the specific breakage rate parameters. Separate charges of balls with diameters of 6, 3, 2 mm were used for the experiments. Since the coarse monosize

feed sample prepared by a sieving technique such as -300+212 microns was above the size measurement limit of the Malvern Particle Sizer, a sieving technique was selected to evaluate the size distribution of the products.

Data derived from the experiments are shown in Figure 7.4 and Table A7.1.9. For each ball size and starting at a small particle size, the rate of breakage increased with increasing particle size, reached a flat maximum value and then decreased with a further increase in size. In all cases the specific breakage curves were of a similar shape and the position of the maximum breakage moved to larger particle sizes as the ball diameter was increased. This concept can be expressed by the empirical Equation 7.12.

$$x_m = K d^\lambda \quad (7.12)$$

where x_m (microns) is the size at which the maximum specific breakage rate occurs, d (mm) is the ball diameter and K is a constant.

Figure 7.5 and Table A7.1.10 show the relationship between the particle size which produces the maximum breakage rate and the ball diameter. The results can be fitted to a straight line. K and λ values were found to be 26.9 and 0.95. The regression coefficient of the correlation was 0.999

The results showed that the particle size giving the maximum breakage rate is directly proportional to the ball diameter, therefore there is a definite relationship between the particle size and the ball diameter. An optimum particle to ball diameter ratio was found to be 26.9.

An attempt was made by Mankosa et. al. (42) to relate the optimum ratio of ball size to feed size by the angle of nip theory for a stirred ball mill. On a coal sample used for their investigation, it was found that the maximum breakage rate was achieved when the ball size to feed size ratio was 20:1. The variations in K values is probably due to the material type and the grinding conditions.

The relationship between the ball diameter and the particle size could be explained by the "angle of nip" theory which is used to calculate the maximum feed size based on the roller size of the roller crushers (8,42,46). Since the balls rotate individually while they are moved around by the rotating shaft pins in the stirred ball

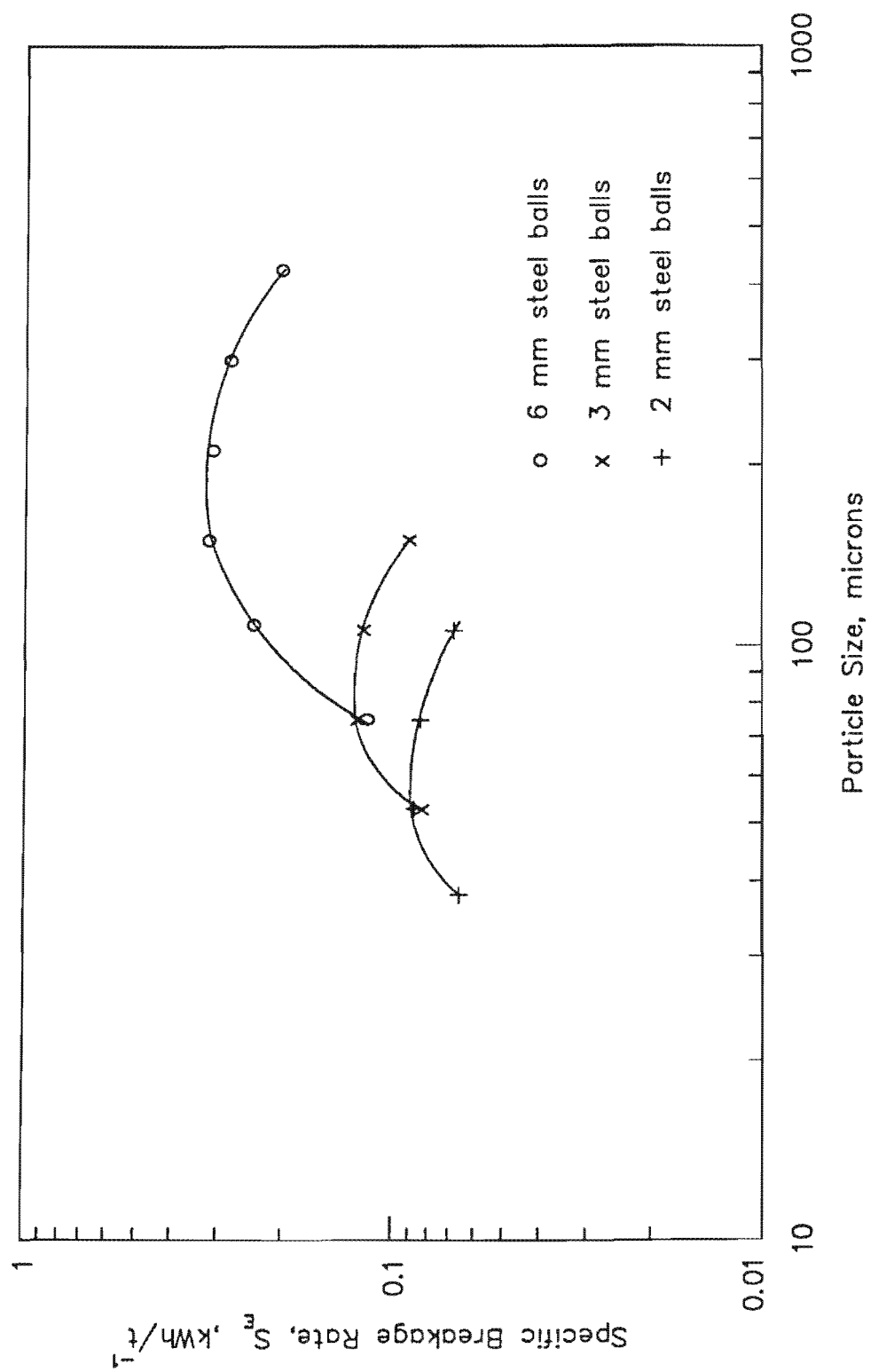


Figure 7.4. Specific breakage rate as a function of particle size using balls of various diameters: pulp density = 1950 kg/m³, media type = steel, pin tip velocity = 3.66 m/s (data given in Table A7.1.9).

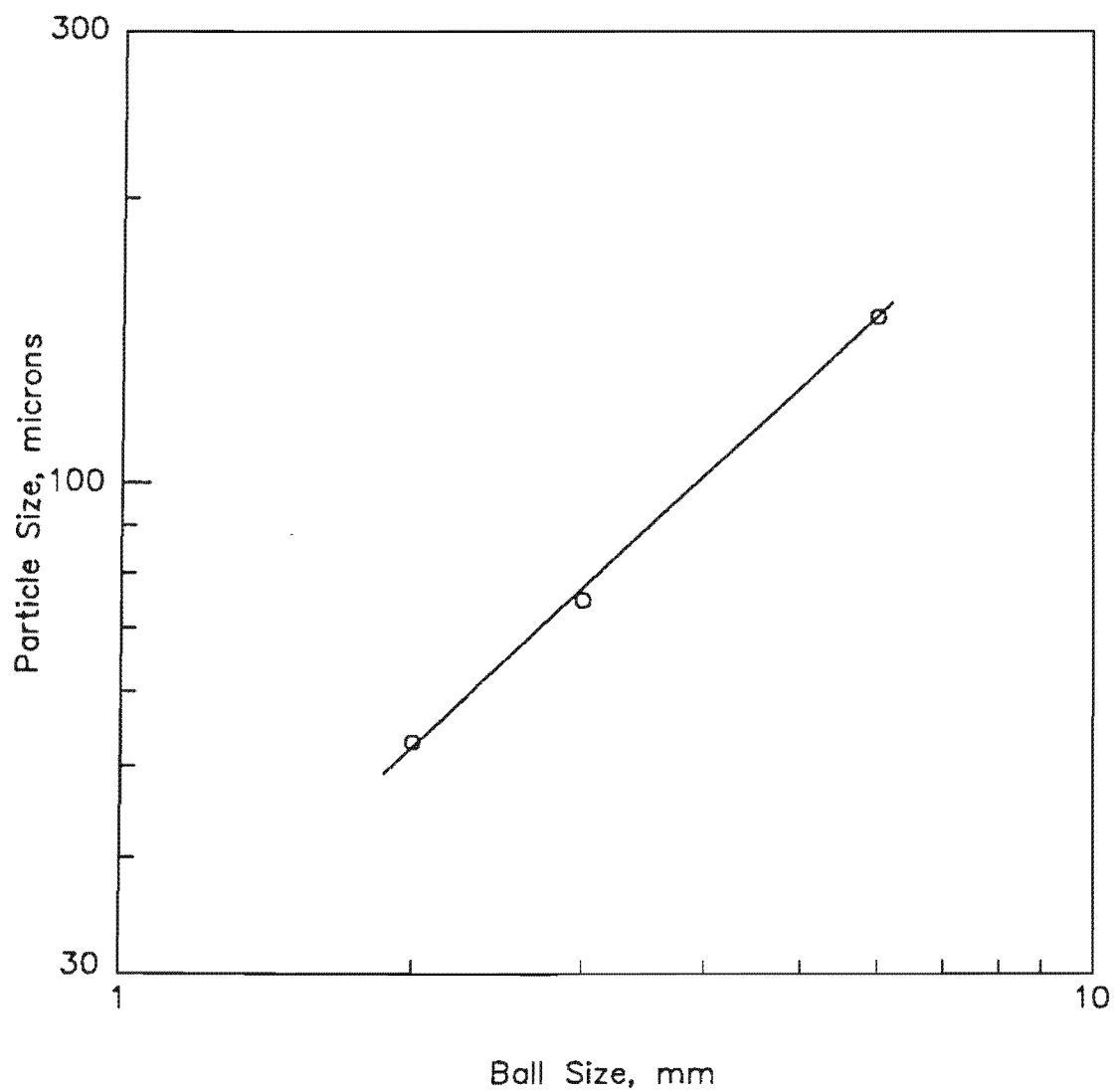


Figure 7.5. Particle size at which maximum breakage rate occurs as function of ball diameter: pulp density = 1950 kg/m^3 , media type = steel, pin tip velocity = 3.66 m/s (data given in Table A7.1.10).

individually while they are moved around by the rotating shaft pins in the stirred ball mill, the breakage might be effected by the ball surfaces gripping the particles between them. An illustration of a spherical particle held between two balls is shown in Figure 7.6.

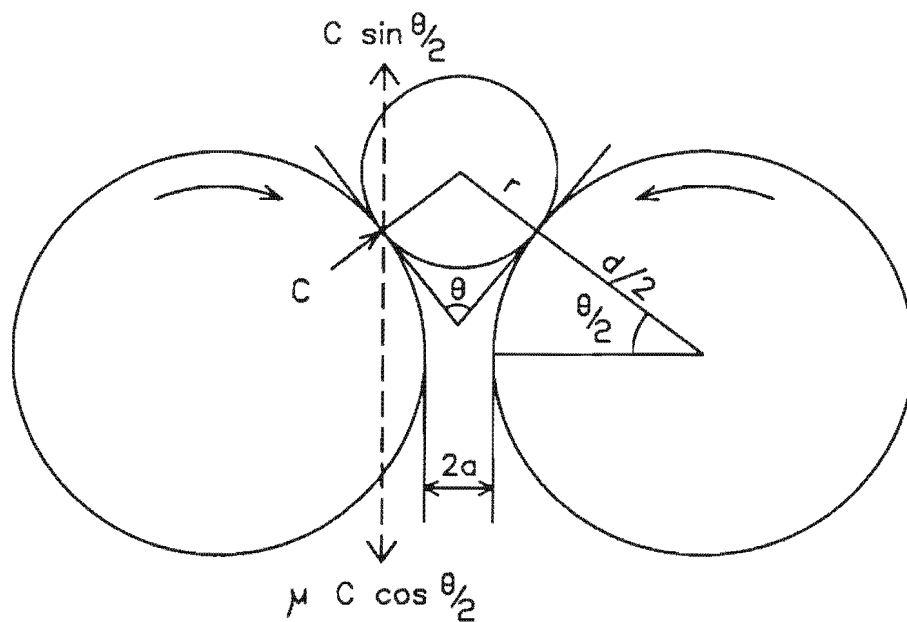


Figure 7.6. Forces exerted on the particles by two rotating balls according to the angle of nip theory

If we consider a spherical particle of radius r , being crushed by a pair of balls of radius $d/2$, the gap between the balls being $2a$, μ is the coefficient of friction between the surfaces of the balls and the particle. θ is the angle between the tangents at the two points of contact between the particle and the ball surfaces which is called the angle of nip and C is the compressive force exerted by the balls, acting from the ball centres through the particle centre. Then for a particle to be gripped by the balls,

$$C \sin \theta/2 > \mu C \cos \theta/2 \quad (7.13)$$

$$\mu > \tan \theta/2 \quad (7.14)$$

There is a maximum angle of nip at which a particle can be gripped between two balls. Beyond this maximum angle, the balls fail to nip the particles which would then slip. It should also be noted that the value of the coefficient of friction decreases with speed, so that the angle of nip also depends on the peripheral speeds of the balls. A slower peripheral speed of the balls allows the coarser particles to be nipped.

The critical ratio of ball size to particle size can be calculated by following formula 7.15 from Figure 7.6.

$$\cos \theta/2 = \frac{d + 2a}{d + 2r} \quad (7.15)$$

If the distance between two balls is considered to be negligible, the equation can be written as

$$\cos \theta/2 = \frac{R}{R + r} \quad (7.16)$$

If the optimum feed size to particle ratio is substituted in Equation 7.14, the value of 0.28 is obtained for the friction coefficient. This value is quite reasonable because the coefficient of friction between steel and most ore particles is in the range of 0.2-0.3 (46).

Although, the optimum particle size to ball size ratio can be related to the angle of nip theory applied for the roller crushers, the following parameters should be considered when the angle of nip approach is used for the stirred ball mills: (1) the nature and shape of particles, (2) pulp density and viscosity of pulp, (3) the difference in the peripheral velocity of balls depending on their location in the grinding vessel.

It can be concluded that the rate of grinding increases with decreasing ball size provided that the particles are not too big in relation to the ball diameter and that the balls contain sufficient energy for the fracture of particles. There is an optimum ball size for a given feed size which decreases with decreasing feed size. When the grinding proceeds for a long time (high energy input), an efficient size reduction can be obtained by multiple grinding stages and a progressive reduction in media size.

7.4.5. Prediction of monosize and natural size distribution by simulation

The predictive capability of the model was tested by using experimental data from monosize and natural size grinding tests. Having obtained estimates of parameters in the model Equations 7.10 and 7.11, these were used to predict the product size distributions for the grinding experiments.

Typical examples of the comparison between the experimental product size distributions of monosize and the natural feed from test 8 and linear model fit are shown in Figures 7.7 and Figure 7.8. The model simulation and the experimental results correlated very well. The model predictions and experimental results obtained from all the grinding tests are given in Appendix 7.1.

The Student t-test was carried out to measure the quality of the data fit by the linear model. The null hypothesis that there was no difference between the means of the observed and predicted data by the linear population balance model was tested. t-values and degrees of freedom ranged from 0.005 to 0.369 and from 126 to 154 respectively. The critical t-value = 1.960 at 95% confidence level given in tables (65) was much higher than those reported in Appendix 7.1 with the same degrees of freedom. As a result of this, the null hypothesis could not be rejected. R-squared values obtained from the tests ranged from 0.997 to 0.999. These results indicate that a population balance model would provide adequate predictions of the size distributions produced in the stirred ball mill.

7.4.6. Links between the empirical model in Chapter 6 and the linear population balance model.

In chapter 6, batch grinding tests showed that experimental results could be predicted using the Charles' and Rosin-Rammler equations and in this chapter it was also demonstrated that these results could be computed using a set of S and normalised B values. Consequently, there is a connection between these two

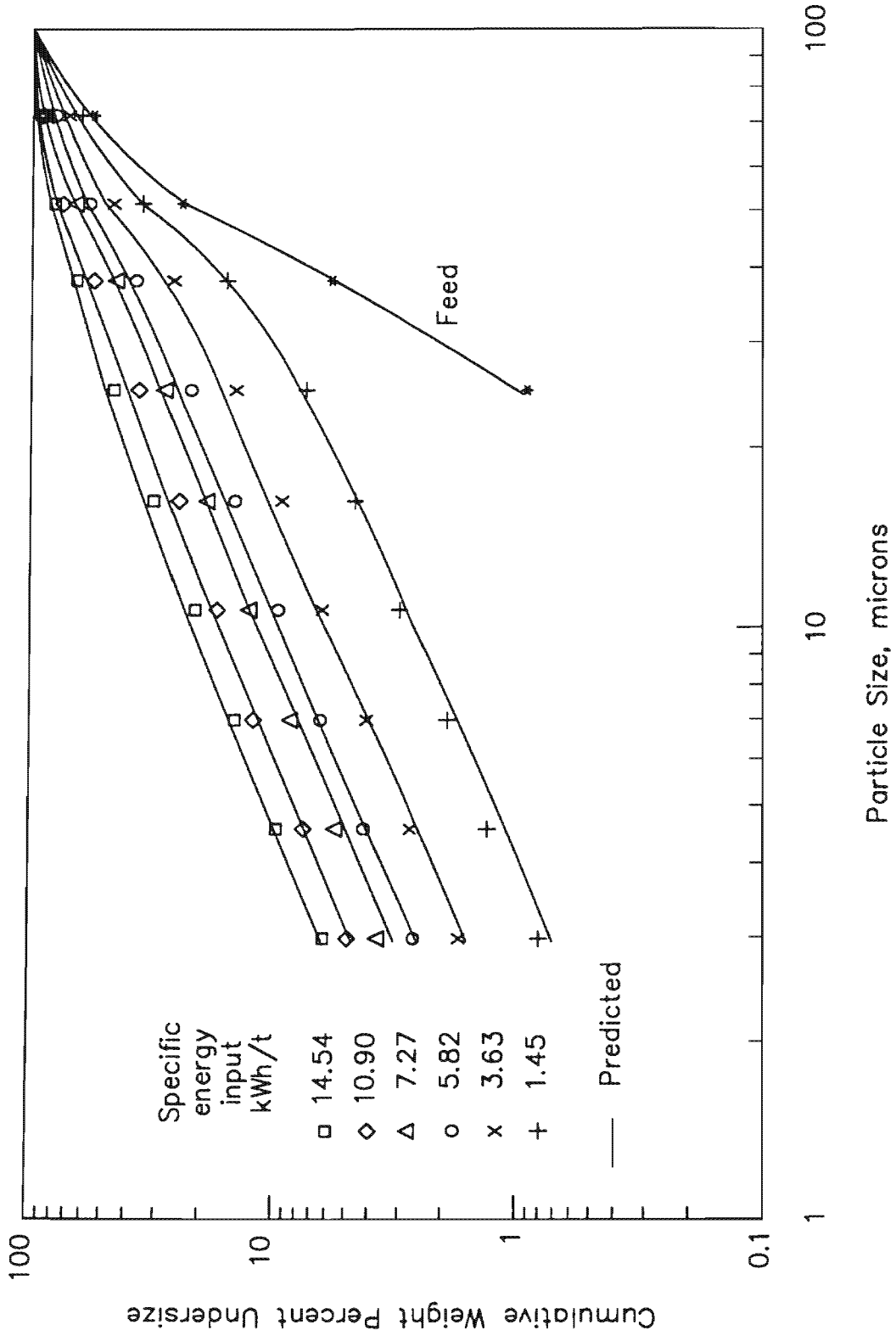


Figure 7.7. Comparison between experimental and predicted product size distributions for -53+38 microns monosize feed using grinding conditions in Table 7.1, test no: 8: pulp density = 1880 kg/m³, pin tip velocity = 3.66 m/s, ball density = 7850 kg/m³, ave. ball size = 0.005 m.

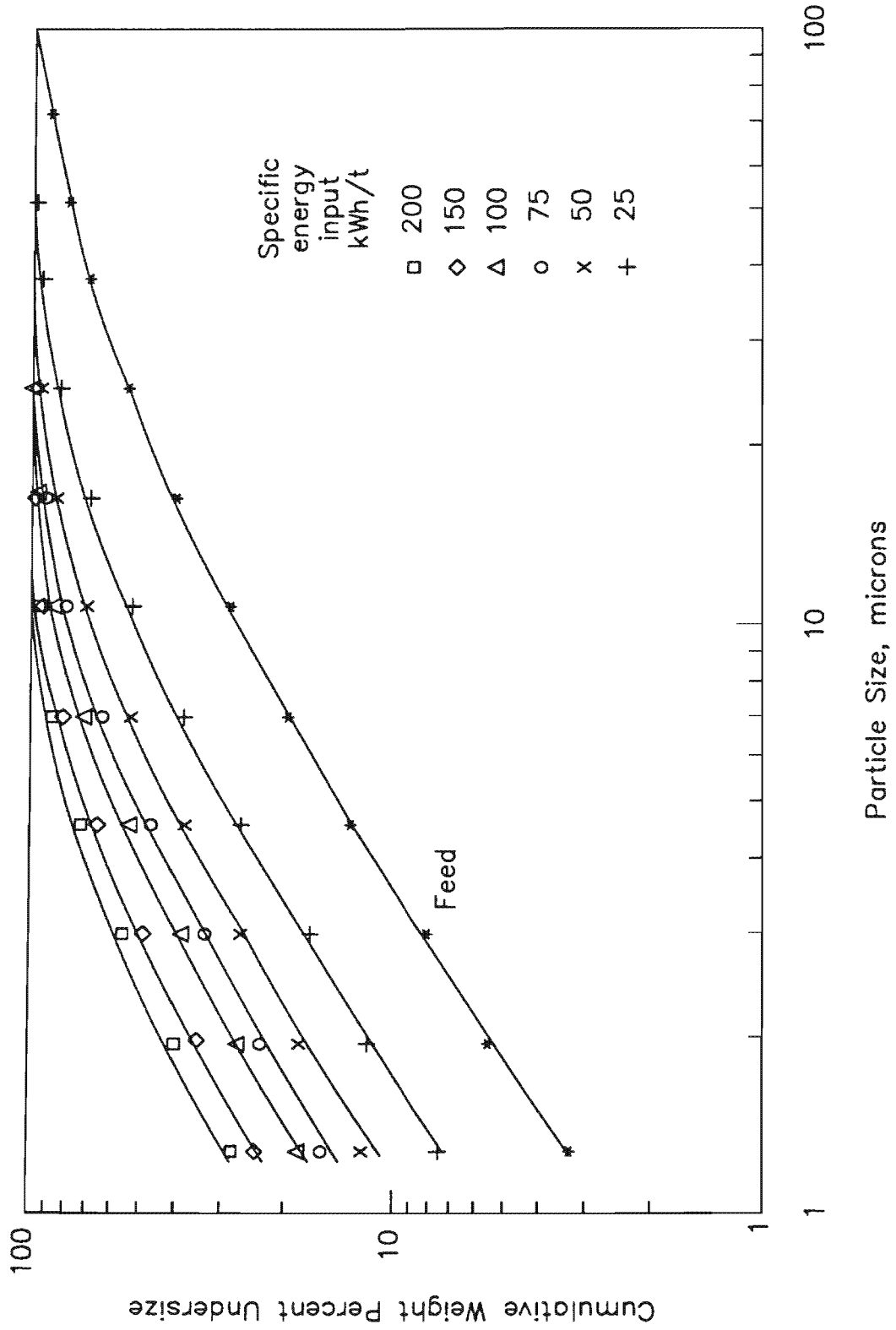


Figure 7.8. Comparison between experimental and predicted product size distributions for natural size feed using grinding conditions in Table 7.1, test no: 8: pulp density = 1880 kg/m³, pin tip velocity = 3.66 m/s, ball density = 7850 kg/m³, ave. ball size = 0.005 m.

approaches. This relationship has been shown by several researchers (67,68,73) that Charles' Law applied to batch grinding can be deduced as a special case of solution of the first order batch grinding equation.

There is a condition that gives a simple analytical solution for the batch grinding equation. It is the compensation condition, that,

$$S_j B_{i,j} = \text{function of } i \text{ only}, i \geq j \quad (7.17)$$

For example, this would apply for

$$S_j = ax_j^\alpha \quad (7.18)$$

and

$$B_{i,j} = \left(\frac{x_{i-1}}{x_j} \right)^\alpha \quad (7.19)$$

This leads to the simple solution of the batch grinding equation (67)

$$P(x,t) = 1 - (1 - P(x,0)) \exp(-S(x)t), \quad 0 \leq x \leq x_{\max} \quad (7.20)$$

Using Equation 7.18 in Equation 7.20 gives

$$P(x,t) = 1 - ((1 - P(x,0)) \exp(-ax^\alpha t)) \quad (7.21)$$

$$P(x,t) = 1 - \left((1 - P(x,0)) \exp\left(-\left(\frac{x}{k}\right)^\alpha\right) \right) \quad (7.22)$$

where

$$k = (1/at)^{1/\alpha} \quad (7.23)$$

Thus, the Rosin-Rammler equation in Equation 6.2 is obtained.

If the feed size distribution is itself a Rosin-rammler distribution,

$$k = \left(\frac{1}{at + (1/k_0)^\alpha} \right)^{1/\alpha} \quad (7.24)$$

The size modulus k varies with grinding time according to the following equation:

$$at = \frac{1}{k^\alpha} - \frac{1}{k_0^\alpha} \quad (7.25)$$

Time is usually directly related to energy in a simple batch laboratory experiment.

$$E = K \left(\frac{1}{k^\alpha} - \frac{1}{k_0^\alpha} \right) \quad (7.26)$$

Equation 7.26 is therefore identical to Charles' Law, shown in Equation 6.2.

From Equations 7.25 and 7.26 the following relationship can be obtained

$$at = \frac{E}{K} \quad (7.27)$$

Substituting Equation 7.27 into Equation 7.24 gives Equation 6.6 in Chapter 6.

In Chapter 6, it was observed that the average value of the exponent (β) of Charles' Equation was 1.25. This is approximately equal to the values of $\alpha = 1.23$ in the specific selection function equation. However, there is no reason that the exponents of the selection function (α) and the breakage distribution function (γ) should always be equal. From experimental data it was found that the selection and breakage distribution functions can be described by simple power laws. The exponents of these functions are not equal but reasonably close ($\alpha = 1.23$, $\gamma = 1.07$). For these cases, Austin (73) gave a method of estimating α , γ , δ (slope of Rosin-Rammler size distribution) values.

CHAPTER 8

CONTINUOUS GRINDING EXPERIMENTS

8.1. TESTWORK

The research was carried out on the continuous grinding operation of the stirred ball mill so that the results could be used for correlation of batch and continuous milling.

The continuous tests were conducted to determine the influence of different feed rates on grinding efficiency and power consumption of the 50 litre stirred ball mill (30 cm in diameter and 71 cm high).

Operating grinding conditions and the results of continuous grinding are presented in Table 8.1.

The feed rate was varied over a range from 428.8 kg/h to 167.0 kg/h. The steady torque was around 590 Nm for all the continuous grinding experiments. The slurry solids content of the new feed for all tests averaged 61.2%. However, it was approximately 4.6% higher in the mill. The batch tests were also run using a 5 litre stirred ball mill under conditions similar to those used for the continuous tests. The 50% passing size of the continuous and batch grinding products as a function of energy input level is plotted in Figure 8.1.

The results show a good fit to the straight line.

$$E = 446.7d_{median}^{-1} \quad \text{corr.coef.} = 0.993 \quad (8.1)$$

Based on the median size of the product, the continuous grinding required the same power as that consumed in batch grinding when the equivalent conditions were used.

Table 8.1. Experimental conditions and results for the continuous and batch tests at equivalent conditions:
 6 mm steel balls, pin tip velocity = 2.45 m/s, pin spacing = 2.5 cm, pin diameter =1.6 cm
 (data shown in Figures 8.1).

Grinding mode (Mill size)	Feed rate kg/h	Water flowrate l/h	Pulp density Solids % by weight		Specific Energy Input kWh/t	Feed d50 microns	Product d50 microns
			Product	In the mill			
Continuous (50 litre)	428.8	252.9	62.9	68.3	30.2	370	15.1
	277.1	159.8	63.4	67.2	44.9	370	9.3
	167.0	124.4	57.3	61.9	75.4	370	6.1
Batch (5 litre)	-	-	68.3	68.3	30.2	370	15.6
	-	-	67.2	67.2	44.9	370	10.0
	-	-	61.9	61.9	75.4	370	5.7

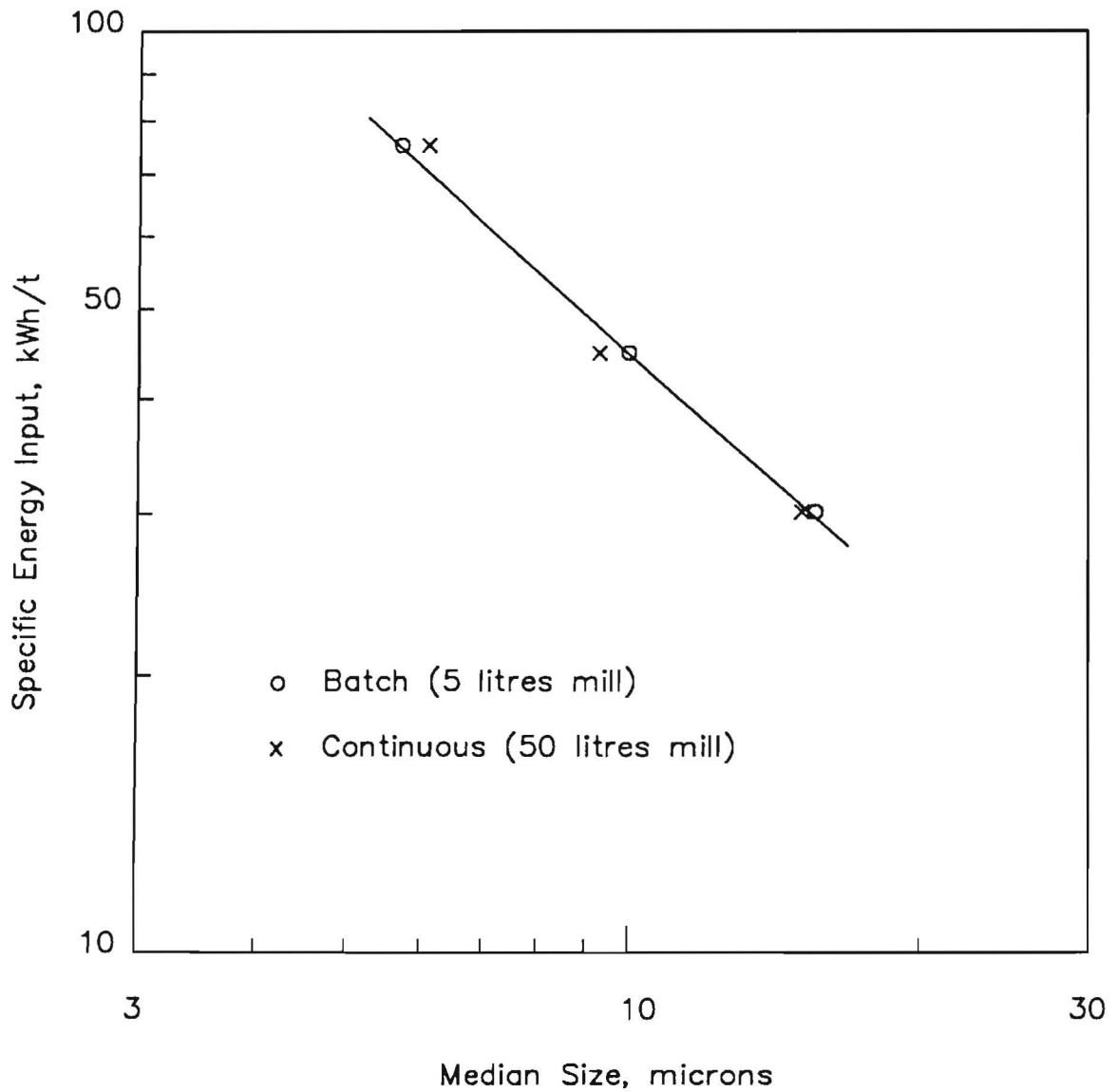


Figure 8.1. Median size of the product from the continuous and batch grinding of stirred ball mill as a function of specific energy input: feed size(d_{50}) = 370 mic., 6 mm steel balls, pin tip velocity = 2.45 m/s, pin spacing = 2.5 cm, pin diameter = 1.6 cm, (data given in Table 8.1).

However, complete evaluation of the grinding efficiency could only be gained by comparing the complete particle size distributions. The complete size distribution of products obtained by the batch and continuous methods are presented graphically in Figure 8.2 (Table A8.2). The plotted data show that the particle size distribution of products in the batch and continuous grind show a reasonably close agreement in the fine size fractions. However, continuous grinding gave a higher percentage of coarse sizes.

8.2. RESIDENCE TIME DISTRIBUTION

No effort has been directed towards determining residence time distribution (RTD) in the vertical stirred ball mill therefore preliminary residence time experiments were run to obtain knowledge of RTD essential for constructing an accurate simulation of the stirred ball mill.

8.2.1. Experimental Methods

Three impulse type experimental techniques were considered to measure the residence time distributions.

a) Radioactive tracer method: Although the use of irradiated chromite samples would give satisfactory results, this method was rejected because it required not only sophisticated instrumentation but also introduced hazards and costs which made the method impractical.

b) Magnetite as a tracer material: Solid flow behaviour was studied using a tracer of magnetite from the Phalaborwa complex. The tracer material used was a single size magnetite mineral which has a specific gravity of 5.17 g/cm³ and a hardness of 6.0 on Moh's scale.

It was assumed that magnetite behaves in the same manner as chromite in the stirred ball mill because of its similarity in hardness and specific gravity.

A 20 litre stirred ball mill was used for the experiments. When steady state conditions were established in the mill, the chromite feed was interrupted for 2.6 minutes and 500 g magnetite was added. By this method the average overall feed rate was maintained. After the tracer material was fed through the shaft into

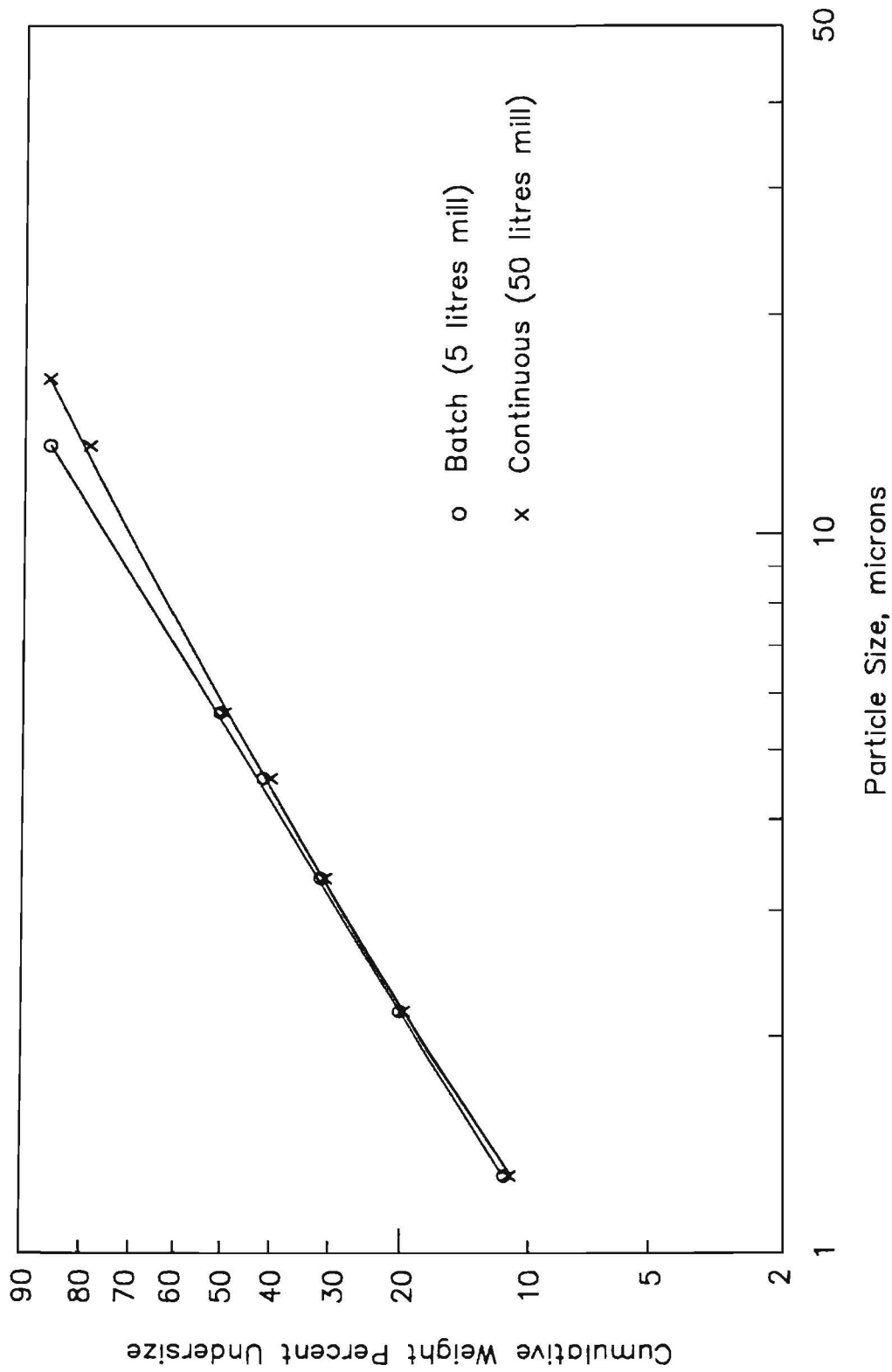


Figure 8.2. Comparison between size distribution of batch and continuous grinding products at 75 kWh/t energy input: feed size(d50) = 370 mic., pulp density = 61.9% solids by weight, 6 mm steel balls, pin tip velocity = 2.45 m/s, pin spacing = 2.5 cm, pin diameter = 1.6 cm (data given in Table A8.2).

the vessel, 1 minute samples were collected at 10 minute intervals in beakers and the tracer of magnetite was separated using a Davis Tube. The RTD's of the tracer were determined by weighing the magnetite sample. However, it was found that the recovery of fine magnetite samples by means of the Davis Tube was not accurate. The method was therefore unsatisfactory.

c) Salt solution: The water flow was investigated by the addition of NaCl as a concentrated solution.

The experiments were performed in the 50 litre stirred ball mill. The following conditions were used. The stirred ball mill was run at a pin tip velocity of 2.45 m/s. The pulp density was approximately 61.2% solids by weight. The ball charge consisted of 6 mm steel balls. The solid feed rate ranged from 428.8 kg/h to 167.0 kg/h

Steady state conditions were established by feeding chromite ore and water at desired feed rates until the pulp density of the mill discharge was the same as the pulp density of the feed and did not change with time. A 50 cc salt solution containing 10 g salt was injected directly into the inlet of the mill by means of a syringe. As soon as the salt solution was added, the slurry which was leaving the mill was collected at constant short time intervals in buckets. The supernatant liquid was filtered and the salt content of each sample was determined by means of a conductivity meter.

8.2.2. Results and Discussions

The mean residence times of the pulse response curve for salt are evaluated by the following formula.

Formula for calculating t_{mean} of salt RTD at equal time increments

$$t_{mean} = \frac{\sum_{i=1}^n t_i C_i}{\sum_{i=1}^n C_i} \quad (8.2)$$

where t_i is the average time in interval and C_i is the tracer concentration at the mill exit at various times.

The mean residence times of solids are defined by dividing the final hold-up weight of solids by the feed rate of solids. The mean residence time of water can also be calculated in the same manner. All data and estimated mean residence times of salt solution are shown in Table 8.2.

Table 8.2. The mean residence times of calculated solids and water and of tracer curves: mill size= 50 liters, feed size (d_{50}) = 370 mic., ave. pulp density = 65.8% solids by weight, 6 mm steel balls, pin tip velocity = 2.45 m/s, pin spacing = 2.5 cm, pin diameter = 1.6 cm

Energy Input KWh/t	t_{mean} minutes		
	Solid	Water	Salt
30.2	5.2	3.8	3.8
44.9	7.8	6.6	6.1
75.4	11.0	9.1	8.5

A comparison of the mean residence times of solids and water shows that for the solids they are greater than that for water and both of the mean residence times for solids and water are higher than those for the salt solution with the exception of 3.8 minutes.

Figure 8.3 illustrates the plot of the normalized concentrations of NaCl in the mill discharge of the impulse sample test against dimensionless time under the grinding conditions mentioned above. Normalization of the tracers was performed by dividing the measured concentration by the input of tracer concentration. The mid-point of each time interval was divided by the mean residence time to give the dimensionless time. The individual sample concentrations were plotted versus the dimensionless time to obtain the instantaneous impulse function. All relevant data is shown in Table A8.1.

One of the methods of treating RTD is to consider the RTD as equivalent to that from a number of fully mixed reactors or tanks in series.

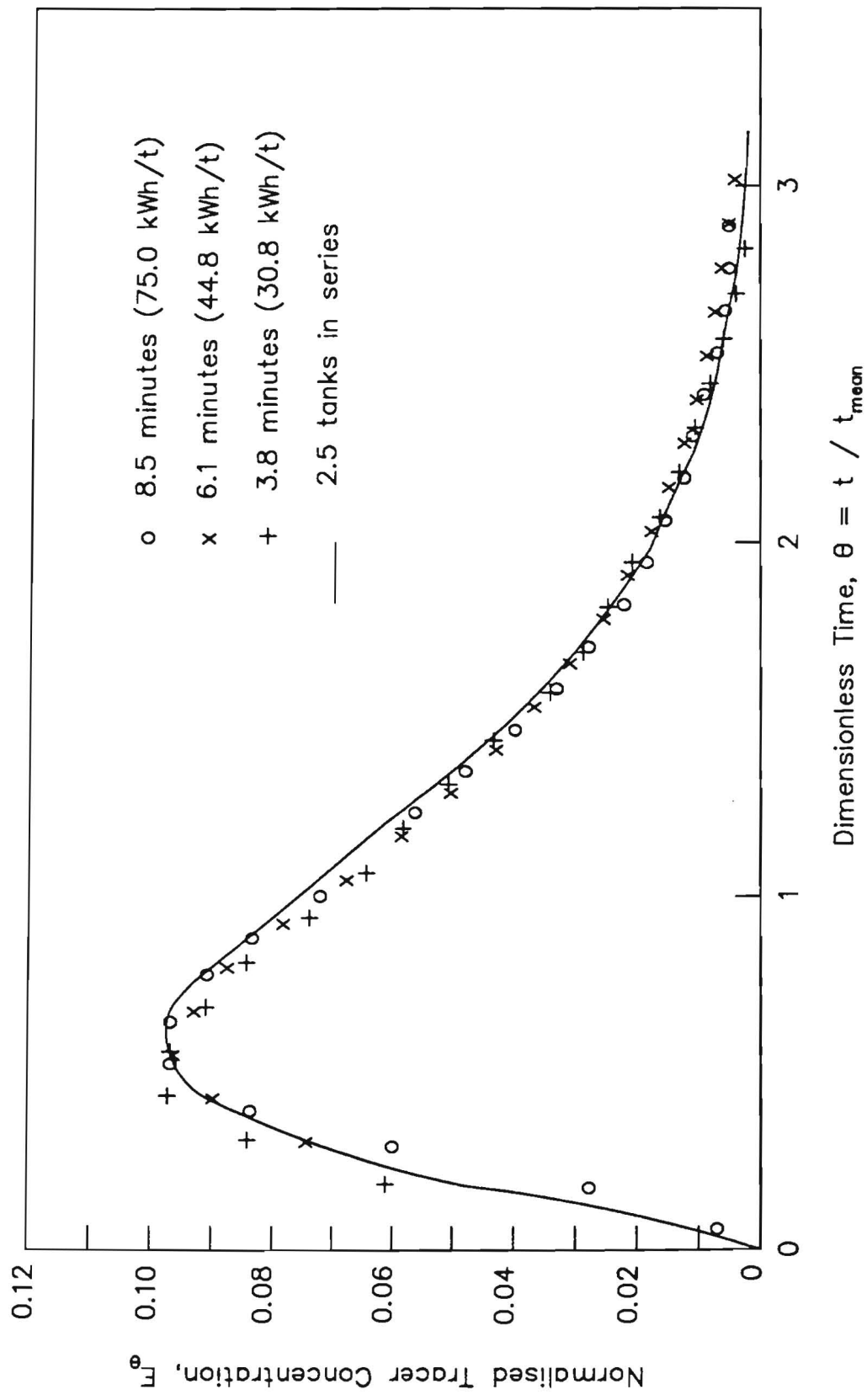


Figure 8.3. Comparison of experimental and model dimensionless R.T.D. functions: feed size(d_{50}) = 370 mic., ave. pulp density = 65.8% solids by weight, 6 mm steel balls, pin tip velocity = 2.45 m/s, pin spacing = 2.5 cm, pin diameter = 1.6 cm (data given in Table A8.1).

The shape of the plots of salt content is essentially the same as that of a theoretical curve 2.5 tanks in series. The solid line represents that curve which would be generated using a 2.5 tanks in series equation which is as follows

$$E_{\theta} = N(N\theta)^{(N-1)} \frac{1}{(N-1)!} e^{-(N\theta)} \quad (8.3)$$

where E_{θ} is the normalised tracer concentration, θ is the dimensionless time and N is number of tanks.

The product size distribution from the batch test and the continuous test at an energy input of 75 kWh/t and simulated results on a Rosin-Rammler graph are shown in Figure 8.4 (Tables A8.2 and A8.3). The results demonstrated that in practice, 2.5 tanks in series model and the real system in continuous system do not meet exactly. The real system has flow characteristics which is intermediate between plug flow and 2.5 tanks in series.

A comparison of the size distribution of products from batch and continuous grinding showed that continuous grinding products contained a higher percentage of coarser fractions. A possible explanation for this is that in the batch laboratory mill, all the solid particles remained inside the mill for the same time. In addition, the average particle size distribution environment within the mill changed with time. On the other hand, in the continuous grinding tests solid particles entering the mill simultaneously left it at different times.

When the tanks in series model was used to study the residence time distribution of water flow, it was assumed that all the particles had the same liquid flow velocity regardless of their size. The reasons for the diversity of the results by continuous grinding and the 2.5 tanks in series model might be due to a consistently smaller mean residence time of water which means that the slurry density is higher in the mill than in the feed and exit streams, which will affect the viscosity in the mill. Besides that, if the solids transportation through the mill is particle size dependant, the fine particles move more rapidly than the coarser material. This size dependence gives rise to internal classification in the mill. As a result of this reasoning, the solid residence time in the stirred ball mill cannot be fully characterised by the behaviour of the salt solution.

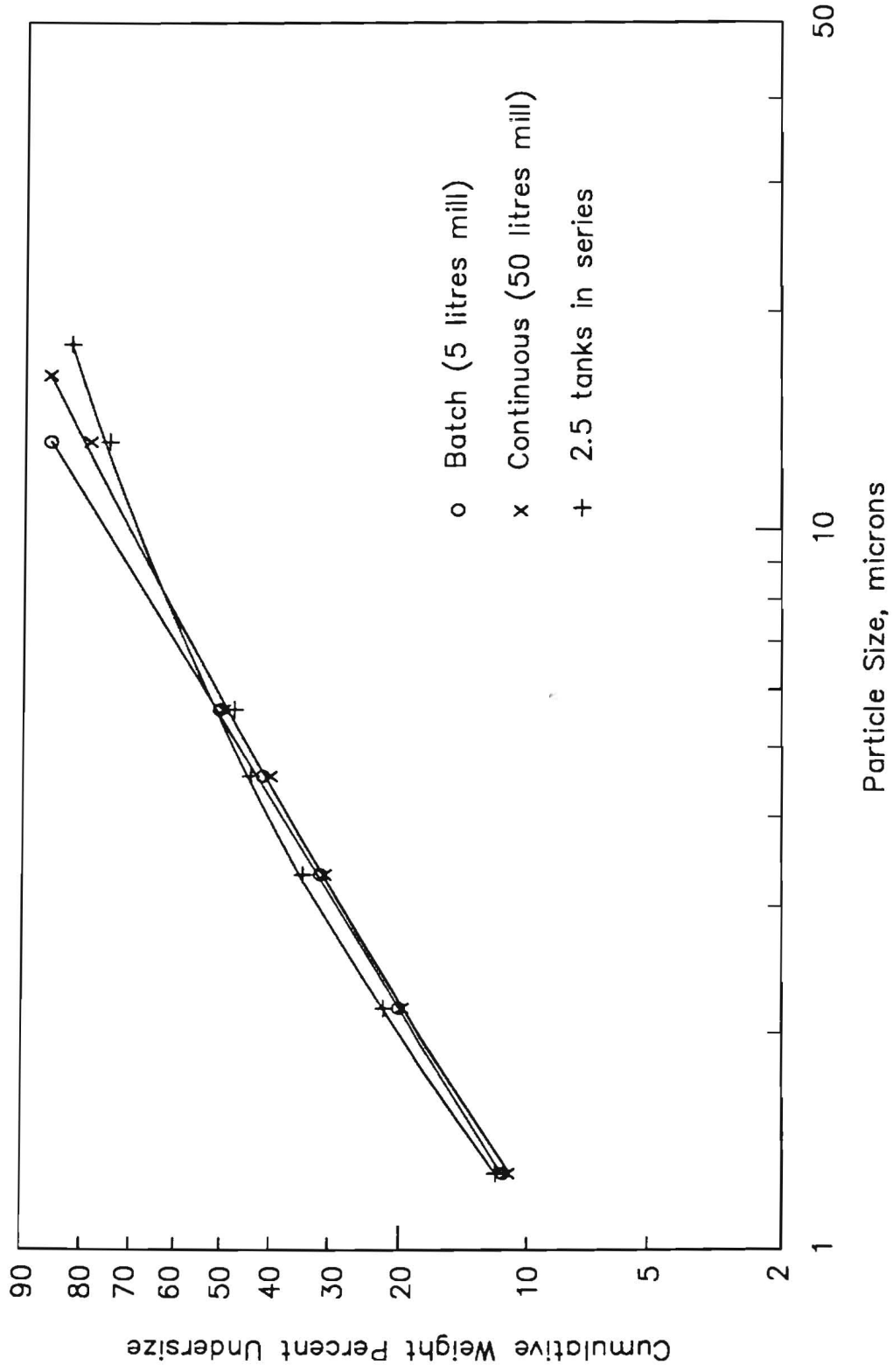


Figure 8.4. Comparison between size distribution of batch and continuous grinding and calculated products at 75 kWh/t energy input: feed size(d50) = 370 mic., pulp density = 61.9% solids by weight, 6 mm steel balls, pin tip velocity = 2.45 m/s, pin spacing = 2.5 cm, pin diameter = 1.6 cm (data given in Table A8.2).

CHAPTER 9

MILL POWER

9.1. INTRODUCTION

Power consumption is one of the prime variables considered in determining the design and operating conditions for any mill. There is very little published data available regarding power correlation specifically for the vertical stirred ball mill. There are even only a few articles in the literature dealing with the shaft torque required in mixing granular materials, although in the process industries, there are many instances where it is necessary to force an object, sometimes in the form of a blade, through a bed of particulate solids. In the beginning, the impracticability of a direct mathematical solution on agitator power correlation led to an empirical approach. The subject however has much in common with the use of dimensional analysis, with methods of analysis in fluid dynamics and with the theory of models.

9.2. LITERATURE SURVEY

A few researchers have studied the effect of moving objects or blades through a granular material. Bagster, D.F., et.al. (51) have made studies on the mixing of granular materials and the forces required to move blades through beds of cohesionless particles. The apparatus for determining the effective force vector such as the horizontal and vertical components of force and the effective point of action is described. The influence of the following parameters on the force vector has been studied: the type of particulate material (angle of friction, bulk density), the roughness of blade, the velocity of blade, the size of blade and its depth of immersion. An attempt was made to provide a semi-empirical correlation based on the elementary soil mechanics theory.

Novasod, J. (52-55) has investigated the movement of the particles around a blade rotating in a vessel with granular material. The space in the vicinity of the blade was divided into three regions in a radial direction and into eleven regions in an axial direction. The slip lines and the stream lines were determined photographically. In some regions theoretical slip lines were constructed and these

were compared with the experimental results. A combination of analytical and graphical methods was used to determine the stress distribution on the blade of an impeller. A dimensionless function of the internal and external friction angles was derived giving the normal stress on a blade in a unit depth in a granular material of unit bulk density. The effects of geometrical parameters and the material properties of the granular material in the vessel on the shaft torque were studied. A semi-empirical correlation was determined to calculate the critical depth above which the torque remained almost constant and the critical moment of the granular bed which was measured at the critical depth of the granular material bed. A dimensionless equation was derived to determine the shaft torque for below the critical depth of the bed.

Impellers of many types have been used to produce agitation and mixing in the liquid phase. White and his co-workers (57) were the first to point out the possibility and advantage of correlating the performance of mixing impellers by use of dimensional analysis and a study of models. Hixson and his colleagues (58) made further theoretical analyses and gave substantiation to the theory by experimentation. An extensive research programme was initiated by Rushton, J.H., et.al. (59,60) to study the properties of the impeller, tank and fluid over wide ranges of power, size and physical properties and they showed the advantage of correlating the performance of the mixing impeller by use of dimensional analysis. Two extremes were identified: the fully baffled mixer and the unbaffled mixer which developed a vortex at higher speeds. Three dimensionless groups were used for a complete correlation for different flow regimes.

Sepulveda, J.L. (28,32) ran a set of tests to provide data to establish the energy consumption characteristics of the stirred ball mill and he stated that the power characteristics of the stirred mill were comparable to those of a completely baffled radial flow turbine mixer.

9.3. POWER EQUATIONS

In this section, the design procedures for agitators using dimensional analysis and the concept of fluid dynamics are outlined. An attempt was made to establish a fundamental concept that formed a basis for a design method to

scale-up the stirred ball mill. Using regression analysis a semi-empirical equation was also developed by using experimental results to determine the stirred ball mill scale-up requirements.

9.3.1. Dimensional analysis

A general dimensionless equation for agitator power may be derived by using dimensional analysis. The impeller power could be a function of the geometrical boundary conditions, shape of the impeller and gravitational force.

It is possible to relate two boundary conditions in similar fluid flow motion and the mathematics derived from the dimensional analysis of similarity can be used for scale-up purposes.

There are three types of similarity.

Geometrical similarity: it requires that all corresponding dimensions have the same ratio as all other corresponding boundary dimensions.

Dynamic similarity: the ratios of masses and forces at corresponding points are equal.

Kinematic similarity: the patterns or paths of motion are alike and the velocities at corresponding points are in the same ratio.

When the fluid motion is analysed using the Buckingham P_i theorem (61), the general dimensionless Equation 9.1 can be obtained for the relationship of the following variables. The variables involved are: fluid viscosity μ_f , impeller diameter L , shaft rotation speed N , fluid density ρ_f , gravitational g and power P . All other dimensionless variables are expressed as ratios to the impeller diameter, such as; tank diameter D , liquid depth H , distance of impeller from bottom C , pitch of impeller O , width of impeller blades W , length of impeller blade M , width of baffles J , number of blades on impeller B , number of baffles R and the reference number No being determined by convenient choice.

$$f\left(\frac{\rho_f L^2 N}{\mu_f}, \frac{LN^2}{g}, \frac{L^5 N^3 \rho_f}{P}, \frac{L}{D}, \frac{L}{H}, \frac{L}{C}, \frac{L}{O}, \frac{L}{W}, \frac{L}{M}, \frac{L}{J}, \frac{B}{No}, \frac{R}{No}\right) = 0 \quad (9.1)$$

Dimensional analysis reduces the number of independently variable quantities that describe a problem by combining the variables into dimensionless groups. Although fluid agitation involves a large number of geometrical, operation and physical variables, a relatively small number of physically significant dimensionless groups can be established.

For geometrically similar systems Equation 9.1 may be stated as

$$f\left(\frac{\rho_f L^2 N}{\mu_f}, \frac{LN^2}{g}, \frac{L^5 N^3 \rho_f}{P}\right) = 0 \quad (9.2)$$

It is possible to simplify Equation 9.2 and write it in the following form

$$N_p = K(N_{Re})^a (N_{Fr})^b \quad (9.3)$$

The power number (N_p) relates imposed forces to inertial forces ($P/L^5 N^3 \rho_f$). The Reynolds number (N_{Re}) can be used to characterize the flow type and it presents the ratio of the inertial forces to viscous forces ($\rho_f L^2 N / \mu_f$). If the tank has no baffles the fluid may form a vortex. Under these conditions, the Froude number (Fr) must be introduced. It is the ratio of the inertia force to the gravitational force (LN^2/g).

For many cases where $(N_{Fr})^b$ is equal to 1 or its effect negligible, Equation 9.3 can be written

$$N_p = K(N_{Re})^a \quad (9.4)$$

To correlate the performance in terms of power equation, Equation 9.4 may be expressed and written:

$$P = \frac{K}{g} \rho_f N^3 L^5 \left(\frac{L^2 N \rho_f}{\mu_f}\right)^a \quad (9.5)$$

where g is the gravitational conversion factor.

A typical graphical representation of a relationship between the power number (N_p) and the Reynolds number (N_{Re}) on a log-log plot is shown in Figure 9.1.

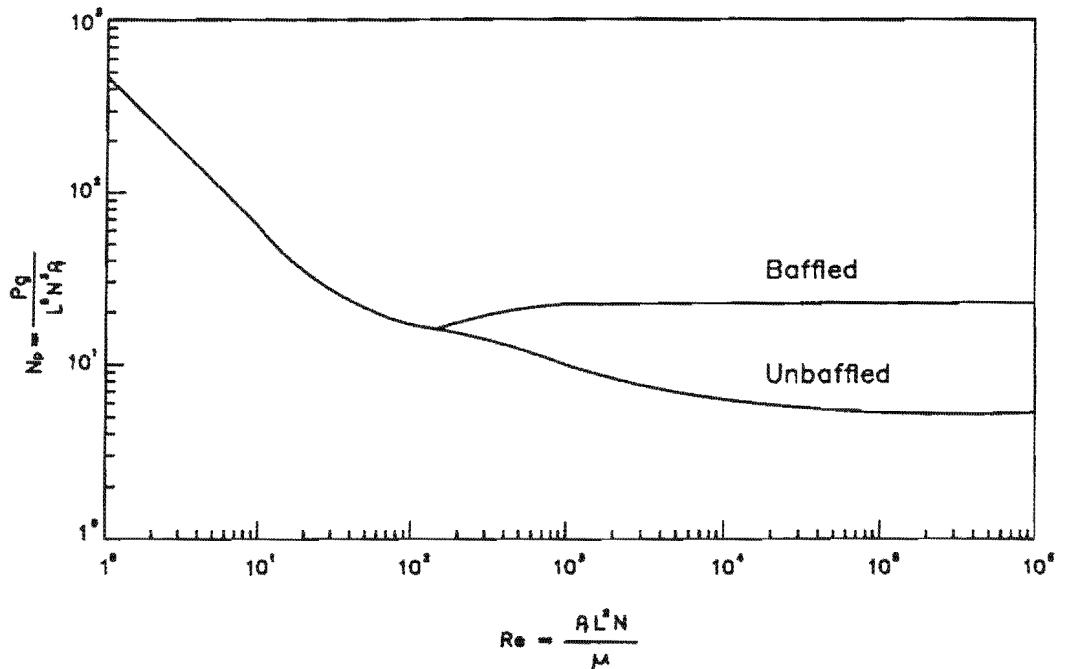


Figure 9.1. Typical power characteristics of a mixing impeller (ref.62).

Turbulent regime:

When the curve has a slope of zero at higher Reynolds numbers, Equation 9.4 reduces to:

$$N_p = K \quad (9.6)$$

$$P = \frac{K}{g} \rho_f N^3 L^5 \quad (9.7)$$

This is in the turbulent range with geometric similarity. Power can be stated to be proportional to density, to impeller speed cubed, to diameter to the fifth power and independent of viscosity.

Laminar regime:

It is apparent from the plot in Figure 9.1 that the slope of the curve is -1.

$$N_p = K(N_{Re})^{-1} \quad (9.8)$$

$$P = \frac{K}{g} \mu_f N^2 L^3 \quad (9.9)$$

For the low Reynolds number range the power is proportional to fluid viscosity, to the square of impeller speed and the cube of impeller diameter.

9.3.2. Fluid dynamics

The power consumption in the stirred ball mill can be related to the pressure distribution over the surface of the pins. The pressure calculations can be based on the integration of Newton's law expressing the friction drag resulting from relative motion between a body and a fluid in contact (Figure 9.2). Newton's law is

$$F = CA \frac{V^2 \rho_f}{2g} \quad (9.10)$$

where F is a drag force, C is a dimensionless constant and is a function of the Reynolds number in the laminar region. However, it is independent of the Reynolds number in the turbulent region, A is an area on which the force is considered to act and ρ_f is fluid density.

When one of the rotating shaft pins which has a diameter of w moves through the bed of grinding media (grinding media density, ρ_b) in the turbulent region at a velocity of V which is at a section at a distance of l from the centre line of the shaft, the resisting force of the grinding media exerted on an element of area ($w dl$) may be expressed

$$df = C \frac{1}{2} \rho_b V^2 w dl \quad (9.11)$$

The pressure distribution over the pins could then be integrated to give the torque acting on the pin. The power could be calculated directly from the total torque and rotation speed of the shaft.

The differential contribution to the ideal shaft torque for the section of the pin from l to $l+dl$ is given by the expression:

$$dT = df \cdot l \quad (9.12)$$

$$dT = C \frac{1}{2} \rho_b V^2 l w dl \quad (9.13)$$

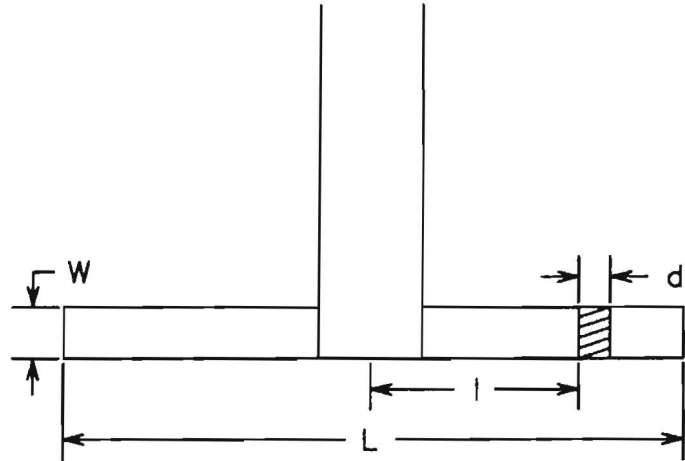


Figure 9.2. Illustration for derivation of power equation based on fluid dynamics

V is directly proportional to the velocity of the differential section and it can also be described by

$$V = C_1(2\pi Nl) \quad (9.14)$$

where N is shaft rotation speed. Substituting Equation 9.14 in Equation 9.13,

$$dT = C \frac{1}{2} \rho_b C_1^2 (2\pi N)^2 l^3 w dl \quad (9.15)$$

On the integration between the limits from $l=0$ to $l=L/2$ the torque acting on a single pin is

$$T = C \frac{1}{2} \rho_b C_1^2 w (2\pi N)^2 \int_0^{L/2} l^3 dl \quad (9.16)$$

$$T = C_2 \rho_b w N^2 L^4 \quad (9.17)$$

The power needed to overcome this force is

$$P = \frac{2\pi}{60} \times \text{torque} \times \text{shaft rotation speed}$$

$$P = \frac{2\pi}{60}TN \quad (9.18)$$

Therefore the power is proportional to

$$P = C_3\rho_b wN^3L^4 \quad (9.19)$$

9.3.3. Theory of mill power

The purpose of this section is to make an attempt to develop a torque model which could produce a basic understanding of the physical processes involved in the mill and to establish a semi-empirical equation which includes the ball diameter and shaft geometry to predict the mill power draw.

To establish the energy consumption characteristics of the stirred ball mill, a vast number of experiments were run to provide data for the construction of a torque model and a semi-empirical power equation by nonlinear regression analysis. The torque required in different operating and design conditions to drive the stirring mechanism was measured directly from the shaft.

A summary of test conditions and experimental results is given in Appendix 9.

For stirred ball mills, there are three regions in the torque versus pin tip velocity plot (Figure 9.3). The start-up torque region (A) where the torque is very high due to the static friction force and locking of the grinding media. In the second region (B) where the grinding media is stirred in a vertical vessel at a low speed, the plot is almost an horizontal straight line, the torque exerted on the vessel is then a function of the torque applied on the bottom (T_b) and the wall of the vessel (T_w) by the mass in the mill. In the third region (C), the torque increases with increasing pin tip velocity and the torque is proportional to the pressure exerted due to the centrifugal force of the mass on the wall of the vessel (T_c).

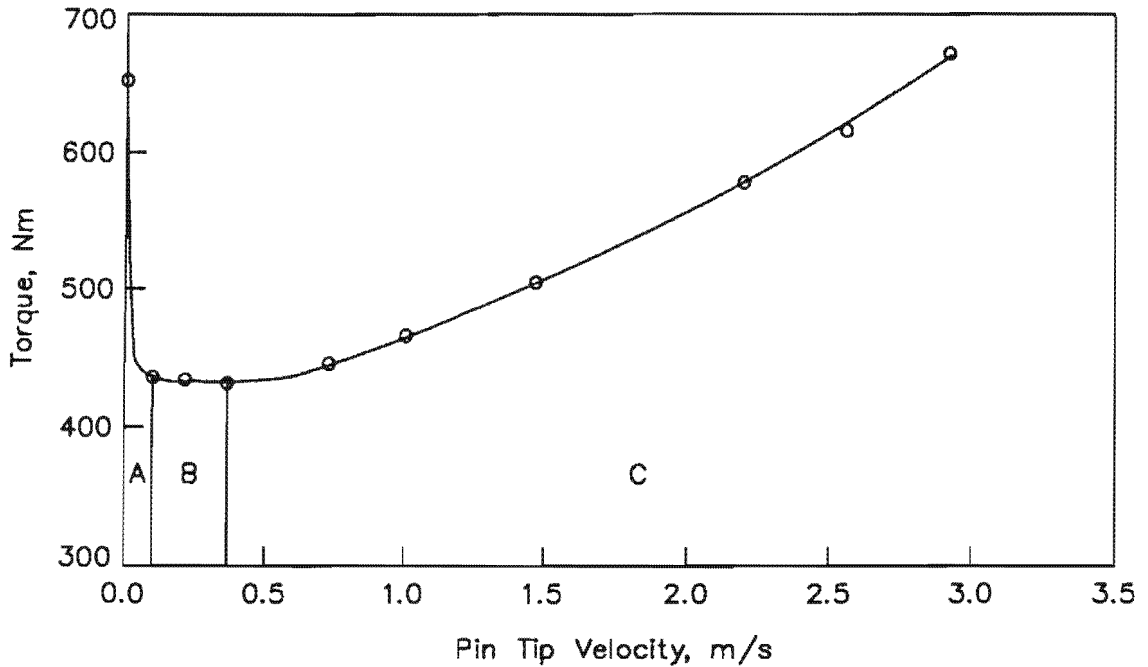


Figure 9.3. Typical torque curve as a function of pin tip velocity for stirred ball mill (Experimental conditions and data given in Table A9.3).

An equation for the total torque exerted on the vessel can be expressed in the following simplified form:-

$$T = A + BV^a \quad (9.20)$$

where V (m/s) is pin tip velocity and a is an exponent.

$A = (T_b + T_w)$ which refers to region B

$BV^a = (T_c)$ which refers to region C

They may also be expressed as a function of the following principal parameters which are considered in developing the torque equation

$$(T_b + T_w) = f(s, w, d, \rho_b, \rho_p, H, D) \quad (9.21)$$

$$T_c = f(s, w, d, \rho_b, \rho_p, H, D, V) \quad (9.22)$$

where s = pin spacing (m)
 w = pin diameter (m)

1 The distance between the centre lines of the nearest two pins

- d = ball diameter (m)
 ρ_b = ball density (kg/m^3)
 ρ_p = pulp density (kg/m^3)
 H = mill load height at rest (m)
 D = mill diameter (m)

The effect of particle size on the torque was clearly evident during the batch grinding experiments up to an energy input of approximately 25 kWh/t when a relatively narrow coarse feed size (-600+100 microns) was used (Figure 4.3). As grinding proceeded, the particles became progressively finer and the torque became stable. However, in the continuous grinding, the mill content contained a mixture of coarse and fine particles. Even when a feed size coarser than 100 microns was used, where the stirred mill was less efficient than the tumbling mill, the torque remained almost constant for various feed rates during the continuous grinding experiments as indicated in Chapter 8. As a result of this, the effect of particle size was not included in the torque equations.

9.3.3.1. Torque model

A torque model based on Equation 9.20 was developed. The relationship between the principal variables and the mill torque was examined in regions B and C as shown in Figure 9.3. The mechanism affecting the torque was explained by the basic physics of the system. The grinding media were influenced by the action of gravitational, centrifugal and frictional forces. The sum of these forces acting on the surface of the vessel should determine the power required to drive the mill. It was assumed that the mill content behaved as a fluidised bed and a $\rho_{eff} g h$ type model for the pressure was applied throughout the grinding media bed. In addition, it was considered that an effective charge velocity was proportional to the pin tip velocity. Based on a simplified model for the forces acting on the bottom and the wall of the vessel, it was possible to derive an equation relating power requirements to the dimensions of the mill, velocity of pin tip and to the amount and the nature of the charge.

The effect of mill load density on the mill torque

The effective mill charge density can be calculated knowing the grinding media density, voidage, ore density, solid concentration and buoyancy effects

ρ_{bulk} can be expressed as

$$\rho_{bulk} = (1 - \varepsilon)\rho_{media} + \varepsilon\rho_{pulp} \quad (9.23)$$

where ρ_{bulk} is the bulk density of the composite load, ρ_{media} is the density of the grinding media, ρ_{pulp} is the density of the pulp and ε is the voids between the balls given in Appendix 3.

Experimental results (Table A9.2) indicated that buoyancy force had an effect on the density of the composite load.

When the buoyancy force is included, equation 9.24 becomes

$$\rho_{eff} = (1 - \varepsilon)\rho_{media} + \varepsilon\rho_{pulp} - \rho_{pulp} \quad (9.24)$$

where ρ_{eff} (kg/m^3) is the effective density of the load in the mill.

The equation 9.24 can be simplified as

$$\rho_{eff} = (1 - \varepsilon)(\rho_{media} - \rho_{pulp}) \quad (9.25)$$

Figure 9.4 shows the effect of effective density of the mill load on the torque at a low pin tip velocity of 0.37 m/s (Table A9.2). The relationship between the torque and effective density of the mill load is

$$(T_b + T_w) \propto \rho_{eff}^{0.91} \quad (9.26)$$

The torque is almost directly proportional to the effective density of the mill load. The accuracy of this view is supported by Figure 9.5 in which the torque is plotted against the pin tip velocity at various effective densities. Pulp buoyancy forces acting on the immersed load lowered its composite load density, therefore the buoyancy force should be included in the analysis of torque requirements.

Region B:

a) Calculation of the torque exerted on the bottom of the vessel by mass (T_{bm})

It is assumed that the mill content behaves as a fluidised bed consequently the pressure at a height h from the top of the mill charge is $\rho_{eff}gh$ and the pressure at the bottom of the mill is $\rho_{eff}gH$ as shown in Figure 9.6.

An infinitesimal area which is shown in Figure 9.6 is taken for examination.

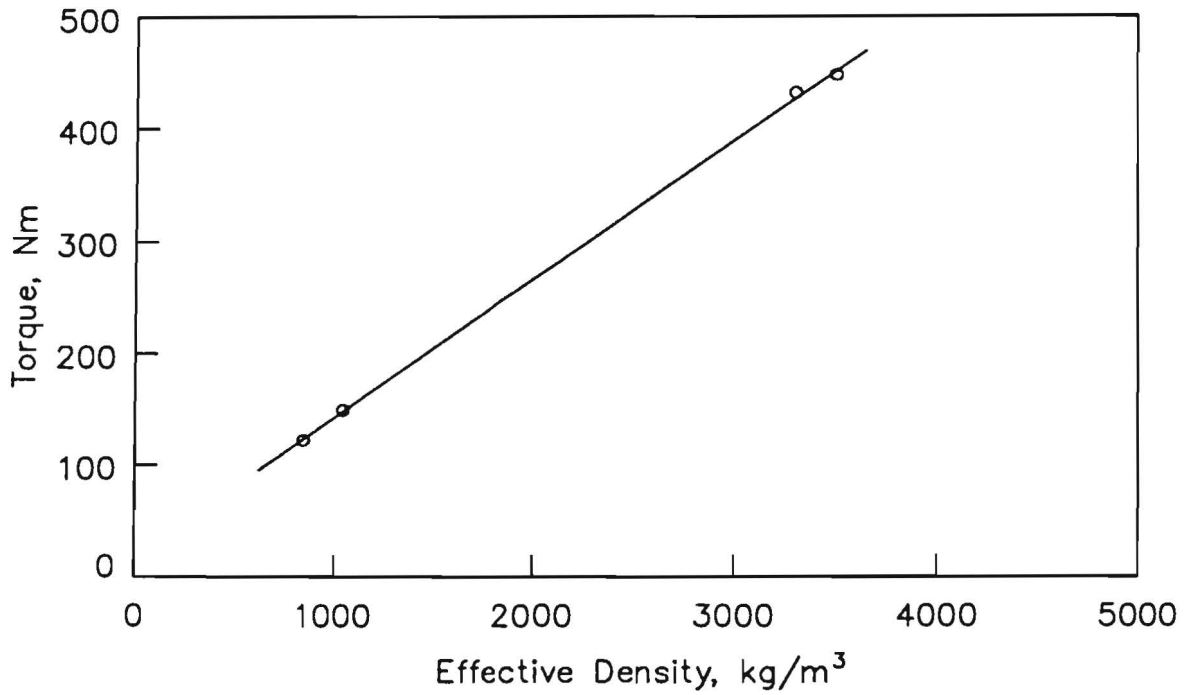


Figure 9.4. Effect of effective density on the mill torque at a pin tip velocity of 0.37 m/s (Experimental conditions and data given in Table A9.2).

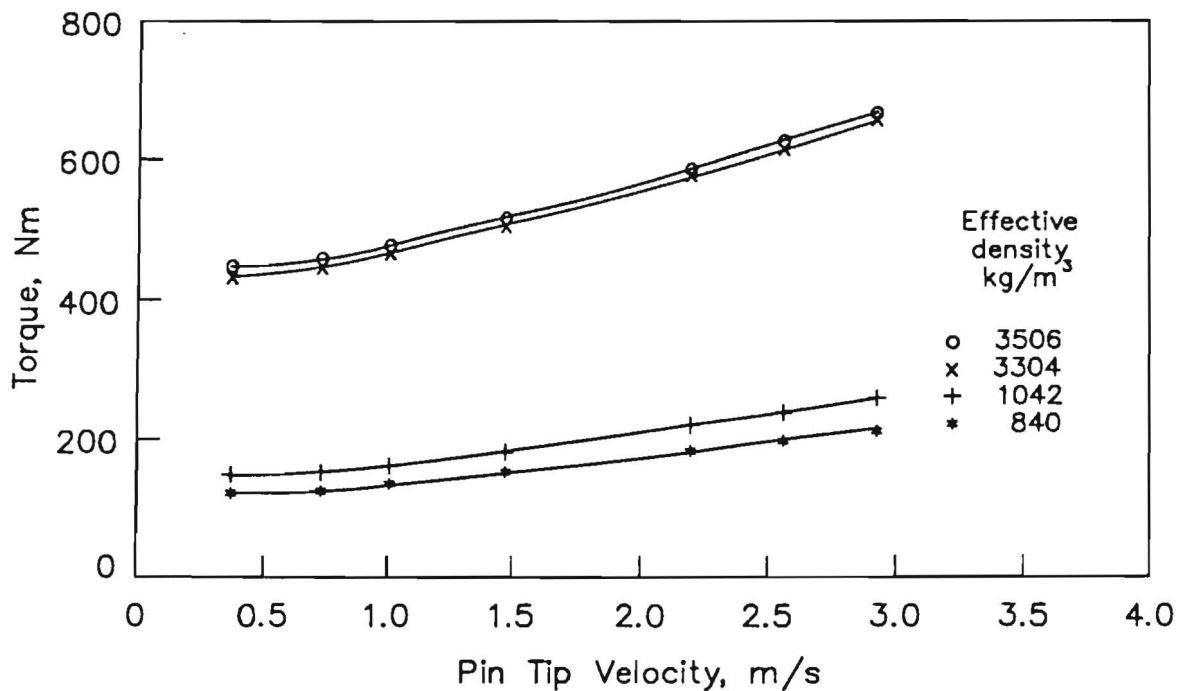


Figure 9.5. Effect of effective density at various pin tip velocities on the mill torque (Experimental conditions and data given in Table A9.2).

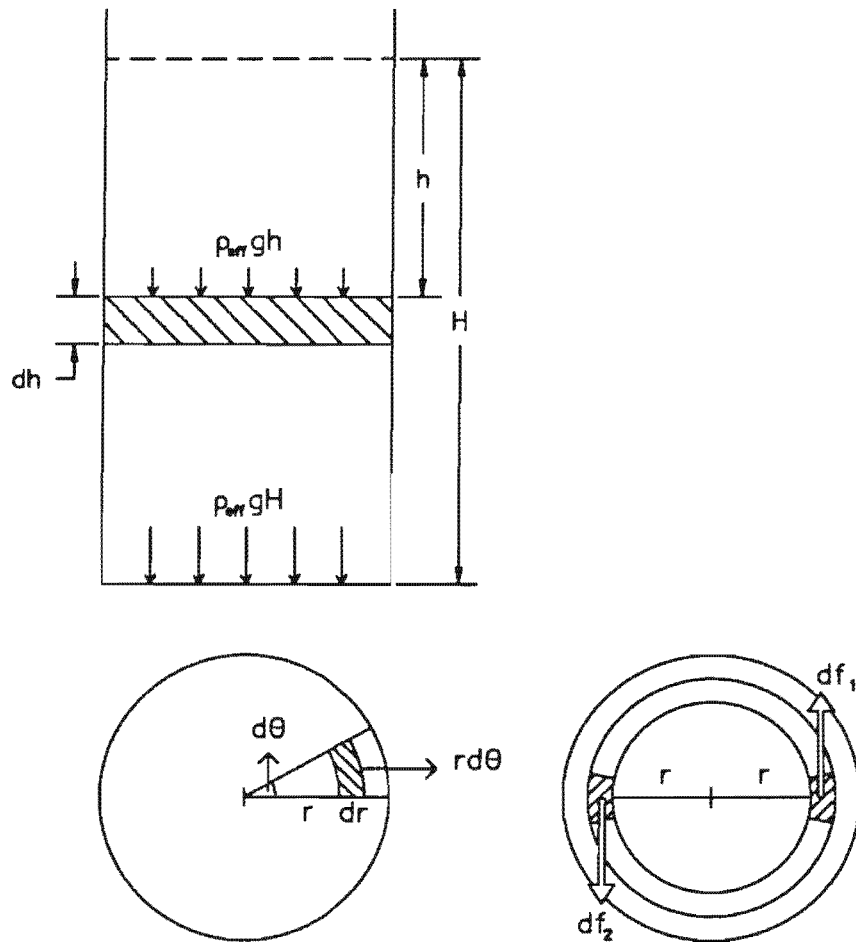


Figure 9.6. Illustration for derivation of torque equation for the bottom of the vessel

It is assumed that the normal force is uniformly distributed over the area of contact in which case then the normal force on the area of element $r d\theta dr$ is

$$dN = gH\rho_{eff}r d\theta dr \quad (9.27)$$

The friction force associated with this force during motion is

$$df = g\mu H\rho_{eff}r d\theta dr \quad (9.28)$$

where μ is the coefficient of friction.

The direction of friction forces must oppose the relative motion between the surfaces. The relative motion is that of concentric circles around the centre line, so the direction of a force df_1 must lie at a tangent to a circle of radius r . At 180° from the position of the area element for df_1 , a similar calculation can be carried out for a force df_2 , thus forming a couple. Since the entire area may be broken up in this way, if the moments about the centre are taken, the magnitude of the total frictional couple is arrived at. If the radius of the ring on which the area of the element is placed is r :

$$T_{bm} = \int_0^{2\pi} g\mu H \rho_{eff} r r d\theta dr \quad (9.29)$$

In order to calculate the frictional torque, it must be integrated between $r=0$ and $r=D/2$. Thus:

$$T_{bm} = \int_0^{D/2} \int_0^{2\pi} g\mu H \rho_{eff} r r d\theta dr \quad (9.30)$$

then the integration becomes

$$T_{bm} = g\mu H \rho_{eff} 2\pi \int_0^{D/2} r^2 dr \quad (9.31)$$

$$T_{bm} = g \frac{\pi}{12} \mu \rho_{eff} H D^3 \quad (9.32)$$

$$T_{bm} = K_1 \frac{1}{12} \rho_{eff} H D^3 \quad (9.33)$$

b) Calculations of the torque exerted on the wall of the vessel by mass (T_{wm})

The torque exerted onto the wall of the vessel is derived as follows. Figure 9.7 shows an infinitesimal area which is $dh dl$ at a distance h from the upper surface of the grinding media at rest.

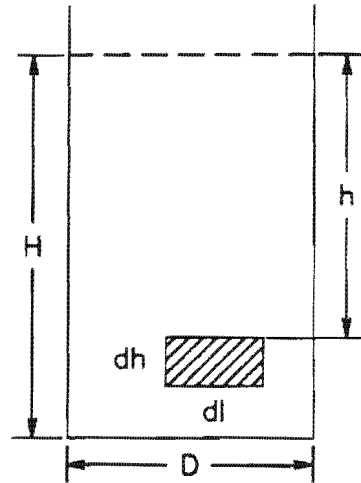


Figure 9.7. Illustration for derivation of torque equation for vessel wall

The normal force acting on this area is therefore

$$dN = g h \rho_{eff} dh dl \quad (9.34)$$

The friction force acting on the unit surface area is expressed as

$$df = g \mu h \rho_{eff} dh dl \quad (9.35)$$

The torque exerted on the vessel wall is

$$T_{wm} = \int_0^{\pi D} \int_0^H g \mu \rho_{eff} h \frac{D}{2} dh dl \quad (9.36)$$

$$T_{wm} = g \mu \rho_{eff} \frac{H^2 D}{2} \int_0^{\pi D} dl \quad (9.37)$$

$$T_{wm} = g \frac{\pi}{4} \mu \rho_{eff} H^2 D^2 \quad (9.38)$$

$$T_{wm} = K_2 \frac{1}{4} \rho_{eff} H^2 D^2 \quad (9.39)$$

Region C:

a) Calculations of the torque on the wall of the vessel by the centrifugal force (T_{cm})

The motion of the balls in the mill is very complex and the balls move both radially inwards and outwards as well as up and down. Consequently, the mill charge velocity varies according to the position in the mill. As an approximation, an effective charge velocity (V_c) was taken to be proportional to pin tip velocity

$$V_c = KV \quad (9.40)$$

The centrifugal force becomes (Figure 9.7)

$$F_c = K_3 M g V^2 \frac{2}{D} = K_3 g \frac{\pi D^2}{4} H \rho_{eff} V^2 \frac{2}{D} = K_3 g \frac{\pi}{2} D H \rho_{eff} V^2 \quad (9.41)$$

The normal force over the unit area of $dh dl$ is

$$dN = K_3 \frac{F_c}{\pi D H} dh dl = K_3 g \frac{1}{2} \rho_{eff} V^2 dh dl \quad (9.42)$$

The friction force on the unit area can be expressed as

$$df = K_3 g \frac{1}{2} \mu \rho_{eff} V^2 dh dl \quad (9.43)$$

The torque due to the centrifugal force is obtained by integration

$$T_{cm} = \int_0^{\pi D} \int_0^H K_3 g \frac{1}{2} \mu \rho_{eff} V^2 \frac{D}{2} dh dl \quad (9.44)$$

$$T_{cm} = K_3 g \frac{\mu}{2} \rho_{eff} H V^2 \frac{D}{2} \int_0^{\pi D} dl \quad (9.45)$$

$$T_{cm} = K_3 g \frac{\pi}{4} \mu \rho_{eff} H D^2 V^2 \quad (9.46)$$

Equation 9.46 may be represented by the following equation

$$T_{cm} = K_4 \rho_{eff} H D^2 V^2 \quad (9.47)$$

Total torque exerted onto the vessel (T)

$$T = K_1 \frac{1}{12} \rho_{eff} H D^3 + K_2 \frac{1}{4} \rho_{eff} H^2 D^2 + K_4 \rho_{eff} H D^2 V^2 \quad (9.48)$$

Equation 9.48 simplifies to

$$T = \rho_{eff} H D^2 \left(K' \left(\frac{D}{3} + H \right) + K'' V^2 \right) \quad (9.49)$$

Experimental and predicted torque results using various grinding conditions and design variables are given in Table A9.1. A 5 litre test-rig, which employed a vessel 20 cm in diameter and 20 cm long and a 50 litre test-rig which accommodated vessels which were 20 cm, 25 cm and 30 cm in diameter and 90 cm long and a vessel 50 cm in diameter and 50 cm long as indicated in Section 3.2 Chapter 3.

A nonlinear regression programme was used to determine constant parameters. The nonlinear programme employed throughout the work obtained least squares estimates of the parameters and used an iterative search algorithm to determine the estimates that minimised the residual sum of squares

$$\text{Sum of squares} = \sum_{i=1}^n (T_i \text{observed} - T_i \text{calculated})^2 \quad (9.50)$$

Constant parameters were determined as:

$$K' = 2.624 \text{ and } K'' = 0.115$$

The power delivered by the shaft P(kW)

$$P = 105 \times 10^{-6} N \left(\rho_{eff} H D^2 \left(K' \left(\frac{D}{3} + H \right) + K'' V^2 \right) \right) \quad (9.51)$$

9.3.3.2. Torque model including the configuration of stirring mechanism and ball diameter

The important variables in the configuration of the stirring mechanism were pin spacing s(m) and pin diameter w(m). In addition to these, the ball size d(m) had an effect on the mill torque. The examination of the results in Table 9.1

(section 9.4) to determine whether these variables were important for the equation revealed high ratios of the size of the estimates of independent variables to their standard errors. This suggested that pin spacing, pin diameter and ball diameter were significantly important. These parameters were therefore entered in the torque equation. The data is correlated by the relation

$$T = w^a s^b d^c \rho_{eff} H D^2 \left(K_1' \left(\frac{D}{3} + H \right) + K_1'' V^2 \right) \quad (9.52)$$

A nonlinear regression analysis programme was used to calculate the exponents of the variables. The relationship between these variables is found experimentally to be

$$T = w^{0.39} s^{-0.39} d^{0.54} \rho_{eff} H D^2 \left(K_1' \left(\frac{D}{3} + H \right) + K_1'' V^2 \right) \quad (9.53)$$

The exponents show how the torque varies with the pin spacing, pin diameter and ball size. The torque in the stirred ball mill is a mild function of these parameters. The exponents of the pin spacing and pin diameter were found to be almost the same. Therefore, equation 9.53 can be simplified to

$$T = (w/s)^{0.39} d^{0.54} \rho_{eff} H D^2 \left(K_1' \left(\frac{D}{3} + H \right) + K_1'' V^2 \right) \quad (9.54)$$

The constant parameters evaluated using nonlinear regression analysis were

$$K_1' = 49.711 \quad \text{and} \quad K_1'' = 2.109$$

The equation can be written as the power delivered by the shaft P (kW)

$$P = 100 \times 10^{-6} N \left((w/s)^{-0.39} d^{0.54} \rho_{eff} H D^2 \left(K_1' \left(\frac{D}{3} + H \right) + K_1'' V^2 \right) \right) \quad (9.55)$$

9.4. DISCUSSIONS

With the present state of knowledge of stirred ball milling, determining the optimum design or operating conditions has some shortcomings. Although theories and equations using dimensional analysis and fluid dynamics can be accepted as fundamentally sound, they provide a basic concept which has some

gaps remaining that need to be filled. To be fully inclusive the equation should be expanded to include the shaft geometry, ball diameter and pulp density. Neglecting these parameters can lead to erroneous conclusions.

By using these power equations, the effect of grinding conditions or equipment design can be only roughly predicted, therefore an attempt was made to develop a method of predicting power requirement as a function of operating and design parameters. An equation was derived and a fundamental concept was developed to establish a framework for stirred ball mill design and the equation was expanded to include the shaft geometry and ball diameter to predict the power requirements.

A typical example of the experimental results from the 50 litre stirred ball mill is graphically shown in Figure 9.3 (Table A9.3). The torque and pin tip velocity curve shows that the torque curve is divided into three different regions relating to the shaft rotation speed. First region; (start-up region) has a high torque which can be related to the high static friction force and locking of the grinding media. Second region; (low shaft rotation speed) the torque drops sharply to the minimum value and remains almost constant up to a pin tip velocity of 0.37 m/s. For the modelling of this region, the torque readings at the pin tip velocity of 0.37 m/s were used. It was not possible to run the mill in region B continuously because the motor tripped when the pin tip velocity was lower than 0.37 m/s. Figure 9.3 and Table A9.3 show the average torque reading for a very short run at 0.37, 0.21, 0.10 m/s. The torque readings were almost the same at these speeds. Therefore it was practical to take the torque reading at 0.37 m/s to represent the region B. Third region; (high pin tip velocity) the torque increased with increasing shaft rotation speed. Since all the experimental data were prevalent in regions B and C, the torque equations were developed for these regions.

Simple torque and semi-empirical torque models were developed relating the mill torque to the various geometrical and operating conditions in the stirred ball mill. The approach that the mill torque was proportional to the total force which was adopted resulted from gravitational, centrifugal and frictional forces acting on the vessel. The basic assumptions underlying the models were :

- 1) it was considered that the mill content behaved as a fluidised bed and a $\rho_{eff}gh$ type model for the pressure was applied throughout the grinding media bed.
- 2) The movement of the grinding balls in the mill was very complex and difficult to

define and the velocity of the balls also differed depending of their location in the vessel. Since most of the grinding activity was performed around the pin tip, it was assumed that the velocity of the composite mill load was proportional to the velocity of the pin tip.

The torque equation was derived relating the power requirements to the dimensions of the vessel, pin tip velocity, amount and nature of charge for given shaft geometry and ball size (Eq.9.49). Model fitting results giving high ratios of the estimates of the exponents to their standard errors for the semi-empirical torque model (Table 9.1) showed that shaft geometry and ball size were important parameters for the torque equation. The stirring mechanism comprised a rotating shaft having radially directed arms at 90° angles to each other. The variables in the configuration of the stirring mechanism were pin spacing and pin diameter. The effect of these factors and ball diameter were expressed by the semi-empirical torque equation (Eq.9.54). The exponents of pin spacing, pin diameter and ball diameter showed that the torque is not a strong function of these variables.

Table 9.1. Model fitting results for torque and semi-empirical models

Torque model	Parameter	Exponent		
		Estimate	Std. error	Ratio
	K'	2.624	0.0242	108.5
	K''	0.115	0.0032	35.1
Semi-empirical torque model	K'_1	49.840	29.017	1.7
	K''_1	2.110	1.233	1.7
	(w/s)	0.393	0.178	22.0
	d	0.540	0.115	4.7

The adequacy of the models was evaluated by analysing the residuals and variance table and employing the t-test.

Overall residuals were examined in order to check the torque model. The plot as shown in Figure 9.8 indicated no abnormality. The residuals appeared to be random. The examination of the plots of residuals against the torque calculated by the semi-empirical torque model also suggested no abnormality. The model would not appear to be invalidated (Figure 9.9).

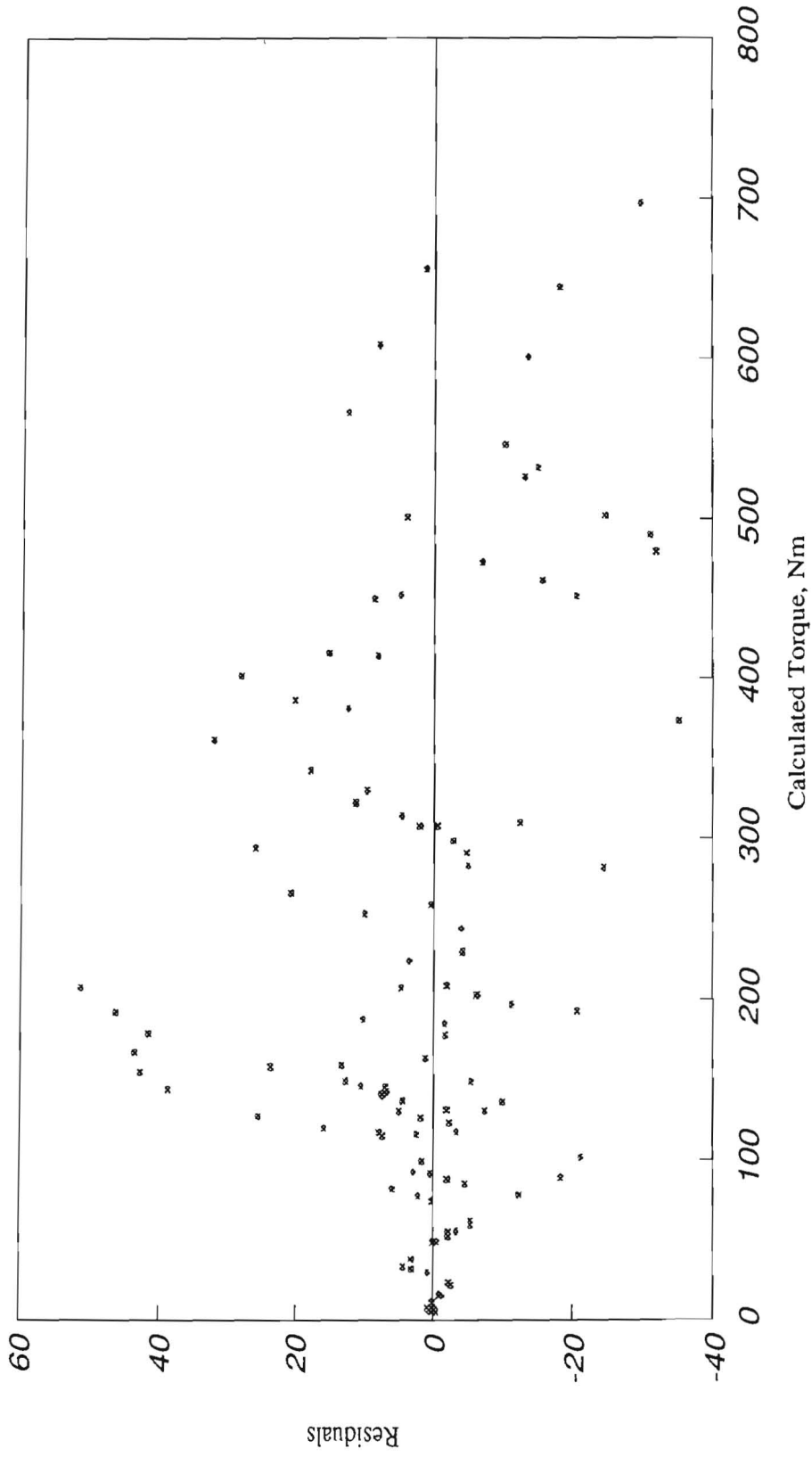


Figure 9.8. Plot of residuals versus torque values calculated by a torque model (Eq.9.49) (data given in Table A9.1)

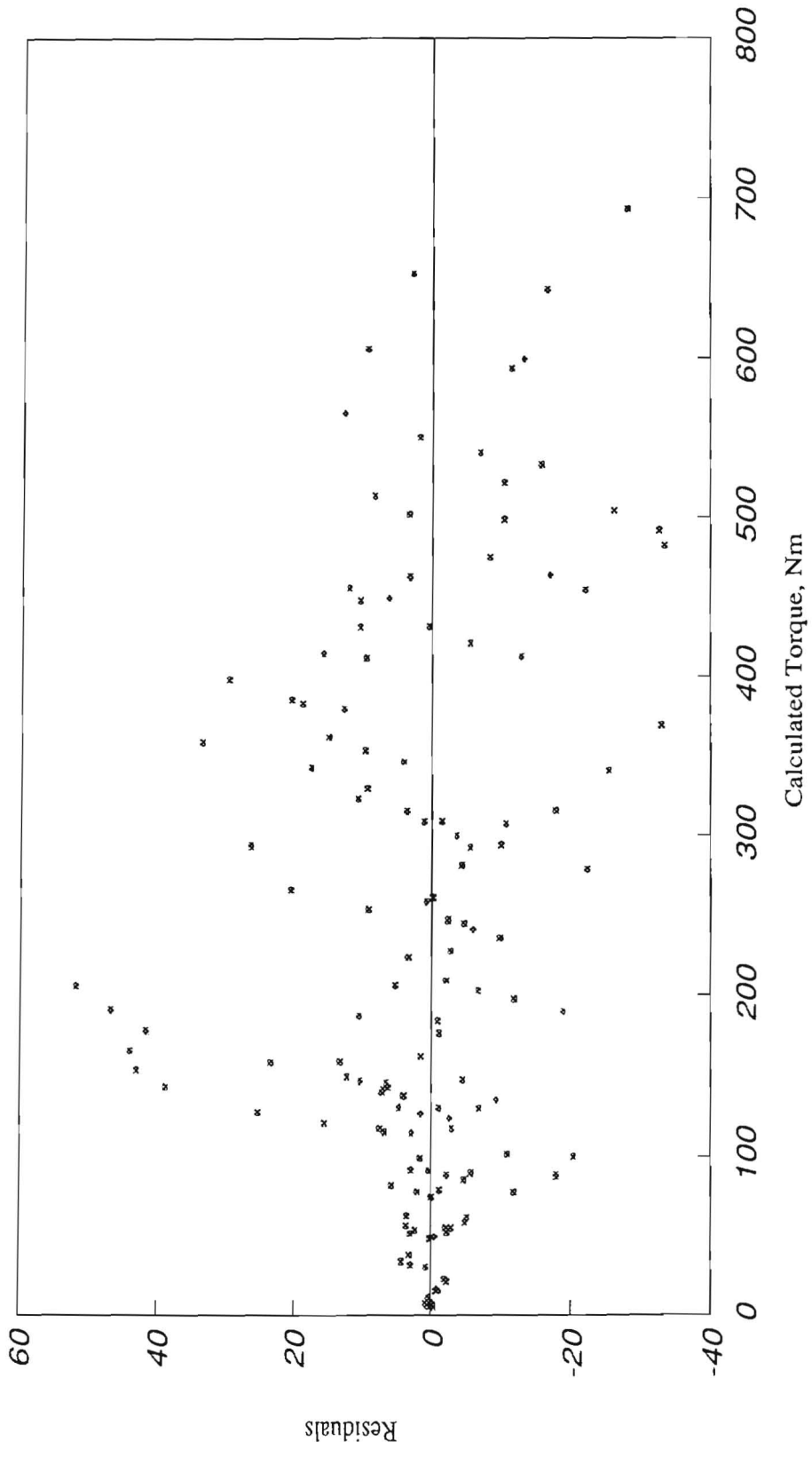


Figure 9.9. Plot of residuals versus torque values calculated by a semi-empirical torque model (Eq.9.54) (data given in Table A9.1)

The analysis of variance (Table 9.1) for both models showed no lack of fit. The values of the mean squares ratio (18505.1 and 13729.0) were significantly large.

Table 9.2. Analysis of variance for the full regression of torque and semi-empirical models

Torque model	Source	Sum of squares	df	Mean square	Ratio
	Model	8845934.7	2	4422967.3	18505.1
	Error	28203.6	118	239.0	
	Total	8874138.2	120		
Total(corr.)	3599512.0	119			
R-squared = 0.992					
Semi-empirical torque model	Source	Sum of squares	df	Mean square	Ratio
	Model	12253228	4	3063307	13729
	Error	32352.7	145	223.1	
	Total	12285581	149		
Total(corr.)	4587634.3	148			
R-squared = 0.993					

The agreement between the measured and calculated torque using the torque and semi-empirical torque model is excellent, giving a very high correlation coefficient of 0.992 and 0.993 respectively.

The values of the torque predicted by the torque model and semi-empirical torque equations are plotted against the observed torque values in Figures 9.10 and 9.11 and they correspond very well. In order to confirm this, the t-test was carried out (63,64).

The null hypothesis denoted H_0 that there is no difference between the observed data and calculated data by the torque models was tested. The null hypothesis is given by

$$H_0: x_1 = x_2 \quad (9.56)$$

where x_1 and x_2 are the means of observed and calculated data.

The analysis of calculated and observed torque values for both models using the student t-test was performed. Two tail t-value $t_{(0.025, \infty)} = 1.960$ from the student's t distribution tables (64) which was bigger than the calculated t-values of

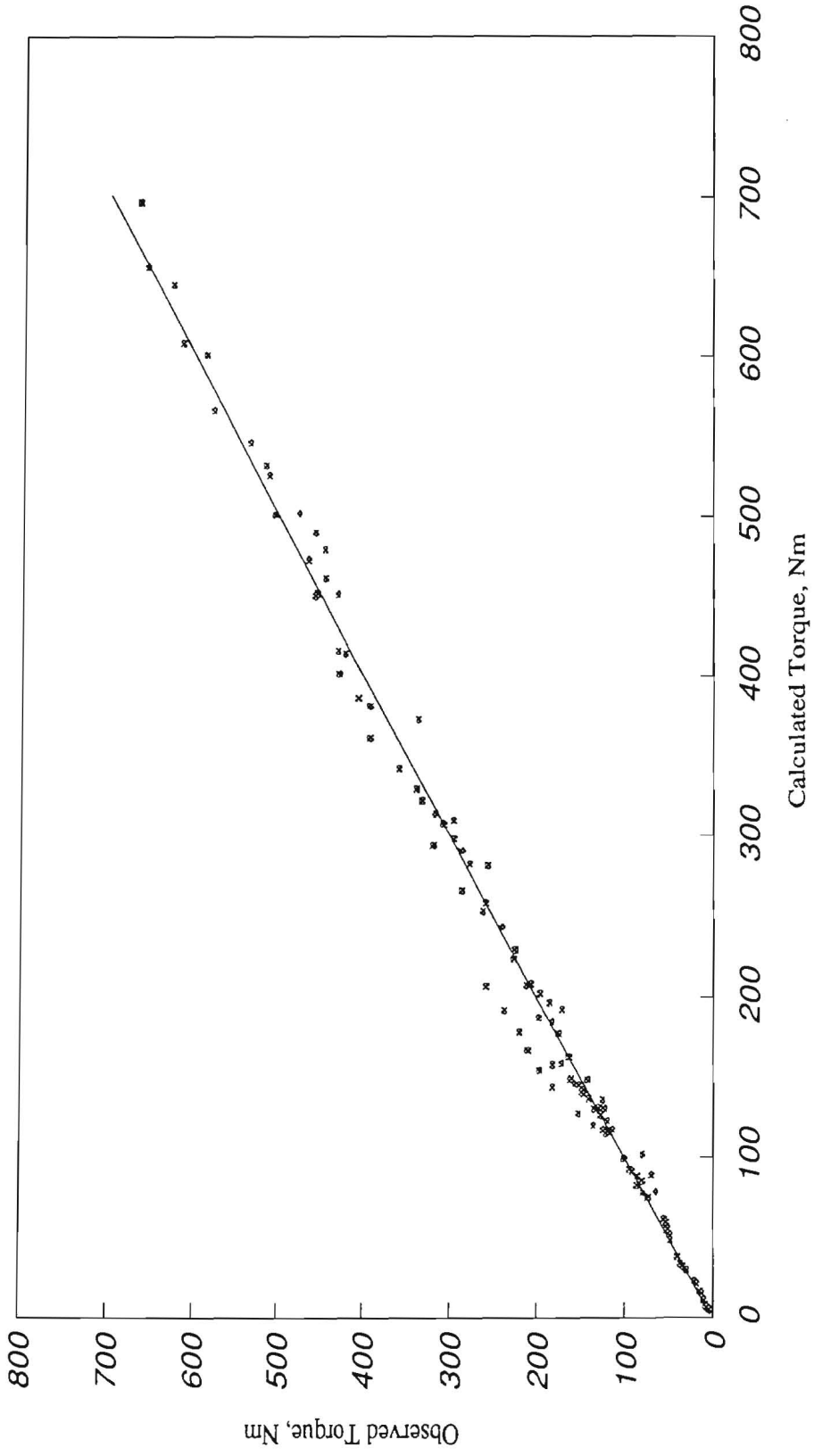


Figure 9.10. Plot of observed torque values versus torque values calculated by a torque model (Eq. 9.49) (data given in Table A9.1)

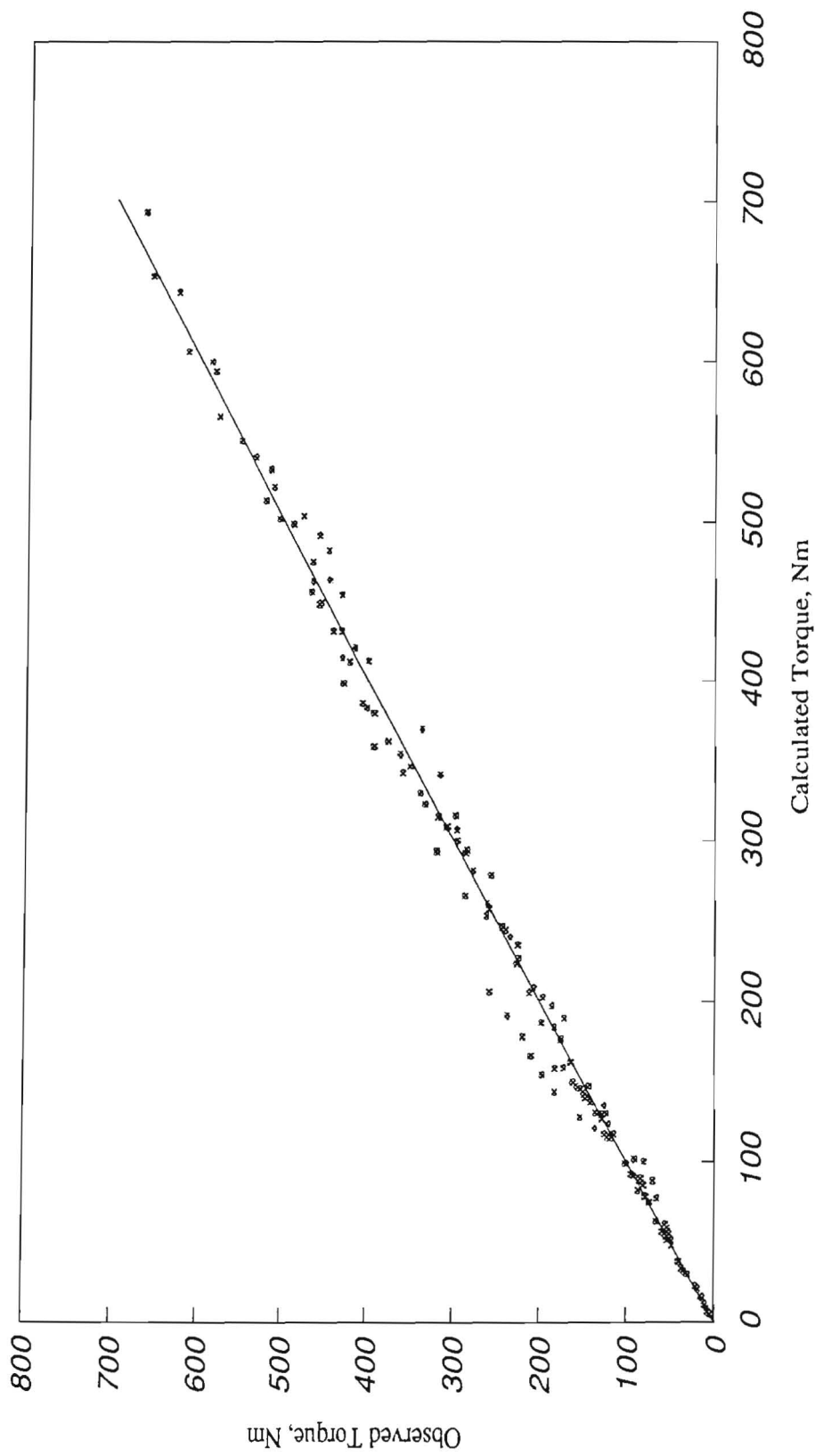


Figure 9.11. Plot of observed torque values versus torque values calculated by a semi-empirical torque model (Eq.9.54) (data given in Table A9.1)

0.086 with 238 degrees of freedom for the torque model and 0.081 with 294 degrees of freedom for the semi-empirical torque model. So the null hypothesis cannot be rejected at 5 percent significance level.

In order to check the validity of the torque equations a 200 litre test-rig was manufactured. The shaft rotation speed was set by means of a D.C. motor, belt, gear and sprocket system. The torque exerted onto the shaft was measured by a strain gauge. Two experiments, run under the various grinding conditions, gave torque readings of 2038 Nm and 2439 Nm. The calculated torque for these experiments using Equation 9.54 were 2041 Nm and 2365 Nm respectively. These results demonstrated that the torque equations developed during this work can be confidently applied to stirred ball mills of up to 200 litres.

CHAPTER 10

CONCLUSIONS

Higher pulp densities lead to an increase in the fineness of grind using balls of a larger diameter (15 mm). When using balls of a smaller diameter (smaller than 10 mm) the pulp density has very little effect on the breakage rate up to an optimum pulp density of 75% solids by weight but beyond this the breakage of material decreases significantly. Additionally the use of a higher pulp density results in a reduction in media wear.

Using grinding media of a smaller size gives a slightly better breakage rate for fine feed material in the stirred ball mill. A decrease in the ball size leads to a decrease in mill torque and an increase in media wear.

Steel balls (7.85 g/cm^3) produce a somewhat finer product than steatite balls (2.65 g/cm^3) at a pulp density of 2.40 g/cm^3 (Chapter 4) and coarser product than alumina (3.45 g/cm^3) at a pulp density of 2.20 g/cm^3 (Chapter 6). A lighter grinding media gives a finer product than denser ones providing that the grinding media density is reasonably higher than the pulp density. The torque to drive the mill at various pin tip velocities is almost directly proportional to the difference between the density of the grinding media and pulp density.

The grinding efficiency is sensitive to changes in the shaft rotation speed when larger balls are used (15 mm and 10 mm) and it decreases with increasing shaft speed. On the other hand, the grinding efficiency is not affected over the range of shaft rotation speeds investigated when the small balls (6 mm) are used.

It can be tentatively concluded that the larger stirred ball mill is more efficient on the basis of the capacity and media wear. Grinding efficiency however remains the same regardless of the mill height.

A decrease in pin spacing and an increase in pin diameter result in an increase in both grinding efficiency and mill torque. The effect of changes in shaft design parameters on media wear is insignificant.

The empirical approach based on the Charles' Equation proved to be useful to calculate the median size of the product for a given energy input level. However, deviations from the formula would perhaps be expected. Charles'

Equation holds for a limited size range. For each narrow size range, the exponent of the equation should be determined experimentally. Thus, this formula should be accepted with caution.

Batch grinding tests show that size reduction of chromite ore using the stirred ball mill is more efficient than when the tumbling ball mill is used in fines production. The energy input per ton of grinding media is much higher (10 fold) in the stirred ball mill than in the tumbling ball mill and therefore for the same capacity, a stirred ball mill of a much smaller size than the tumbling ball mill could be utilized.

The stirred ball mill will not replace the tumbling ball mill but does provide a superior means of comminution in the area of fine or ultrafine grinding where the tumbling mill becomes inefficient.

In the stirred ball mill, grinding media consumption is higher than in the tumbling ball mill in the coarse product size range. However, as the grinding proceeds, the media wear difference disappears and it becomes the same in the fine product size range (median size 4.8 microns).

The grinding conditions required to achieve the desired product specifications can be accurately predicted using the Charles' and the Rosin-Rammler-Bennett equations.

From 2^4 factorial experiments, the main factors influencing grindability are ball size, pin tip velocity and ball density, in decreasing order of importance. The pulp densities between the 1880 kg/m^3 and 2200 kg/m^3 do not influence the grinding results.

Interactions between the variables are shown to be insignificant.

A linear population balance model is applicable to the stirred ball mill grinding.

The primary breakage distribution parameters are normalizable for various mill operating conditions.

There is an optimum ball to feed size ratio which is calculated as 26.9 using the "angle of nip" theory.

Although initial specific breakage function parameters obtained from the monosize tests are fairly accurate, the specific breakage rates are lower than those obtained from the natural size feed sample. As a result of this, final grinding parameters have to be determined from the natural feed size, conditions similar to the real grinding system.

Application of the Charles' and Rosin-Rammler equations to batch grinding can be deduced as a special case of solution of the first-order batch grinding equation.

A comparison between the batch and continuous grinding results, demonstrates that it is possible to predict the median size of the product obtained from the continuous grinding using the results that are attained in the batch test when equivalent conditions are used.

The tanks in series model based on the residence time distribution of the water flow is not in exact agreement with the experimental results. This is due to the longer residence time for solids, the higher pulp density in the mill and the differential settling of the particles.

Existing power equations for the stirred ball mill are empirical and do not cover the all important variables. Regions B and C that are indicated in the torque versus pin tip velocity curve, can be described well by the torque and semi-empirical torque models. Experimental results are shown to be in excellent agreement with the torque model predictions for a wide range of variables in these regions.

REFERENCES

- (1) HUKKI, R.T., "Proposal for a Solomonic Settlement Between the Theories of Von Rittinger, Kick, and Bond" AIME Transactions, Vol.220, 1961, pp.403-408.
- (2) HARRIS, C.C., "On the Limit of Comminution" Transaction SME, March 1967, pp.17-30.
- (3) VOGENO, W., "Vibration Grinding Mill" Chemical and Process Engineering, Sept., 1969, pp.90-97.
- (4) ROSE, H.E.& SULLIVAN, R.M.E. "Vibrating Mills and Vibrating Milling". London: Whitefriars, 1961.
- (5) LICHTER, J.K.H., "A Study of Fine Grinding of Chromite Ore in a Palla Vibration Mill" M.Sc. Thesis, University of Natal, 1985.
- (6) SPINK, K., "Comminution Methods and Machinery" Mining and Minerals Engineering, Jan. 1972, pp.5-21.
- (7) CALLCOTT, T.G., "A Study of the Size Reduction Mechanism of Swing Hammer Mill" Journal of Institute of Fuel, 1960, pp.529-539.
- (8) TARJAN, G., Mineral Processing. Budapest: Akademiai Kiado, 1981.
- (9) DOBSON, B. & ROTHWELL, E., "Particle Size Reduction in a Fluid Energy Mill" Powder Technology, Vol.3, 1969/70, pp.214-217
- (10) GRIMSHAW, C.V. & ALBUS, J.F., "Fluid Energy Grinding and Drying for Fine Powders Production" Ultrafine Grinding and Separation of Industrial Minerals SME-AIME ed. Malghan, G.S., 1983.
- (11) TRASS, O., "The Szego Grinding Mill" Fine Particles Processing, SME-AIME, Vol.1, pp.96-113.
- (12) KLEIN, P., et.al., "Process of and Apparatus for Producing Liquid Dispersion" April 24, 1934, U.S. Patent No. 2,764,359
- (13) SZEGVARI, A., "Treatment of Liquid Systems and Apparatus Therefor" Sept. 25, 1956, U.S. Patent No. 2,764,359.

- (14) DASHER, D.E. & RALSTON, O.C., "New Method of Cleaning Glass Sands" Bulletin of the American Ceramic Society, Vol.20, No.6, June 1941, p.187.
- (15) FELD, I.L. & CLEMMONS, B.H. "Process for wet Grinding Solids to Extreme Fineness" U.S. Patent 3,075,710, Jan. 29, 1963.
- (16) STANLEY, D.A., et.al., "Attrition Milling of Ceramic Oxides" American Ceramic Society Bulletin, Vol.53, No.11, 1974, pp.813-815.
- (17) SADLER III, L. Y., et.al., "Attrition Mill Operating Characteristics" Powder Technology, Vol.12, 1975, pp.19-28.
- (18) FELD, I.L., et.al., "Paper-Coating Clay From Coarse Georgia Kaolins by a New Attrition-grinding Process" U.S. Bureau of Mines R.I. 5697, 1976, p.20.
- (19) STANLEY, D.A., et.al., "Size Reduction of Ceramic powders by Attrition Milling" Proceedings of International Conference in Particle Technology, August 21-24, 1973, pp.813-815.
- (20) STANLEY, D.A., et.al., "Attrition Milling of Ceramic Oxides" American Ceramic Society Bulletin, Vol.53, No.11, 1974, pp.813-815.
- (21) WITTMER, D.E., "Use of Bureau of Mines Turbomill to Produce High-Purity Ultrafine Nonoxide Ceramic Powders" U.S. Bureau of Mines R.I. 8854, 1984, pp.1-12.
- (22) STEHR, R., "Recent Development in Stirred Ball Milling" Engineering Foundation Conference, Dec. 8-13, 1985, p.14.
- (23) ENGELS, E., et.al., "Stirring Mill" March 28, 1967, U.S. Patent No.3,311,310.
- (24) CONLEY, R.F., "Effects of Crystal Structure and Grinder Energy on Fine Grinding of Pigments" Journal of Paint and Technology, Vol.44, No.567, April 1972, pp.67-87.
- (25) JENCZEWSKI, T.J., "The Grinding of Organic Dyestuffs" The Canadian Journal of Chemical Engineering, Vol.50, Feb. 1972, pp.59-65.

- (26) Fifth International Symposium on Coal Combustion and Technology, Proceedings Vol.1&2, Apr. 25-27, 1983, Tampa, Florida.
- (27) WESTERLUND, P., "Preliminary Report on Grinding Tests in a Vertical Laboratory Mill" International Mineral Processing Congress, 1960, pp.81-87.
- (28) SEPULVEDA, J.L., "Stirred Ball Milling: An Energy Efficient Approach To Produce Coal/Oil Mixtures" AIME-SME, Mini-Symposium "Coal Slurry Fuels", 6-10 March 1983, Atlanta, G.A. (N 83-Coal-02).
- (29) HERBST, J.L. & SEPULVEDA, J.L., "Fundamentals of Fine and Ultrafine Grinding in a Stirred Ball Mill" Powder and Bulk Solids Handling and Processing, Proceedings of the Tech. Prog., May 16-18 1978, pp.452-470.
- (30) SHALL, G., "Advances in Microfine Wet Grinding" Perth Gold 88, pp.53-60.
- (31) POKORNY, J., "Dry Grinding in Agitated Ball Mills" Powder Technology, 1976, Vol.15, pp.181-186.
- (32) SEPULVEDA, J.L., "A Detailed Study of Stirred Ball Milling" Ph.D. thesis, Metallurgy Department, University of Utah, 1981.
- (33) MATTER, F., "The Use of Fine Size Media to Grind Industrial Minerals by Wet or Dry Process" Ultrafine Grinding and Separation of Industrial Minerals SME-AIME Ed. Malghan, G.S., 1983.
- (34) RAMSEY, T.L., "Reducing Grinding Costs: The Potential is great" World Mining, Oct. 1982, pp.78-81.
- (35) ANON., "Grinding Mills-Rod, Ball and Autogenous" Mining Magazine, Sept. 1982, pp.197-225.
- (36) BIGNELL, J.D. & NEWTON, S., "Recent Progress in Solids Processing: Comminution - A Review" Chemical Engineering Research & Design, Vol.64, No.2, March 1986, pp.91-93.
- (37) ADORJAN, L.A., "Mineral Processing" Min. Annual Review, 1983, pp.217-248.

- (38) DONALD, E.S., et.al., "Tower Mill and its Application to Fine Grinding" SME-AIME Annual Meeting Los Angeles, California. Feb. 26 - March 1 1984, pp.10.
- (39) SEPULVEDA, J.L. & FLETCHER, P.C., "On the Regrind of Molybdenite Concentrates with a Tower Mill" SME-AIME Annual Meeting, Los Angeles, California, Feb. 26 - March 1 1984, p.17.
- (40) HOYER, D.I., "Fine Grinding with The Tower Mill: A Comparison with a Ball Mill" Mintek No.C336M, Sept. 3 1984.
- (41) MasterSizer Instruction Manual, Malvern Instruments.
- (42) MANKOSA, M.J., et.al., "Effect of Media Size in Stirred Ball Mill Grinding of Coal" Powder Technology, Vol.49, 1986, pp.75-82.
- (43) CHARLES, R.J., "Energy-Size Reduction Relationship in Comminution" AIME Transactions, Vol.208, 1957, pp.80-88.
- (44) SCHUHMANN, J.R., "Energy Input and Size Distribution in Comminution" AIME Transactions, Vol.217, 1960, pp.22-25.
- (45) PRYOR, N., Mineral Processing. London: Applied Science Publishers Limited, 1978.
- (46) WILLS, B.A., Mineral Processing Technology, Pergamon Press, 1988
- (47) STEHR, N., et.al., "Comparison of Energy Requirements for Conventional and Stirred Ball Milling of Coal-Water Slurries" Coal Preparation, Vol.4, 1987, pp.209-226.
- (48) SCHUHMANN, R.Jr., "Principles of Comminution. 1- Size distribution and Surface Calculations" AIME Technical Publications No. 1189, p.11.
- (49) ROSIN, R.&RAMMLER, E., J. Inst. Fuel, 7,1933, pp.29-35.
- (50) BENNETT, J.G., J. Inst. Fuel, 10, 1936, pp.22-39.
- (51) BAGSTER, D.F., "The Measurement of the Force Needed to Move Blades Through a Bed of Cohensionless Granulas" Powder Technology, Vol.1, 1967, pp.109-115.

- (52) NOVASAD, J., "Studies on Granular Materials I. Kinematic of Granular Materials Mixed by a Mechanical Impeller" Collection of Czechoslovak Chemical Communications, Vol.29, 1964, pp.2681-2696.
- (53) NOVOSAD, J., "Studies on Granular Materials II. Apparatus for Measuring the Dynamic Angle of Internal and External Friction of Granular Materials" Collection of Czechoslovak Chemical Communications, Vol.29, 1964, pp.2697-2701.
- (54) NOVOSAD, J., "Studies on Granular Materials III. Stress Distribution in a Granular Material Mixed by a Mechanical Impeller" Collection of Czechoslovak Chemical Communications, Vol.29, 1964, pp.2703-2709.
- (55) NOVASAD, J., "Studies on Granular Materials IV. Calculation of the Shaft Torque for Mixing Granular Materials" Czechoslovak Chemical Communications, Vol.30, 1965, pp.3247-3262.
- (56) UHL, V.W., "Mixing" Academic Press, New York & London, Vol.46, No.8, pp.111-179.
- (57) WHITE, A. McL., et.al., "Studies in Agitation" Transactions. American Institute of Chemical Engineers, Vol.30, 1934, pp.570-597.
- (58) HIXSON, A.W. & LUEDEKE, V.D. "Wall Friction in Liquid Agitation Systems" Industrial and Engineering Chemistry, Vol.29, 1937, pp.927-933.
- (59) RUSHTON, J.H., et.al., "Power Characteristic of Mixing Impellers. Part 1" Chemical Engineering Progress, Vol.46, No.8, pp.395-404.
- (60) RUSHTON, J.H., et.al., "Power Characteristics of Mixing Impellers. Part.2" Chemical Engineering Progress, Vol.46, No.9, pp.467-476.
- (61) BUCKINGHAM, E., Transactions. American Society of Mechanical Engineers, Vol.37, 1915, pp.263.
- (62) RUSHTON, J.H., et.al., "Mixing of Liquids" Chem. Eng. Progress, Vol.55, No.9, pp.181-198.

- (63) MILLER, I.& FREUND, J.E., Probability and Statistics for Engineers, New Jersey, Prentice-Hall, Inc., 1977.
- (64) CHATFIELD, C., Statistics for Techonolgy, Chapman and Hall, 1978.
- (65) HALD, A., Statistical Tables and Formulas, New York, John Wiley & Sons, Inc., 1960.
- (66) BOX, G.E.P., et.al., "Statistics for Experimenters", John Wiley & Sons, 1978.
- (67) AUSTIN, L.G., et.al, "Simple Solutions to Grinding Equations" Process Engineering of Size Reduction: Ball Milling, Guinn Printing Inc., New Jersey, 1984, pp.169-175.
- (68) LOVEDAY, B.K., "An Analysis of Comminution Kinetics in Terms of Size Distribution Parameters" Journal of the South African Institute of Mining and Metallurgy, Vol.6, No.3, Oct.1967, pp.111-131
- (69) AUSTIN, L.G., et.al, Process Engineering of Size Reduction: Ball Milling, Guinn Printing Inc., New Jersey, 1984.
- (70) REID, K.J., "A Solution to the Batch Grinding Equation" Chemical Engineering Science, Vol.20, 1965, pp.953-963.
- (71) HERBST, J.A., et.al., "Scale-up Procedure for Continuous Grinding Mill Design Using Population Balance Models", International Journal of Mineral Processing", Vol.7, 1980, pp.1-31.
- (72) HERBST, J.A., et.al, "The Zero Order Production of Fine Sizes in Comminution and Its Implications in Simulation", AIME Transactions, Vol.241, 1968, pp.538-548.
- (73) AUSTIN, L.G., et.al., "Solutions of the Batch Grinding Equation Leading to Rosin-Rammler Distributions", AIME Transactions, Vol.252, 1972, pp.87-94.

APPENDIX 1

SIEVING TESTS TO DETERMINE THE OPTIMUM SIEVING TIME

A representative sample was wet-sieved at 38 microns and then dry-sieved to a constant rate of weight loss of the +38 micron material at 10 minutes intervals up to 50 minutes.

After each time interval, the sample was removed and the underside of the inverted screens were brushed to remove the material stuck in the mesh. The size fractions were weighed and the sample was replaced on the sieves and sieved for a further 10 minutes. The results of the sieving tests on chromite ore are given in Table A1.1. It was concluded that the sieving time should be 30 minutes.

Table A1.1. Tests of dry sieving schedule for chromite ore

Screen size mic. ¹	Wt % less than in sieving time, minutes				
	10	20	30	40	50
75	91.49	92.13	92.55	92.80	92.92
53	78.49	79.35	79.77	80.07	80.42
38	62.19	62.99	63.50	63.88	64.26
-38 mic. wt% increase	0.80	0.51	0.38	0.38	

¹ microns

APPENDIX 2

ENERGY CONSUMPTION CALCULATIONS FOR THE STIRRED BALL MILL

The energy input to the mill was measured either with the torque table to which the stationary grinding vessel was attached or with the torque arm on the rotating shaft. The torque amplifier was previously calibrated with two different known weights when the grinding vessel was empty. The power consumption was calculated from the rotating shaft angular velocity together with either the torque on the turn-table or the torque on the rotating shaft.

$$P = \omega T \quad (\text{A2.1})$$

$P =$ power delivered by the shaft, W

$\omega =$ angular velocity, rad/s

$T =$ the torque applied to the turntable or the rotating shaft, Nm

Short term averages of the torques were recorded periodically during the experiment from a load cell attached to the extension arm via a spring. The torque versus grinding time was plotted. The energy input was calculated integrating the torque-time curve.

$$E = \int_0^t \omega T \Delta t \quad (\text{A2.2})$$

APPENDIX 3

CALCULATIONS FOR THE WEIGHT OF CHARGE MATERIAL

The weight of the charge material depends on the porosity volume of the grinding media and the pulp density of the slurry.

The vessel was filled with the balls and they were covered with water to determine the grinding media porosity at rest. The bed porosity varied slightly from 44.0% to 41.0% depending on the mill size. The experimentally observed grinding media porosity was 44.0% for the 5 litre stirred ball mill and 41.0% for the 50 litre stirred ball mill. The value of 44.0% was used for the porosity of the grinding media for the following calculations.

The grinding media porosity of 44.0% is the volume fraction of voids in a true grinding media plus porosity volume of 100.

$$\begin{array}{rclcl} \text{True grinding media} & + & \text{Grinding media} & = & 100 \\ \text{volume} & & \text{porosity} & & \\ 56.0 & + & 44.0 & = & 100 \end{array}$$

$$\text{Porosity volume of grinding media} = \frac{\text{mass of balls} \times 44.0}{\text{ball density} \times 56.0} \quad (\text{A3.1})$$

If the spaces between the balls are filled with slurry,

$$\text{Porosity volume of grinding media} = \frac{x}{\rho_s} + \frac{y}{\rho_l} \quad (\text{A3.2})$$

$$\text{Fraction of solids by volume} = \frac{x / \rho_s}{(x / \rho_s) + (y / \rho_l)} \quad (\text{A3.3})$$

where,

- x ; weight of solids, g
- y ; weight of liquid, g
- ρ_s ; density of solids, g/cm³
- ρ_l ; density of liquid, g/cm³

APPENDIX 4

DRAWING OF 20 LITRE STIRRED BALL MILL

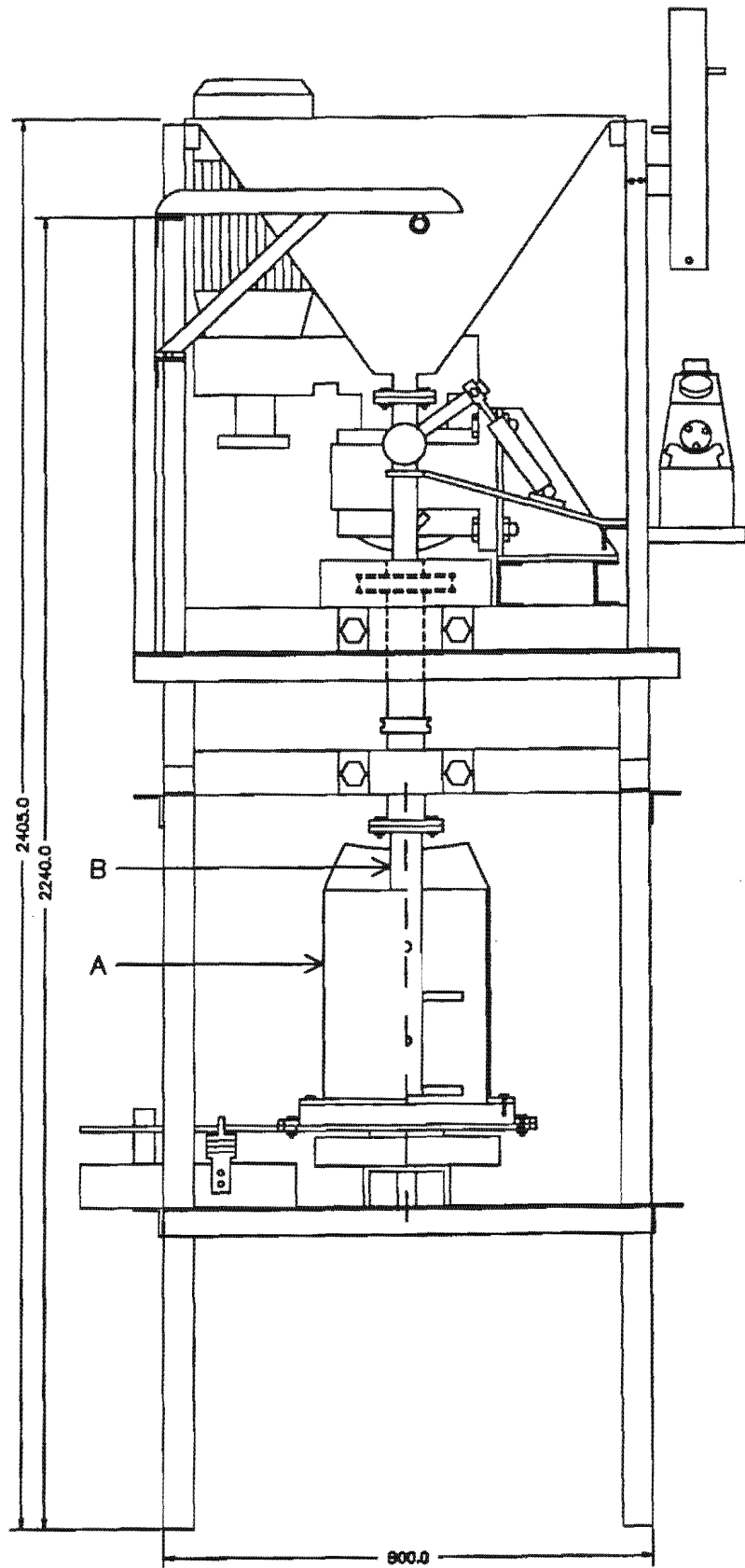


Figure A4.1. Drawing of 20 litre stirred ball mill test rig (Front elevation)

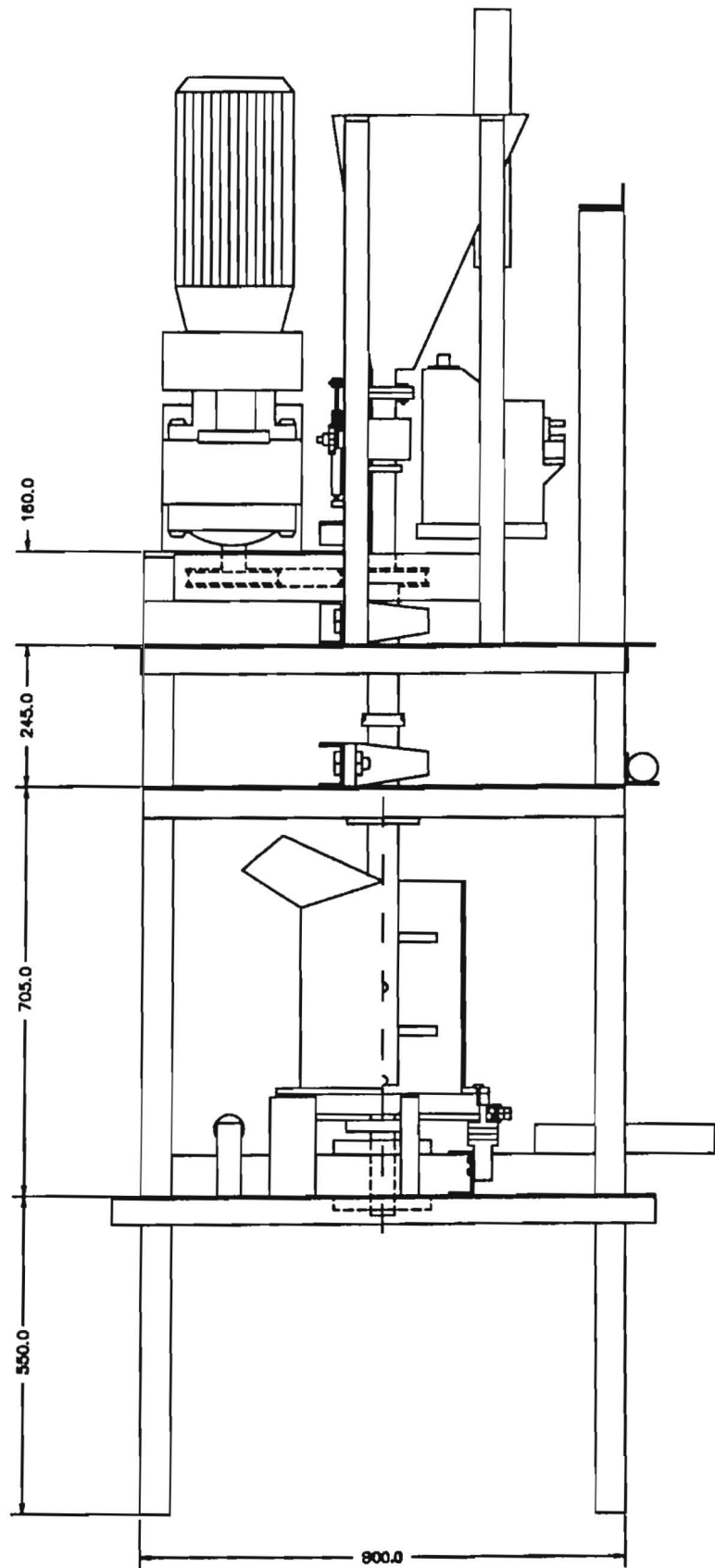
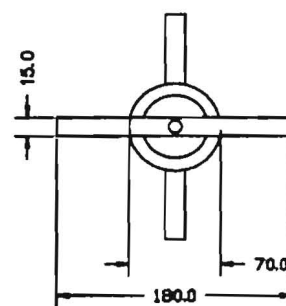
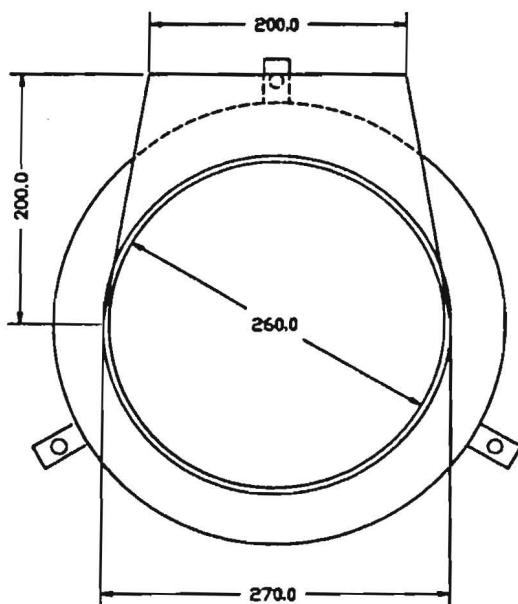
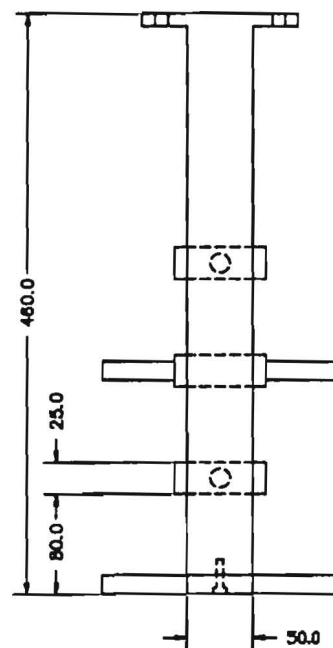
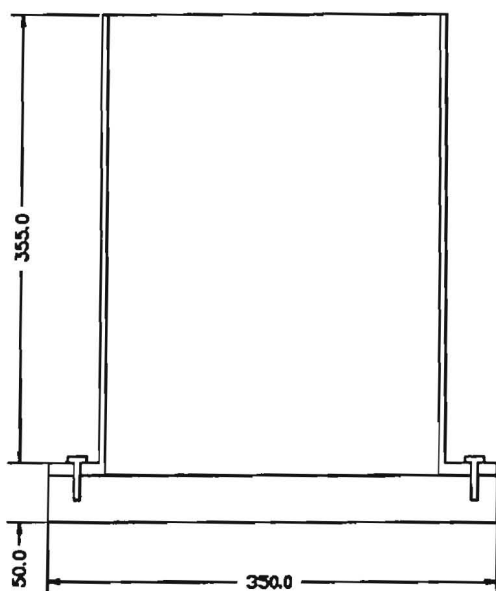


Figure A4.2. Drawing of 20 litre stirred ball mill test rig
(End elevation)



A. Vessel

B. Rotating shaft
(Adjustable pin
spacing and
diameter)

Figure A4.3. Drawing of components for 20 litre stirred ball mill test rig

BATCH GRINDING RESULTS FROM A 20 LITRE STIRRED BALL MILL

Table A4.1. Variation of median size of products with slurry density (Vol. % solids): load depth = 32 cm, pin spacing = 8.6 cm, pin diameter = 1.6 cm, energy input = 66 kWh/t (data shown in Figure 4.1).

Weight % solids	Vol. % solids	Median Size, mic.				
		Ball type	Steatite	Steel		
		Balls size, mm	6	15	6	
		Shaft speed, r.p.m.	300	72	164	300
62.5	27		8.6	10.0	7.9	8.2
70.0	34		8.8	9.3	7.5	7.8
75.0	40		9.2	8.8	7.8	7.8
80.0	47		-	8.5	8.8	8.7
85.0	56		-	*	-	-

* The mill jammed

Table A4.2. Median size of chromite ore as a function of energy input at various pulp densities: 6 mm steel balls, load depth = 32 cm, shaft speed = 164 r.p.m., pin spacing = 8.6 cm, pin diameter = 1.6 cm (data shown in Figure 4.2).

Energy input kWh/t	Median size, mic.	
	Pulp density, % solids by weight	
	62.5	75.0
28.0	-	23.0
36.0	14.7	14.8
52.5	-	10.1
66.0	7.9	7.8
90.0	5.6	5.6
150.0	4.1	4.1
200.0	3.3	3.4

Table A4.3. Variation of mill torque as a function of energy input at various pulp densities: 6 mm steel balls, load depth = 32 cm, shaft speed = 164 r.p.m., pin spacing = 8.6 cm, pin diameter = 1.6 cm (data shown in Figure 4.3).

Energy input kWh/t	Torque, Nm			
	Pulp density, % solids by weight			
	62.5	70.0	75.0	80.0
1.0	52.5	57.6	60.3	61.3
10.0	50.7	47.9	51.1	50.4
20.0	43.0	42.1	40.6	39.4
30.0	38.2	37.5	36.2	35.3
40.0	37.7	36.1	35.2	34.7
50.0	37.0	35.2	33.6	32.5
60.0	36.8	34.2	33.2	31.5
66.0	35.8	33.1	32.1	31.0

Table A4.4. Media wear as a function of energy input at various percent solids: 6 mm steel balls load depth = 32 cm, shaft speed 164 r.p.m., pin spacing = 8.6 cm, pin diameter = 1.6 cm (data shown in Figure 4.4).

Energy Input kWh/t	Media wear, kg/t					
	Pulp density, % solids by weight					
	62.5		70.0		75.0	
	Feed	-10 mic. produced	Feed	-10 mic. produced	Feed	-10 mic. produced
20.0	4.1	13.8	4.0	13.2	3.4	12.8
37.5	7.4	18.8	7.3	16.0	6.4	13.5
52.5	9.2	17.4	9.1	15.5	8.0	13.4
66.0	9.8	14.8	9.5	14.0	8.3	12.7

Table A4.5. Effect of pulp density on media wear: ball type = steel, load depth = 32 cm, pin spacing = 8.6 cm, pin diameter = 1.6 cm, energy input = 66 kWh/t (data shown in Figure 4.5).

Weight % solids	Vol % solids		Media wear, kg/t feed		
		Ball size, mm	15	6	
		Shaft speed, r.p.m.	72	164	300
62.5	27		5.9	9.8	10.0
70.0	34		6.0	9.5	9.9
75.0	40		5.5	8.3	8.2
80.0	47		5.1	7.0	7.1

Table A4.6. Median size of chromite ore as a function of energy input for various ball sizes at 72 r.p.m.: pulp density = 75% solids by weight, media type = steel, load depth = 32 cm, pin spacing = 8.6 cm, pin diameter = 1.6 cm (data shown in Figure 4.6)

Ball size mm	Energy input kWh/t	Median size mic.
15	20.0	26.8
	36.0	14.3
	52.5	10.3
	66.0	8.8
10	20.0	32.3
	36.0	14.4
	52.5	9.6
	66.0	7.8

Table A4.7. Median size of chromite ore as a function of energy input for various ball sizes at 164 r.p.m.: pulp density = 75% solids by weight, media type = steel, load depth = 32 cm, pin spacing = 8.6 cm, pin diameter = 1.6 cm (data shown in Figure 4.7).

Ball size mm	Energy input kWh/t	Median size mic.
10	20.0	27.7
	36.0	14.3
	49.5	10.1
	66.0	8.3
	90.0	5.9
	150.0	4.5
	200.0	3.6
6	20.0	-
	28.0	23.0
	36.0	14.8
	52.5	10.1
	66.0	7.8
	90.0	5.6
	150.0	4.1
	200.0	3.4

Table A4.8. Media wear and torque as a function of ball sizes: pulp density = 75% solids by weight, media type = steel, load depth = 32 cm, pin spacing = 8.6 cm, pin diameter = 1.6 cm, energy input = 66 kWh/t (data shown in Figures 4.8 and 4.9).

Ball size mm	Shaft rotation speed, r.p.m.					
	72			164		
	Torque	Media wear, kg/t		Torque	Media wear, kg/t	
	Nm	Feed	-10 mic. produced	Nm	Feed	-10 mic. produced
15	54.5	5.5	9.8	69.1	5.4	10.4
10	37.6	7.8	12.1	45.2	7.4	12.1
6	28.2	9.4	14.2	32.1	8.3	12.7

Table A4.9. Mill torque, median size and media wear as a function of load depth: pulp density = 75% solids by weight, media type = steel, pin spacing = 8.6 cm, pin diameter = 1.6 cm, energy input = 66 kWh/t (data shown in Figures 4.10, 4.11, 4.12).

Load depth cm	Ball size : 15 mm				Ball size : 6 mm			
	Shaft speed : 72 r.p.m.				Shaft speed : 164 r.p.m.			
	Median size mic.	Torque Nm	Media wear kg/t		Median size mic.	Torque Nm	Media wear kg/t	
			Feed	-10 mic. prod.			Feed	-10 mic. prod.
13.7	8.8	13.8	6.3	11.3	7.6	9.2	9.3	13.9
22.9	8.8	29.9	5.7	10.1	7.7	21.9	8.5	12.5
32.0	8.8	54.5	5.5	9.8	7.8	32.1	8.3	12.7

Table A4.10. Effect of shaft rotation speed on median size, torque, media wear using grinding media of various sizes and densities: pulp density = 75% solids by weight, load depth = 32 cm, pin spacing = 8.6 cm, pin diameter = 1.6 cm, energy input = 66 kWh/t (data shown in Figure 4.13, 4.14, 4.15).

Ball density g/cm ³	Ball size mm	Shaft rotation speed r.p.m.	Median size mic.	Torque Nm	Media wear, kg/t	
					Feed	- 10 mic. produced
7.85	15	50	8.7	52.0	6.1	10.5
		72	8.8	54.5	5.5	9.8
		164	9.8	69.1	5.4	10.6
	10	72	7.8	37.6	7.8	12.1
		164	8.3	45.2	7.4	12.1
		300	9.2	57.4	7.4	13.6
	6	72	-	28.2	9.4	14.2
		164	7.8	32.1	8.3	12.7
		300	7.8	40.2	8.2	12.9
		400	7.8	49.3	8.2	13.1
2.65	6	164	107.6	7.4	-	-
		300	9.9	9.6	-	-
		400	14.4	14.4	-	-

Table A4.11. Effect of pin spacing on median size, torque and media wear using grinding media of varying sizes: pulp density = 75% solids by weight, media type = steel, load depth = 32 cm, shaft speed = 164 r.p.m., pin diameter = 1.6 cm, energy input = 66 kWh/t (data shown in Figures 4.16, 4.17, 4.18).

Ball size mm	¹ Pin spacing cm	² Pin spacing cm	median size mic.	Torque Nm	Media wear, kg/t	
					Feed	- 10 mic. produced
10	5.6	4.0	7.9	52.4	7.8	12.6
	8.6	7.0	8.3	45.2	7.4	12.1
	13.1	11.5	8.5	37.3	7.4	12.5
	20.8	19.2	8.9	29.4	7.1	12.6
6	3.6	2.0	7.2	51.8	8.5	12.3
	5.6	4.0	7.7	45.0	8.2	12.6
	8.6	7.0	7.8	32.1	8.3	12.7
	13.1	11.5	8.5	30.7	7.8	13.2

¹ The distance between the centre lines of the nearest two pins

² The distance between the nearest edges of two pins

APPENDIX 5

OPTIMUM BATCH GRINDING CONDITIONS IN TUMBLING BALL MILL

A series of experiments were carried out to determine the optimum grinding conditions for a batch tumbling ball mill in order to compare it with the stirred ball mill. The following variables were kept constant during the experiments. The ball charge was 42.7 kg (40% of mill volume). All tests were run at 54.8 r.p.m which was 70% of the critical speed and mill slurry loadings corresponded to the media void volume filling of 100%. The effect of the grinding media size and pulp density on the size reduction were investigated. Experimental factors were varied one at a time, with the remaining factors held constant.

Figure A5.1 and Table A5.1 show the variation in median size as a function of energy input using ball diameters of various sizes. The breakage rates for 23 mm steel balls were somewhat higher than for 40 & 30 mm steel balls (38.2% of 40 mm & 61.8% of 30 mm balls by weight). This results from the increase in the rate of ball to ball contact per unit time because as the ball diameter decreases, the number of balls in the mill increases.

The median size versus pulp density curve is shown in Figure A5.2 and Table A5.2. Test results demonstrated that the median size of the product decreased for up to 75% pulp density. After reaching a minimum value, it increased significantly at higher slurry densities. At a pulp density of 85%, after an energy input of 25 kWh/t the power draw fell to almost zero, the grinding media ceased to tumble and the grinding action stopped.

The increase in grinding efficiency with an increase in pulp density from up to 75% was probably due to a greater solid packing in the grinding media voids. When the grinding was carried out on high pulp densities (above 75%) the viscosity increased with pulp density, resulting in a slowing down of breakage rates. It can therefore be concluded that the optimum pulp density is 75%.

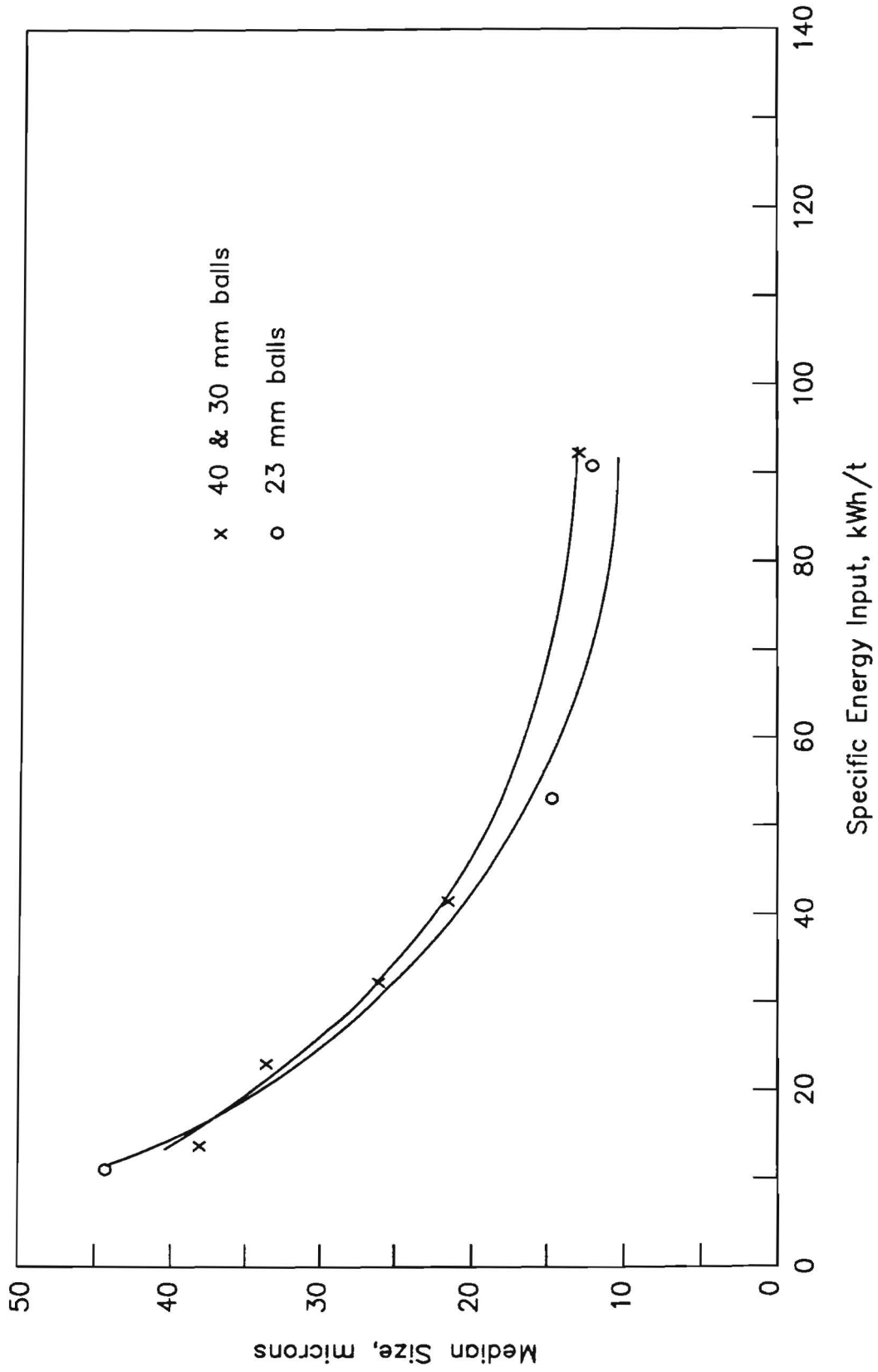


Figure A5.1. Effect of ball size as a function of energy input at a pulp density of 62.5%: ball charge = 42.7 kg, mill speed = 54.8 r.p.m. (data given in Table A5.1).

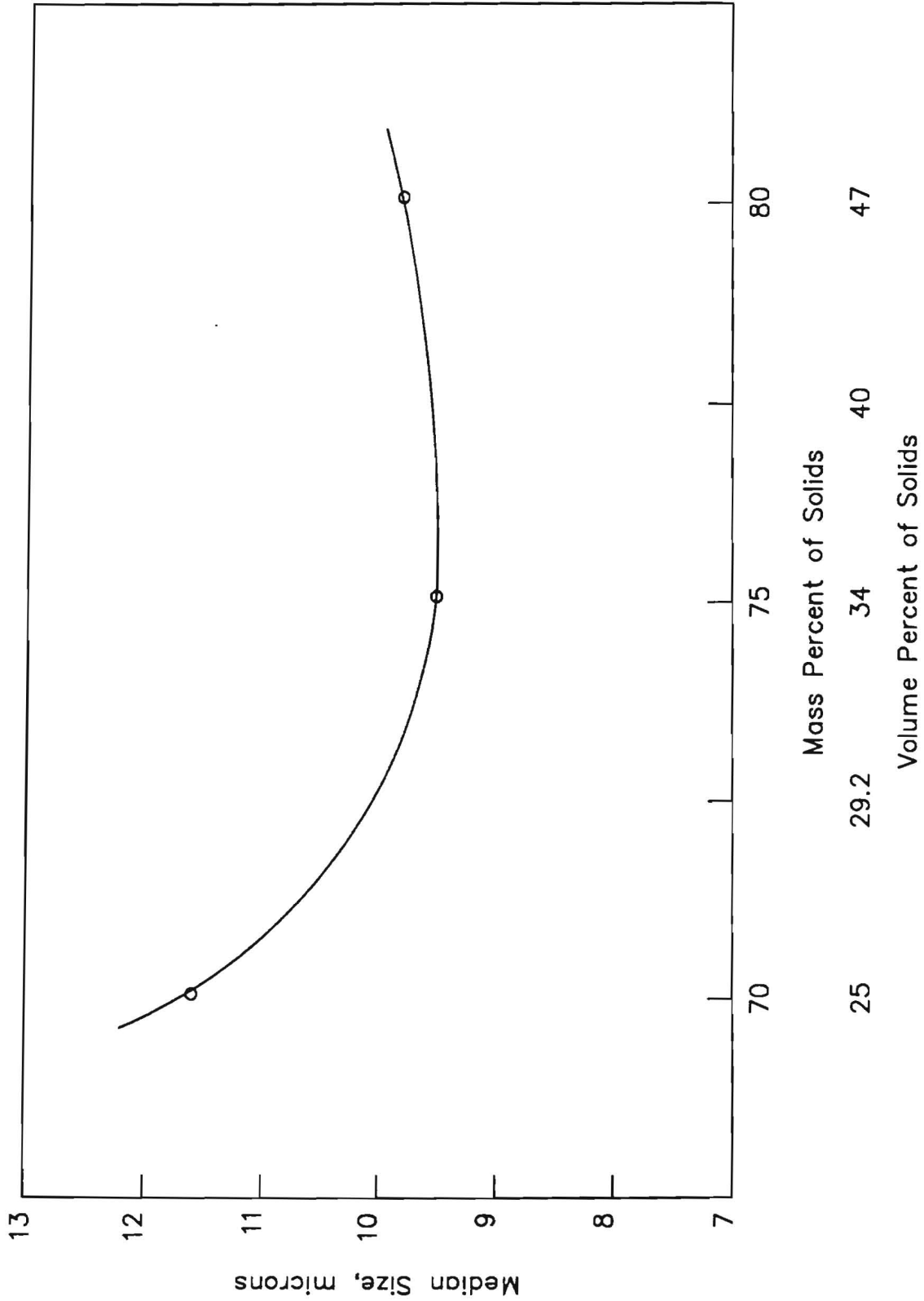


Figure A5.2. Variation of median size of product with slurry density at 66 kWh/t energy input using 23 mm balls; ball charge = 42.7 kg, mill speed = 54.8 r.p.m. (data given in Table A5.2).

Table A5.1. Effect of ball size as a function of energy input at 62.5% pulp density in tumbling ball mill: ball charge = 42.7 kg, mill speed = 54.8 r.p.m. (data shown in Figure A5.1).

Energy input kWh/t	Median size, mic.	
	Ball size, mm	
	40 & 30	23
10.4	-	44.3
13.2	38.1	-
22.5	33.6	-
31.7	26.1	-
40.9	21.6	-
52.5	-	14.7
90.2	-	12.1
91.7	13.0	-

Table A5.2. Variation of median size of product with slurry density (vol. % solids) at 66.0 kWh/t energy input using 23 mm steel balls in tumbling ball mill: ball charge = 42.7 kg, mill speed = 54.8 r.p.m. (data shown in Figure A5.2).

Weight % solids	Vol. % solids	Median size, mic.
70.0	34.0	11.6
75.0	40.0	9.5
80.0	47.0	9.8
85.0	56.0	*

* Tumbling action of the grinding media almost stopped after an energy input of 25 kWh/t

COMPARISON BETWEEN STIRRED AND TUMBLING BALL MILLS

Table A5.3. Size distribution of products from stirred and tumbling ball mill at various levels of energy input (experimental conditions given in Table 5.1 and data shown in Figure 5.1).

Particle size mic.	Cumulative weight percent passing			
	Energy input levels, kWh/t			
	Stirred ball mill		Tumbling ball	
	28.0	66.0	28.0	66.0
425.0	100.0	100.0	100.0	100.0
300.0	95.8	100.0	100.0	100.0
212.0	93.3	100.0	100.0	100.0
150.0	91.8	100.0	100.0	100.0
106.0	90.4	100.0	100.0	100.0
75.0	89.2	100.0	98.7	100.0
38.0	87.4	100.0	94.9	99.9
38.0	83.1	100.0	84.1	98.6
28.1	71.8	99.4	71.0	95.2
21.5	59.6	97.4	57.8	87.0
16.7	47.6	91.8	45.3	76.1
12.9	38.9	80.9	37.3	63.7
10.1	31.6	69.0	30.8	52.9
7.9	22.8	56.9	22.0	42.0
6.2	16.0	40.5	15.5	31.8

Table A5.4. Median size, torque, media wear from stirred and tumbling ball mills at various levels of energy input (experimental conditions given in Table 5.1 and data shown in Figures 5.2, 5.4, 5.5, 5.7 and 5.8).

Energy input kWh.t	Stirred ball mill				Tumbling ball mill			
	Median size mic.	Torque Nm	Media wear kg/t		Median size mic.	Torque Nm	Media wear kg/t	
			Feed	-10 mic. prod.			Feed	-10 mic. prod.
1.0	-	82.0	-	-	-	24.3	-	-
10.0	-	72.1	-	-	-	23.2	-	-
20.0	28.7	57.4	3.8	-	22.5	24.9	3.0	12.3
28.0	17.7	54.9	4.5	17.4	18.5	25.2	3.9	12.6
36.0	13.2	53.7	5.8	14.2	15.1	25.2	4.5	12.8
52.5	8.8	52.5	7.6	12.7	11.2	26.2	5.5	11.7
66.0	7.2	51.0	8.5	12.2	9.5	27.0	6.0	11.3
90.0	5.2	48.1	11.0	11.9	-	-	-	-
130.8	-	-	-	-	6.6	28.4	8.9	11.7

Table A5.5. Energy reduction in percent for the 50% passing product size when stirred ball mill is used instead of tumbling ball mill (experimental conditions given in Table 5.1 and data shown in Figure 5.3).

Median size mic.	Energy reduction %
17	3.3
13	16.3
10	25.8
8	34.9
7	40.4
6	50.0

Table A5.6. Comparison between the energy input per ton grinding media as a function of mill speed for stirred and tumbling mills (experimental conditions given in Table 5.1 and data shown in Figure 5.6).

Mill speed r.p.m.	Power density, kW per ton grinding media	
	Stirred ball mill	Tumbling ball mill
39.2	-	2.2
54.8	-	3.1
70.5	-	4.1
164.0	12.5	-
300.0	26.2	-
400.0	40.4	-

APPENDIX 6.1**EXPERIMENTAL AND CALCULATED PRODUCT SIZE DISTRIBUTIONS AT
VARIOUS GRINDING CONDITIONS IN A BATCH 5 LITRE STIRRED BALL
MILL**

Table A6.1.1. Experimental and calculated product size distributions at different energy input levels using grinding conditions in Table 6.1, test no:1.

Particle size mic.	Cumulative weight percent passing												
	Feed	Energy input levels, kWh/t											
		25			50		75		100		150		200
Exp.	Exp. ¹	Calc. ²	Exp.	Calc.									
71.9	89.9	100.0	100.0										
58.2	84.3	99.9	100.0	100.0	100.0								
47.1	77.6	99.7	99.9	99.9	100.0								
38.1	70.2	99.2	99.4	99.9	100.0								
30.8	62.4	98.3	98.2	99.7	99.9	100.0	100.0	100.0	100.0				
24.9	54.7	96.6	95.7	99.4	99.5	99.9	99.9	99.9	100.0				
20.1	47.3	93.2	91.5	98.6	98.5	99.7	99.7	99.8	99.9				
16.3	40.4	87.7	85.7	97.2	96.3	99.2	99.0	99.5	99.7	100.0	100.0	100.0	100.0
13.2	34.2	79.9	78.3	94.3	92.5	98.0	97.3	98.9	99.0	99.9	99.9	99.9	100.0
10.7	28.6	70.5	70.0	89.6	86.9	95.9	94.1	97.7	97.3	99.7	99.4	99.9	99.9
8.62	23.8	60.3	60.9	82.4	79.6	92.1	89.1	95.5	94.1	98.9	98.2	99.7	99.4
6.97	19.7	50.5	52.2	73.0	71.3	86.0	82.4	91.6	89.1	96.9	95.7	98.8	98.2
5.64	16.2	41.7	44.0	62.6	62.5	77.6	74.5	85.4	82.5	93.1	91.5	96.7	95.8
4.56	13.2	34.2	36.6	52.3	53.7	67.6	65.8	76.9	74.5	87.4	85.6	92.8	91.7
3.69	10.8	28.1	30.1	43.2	45.4	57.2	56.9	67.0	65.8	79.7	78.2	86.9	85.9
2.98	8.1	23.2	24.4	35.8	37.7	47.5	48.3	56.8	56.9	70.8	69.7	79.2	78.5
2.41	6.9	19.0	19.7	29.5	31.1	39.0	40.4	47.1	48.3	61.2	60.8	70.1	70.0
1.95	5.5	15.6	15.9	24.2	25.3	31.9	33.4	38.7	40.5	51.8	52.1	60.6	61.2
1.58	4.2	12.6	12.7	19.7	20.5	26.0	27.4	31.6	33.5	43.0	43.9	51.2	52.5
1.28	3.3	10.0	10.1	16.0	16.5	21.0	22.3	25.7	27.5	35.0	36.6	42.4	44.3
1.03	2.5	8.0	8.0	12.9	13.2	16.9	17.8	20.7	22.2	28.2	29.9	34.5	36.7
0.83	1.9	6.2	6.3	10.2	10.4	13.4	14.2	16.5	17.8	22.4	24.3	27.7	30.1
0.68	1.4	4.8	5.1	7.9	8.4	10.4	11.5	12.8	14.4	17.6	19.9	22.0	24.8
$d_{63.2}$	30.5	9.15		5.63		4.10		3.33		2.50		2.05	
δ	1.03	1.16	1.14	1.19	1.14	1.20	1.14	1.21	1.14	1.22	1.14	1.22	1.14
β		-1.25	-1.25	-1.25	-1.25	-1.25	-1.25	-1.25	-1.25	-1.25	-1.25	-1.25	-1.25
1/K	1.97 x 10 ⁻³												
Computed t statistic = -0.017 with 226 d.f.													

Grinding conditions : Pulp density : 1880 kg/m³
 Pin tip velocity : 2.56 m/s
 Ball density : 3450 kg/m³
 Ave. ball size : 0.0036 m
 Mill size : 5 litre

1 Exp. : experimental product size distribution.

2 Calc : calculated product size distribution using Equation 6.8.

Table A6.1.2. Experimental and calculated product size distributions at different energy input levels using grinding conditions in Table 6.1, test no:2.

Particle size mic.	Cumulative weight percent passing												
	Feed	Energy input levels, kWh/t											
		25		50		75		100		150		200	
	Exp.	Exp.	Calc.	Exp.	Calc.	Exp.	Calc.	Exp.	Calc.	Exp.	Calc.	Exp.	Calc.
71.9	89.9												
58.2	84.3	100.0	100.0										
47.1	77.6	99.8	99.9										
38.1	70.2	99.2	99.4	100.0	100.0								
30.8	62.4	97.8	98.2	99.9	99.9								
24.9	54.7	95.0	95.7	99.6	99.5	100.0	99.9						
20.1	47.3	90.4	91.5	98.6	98.5	99.8	99.7	100.0	99.9				
16.3	40.4	84.2	85.7	96.3	96.3	99.2	99.0	99.8	99.7	100.0	100.0		
13.2	34.2	76.4	78.3	92.4	92.5	97.6	97.3	99.2	99.0	99.9	99.9	100.0	100.0
10.7	28.6	67.8	70.0	86.5	86.9	94.6	94.1	97.6	97.3	99.4	99.4	99.9	99.9
8.62	23.8	58.9	60.9	79.0	79.6	89.6	89.1	94.5	94.1	98.1	98.2	99.4	99.4
6.97	19.7	50.3	52.2	70.3	71.3	82.8	82.4	89.5	89.1	95.4	95.7	98.2	98.2
5.64	16.2	42.2	44.0	61.1	62.5	74.6	74.5	82.7	82.5	90.9	91.5	95.7	95.8
4.56	13.2	34.9	36.6	52.0	53.7	65.6	65.8	74.4	74.5	84.5	85.6	91.4	91.7
3.69	10.8	28.6	30.1	43.5	45.4	56.7	56.9	65.3	65.8	76.6	78.2	85.3	85.9
2.98	8.1	23.2	24.4	35.8	37.7	47.8	48.3	56.1	56.9	67.7	69.7	77.5	78.5
2.41	6.9	18.7	19.7	29.1	31.1	39.9	40.4	47.2	48.3	58.4	60.8	68.8	70.0
1.95	5.5	14.9	15.9	23.4	25.3	32.5	33.4	39.0	40.5	49.5	52.1	59.6	61.2
1.58	4.2	11.9	12.7	18.7	20.5	26.5	27.4	31.8	33.5	41.1	43.9	50.6	52.5
1.28	3.3	9.4	10.1	14.8	16.5	21.6	22.3	25.7	27.5	33.7	36.6	42.2	44.3
1.03	2.5	7.4	8.0	11.7	13.2	17.2	17.8	20.5	22.2	27.2	29.9	34.7	36.7
0.83	1.9	5.8	6.3	9.1	10.4	13.8	14.2	16.2	17.8	21.8	24.3	28.1	30.1
0.68	1.4	4.5	5.1	7.1	8.4	11.5	11.5	12.7	14.4	17.3	19.9	22.5	24.8
$d_{63.2}$	30.5	9.52		5.90		4.32		3.49		2.67		2.10	
δ	1.03	1.14	1.14	1.18	1.14	1.18	1.14	1.18	1.14	1.17	1.14	1.16	1.14
β		-1.23	-1.25	-1.23	-1.25	-1.23	-1.25	-1.23	-1.25	-1.23	-1.25	-1.23	-1.25
1/K	1.94 x 10 ⁻³												
Computed t statistic = -0.200 with 212 d.f.													

Grinding conditions :

- Pulp density : 2200 kg/m³
- Pin tip velocity : 2.56 m/s
- Ball density : 3450 kg/m³
- Ave. ball size : 0.0036 m
- Mill size : 5 litre

Table A6.1.3. Experimental and calculated product size distributions at different energy input levels using grinding conditions in Table 6.1, test no:3.

Particle Size mic.	Cumulative weight percent passing												
	Feed	Energy input levels, kWh/t											
		25		50		75		100		150		200	
	Exp.	Exp.	Calc.	Exp.	Calc.	Exp.	Calc.	Exp.	Calc.	Exp.	Calc.	Exp.	Calc.
71.9	89.9	100.0	100.0	100.0	100.0								
58.2	84.3	99.9	99.9	99.9	100.0								
47.1	77.6	99.7	99.7	99.9	100.0								
38.1	70.2	99.2	99.0	99.7	100.0	100.0	100.0						
30.8	62.4	98.1	97.3	99.4	99.8	99.9	100.0	100.0	100.0	100.0	100.0	100.0	100.0
24.9	54.7	95.9	94.1	98.9	99.1	99.8	99.9	99.9	100.0	99.9	100.0	99.9	100.0
20.1	47.3	92.1	89.1	97.8	97.5	99.5	99.4	99.7	99.8	99.8	100.0	99.8	100.0
16.3	40.4	86.2	82.5	95.7	94.5	98.7	98.2	99.2	99.4	99.6	99.9	99.6	100.0
13.2	34.2	78.1	74.6	92.1	89.8	97.0	95.8	98.3	98.2	99.1	99.7	99.3	99.9
10.7	28.6	68.8	66.0	86.6	83.4	94.0	91.7	96.6	95.8	98.3	98.9	98.9	99.7
8.62	23.8	59.2	57.0	79.1	75.5	89.1	85.7	93.6	91.6	96.8	97.0	98.1	98.9
6.97	19.7	49.9	48.4	69.8	66.8	82.0	78.3	88.6	85.6	94.1	93.6	96.6	97.1
5.64	16.2	41.6	40.5	59.7	58.0	73.0	69.9	81.4	78.2	89.7	88.4	93.9	93.7
4.56	13.2	34.5	33.5	49.9	49.3	62.9	61.0	72.3	69.8	83.1	81.6	89.5	88.6
3.69	10.8	28.6	27.4	41.0	41.4	53.0	52.3	62.3	60.9	74.5	73.5	83.1	81.9
2.98	8.1	23.7	22.2	33.5	34.2	44.2	44.0	52.7	52.1	65.0	64.7	74.8	73.8
2.41	6.9	19.5	17.9	27.0	28.0	36.5	36.6	43.8	43.9	55.3	55.9	64.8	65.0
1.95	5.5	16.0	14.3	21.5	22.8	30.0	30.1	36.2	36.5	46.2	47.4	55.7	56.2
1.58	4.2	13.0	11.5	17.0	18.4	24.6	24.5	29.8	30.1	38.3	39.7	46.1	47.8
1.28	3.3	10.4	9.1	13.3	14.8	19.9	19.9	24.3	24.5	31.4	32.8	38.8	40.0
1.03	2.5	8.3	7.2	10.4	11.7	16.1	15.9	19.8	19.7	25.5	26.7	32.1	32.9
0.83	1.9	6.5	5.7	8.0	9.3	12.7	12.6	15.9	15.8	20.4	21.5	25.9	26.8
0.68	1.4	5.0	4.6	6.1	7.5	9.8	10.2	12.4	12.8	16.9	17.6	19.9	22.0
$d_{63.2}$	30.5	9.44		6.03		4.52		3.64		2.76		2.16	
δ	1.03	1.12	1.14	1.16	1.14	1.16	1.14	1.17	1.14	1.16	1.14	1.15	1.14
β		-1.27	-1.25	-1.27	-1.25	-1.27	-1.25	-1.27	-1.25	-1.27	-1.25	-1.27	-1.25
1/K	1.82×10^{-3}												
Computed t statistic = 0.102 with 242 d.f.													

Grinding conditions :

Pulp density	: 1880 kg/m ³
Pin tip velocity	: 3.66 m/s
Ball density	: 3450 kg/m ³
Ave. ball size	: 0.0036 m
Mill size	: 5 litre

Table A6.1.4. Experimental and calculated product size distributions at different energy input levels using grinding conditions in Table 6.1, test no:4.

Particle size mic.	Cumulative weight percent passing												
	Feed	Energy input levels, kWh/t											
		25		50		75		100		150		200	
	Exp.	Exp.	Calc.	Exp.	Calc.	Exp.	Calc.	Exp.	Calc.	Exp.	Calc.	Exp.	Calc.
71.9	89.9	100.0	100.0										
58.2	84.3	99.9	99.9										
47.1	77.6	99.7	99.7										
38.1	70.2	98.9	99.0	100.0	100.0								
30.8	62.4	97.2	97.3	99.8	99.8	100.0	100.0						
24.9	54.7	94.1	94.1	99.3	99.1	99.9	99.9	100.0	100.0				
20.1	47.3	89.2	89.1	98.0	97.5	99.6	99.4	99.9	99.8	100.0	100.0		
16.3	40.4	82.7	82.5	95.3	94.5	98.6	98.2	99.5	99.4	99.9	99.9	100.0	100.0
13.2	34.2	75.0	74.6	90.0	89.8	96.5	95.8	98.5	98.2	99.6	99.7	99.9	99.9
10.7	28.6	66.4	66.0	84.8	83.4	92.9	91.7	96.3	95.8	98.8	98.9	99.6	99.7
8.62	23.8	57.7	57.0	77.1	75.5	87.4	85.7	92.5	91.6	96.9	97.0	98.6	98.9
6.97	19.7	49.2	48.4	68.5	66.8	80.2	78.3	87.0	85.6	93.5	93.6	96.6	97.1
5.64	16.2	41.4	40.5	59.6	58.0	71.9	69.9	79.8	78.2	88.4	88.4	93.1	93.7
4.56	13.2	34.3	33.5	50.8	49.3	63.0	61.0	71.5	69.8	81.7	81.6	87.9	88.6
3.69	10.8	28.2	27.4	42.6	41.4	54.1	52.3	62.6	60.9	73.8	73.5	81.1	81.9
2.98	8.1	22.9	22.2	35.2	34.2	45.6	44.0	53.8	52.1	65.1	64.7	73.1	73.8
2.41	6.9	18.5	17.9	28.8	28.0	37.9	36.6	45.4	43.9	56.3	55.9	64.5	65.0
1.95	5.5	14.9	14.3	23.3	22.8	31.1	30.1	37.7	36.5	47.9	47.4	55.8	56.2
1.58	4.2	11.9	11.5	18.7	18.4	25.2	24.5	31.0	30.1	40.0	39.7	47.4	47.8
1.28	3.3	9.4	9.1	14.9	14.8	20.3	19.9	25.1	24.5	33.0	32.8	39.6	40.0
1.03	2.5	7.5	7.2	11.8	11.7	16.2	15.9	20.2	19.7	26.9	26.7	32.7	32.9
0.83	1.9	5.9	5.7	9.3	9.3	12.8	12.6	16.1	15.8	21.8	21.5	26.7	26.8
0.68	1.4	4.6	4.6	7.3	7.5	11.4	10.2	12.8	12.8	17.4	17.6	21.5	22.0
$d_{63.2}$	30.5	9.83		6.12		4.56		3.71		2.82		2.31	
δ	1.03	1.12	1.14	1.15	1.14	1.15	1.14	1.14	1.14	1.14	1.14	1.14	1.14
β		-1.28	-1.25	-1.28	-1.25	-1.28	-1.25	-1.28	-1.25	-1.28	-1.25	-1.28	-1.25
1/K	1.65×10^{-3}												
Computed t statistic = 0.103 with 222 d.f.													

Grinding conditions :

Pulp density	: 2200 kg/m ³
Pin tip velocity	: 3.66 m/s
Ball density	: 3450 kg/m ³
Ave. Ball size	: 0.0036 m
Mill size	: 5 litre

Table A6.1.5. Experimental and calculated product size distributions at different energy input levels using grinding conditions in Table 6.1, test no:5.

Particle size mic.	Cumulative weight percent passing												
	Feed	Energy input levels, kWh/t											
		25		50		75		100		150		200	
Exp.	Exp.	Calc.	Exp.	Calc.	Exp.	Calc.	Exp.	Calc.	Exp.	Calc.	Exp.	Calc.	
71.9	89.9	99.9	100.0										
58.2	84.3	99.7	100.0										
47.1	77.6	99.2	99.7	100.0	100.0								
38.1	70.2	98.3	99.1	99.9	100.0	100.0	100.0						
30.8	62.4	96.7	97.5	99.8	99.8	99.9	100.0	100.0	100.0				
24.9	54.7	93.9	94.5	99.3	99.2	99.9	99.9	99.9	100.0	100.0	100.0		
20.1	47.3	89.2	89.6	97.9	97.7	99.7	99.5	99.9	99.9	99.9	100.0		
16.3	40.4	82.4	83.2	95.1	94.9	98.8	98.4	99.7	99.5	99.9	99.9	100.0	100.0
13.2	34.2	73.7	75.4	90.4	90.4	96.7	96.1	98.8	98.4	99.9	99.7	99.9	99.9
10.7	28.6	64.1	66.9	83.8	84.2	92.8	92.3	96.7	96.2	99.4	99.0	99.9	99.7
8.62	23.8	54.6	57.8	75.7	76.4	87.0	86.5	92.8	92.2	98.1	97.3	99.5	99.0
6.97	19.7	45.7	49.2	66.7	67.8	79.4	79.2	86.8	86.4	95.3	94.1	98.3	97.4
5.64	16.2	37.8	41.3	57.5	59.0	70.5	70.9	79.1	79.2	90.6	89.2	95.7	94.2
4.56	13.2	31.1	34.1	48.6	50.3	61.2	62.1	70.2	70.8	84.0	82.5	91.2	89.4
3.69	10.8	25.6	28.0	40.4	42.2	51.9	53.3	60.7	62.0	76.5	74.6	84.6	82.8
2.98	8.1	21.0	22.7	33.1	35.0	43.2	44.9	51.3	53.2	66.4	65.8	76.4	74.8
2.41	6.9	17.2	18.3	26.8	28.7	35.4	37.4	42.6	44.9	56.9	56.9	67.1	66.1
1.95	5.5	14.0	14.7	21.5	23.3	28.7	30.8	34.8	37.4	47.7	48.4	57.6	57.3
1.58	4.2	11.3	11.7	17.1	18.8	23.0	25.1	28.0	30.8	39.3	40.6	48.3	48.8
1.28	3.3	9.1	9.3	13.5	15.1	18.2	20.4	22.4	25.1	31.9	33.6	39.8	40.9
1.03	2.5	7.2	7.4	10.6	12.0	14.4	16.3	17.7	20.2	25.6	27.4	32.3	33.7
0.83	1.9	5.6	5.8	8.3	9.5	11.2	13.0	13.9	16.2	20.3	22.1	25.8	27.5
0.68	1.4	4.4	4.7	6.4	7.7	8.7	10.5	10.8	13.1	15.9	18.1	20.4	22.6
$d_{63.2}$	30.5	9.92		6.41		4.76		3.89		2.76		2.22	
δ	1.03	1.14	1.14	1.18	1.14	1.20	1.14	1.22	1.14	1.21	1.14	1.22	1.14
β		-1.23	-1.25	-1.23	-1.25	-1.23	-1.25	-1.23	-1.25	-1.23	-1.25	-1.23	-1.25
1/K	1.80×10^{-3}												
Computed t statistic = -0.161 with 230 d.f.													

Grinding conditions :

Pulp density	: 1880 kg/m ³
Pin tip velocity	: 2.56 m/s
Ball density	: 7850 kg/m ³
Ave. ball size	: 0.0036 m
Mill size	: 5 litre

Table A6.1.6. Experimental and calculated product size distributions at different energy input levels using grinding conditions in Table 6.1, test no:6.

Particle size mic.	Cumulative weight percent passing												
	Feed	Energy input levels, kWh/t											
		25		50		75		100		150		200	
	Exp.	Exp.	Calc.	Exp.	Calc.	Exp.	Calc.	Exp.	Calc.	Exp.	Calc.	Exp.	Calc.
71.9	89.9	100.0	100.0										
58.2	84.3	99.9	100.0	100.0	100.0								
47.1	77.6	99.6	99.7	99.9	100.0								
38.1	70.2	99.1	99.1	99.8	100.0								
30.8	62.4	98.1	97.5	99.6	99.8	100.0	100.0	100.0	100.0			100.0	100.0
24.9	54.7	96.0	94.5	99.2	99.2	99.9	99.9	99.9	100.0	100.0	100.0	99.9	100.0
20.1	47.3	92.1	89.6	98.3	97.7	99.7	99.6	99.8	99.9	99.9	100.0	99.8	100.0
16.3	40.4	85.7	83.2	96.5	94.9	99.1	98.6	99.5	99.5	99.7	99.9	99.7	100.0
13.2	34.2	76.9	75.4	92.9	90.4	97.7	96.6	98.8	98.4	99.4	99.7	99.5	99.9
10.7	28.6	66.9	66.9	87.1	84.2	94.9	92.9	97.4	96.2	98.8	99.0	99.1	99.7
8.62	23.8	56.8	57.8	78.6	76.4	90.1	87.4	94.7	92.2	97.7	97.3	98.4	99.0
6.97	19.7	47.5	49.2	68.3	67.8	82.6	80.3	89.9	86.4	95.5	94.1	97.0	97.4
5.64	16.2	39.5	41.3	57.6	59.0	72.9	72.1	82.6	79.2	91.6	89.2	94.6	94.2
4.56	13.2	32.7	34.1	47.9	50.3	62.2	63.3	73.1	70.8	85.4	82.5	90.3	89.4
3.69	10.8	27.2	28.0	39.9	42.2	52.1	54.5	62.7	62.0	76.9	74.6	83.9	82.8
2.98	8.1	22.6	22.7	33.3	35.0	43.3	46.1	52.8	53.2	67.2	65.8	75.4	74.8
2.41	6.9	18.6	18.3	27.5	28.7	35.8	38.4	43.9	44.9	58.4	56.9	65.1	66.1
1.95	5.5	15.1	14.7	22.6	23.3	29.4	31.7	36.2	37.4	49.1	48.4	57.0	57.3
1.58	4.2	12.1	11.7	18.2	18.8	24.0	25.9	29.6	30.8	40.5	40.6	47.6	48.8
1.28	3.3	9.5	9.3	14.4	15.1	19.2	21.0	23.8	25.1	33.0	33.6	39.0	40.9
1.03	2.5	7.4	7.4	11.3	12.0	15.2	16.8	19.0	20.2	26.4	27.4	31.5	33.7
0.83	1.9	5.7	5.8	8.7	9.5	11.8	13.4	14.8	16.2	21.0	22.1	25.1	27.5
0.68	1.4	4.3	4.7	6.6	7.7	8.9	10.8	11.3	13.1	16.5	18.1	19.7	22.6
$d_{63.2}$	30.5	9.85		6.13		4.55		3.61		2.67		2.25	
δ	1.03	1.14	1.14	1.18	1.14	1.20	1.14	1.20	1.14	1.21	1.14	1.22	1.14
β		-1.26	-1.25	-1.26	-1.25	-1.26	-1.25	-1.26	-1.25	-1.26	-1.25	-1.26	-1.25
1/K	1.74 X 10 ⁻³												
Computed t statistic = -0.022 with 236 d.f.													

Grinding conditions :

Pulp density	: 2200 kg/m ³
Pin tip velocity	: 2.56 m/s
Ball density	: 7850 kg/m ³
Ave. ball size	: 0.0036 m
Mill size	: 5 litre

Table A6.1.7. Experimental and calculated product size distributions at different energy input levels using grinding conditions in Table 6.1, test no:7.

Particle size mic.	Cumulative weight percent passing												
	Feed	Energy input levels, kWh/t											
		25		50		75		100		150		200	
	Exp.	Exp.	Calc.	Exp.	Calc.	Exp.	Calc.	Exp.	Calc.	Exp.	Calc.	Exp.	Calc.
71.9	89.9	99.9	100.0	100.0	100.0	100.0	100.0						
58.2	84.3	99.7	99.9	99.9	100.0	99.9	100.0						
47.1	77.6	99.1	99.5	99.8	100.0	99.8	100.0						
38.1	70.2	98.0	98.5	99.5	99.9	99.7	100.0	100.0	100.0				
30.8	62.4	96.1	96.4	99.0	99.6	99.4	99.9	99.9	100.0				
24.9	54.7	92.8	92.6	98.0	98.6	99.0	99.7	99.8	99.9	100.0	100.0		
20.1	47.3	87.7	87.0	96.1	96.5	98.2	99.0	99.4	99.7	99.9	100.0	100.0	100.0
16.3	40.4	80.6	79.9	92.8	92.9	96.7	97.4	98.6	99.0	99.9	99.9	99.9	100.0
13.2	34.2	71.9	71.7	87.7	87.5	94.0	94.3	96.9	97.3	99.7	99.4	99.9	99.9
10.7	28.6	62.6	63.0	80.7	80.5	89.7	89.5	94.2	94.3	98.8	98.2	99.7	99.4
8.62	23.8	53.6	54.0	72.2	72.2	83.6	82.8	89.8	89.3	96.9	95.7	98.9	98.2
6.97	19.7	45.2	45.6	62.8	63.4	75.5	74.9	83.5	82.7	93.2	91.6	97.1	95.8
5.64	16.2	37.8	38.0	53.6	54.6	66.3	66.3	75.4	74.8	87.7	85.6	93.5	91.7
4.56	13.2	31.4	31.3	45.0	46.1	56.8	57.4	66.2	66.1	80.5	78.2	88.0	85.8
3.69	10.8	26.0	25.6	37.6	38.5	48.0	48.8	56.8	57.2	72.0	69.8	80.7	78.5
2.98	8.1	21.6	20.7	31.3	31.7	40.3	40.9	48.1	48.6	62.9	60.9	72.1	70.0
2.41	6.9	17.7	16.6	25.8	25.9	33.4	33.8	40.1	40.7	53.7	52.1	62.9	61.1
1.95	5.5	14.5	13.3	21.0	20.9	27.3	27.7	33.1	33.7	45.1	43.9	53.6	52.4
1.58	4.2	11.6	10.6	16.8	16.9	21.9	22.5	27.0	27.6	37.2	36.6	44.8	44.2
1.28	3.3	9.2	8.5	13.2	13.5	17.3	18.2	21.7	22.4	30.3	30.1	36.8	36.8
1.03	2.5	7.2	6.7	10.2	10.7	13.5	14.5	17.2	18.0	24.4	24.4	29.8	30.1
0.83	1.9	5.5	5.2	7.8	8.5	10.3	11.5	13.3	14.4	19.5	19.6	23.9	24.4
0.68	1.4	4.2	4.2	5.9	6.8	7.8	9.3	10.8	11.6	15.4	16.0	18.9	20.0
$d_{63.2}$	30.5	10.72		6.87		5.09		4.13		2.98		2.41	
δ	1.03	1.10	1.14	1.14	1.14	1.15	1.14	1.14	1.14	1.17	1.14	1.19	1.14
β		-1.22	-1.25	-1.22	-1.25	-1.22	-1.25	-1.22	-1.25	-1.22	-1.25	-1.22	-1.25
1/K	1.64 x 10 ₋₃												
Computed t statistic = 0.019 with 244 d.f.													

Grinding conditions :

Pulp density	: 1880 kg/m ³
Pin tip velocity	: 3.66 m/s
Ball density	: 7850 kg/m ³
Ave. ball size	: 0.0036 m
Mill size	: 5 litre

Table A6.1.8. Experimental and calculated product size distributions at different energy input levels using grinding conditions in Table 6.1, test no:8.

Particle size mic.	Cumulative weight percent passing												
	Feed	Energy input levels, kWh/t											
		25		50		75		100		150		200	
	Exp.	Exp.	Calc.	Exp.	Calc.	Exp.	Calc.	Exp.	Calc.	Exp.	Calc.	Exp.	Calc.
71.9	89.9	99.9	100.0			100.0	100.0						
58.2	84.3	99.8	99.9	100.0	100.0	99.9	100.0						
47.1	77.6	99.4	99.5	99.9	100.0	99.8	100.0						
38.1	70.2	98.6	98.5	99.7	99.9	99.7	100.0						
30.8	62.4	97.1	96.4	99.4	99.6	99.6	99.9	100.0	100.0	100.0	100.0	100.0	100.0
24.9	54.7	94.3	92.6	98.8	98.6	99.3	99.7	99.9	99.9	99.9	100.0	99.9	100.0
20.1	47.3	89.7	87.0	97.4	96.5	98.7	99.0	99.7	99.7	99.8	100.0	99.8	100.0
16.3	40.4	82.7	79.9	94.8	92.9	97.5	97.4	99.2	99.0	99.6	99.9	99.7	100.0
13.2	34.2	73.9	71.7	90.3	87.5	95.4	94.3	98.1	97.3	99.2	99.4	99.4	99.9
10.7	28.6	64.3	63.0	83.6	80.5	91.6	89.5	95.9	94.3	98.4	98.2	99.0	99.4
8.62	23.8	54.8	54.0	74.8	72.2	85.7	82.8	92.2	89.3	96.8	95.7	98.1	98.2
6.97	19.7	46.1	45.6	64.8	63.4	77.5	74.9	86.2	82.7	93.8	91.6	96.5	95.8
5.64	16.2	38.4	38.0	54.7	54.6	67.5	66.3	77.8	74.8	88.9	85.6	93.6	91.7
4.56	13.2	31.9	31.3	45.6	46.1	57.3	57.4	67.8	66.1	81.7	78.2	88.7	85.8
3.69	10.8	26.5	25.6	37.9	38.5	47.9	48.8	57.6	57.2	72.7	69.8	81.8	78.5
2.98	8.1	22.1	20.7	31.6	31.7	40.0	40.9	48.1	48.6	62.8	60.9	73.0	70.0
2.41	6.9	18.2	16.6	26.1	25.9	33.1	33.8	39.8	40.7	53.0	52.1	63.0	61.1
1.95	5.5	14.9	13.3	21.5	20.9	27.1	27.7	32.6	33.7	44.0	43.9	52.8	52.4
1.58	4.2	12.0	10.6	17.4	16.9	21.9	22.5	26.6	27.6	36.2	36.6	43.4	44.2
1.28	3.3	9.6	8.5	13.9	13.5	17.4	18.2	21.5	22.4	29.3	30.1	36.1	36.8
1.03	2.5	7.5	6.7	11.0	10.7	13.7	14.5	17.3	18.0	23.6	24.4	28.9	30.1
0.83	1.9	5.9	5.2	8.5	8.5	10.6	11.5	13.6	14.4	18.7	19.6	22.6	24.4
0.68	1.4	4.5	4.2	6.5	6.8	7.9	9.3	10.5	11.6	14.4	16.0	17.8	20.0
$d_{63.2}$	30.5	10.47		6.64		4.97		4.06		2.91		2.33	
δ	1.03	1.10	1.14	1.15	1.14	1.18	1.14	1.19	1.14	1.19	1.14	1.22	1.14
β		-1.21	-1.25	-1.21	-1.25	-1.21	-1.25	-1.21	-1.25	-1.21	-1.25	-1.21	-1.25
1/K	1.72 x 10 ⁻³												
Computed t statistic = 0.112 with 246 d.f.													

Grinding conditions :

Pulp density	: 2200 kg/m ³
Pin tip velocity	: 3.66 m/s
Ball density	: 7850 kg/m ³
Ave. ball size	: 0.0036 m
Mill size	: 5 litre

Table A6.1.9. Experimental and calculated product size distributions at different energy input levels using grinding conditions in Table 6.1, test no:9.

Particle size mic.	Cumulative weight percent passing												
	Feed	Energy input levels, kWh/t											
		25		50		75		100		150		200	
		Exp.	Calc.	Exp.	Calc.	Exp.	Calc.	Exp.	Calc.	Exp.	Calc.	Exp.	Calc.
71.9	89.9	100.0	100.0	100.0	100.0								
58.2	84.3	99.8	99.9	99.9	100.0								
47.1	77.6	99.6	99.5	99.9	100.0								
38.1	70.2	98.8	98.5	99.7	99.9	100.0	100.0						
30.8	62.4	96.8	96.3	99.4	99.6	99.9	99.9	100.0	100.0	100.0	100.0	100.0	100.0
24.9	54.7	93.5	92.5	98.7	98.6	99.8	99.7	99.9	99.9	99.9	100.0	99.9	100.0
20.1	47.3	89.2	86.9	97.5	96.5	99.3	99.0	99.6	99.7	99.8	100.0	99.9	100.0
16.3	40.4	82.4	79.8	95.1	92.8	98.3	97.3	99.1	99.0	99.5	99.8	99.7	100.0
13.2	34.2	74.4	71.5	91.0	87.3	96.2	94.2	97.9	97.3	98.9	99.4	99.4	99.9
10.7	28.6	64.7	62.8	84.8	80.4	92.6	89.4	95.8	94.2	97.9	98.2	98.8	99.4
8.62	23.8	55.7	53.8	76.6	72.0	87.1	82.7	92.2	89.1	96.0	95.6	97.8	98.2
6.97	19.7	47.2	45.5	66.9	63.1	79.4	74.7	86.4	82.5	92.7	91.4	95.8	95.7
5.64	16.2	39.0	37.9	56.8	54.4	70.1	66.1	78.5	74.6	87.3	85.5	92.2	91.6
4.56	13.2	32.7	31.2	47.3	46.0	59.9	57.2	68.9	65.8	79.7	78.0	86.6	85.7
3.69	10.8	27.0	25.5	39.3	38.3	50.2	48.6	58.8	57.0	70.4	69.6	78.8	78.2
2.98	8.1	21.5	20.6	32.6	31.5	41.7	40.7	49.4	48.4	60.5	60.6	69.5	69.7
2.41	6.9	17.1	16.5	26.9	25.7	34.3	33.6	41.0	40.5	50.8	51.9	59.5	60.9
1.95	5.5	13.7	13.2	22.1	20.8	28.1	27.5	33.7	33.5	42.1	43.7	49.8	52.2
1.58	4.2	11.1	10.6	18.1	16.8	23.0	22.4	27.7	27.4	34.7	36.4	41.2	44.0
1.28	3.3	8.8	8.4	14.6	13.5	18.6	18.1	22.5	22.3	28.3	29.9	33.7	36.6
1.03	2.5	6.8	6.6	11.8	10.7	15.0	14.4	18.2	17.9	23.0	24.2	27.4	30.0
0.83	1.9	5.1	5.2	9.3	8.4	11.9	11.4	14.5	14.3	18.4	19.5	21.8	24.3
0.68	1.4	4.1	4.2	7.2	6.8	9.2	9.2	11.2	11.5	14.4	15.9	16.9	19.9
$d_{63.2}$	30.5	10.35		6.40		4.80		3.96		3.06		2.49	
δ	1.03	1.14	1.14	1.15	1.14	1.17	1.14	1.17	1.14	1.18	1.14	1.18	1.14
β		-1.30	-1.25	-1.30	-1.25	-1.30	-1.25	-1.30	-1.25	-1.30	-1.25	-1.30	-1.25
1/K	1.48×10^{-3}												
Computed t statistic = 0.150 with 242 d.f.													

Grinding conditions :

Pulp density	: 1880 kg/m ³
Pin tip velocity	: 2.56 m/s
Ball density	: 3450 kg/m ³
Ave. ball size	: 0.005 m
Mill size	: 5 litre

Table A6.1.10. Experimental and calculated product size distributions at different energy input levels using grinding conditions in Table 6.1, test no:10.

Particle size mic.	Cumulative weight percent passing												
	Feed	Energy input levels, kWh/t											
		25		50		75		100		150		200	
	Exp.	Exp.	Calc.	Exp.	Calc.	Exp.	Calc.	Exp.	Calc.	Exp.	Calc.	Exp.	Calc.
71.9	89.9	100.0	100.0	100.0	100.0								
58.2	84.3	99.9	99.9	99.9	100.0								
47.1	77.6	99.7	99.5	99.9	100.0								
38.1	70.2	98.2	98.5	99.7	99.9								
30.8	62.4	96.9	96.3	99.5	99.6	100.0	99.9	100.0	100.0	100.0	100.0	100.0	100.0
24.9	54.7	93.0	92.5	99.0	98.6	99.9	99.7	99.9	99.9	99.9	100.0	99.9	100.0
20.1	47.3	87.6	86.9	98.0	96.5	99.5	99.0	99.8	99.7	99.8	100.0	99.8	100.0
16.3	40.4	80.3	79.8	95.9	92.8	98.7	97.3	99.4	99.0	99.6	99.8	99.6	100.0
13.2	34.2	72.6	71.5	92.1	87.3	97.0	94.2	98.8	97.3	99.1	99.4	99.3	99.9
10.7	28.6	63.5	62.8	85.9	80.4	93.7	89.4	95.5	94.2	98.3	98.2	98.7	99.4
8.62	23.8	54.8	53.8	77.3	72.0	88.3	82.7	91.1	89.1	96.6	95.6	97.7	98.2
6.97	19.7	46.4	45.5	67.0	63.1	80.3	74.7	84.8	82.5	93.4	91.4	95.7	95.7
5.64	16.2	38.1	37.9	56.5	54.4	70.2	66.1	76.7	74.6	88.0	85.5	92.2	91.6
4.56	13.2	31.8	31.2	46.8	46.0	59.4	57.2	68.4	65.8	80.0	78.0	86.4	85.7
3.69	10.8	26.1	25.5	38.8	38.3	49.4	48.6	59.3	57.0	70.2	69.6	78.3	78.2
2.98	8.1	21.0	20.6	32.3	31.5	40.9	40.7	50.3	48.4	59.9	60.6	68.6	69.7
2.41	6.9	17.4	16.5	26.8	25.7	33.7	33.6	42.9	40.5	50.0	51.9	58.4	60.9
1.95	5.5	13.8	13.2	22.1	20.8	27.8	27.5	35.1	33.5	41.4	43.7	48.7	52.2
1.58	4.2	10.8	10.6	18.2	16.8	22.8	22.4	29.0	27.4	34.2	36.4	40.3	44.0
1.28	3.3	8.9	8.4	14.8	13.5	18.7	18.1	23.9	22.3	28.2	29.9	33.3	36.6
1.03	2.5	6.8	6.6	12.0	10.7	15.2	14.4	18.8	17.9	23.2	24.2	27.3	30.0
0.83	1.9	5.5	5.2	9.5	8.4	12.1	11.4	15.1	14.3	18.7	19.5	22.0	24.3
0.68	1.4	4.3	4.2	7.4	6.8	9.5	9.2	11.9	11.5	14.8	15.9	17.3	19.9
$d_{63.2}$	30.5	10.55		6.40		4.83		4.02		3.08		2.53	
δ	1.03	1.13	1.14	1.16	1.14	1.18	1.14	1.19	1.14	1.19	1.14	1.17	1.14
β		-1.29	-1.25	-1.29	-1.25	-1.29	-1.25	-1.29	-1.25	-1.29	-1.25	-1.29	-1.25
1/K	1.45×10^{-3}												
Computed t statistic = 0.143 with 240 d.f.													

Grinding conditions :

Pulp density	: 2200 kg/m ³
Pin tip velocity	: 2.56 m/s
Ball density	: 3450 kg/m ³
Ave. ball size	: 0.005 m
Mill size	: 5 litre

Table A6.1.11. Experimental and calculated product size distributions at different energy input levels using grinding conditions in Table 6.1, test no:11.

Particle size mic.	Cumulative weight percent passing												
	Feed	Energy input levels, kWh/t											
		25		50		75		100		150		200	
	Exp.	Exp.	Calc.	Exp.	Calc.	Exp.	Calc.	Exp.	Calc.	Exp.	Calc.	Exp.	Calc.
71.9	89.9	99.9	100.0	100.0	100.0	100.0	100.0						
58.2	84.3	99.6	99.8	99.9	100.0	99.9	100.0						
47.1	77.6	98.7	99.2	99.7	100.0	99.8	100.0						
38.1	70.2	96.7	97.8	99.4	99.8	99.7	100.0	100.0	100.0				
30.8	62.4	93.0	94.9	98.7	99.2	99.3	99.9	99.9	100.0	100.0	100.0	100.0	100.0
24.9	54.7	87.8	90.4	97.5	97.7	98.7	99.4	99.6	99.9	99.9	100.0	99.9	100.0
20.1	47.3	80.9	84.0	95.2	94.8	97.5	98.3	99.0	99.4	99.6	99.9	99.8	100.0
16.3	40.4	72.7	76.4	91.2	90.3	95.3	95.9	97.7	98.2	99.1	99.7	99.5	99.9
13.2	34.2	64.0	67.9	85.2	84.1	91.6	91.9	95.2	95.8	97.9	98.8	98.9	99.7
10.7	28.6	55.2	59.1	77.3	76.4	85.9	86.2	91.2	91.8	95.8	97.0	97.6	98.9
8.62	23.8	46.8	50.3	68.3	67.7	78.3	78.7	85.3	85.8	92.2	93.5	95.3	97.0
6.97	19.7	39.8	42.2	59.0	58.8	69.3	70.3	77.6	78.4	86.7	88.3	91.4	93.6
5.64	16.2	32.1	35.0	50.1	50.2	59.8	61.4	68.7	70.0	79.3	81.5	85.6	88.5
4.56	13.2	26.2	28.7	41.9	42.1	50.6	52.7	59.2	61.1	70.4	73.4	77.7	81.7
3.69	10.8	21.3	23.3	34.8	34.9	42.5	44.4	50.2	52.4	60.9	64.7	68.6	73.6
2.98	8.1	17.1	18.8	28.7	28.6	35.7	36.9	42.1	44.1	51.9	55.8	59.2	64.8
2.41	6.9	13.7	15.1	23.1	23.2	29.7	30.3	35.1	36.6	43.6	47.3	50.1	55.9
1.95	5.5	10.9	12.0	18.3	18.7	24.6	24.7	29.1	30.1	36.3	39.5	41.9	47.5
1.58	4.2	8.7	9.6	14.4	15.1	20.2	20.0	24.0	24.6	30.1	32.7	34.9	39.7
1.28	3.3	6.8	7.6	11.2	12.1	16.5	16.1	19.6	19.9	24.8	26.8	28.7	32.9
1.03	2.5	5.2	6.0	8.6	9.5	13.4	12.8	16.0	15.9	20.2	21.6	23.5	26.7
0.83	1.9	4.1	4.7	6.6	7.5	10.6	10.2	12.7	12.7	16.2	17.3	18.9	21.6
0.68	1.4	3.2	3.8	5.2	6.1	8.2	8.2	9.9	10.2	12.7	14.0	14.8	17.6
$d_{63.2}$	30.5	12.95		7.48		5.96		4.88		3.76		3.15	
δ	1.03	1.09	1.14	1.09	1.14	1.10	1.14	1.09	1.14	1.10	1.14	1.11	1.14
β		-1.23	-1.25	-1.23	-1.25	-1.23	-1.25	-1.23	-1.25	-1.23	-1.25	-1.23	-1.25
1/K	1.14 x 10 ⁻³												
Computed t statistic = -0.285 with 250 d.f.													

Grinding conditions :

Pulp density	: 1880 kg/m ³
Pin tip velocity	: 3.66 m/s
Ball density	: 3450 kg/m ³
Ave. ball size	: 0.005 m
Mill size	: 5 litre

Table A6.1.12. Experimental and calculated product size distributions at different energy input levels using grinding conditions in Table 6.1, test no:12.

Particle size mic.	Cumulative weight percent passing												
	Feed	Energy input levels, kWh/t											
		25		50		75		100		150		200	
	Exp.	Exp.	Calc.	Exp.	Calc.	Exp.	Calc.	Exp.	Calc.	Exp.	Calc.	Exp.	Calc.
71.9	89.9	99.9	100.0	100.0	100.0	100.0	100.0						
58.2	84.3	99.6	99.8	99.8	100.0	99.9	100.0						
47.1	77.6	98.8	99.2	99.7	100.0	99.8	100.0						
38.1	70.2	97.1	97.8	99.3	99.8	99.7	100.0	100.0	100.0				
30.8	62.4	93.9	94.9	98.8	99.2	99.4	99.9	99.9	100.0	100.0	100.0	100.0	100.0
24.9	54.7	89.3	90.4	97.8	97.7	99.0	99.4	99.8	99.9	99.9	100.0	99.9	100.0
20.1	47.3	83.4	84.0	95.9	94.8	98.1	98.3	99.4	99.4	99.6	99.9	99.8	100.0
16.3	40.4	75.5	76.4	92.4	90.3	96.4	95.9	98.4	98.2	99.2	99.7	99.5	99.9
13.2	34.2	69.4	67.9	86.9	84.1	93.2	91.9	96.4	95.8	98.2	98.8	98.9	99.7
10.7	28.6	59.1	59.1	79.4	76.4	88.1	86.2	92.8	91.8	96.4	97.0	97.9	98.9
8.62	23.8	51.0	50.3	70.4	67.7	80.7	78.7	87.2	85.8	93.3	93.5	96.0	97.0
6.97	19.7	43.6	42.2	60.8	58.8	71.6	70.3	79.5	78.4	88.4	88.3	92.8	93.6
5.64	16.2	36.4	35.0	51.7	50.2	61.8	61.4	70.1	70.0	81.3	81.5	87.7	88.5
4.56	13.2	30.6	28.7	43.4	42.1	52.3	52.7	60.0	61.1	72.5	73.4	80.6	81.7
3.69	10.8	25.2	23.3	36.3	34.9	44.0	44.4	50.6	52.4	63.0	64.7	72.0	73.6
2.98	8.1	20.5	18.8	30.4	28.6	37.0	36.9	42.3	44.1	53.6	55.8	62.9	64.8
2.41	6.9	16.5	15.1	25.3	23.2	30.9	30.3	35.3	36.6	45.4	47.3	54.0	55.9
1.95	5.5	13.5	12.0	21.0	18.7	25.8	24.7	29.3	30.1	38.1	39.5	45.9	47.5
1.58	4.2	11.2	9.6	17.3	15.1	21.3	20.0	24.4	24.6	31.9	32.7	38.7	39.7
1.28	3.3	8.8	7.6	14.1	12.1	17.5	16.1	20.1	19.9	26.5	26.8	32.4	32.9
1.03	2.5	6.9	6.0	11.4	9.5	14.3	12.8	16.5	15.9	21.9	21.6	26.8	26.7
0.83	1.9	5.5	4.7	9.1	7.5	11.4	10.2	13.3	12.7	17.7	17.3	21.8	21.6
0.68	1.4	4.3	3.8	7.1	6.1	9.0	8.2	10.4	10.2	14.0	14.0	17.3	17.6
$d_{63.2}$	30.5	11.75		7.23		5.68		4.76		3.55		2.83	
δ	1.03	1.07	1.14	1.09	1.14	1.10	1.14	1.12	1.14	1.09	1.14	1.09	1.14
β		-1.26	-1.25	-1.26	-1.25	-1.26	-1.25	-1.26	-1.25	-1.26	-1.25	-1.26	-1.25
1/K	1.29×10^{-3}												
Computed t statistic = 0.039 with 250 d.f.													

Grinding conditions :

Pulp density	: 2200 kg/m ³
Pin tip velocity	: 3.66 m/s
Ball density	: 3450 kg/m ³
Ave. ball size	: 0.005 m
Mill size	: 5 litre

Table A6.1.13. Experimental and calculated product size distributions at different energy input levels using grinding conditions in Table 6.1, test no:13.

Particle size mic.	Cumulative weight percent passing												
	Feed	Energy input levels, kWh/t											
		25		50		75		100		150		200	
	Exp.	Exp.	Calc.	Exp.	Calc.	Exp.	Calc.	Exp.	Calc.	Exp.	Calc.	Exp.	Calc.
71.9	89.9	99.9	100.0	100.0	100.0	100.0	100.0						
58.2	84.3	99.4	99.8	99.8	100.0	99.9	100.0						
47.1	77.6	98.5	99.3	99.6	100.0	99.8	100.0						
38.1	70.2	97.1	97.9	99.1	99.8	99.5	100.0	100.0	100.0	100.0	100.0	100.0	100.0
30.8	62.4	94.6	95.3	98.2	99.3	99.1	99.9	99.9	100.0	99.9	100.0	99.9	100.0
24.9	54.7	90.9	90.9	96.7	97.9	98.4	99.5	99.6	99.9	99.8	100.0	99.8	100.0
20.1	47.3	85.3	84.7	94.0	95.2	97.1	98.5	98.9	99.5	99.6	99.9	99.6	100.0
16.3	40.4	77.9	77.1	89.8	90.9	94.8	96.3	97.6	98.4	99.0	99.7	99.3	99.9
13.2	34.2	69.2	68.7	83.8	84.8	91.2	92.4	95.2	96.2	97.9	99.0	98.6	99.7
10.7	28.6	60.3	59.9	76.4	77.3	86.0	86.9	91.5	92.3	96.1	97.3	97.4	99.0
8.62	23.8	51.5	51.0	67.8	68.6	79.1	79.6	86.1	86.6	92.9	94.0	95.5	97.3
6.97	19.7	43.4	42.9	58.7	59.8	70.7	71.3	79.0	79.3	88.2	89.1	92.4	94.1
5.64	16.2	36.2	35.6	49.8	51.1	61.5	62.5	70.4	71.0	81.6	82.4	87.7	89.2
4.56	13.2	30.0	29.2	41.8	42.9	52.5	53.6	61.3	62.1	73.3	74.4	81.2	82.6
3.69	10.8	24.9	23.8	34.8	35.6	44.2	45.3	52.3	53.4	64.3	65.8	73.4	74.7
2.98	8.1	20.7	19.2	29.0	29.2	37.0	37.7	44.1	45.0	55.3	56.8	64.7	65.9
2.41	6.9	17.1	15.4	24.0	23.8	30.8	31.0	36.8	37.5	46.6	48.3	55.7	57.0
1.95	5.5	14.1	12.3	19.8	19.2	25.5	25.3	30.5	30.8	39.0	40.4	47.2	48.5
1.58	4.2	11.6	9.8	16.2	15.4	21.1	20.5	25.2	25.2	32.4	33.5	39.7	40.7
1.28	3.3	9.4	7.8	13.1	12.4	17.2	16.5	20.6	20.4	26.6	27.4	32.9	33.7
1.03	2.5	7.6	6.1	10.5	9.8	13.9	13.2	16.8	16.3	21.6	22.1	27.0	27.4
0.83	1.9	6.0	4.8	8.3	7.7	11.1	10.4	13.3	13.0	17.3	17.8	21.7	22.2
0.68	1.4	4.7	3.9	6.4	6.2	8.7	8.4	10.4	10.5	13.5	14.4	17.1	18.1
$d_{63.2}$	30.5	11.52		7.65		5.74		4.64		3.48		2.74	
δ	1.03	1.07	1.14	1.08	1.14	1.08	1.14	1.07	1.14	1.09	1.14	1.07	1.14
β		-1.25	-1.25	-1.25	-1.25	-1.25	-1.25	-1.25	-1.25	-1.25	-1.25	-1.25	-1.25
1/K	1.35×10^{-3}												
Computed t statistic = -0.088 with 254 d.f.													

Grinding conditions :

Pulp density	: 1880 kg/m ³
Pin tip velocity	: 2.56 m/s
Ball density	: 7850 kg/m ³
Ave. ball size	: 0.005 m
Mill size	: 5 litre

Table A6.1.14. Experimental and calculated product size distributions at different energy input levels using grinding conditions in Table 6.1, test no:14.

Particle size mic.	Cumulative weight percent passing												
	Feed	Energy input levels, kWh/t											
		25		50		75		100		150		200	
	Exp.	Exp.	Calc.	Exp.	Calc.	Exp.	Calc.	Exp.	Calc.	Exp.	Calc.	Exp.	Calc.
71.9	89.9	99.9	100.0	100.0	100.0	100.0	100.0						
58.2	84.3	99.7	99.8	99.9	100.0	99.9	100.0						
47.1	77.6	99.2	99.3	99.7	100.0	99.9	100.0						
38.1	70.2	98.3	97.9	99.4	99.8	99.7	100.0	100.0	100.0	100.0	100.0	100.0	100.0
30.8	62.4	96.4	95.3	98.8	99.3	99.4	99.9	99.9	100.0	99.9	100.0	99.9	100.0
24.9	54.7	93.2	90.9	97.8	97.9	99.0	99.5	99.7	99.9	99.8	100.0	99.8	100.0
20.1	47.3	87.9	84.7	95.8	95.2	98.0	98.5	99.3	99.5	99.6	99.9	99.6	100.0
16.3	40.4	80.4	77.1	92.4	90.9	96.3	96.3	98.4	98.4	99.2	99.7	99.3	99.9
13.2	34.2	71.2	68.7	87.1	84.8	93.3	92.4	96.7	96.2	98.4	99.0	98.8	99.7
10.7	28.6	61.6	59.9	80.0	77.3	88.7	86.9	93.7	92.3	97.0	97.3	97.9	99.0
8.62	23.8	52.3	51.0	71.1	68.6	81.8	79.6	88.7	86.6	94.4	94.0	96.2	97.3
6.97	19.7	43.9	42.9	61.4	59.8	72.9	71.3	81.6	79.3	90.1	89.1	93.3	94.1
5.64	16.2	36.6	35.6	51.6	51.1	62.9	62.5	72.5	71.0	83.6	82.4	88.6	89.2
4.56	13.2	30.4	29.2	43.0	42.9	53.2	53.6	62.7	62.1	75.3	74.4	81.9	82.6
3.69	10.8	25.2	23.8	35.7	35.6	44.5	45.3	53.2	53.4	66.0	65.8	73.5	74.7
2.98	8.1	20.9	19.2	29.7	29.2	37.3	37.7	44.8	45.0	56.8	56.8	64.4	65.9
2.41	6.9	17.2	15.4	24.7	23.8	31.2	31.0	37.6	37.5	48.2	48.3	55.2	57.0
1.95	5.5	14.1	12.3	20.6	19.2	26.0	25.3	31.5	30.8	40.7	40.4	46.8	48.5
1.58	4.2	11.4	9.8	17.1	15.4	21.7	20.5	26.3	25.2	34.2	33.5	39.5	40.7
1.28	3.3	9.2	7.8	14.0	12.4	18.0	16.5	21.8	20.4	28.6	27.4	33.1	33.7
1.03	2.5	7.3	6.1	11.5	9.8	14.8	13.2	17.9	16.3	23.7	22.1	27.6	27.4
0.83	1.9	5.8	4.8	9.2	7.7	11.9	10.4	14.4	13.0	19.3	17.8	22.6	22.2
0.68	1.4	4.5	3.9	7.3	6.2	9.5	8.4	11.3	10.5	15.4	14.4	18.1	18.1
$d_{63.2}$	30.5	11.14		7.26		5.55		4.48		3.30		2.74	
δ	1.03	1.10	1.14	1.11	1.14	1.11	1.14	1.09	1.14	1.07	1.14	1.07	1.14
β		-1.30	-1.25	-1.30	-1.25	-1.30	-1.25	-1.30	-1.25	-1.30	-1.25	-1.30	-1.25
1/K	1.29×10^{-3}												
Computed t statistic = 0.130 with 254 d.f.													

Grinding conditions :

Pulp density	: 2200 kg/m ³
Pin tip velocity	: 2.56 m/s
Ball density	: 7850 kg/m ³
Ave. ball size	: 0.005 m
Mill size	: 5 litre

Table A6.1.15. Experimental and calculated product size distributions at different energy input levels using grinding conditions in Table 6.1, test no:15.

Particle size mic.	Cumulative weight percent passing												
	Feed	Energy input levels, kWh/t											
		25		50		75		100		150		200	
	Exp.	Exp.	Calc.	Exp.	Calc.	Exp.	Calc.	Exp.	Calc.	Exp.	Calc.	Exp.	Calc.
71.9	89.9	99.7	99.9	99.9	100.0	100.0	100.0	100.0	100.0				
58.2	84.3	98.7	99.7	99.7	100.0	99.8	100.0	99.9	100.0				
47.1	77.6	97.1	98.9	99.3	99.9	99.6	100.0	99.7	100.0				
38.1	70.2	94.3	97.1	98.5	99.6	99.3	100.0	99.4	100.0	100.0	100.0	100.0	100.0
30.8	62.4	89.8	93.7	97.1	98.8	98.6	99.8	99.0	99.9	99.9	100.0	99.9	100.0
24.9	54.7	83.9	88.6	94.8	96.9	97.4	99.1	98.2	99.7	99.6	100.0	99.8	100.0
20.1	47.3	76.7	81.7	91.1	93.4	95.2	97.5	96.7	99.0	99.0	99.8	99.4	100.0
16.3	40.4	69.1	73.8	85.7	88.2	91.8	94.5	94.3	97.4	97.8	99.4	98.7	99.9
13.2	34.2	61.0	65.1	78.7	81.3	86.8	89.8	90.5	94.3	95.8	98.2	97.4	99.4
10.7	28.6	52.9	56.3	70.6	73.3	80.3	83.4	85.3	89.6	92.6	95.8	95.3	98.2
8.62	23.8	45.1	47.7	62.0	64.4	72.4	75.4	78.4	82.9	88.0	91.5	92.0	95.7
6.97	19.7	38.3	39.8	53.3	55.5	63.8	66.8	70.2	75.0	81.7	85.6	87.2	91.6
5.64	16.2	32.0	32.9	45.2	47.1	55.1	57.9	61.3	66.3	74.0	78.2	80.6	85.7
4.56	13.2	26.5	26.9	38.0	39.3	46.8	49.3	52.6	57.5	65.5	69.7	72.7	78.3
3.69	10.8	22.1	21.8	31.7	32.5	39.6	41.4	44.7	48.9	56.9	60.9	64.1	69.9
2.98	8.1	17.0	17.5	26.5	26.5	33.3	34.2	37.9	40.9	48.9	52.1	55.6	60.9
2.41	6.9	14.5	14.1	22.0	21.5	27.9	28.0	31.8	33.8	41.5	43.9	47.5	52.2
1.95	5.5	11.8	11.2	18.2	17.3	23.3	22.7	26.5	27.7	34.9	36.5	40.1	44.0
1.58	4.2	9.5	8.9	15.0	13.9	19.3	18.4	22.0	22.5	29.1	30.0	33.7	36.6
1.28	3.3	7.5	7.1	12.2	11.1	15.8	14.8	18.0	18.2	24.0	24.5	27.9	30.1
1.03	2.5	6.1	5.6	9.8	8.8	12.9	11.7	14.6	14.5	19.6	19.7	23.0	24.4
0.83	1.9	4.8	4.4	7.8	6.9	10.3	9.3	11.6	11.5	15.7	15.8	18.6	19.7
0.68	1.4	3.7	3.5	6.1	5.5	8.2	7.5	9.1	9.3	12.3	12.8	14.7	16.0
$d_{63.2}$	30.5	14.03		8.83		6.76		5.74		4.21		3.22	
δ	1.03	1.04	1.14	1.05	1.14	1.04	1.14	1.04	1.14	1.04	1.14	1.04	1.14
β		-1.21	-1.25	-1.21	-1.25	-1.21	-1.25	-1.21	-1.25	-1.21	-1.25	-1.21	-1.25
1/K	1.13 x 10 ⁻³												
Computed t statistic = -0.390 with 260 d.f.													

Grinding conditions :

Pulp density	: 1880 kg/m ³
Pin tip velocity	: 3.66 m/s
Ball density	: 7850 kg/m ³
Ave. ball size	: 0.005 m
Mill size	: 5 litre

Table A6.1.16. Experimental and calculated product size distributions at different energy input levels using grinding conditions in Table 6.1, test no:16.

Particle Size mic.	Cumulative weight percent passing												
	Feed	Energy input levels, kWh/t											
		25		50		75		100		150		200	
		Exp.	Calc.	Exp.	Calc.	Exp.	Calc.	Exp.	Calc.	Exp.	Calc.	Exp.	Calc.
71.9	89.9	99.9	99.9	100.0	100.0	100.0	100.0						
58.2	84.3	99.5	99.7	99.9	100.0	99.9	100.0						
47.1	77.6	98.5	98.9	99.7	99.9	99.8	100.0						
38.1	70.2	96.6	97.1	99.3	99.6	99.6	100.0	100.0	100.0			100.0	100.0
30.8	62.4	93.2	93.7	98.5	98.8	99.2	99.8	99.9	99.9	100.0	100.0	99.9	100.0
24.9	54.7	88.4	88.6	97.1	96.9	98.5	99.1	99.6	99.7	99.8	100.0	99.9	100.0
20.1	47.3	82.2	81.7	94.4	93.4	97.1	97.5	99.0	99.0	99.6	99.8	99.7	100.0
16.3	40.4	74.9	73.8	89.9	88.2	94.6	94.5	97.6	97.4	99.0	99.4	99.3	99.9
13.2	34.2	66.9	65.1	83.4	81.3	90.5	89.8	95.0	94.3	97.8	98.2	98.5	99.4
10.7	28.6	58.7	56.3	75.3	73.3	84.5	83.4	90.9	89.6	95.7	95.8	97.3	98.2
8.62	23.8	50.2	47.7	66.3	64.4	76.8	75.4	84.9	82.9	92.2	91.5	95.1	95.7
6.97	19.7	42.4	39.8	57.1	55.5	67.8	66.8	77.2	75.0	86.9	85.6	91.5	91.6
5.64	16.2	35.6	32.9	48.4	47.1	58.5	57.9	68.3	66.3	79.8	78.2	86.2	85.7
4.56	13.2	29.7	26.9	40.7	39.3	49.7	49.3	59.1	57.5	71.3	69.7	79.0	78.3
3.69	10.8	24.8	21.8	34.1	32.5	42.1	41.4	50.4	48.9	62.3	60.9	70.7	69.9
2.98	8.1	20.6	17.5	28.6	26.5	35.6	34.2	42.8	40.9	53.7	52.1	62.0	60.9
2.41	6.9	16.8	14.1	23.9	21.5	30.0	28.0	36.0	33.8	45.8	43.9	53.5	52.2
1.95	5.5	13.7	11.2	19.8	17.3	25.1	22.7	30.2	27.7	38.8	36.5	45.6	44.0
1.58	4.2	11.0	8.9	16.4	13.9	20.9	18.4	25.3	22.5	32.7	30.0	38.8	36.6
1.28	3.3	8.9	7.1	13.4	11.1	17.2	14.8	21.0	18.2	27.4	24.5	32.7	30.1
1.03	2.5	7.1	5.6	10.9	8.8	14.1	11.7	17.3	14.5	22.8	19.7	27.4	24.4
0.83	1.9	5.7	4.4	8.6	6.9	11.2	9.3	13.9	11.5	18.6	15.8	22.4	19.7
0.68	1.4	4.5	3.5	6.7	5.5	8.8	7.5	11.0	9.3	14.8	12.8	17.9	16.0
$d_{63.2}$	30.5	11.75		7.95		6.10		4.87		3.57		2.88	
δ	1.03	1.05	1.14	1.06	1.14	1.05	1.14	1.05	1.14	1.05	1.14	1.05	1.14
β		-1.28	-1.25	-1.28	-1.25	-1.28	-1.25	-1.28	-1.25	-1.28	-1.25	-1.28	-1.25
1/K	1.23×10^{-3}												
Computed t statistic = -0.280 with 252 d.f.													

Grinding conditions :

Pulp density	: 2200 kg/m ³
Pin tip velocity	: 3.66 m/s
Ball density	: 7850 kg/m ³
Ave. ball size	: 0.005 m
Mill size	: 5 litre

APPENDIX 6.2

PRESENTATION OF SIZE DISTRIBUTIONS

Size distributions are usually presented graphically and it is useful to find a way of plotting which gives approximately straight lines, since curve fitting and subsequent interpolation or extrapolation may be carried out with greater confidence. In addition, if a function can be found which gives an acceptably straight-line graph, the function itself or parameters derived from it, may be used to describe the size distribution. This facilitates data comparisons and also offers major advantages in computer modelling.

A number of mathematical descriptions of size distribution have been developed but two are of special importance; the Gates-Gaudin-Shuhmann (48) and the Rosin-Rammler (49).

As an example, the data from Table 6.3, Test no 3, an energy input level of 75 kWh/t was used to compare these two methods. Figure A6.2.1 shows the Gates-Gaudin-Shuhmann plot which is Log X versus Log Y where Y is the cumulative mass percentage passing size X. In this way, a straight line fits the finer portion of the size distribution and a curved section concaves downwards at the upper end. Only about 50% of the material is presented by the straight line in this example.

For data which yield a straight line on this graph, the distribution may be represented by the following equation:

$$Y = \left(\frac{X}{k} \right)^m \quad (\text{A6.2.1})$$

where Y is the cumulative fraction finer than size X, m is the distribution modulus (i.e. the slope of the distribution line on a log-log plot) and k is the size modulus (i.e. the maximum size of the distribution) which may be determined from the intercept at Y = 100%.

The Gaudin-Shuhmann equation gives a linear log-log plot however it is not a good fit to the observed size distribution in the coarse sizes. The log-log plot is very popular due to its simplicity but the deviation from the linearity reduces its value.

The method derived by Rosin and Rammler to describe the distribution of comminuted coal particles is slightly more complicated.

The Rosin-Rammler equation is:

$$Y = 1 - \exp(-bX^\delta) \quad (\text{A6.2.2})$$

in which Y is the fraction passing size X and b and δ are "characteristic constants". An alternate form of the Rosin-Rammler equation given by Bennett (50) is:

$$Y = 1 - e^{-\left(\frac{X}{k}\right)^\delta} \quad (\text{A6.2.3})$$

where Y is the fraction passing X, k is the size modulus.

Figure A6.2.2 shows a linear relationship between log particle size and log-log inverse retained weight. Comparing Figures A6.2.1 and A6.2.2, the Rosin-Rammler method provides a better clarity and fit to the region approximately above 60% and this contrasts sharply with the congestion of the Gates-Gaudin-Shuhmann method in the same region. Overall, the Rosin-Rammler method provides adequate uniform spacing.

It can be concluded that the Rosin-Rammler method has been found to be more applicable to the stirred ball mill products than the Gaudin-Schuhmann equation with regard to displaying data with optimum clarity, obtaining proper empirical relationships and testing theoretical predictions against experimental data.

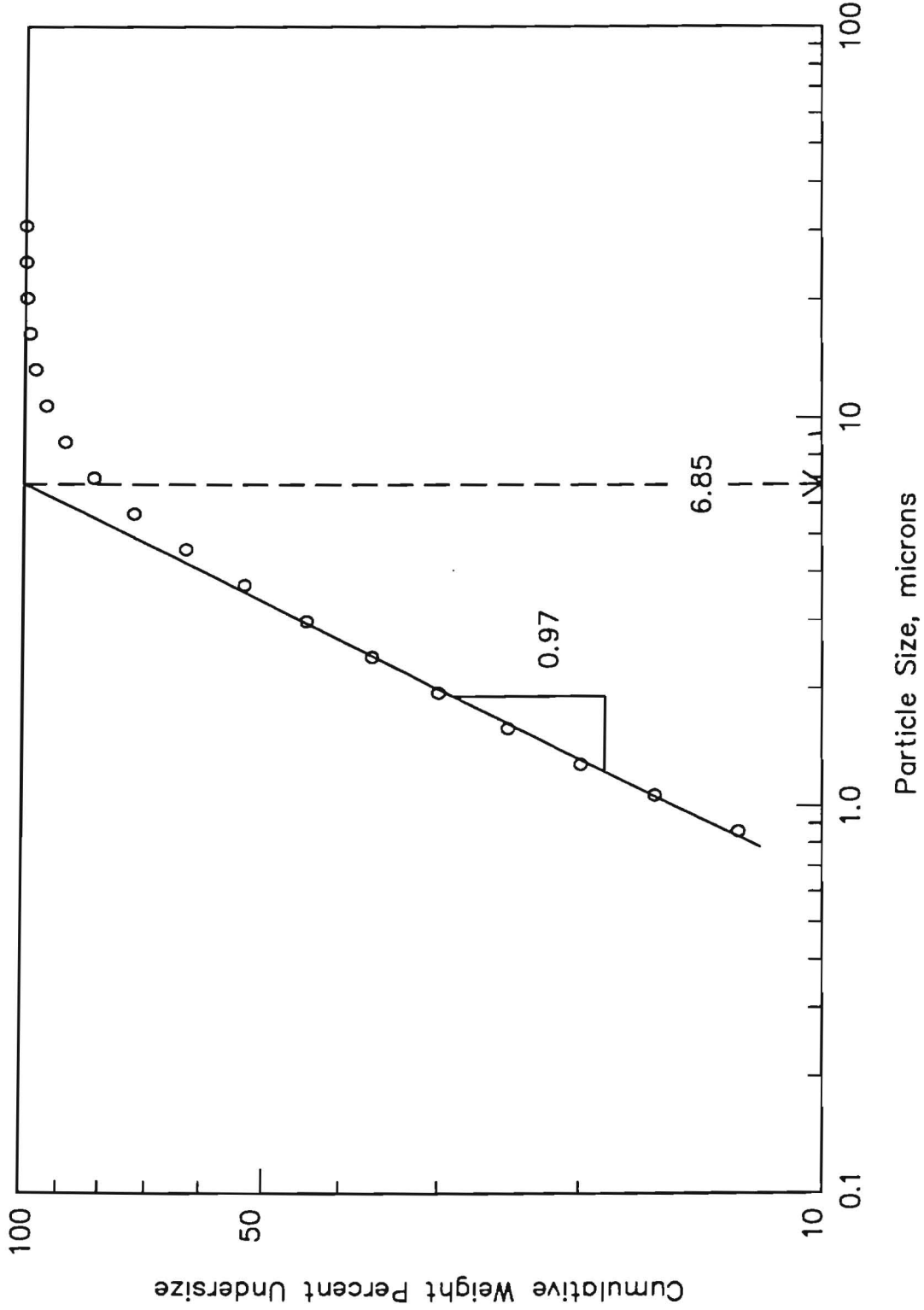


Figure A6.2.1. A typical example of Gaudin-Schuhmann size distribution at 75 kWh/t energy input using grinding conditions in Table 6.1, test no: 3: (data given in Table A6.1.3) Pulp density = 1880 kg/m³, pin tip velocity = 3.66 m/s, ball density = 7850 kg/m³, ave. ball size = 0.0036 m, mill size = 5 litres.

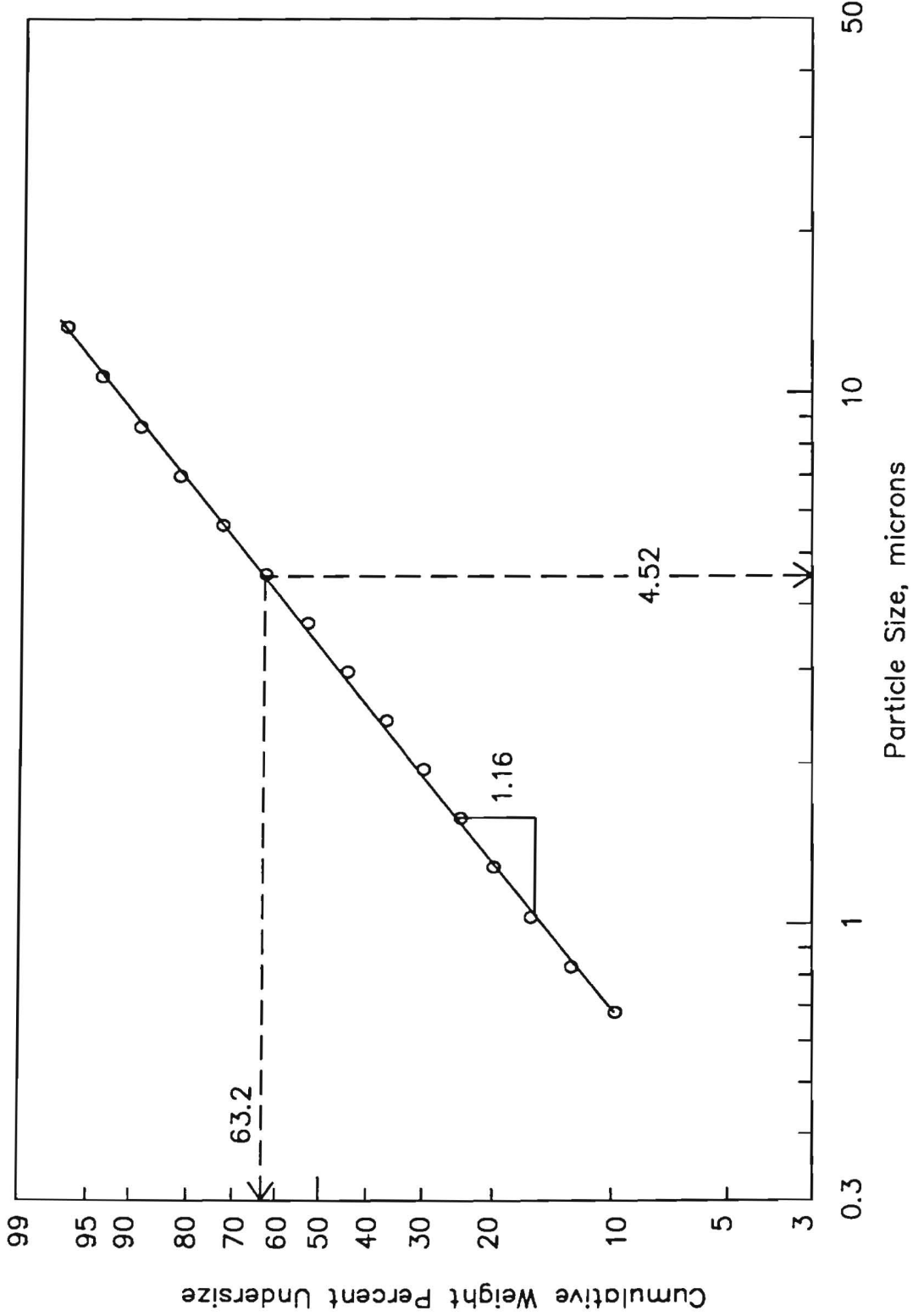


Figure A6.2.2. A typical example of Rosin-Rammler size distribution at 75 kW/t energy input using grinding conditions in Table 6.1, test no: 3: (data given in Table A6.1.3) Pulp density = 1880 kg/m³, pin tip velocity = 3.66 m/s, ball density = 3450 kg/m³, ave. ball size = 0.0036 m, mill size = 5 litres.

APPENDIX 6.3

CALCULATIONS OF STANDARD ERRORS FOR EFFECTS USING
HIGHER-ORDER INTERACTIONS

If there were no replicates and direct estimates of σ^2 , certain assumptions can be made that three and four factor interactions will supposedly be negligible and they would measure differences arising principally from experimental error (66). They could provide an appropriate reference set for the remaining effects. We can find

Table A6.3.1. Calculation for the variance effect.

Interactions	Effect	Effect ²
$\rho_p V \rho_b$	0.325×10^{-4}	10.563×10^{-10}
$\rho_p V d$	0.425×10^{-4}	18.063×10^{-10}
$\rho_p \rho_b d$	-0.375×10^{-4}	14.063×10^{-10}
$V \rho_b d$	0.050×10^{-4}	0.250×10^{-10}
$\rho_p V \rho_b d$	-0.375×10^{-4}	14.063×10^{-10}
Total	-	57.002×10^{-10}

An estimated value for the variance of an effect, having 5 degrees of freedom, is $57.002 \times 10^{-10} / 5 = 11.400 \times 10^{-10}$

The estimated standard error of an effect is therefore $\sqrt{11.400 \times 10^{-10}} = 0.338 \times 10^{-4}$.

In order to select the effects, a reference t-value is used. A reference t-value having 5 degrees of freedom at 95% confidence level with a scale factor of 0.338×10^{-4} is 0.869×10^{-4} .

APPENDIX 6.4

STATISTICAL DATA FOR NONLINEAR REGRESSION ANALYSIS

Nonlinear regression analysis was used to compute the exponents of the independent variables. The programme obtained least squares estimates of the parameters and the objective function was to minimize the residual sum of squares. Statistical analysis of the estimated exponents of the independent variables and variance of the empirical model are given in Tables A6.4.1 and A6.4.2.

Table A6.4.1. Model fitting results.

Parameter	Exponent		
	Estimate	Std. error	Ratio
Constant	13302.0	919.7510	14.46
V	0.437	0.0105	41.49
ρ_b	0.148	0.0046	32.29
d	0.868	0.0101	85.81

Table A6.4.2. Analysis of variance for the full regression.

Source	Sum. of squares	df	Mean square	Ratio
Model	9767114.0	4	2441778.5	99999.0
Error	4326.5	1963	2.2040	
Total	9771440.5	1967		
Total (corr.)	2300873.8	1966		
R-squared = 0.998				

The high ratio of the estimates to their standard errors in Table A6.4.1 indicated that the variables were significantly important. The model accounted for a substantial amount of variance.

APPENDIX 7.1

SIMULATION OF BATCH GRINDING IN A 5 LITRE STIRRED BALL MILL

Table A7.1.1. Experimental and calculated product size distributions at various levels of energy input for -100 microns natural feed using grinding conditions in Table 7.1, test no:1.

Particle Size mic.	Cumulative weight percent passing												
	Feed	Energy input levels, kWh/t											
		25		50		75		100		150		200	
Exp.	Exp.	Calc.	Exp.	Calc.	Exp.	Calc.	Exp.	Calc.	Exp.	Calc.	Exp.	Calc.	
100.00	100.0												
71.90	89.9	100.0	100.0										
52.30	80.0	99.8	99.9										
38.10	70.2	99.2	99.0	99.9	100.0	100.0	100.0	100.0	100.0				
24.90	54.7	96.6	94.9	99.4	99.4	99.9	99.9	99.9	100.0				
16.30	40.4	87.7	84.5	97.2	95.9	99.2	98.9	99.5	99.7	100.0	100.0	100.0	100.0
10.70	28.6	70.5	68.7	89.6	86.0	95.9	93.7	97.7	97.1	99.7	99.4	99.9	99.9
6.97	19.7	50.5	51.5	73.0	70.2	86.0	81.5	91.6	88.5	96.9	95.5	98.8	98.3
4.56	13.2	34.2	36.3	52.3	52.7	67.6	64.6	76.9	73.4	87.4	84.9	92.8	91.4
2.98	8.1	23.2	24.1	35.8	36.6	47.5	46.9	56.8	55.3	70.8	68.3	79.2	77.4
1.95	5.5	15.6	16.0	24.2	24.9	31.9	32.6	38.7	39.4	51.8	50.8	60.6	59.9
1.28	3.3	10.0	10.2	16.0	16.2	21.0	21.6	25.7	26.5	35.0	35.3	42.4	42.9
0.83	1.9	6.2	6.3	10.2	10.2	13.4	13.8	16.5	17.1	22.4	23.3	27.7	28.9
Grinding kinetic parameters													
A	0.292												
α	1.23												
γ	1.07												
Computed t statistic = 0.089 with 116 d.f.													
$R^2 = 0.999$													

Grinding conditions :

Feed size	: -100 microns
Pulp density	: 1880 kg/m ³
Pin tip velocity	: 2.56 m/s
Ball density	: 3450 kg/m ³
Ave. ball size	: 0.0036 m
Mill size	: 5 litre

Table A7.1.2.1. Experimental and calculated product size distributions at various levels of energy input for -100 microns natural feed using grinding conditions in Table 7.1, test no:2.

Particle Size mic.	Cumulative weight percent passing												
	Energy input levels, kWh/t												
	Feed	25		50		75		100		150		200	
	Exp.	Calc.	Exp.	Calc.	Exp.	Calc.	Exp.	Calc.	Exp.	Calc.	Exp.	Calc.	
100.00	100.0												
71.90	89.9	100.0	100.0	100.0	100.0								
52.30	80.0	99.8	99.7	99.9	100.0								
38.10	70.2	99.2	98.3	99.7	99.9	100.0	100.0	100.0	100.0	100.0	100.0	100.0	100.0
24.90	54.7	95.9	92.8	98.9	98.9	99.8	99.8	99.9	100.0	99.9	100.0	99.9	100.0
16.30	40.4	86.2	80.9	95.7	93.8	98.7	98.0	99.2	99.3	99.6	99.9	99.6	100.0
10.70	28.6	68.8	64.5	86.6	82.1	94.0	90.9	96.6	95.3	98.3	98.8	98.9	99.7
6.97	19.7	49.9	47.6	69.8	65.4	82.0	77.0	88.6	84.6	94.1	93.1	96.6	96.9
4.56	13.2	34.5	33.3	49.9	48.2	62.9	59.5	72.3	68.3	83.1	80.4	89.5	87.8
2.98	8.1	23.7	21.9	33.5	33.0	44.2	42.4	52.7	50.3	65.0	62.9	74.8	72.1
1.95	5.5	16.0	14.5	21.5	22.3	30.0	29.2	36.2	35.3	46.2	45.8	55.7	54.5
1.28	3.3	10.4	9.2	13.3	14.4	19.9	19.1	24.3	23.5	31.4	31.4	38.8	38.4
0.83	1.9	6.5	5.6	8.0	9.0	12.7	12.1	15.9	15.1	20.4	20.5	25.9	25.6
Grinding kinetic parameters													
A	0.247												
α	1.23												
γ	1.07												
Computed t statistic = 0.191 with 126 d.f.													
$R^2 = 0.998$													

Grinding conditions :

Feed size	: -100 microns
Pulp density	: 1880 kg/m ³
Pin tip velocity	: 3.66 m/s
Ball density	: 3450 kg/m ³
Ave. ball size	: 0.0036 m
Mill size	: 5 litre

Table A7.1.2.2. Experimental and calculated product size distributions at various levels of energy input for -53+38 microns monosize feed using grinding conditions in Table 7.1, test no:2.

Particle Size mic.	Cumulative weight percent passing												
	Energy input levels, kWh/t												
	Feed	1.34		2.68		5.77		8.48		11.11		12.92	
	Exp.	Calc.	Exp.	Calc.	Exp.	Calc.	Exp.	Calc.	Exp.	Calc.	Exp.	Calc.	
100.00	100.0	100.0	100.0	100.0	100.0	100.0	100.0	100.0	100.0	100.0	100.0	100.0	100.0
71.90	63.9	70.2	74.0	75.9	81.3	85.0	91.3	90.9	95.5	93.8	97.7	95.9	98.5
52.30	28.0	39.1	42.6	53.5	54.1	69.5	72.6	80.5	82.6	86.5	88.8	89.5	91.7
38.10	7.1	16.8	20.6	30.1	32.0	48.3	52.4	62.6	65.1	73.9	74.1	77.9	78.9
24.90	1.1	6.7	10.4	15.5	18.7	29.3	35.1	41.5	46.7	53.1	56.0	58.0	61.4
16.30	0.3	3.7	6.3	9.1	11.8	18.4	23.4	26.8	32.3	35.0	39.9	39.3	44.6
10.70	0.2	2.1	4.0	5.7	7.6	11.9	15.4	17.4	21.7	22.4	27.3	25.5	30.9
6.97	0.1	1.3	2.5	3.7	4.8	7.8	9.9	11.5	14.0	14.4	17.9	16.7	20.4
4.56	0.1	0.8	1.6	2.3	3.1	5.1	6.3	7.5	9.0	9.4	11.6	11.0	13.3
2.98	0.1	0.5	1.0	1.6	2.0	3.4	4.0	4.9	5.8	6.1	7.4	7.3	8.6
1.95	0.0	0.3	0.6	1.1	1.2	2.1	2.5	3.1	3.6	3.9	4.7	4.7	5.4
1.28	0.0	0.1	0.4	0.7	0.7	1.3	1.6	1.9	2.3	2.3	2.9	2.9	3.4
0.83	0.0	0.0	0.2	0.4	0.5	0.8	1.0	1.2	1.4	1.2	1.8	1.7	2.1
Grinding kinetic parameters													
A	0.247												
α	1.23												
γ	1.07												
Computed t statistic = -0.363 with 154 d.f.													
$R^2 = 0.997$													

Grinding conditions :

Feed size	: -53+38 microns
Pulp density	: 1880 kg/m ³
Pin tip velocity	: 3.66 m/s
Ball density	: 3450 kg/m ³
Ave. ball size	: 0.0036 m
Mill size	: 5 litre

Table A7.1.2.3. Experimental and calculated product size distributions at various levels of energy input for -38+25 microns monosize feed using grinding conditions in Table 7.1, test no:2.

Particle Size mic.	Cumulative weight percent passing												
	Energy input levels, kWh/t												
	Feed	1.34		2.68		5.63		8.58		11.39		19.07	
	Exp.	Calc.	Exp.	Calc.	Exp.	Calc.	Exp.	Calc.	Exp.	Calc.	Exp.	Calc.	
100.00	100.0	100.0	100.0	100.0	100.0	100.0	100.0	100.0	100.0	100.0	100.0	100.0	100.0
71.90	94.0	95.0	95.7	96.0	96.9	97.4	98.5	97.4	99.3	98.6	99.6	99.2	99.9
52.30	73.4	78.4	78.5	82.2	82.5	88.3	89.0	90.9	93.0	94.6	95.5	97.2	98.6
38.10	32.6	44.3	41.5	52.2	49.3	65.4	62.8	75.5	72.7	83.5	79.7	91.8	90.9
24.90	2.9	13.6	11.3	21.1	19.0	34.2	33.6	48.4	45.6	59.7	55.1	76.7	73.4
16.30	0.1	5.3	5.6	10.4	10.8	18.8	21.3	28.4	30.5	38.2	38.3	55.1	55.4
10.70	0.0	2.8	3.5	6.2	6.9	11.3	13.9	17.3	20.3	24.0	26.0	35.9	39.5
6.97	0.0	1.6	2.2	4.0	4.3	7.1	8.9	11.0	13.2	15.5	17.0	23.3	26.7
4.56	0.0	1.0	1.4	2.6	2.7	4.6	5.6	7.2	8.4	10.1	11.0	15.3	17.6
2.98	0.0	0.6	0.9	1.8	1.7	3.0	3.6	4.7	5.4	6.6	7.0	9.9	11.3
1.95	0.0	0.3	0.5	1.2	1.1	1.9	2.2	3.0	3.4	4.2	4.4	6.3	7.2
1.28	0.0	0.1	0.3	0.8	0.7	1.2	1.4	1.9	2.1	2.7	2.8	3.9	4.6
0.83	0.0	0.0	0.2	0.5	0.4	0.7	0.9	1.1	1.3	1.6	1.8	2.3	2.9
Grinding kinetic parameters													
A	0.247												
α	1.23												
γ	1.07												
Computed t statistic = -0.046 with 154 d.f.													
$R^2 = 0.998$													

Grinding conditions :

Feed size	: -38+25 microns
Pulp density	: 1880 kg/m ³
Pin tip velocity	: 3.66 m/s
Ball density	: 3450 kg/m ³
Ave. ball size	: 0.0036 m
Mill size	: 5 litre

Table A7.1.3.1. Experimental and calculated product size distributions at various levels of energy input for -100 microns natural feed using grinding conditions in Table 7.1, test no:3.

Particle Size mic.	Cumulative weight percent passing												
	Feed	Energy input levels, kWh/t											
		25		50		75		100		150		200	
Exp.	Exp.	Calc.	Exp.	Calc.	Exp.	Calc.	Exp.	Calc.	Exp.	Calc.	Exp.	Calc.	
100.00	100.0	100.0	100.0										
71.90	89.9	99.9	100.0										
52.30	80.0	99.5	99.7										
38.10	70.2	98.3	98.5	99.9	99.9	100.0	100.0	100.0	100.0				
24.90	54.7	93.9	93.4	99.3	99.1	99.9	99.9	99.9	100.0	100.0	100.0		
16.30	40.4	82.4	81.9	95.1	94.4	98.8	98.3	99.7	99.5	99.9	99.9	100.0	100.0
10.70	28.6	64.1	65.6	83.8	83.2	92.8	91.7	96.7	95.9	99.4	99.0	99.9	99.7
6.97	19.7	45.7	48.6	66.7	66.6	79.4	78.2	86.8	85.7	95.3	93.8	98.3	97.3
4.56	13.2	31.1	34.0	48.6	49.3	61.2	60.8	70.2	69.6	84.0	81.6	91.2	88.8
2.98	8.1	21.0	22.4	33.1	33.9	43.2	43.5	51.3	51.6	66.4	64.3	76.4	73.5
1.95	5.5	14.0	14.9	21.5	23.0	28.7	30.0	34.8	36.3	47.7	47.1	57.6	55.9
1.28	3.3	9.1	9.4	13.5	14.8	18.2	19.7	22.4	24.3	31.9	32.4	39.8	39.5
0.83	1.9	5.6	5.8	8.3	9.3	11.2	12.5	13.9	15.6	20.3	21.2	25.8	26.4
Grinding kinetic parameters													
A	0.258												
α	1.23												
γ	1.07												
Computed t statistic = -0.010 with 120 d.f.													
$R^2 = 0.999$													

Grinding conditions :

Feed size	: -100 microns
Pulp density	: 1880 kg/m ³
Pin tip velocity	: 2.56 m/s
Ball density	: 7850 kg/m ³
Ave. ball size	: 0.0036 m
Mill size	: 5 litre

Table A7.1.3.2. Experimental and calculated product size distributions at various levels of energy input for -53+38 microns monosize feed using grinding conditions in Table 7.1, test no:3.

Particle Size mic.	Cumulative weight percent passing												
	Energy input levels, kWh/t												
	Feed	1.29		2.59		5.82		7.11		8.08		11.32	
	Exp.	Calc.	Exp.	Calc.	Exp.	Calc.	Exp.	Calc.	Exp.	Calc.	Exp.	Calc.	
100.00	100.0	100.0	100.0	100.0	100.0	100.0	100.0	100.0	100.0	100.0	100.0	100.0	100.0
71.90	56.1	70.3	68.6	76.7	77.5	85.6	90.0	89.1	93.0	90.3	94.5	94.3	97.6
52.30	24.8	40.4	39.8	50.7	51.7	72.6	72.0	75.0	77.5	78.1	80.8	86.3	88.8
38.10	6.0	18.5	19.3	28.9	30.7	52.4	52.3	56.2	58.8	61.4	63.1	73.2	74.3
24.90	0.9	7.8	10.0	15.4	18.1	32.7	35.2	35.2	41.0	41.3	44.9	53.1	56.3
16.30	0.3	4.4	6.1	9.5	11.5	20.6	23.6	23.8	27.9	27.0	30.9	35.9	40.2
10.70	0.1	2.6	3.8	6.0	7.3	13.3	15.4	15.3	18.4	17.5	20.6	23.7	27.4
6.97	0.1	1.6	2.4	3.8	4.7	8.9	9.9	10.5	11.9	11.4	13.4	15.6	18.0
4.56	0.0	1.0	1.5	2.5	2.9	5.9	6.3	6.3	7.6	7.4	8.5	10.3	11.6
2.98	0.0	0.6	0.9	1.7	1.9	3.8	4.0	4.2	4.8	4.8	5.4	6.6	7.4
1.95	0.0	0.3	0.6	1.1	1.8	2.5	2.5	2.7	3.0	2.9	3.4	4.1	4.7
1.28	0.0	0.1	0.4	0.8	1.7	1.6	1.6	1.7	1.9	1.8	2.2	2.5	3.0
0.83	0.0	0.0	0.2	0.5	0.4	1.0	1.0	1.0	1.2	1.0	1.3	1.4	1.9
Grinding kinetic parameters													
A	0.258												
α	1.23												
γ	1.07												
Computed t statistic = -0.241 with 154 d.f.													
$R^2 = 0.998$													

Grinding conditions :

Feed size	: -53+38 microns
Pulp density	: 1880 kg/m ³
Pin tip velocity	: 2.56 m/s
Ball density	: 7850 kg/m ³
Ave. ball size	: 0.0036 m
Mill size	: 5 litre

Table A7.1.3.3. Experimental and calculated product size distributions at various levels of energy input for -38+25 microns monosize feed using grinding conditions in Table 7.1, test no:3.

Particle Size mic.	Cumulative weight percent passing												
	Energy input levels, kWh/t												
	Feed	1.29		2.59		5.82		7.11		8.08		11.32	
	Exp.	Calc.	Exp.	Calc.	Exp.	Calc.	Exp.	Calc.	Exp.	Calc.	Exp.	Calc.	
100.00	100.0	100.0	100.0	100.0	100.0	100.0	100.0	100.0	100.0	100.0	100.0	100.0	100.0
71.90	93.6	91.7	95.4	95.9	96.7	96.3	98.6	96.2	99.0	95.0	99.2	98.1	99.7
52.30	73.6	75.2	78.7	77.1	82.8	83.7	89.8	86.9	91.8	88.8	93.0	93.1	95.8
38.10	35.6	39.5	44.2	48.0	51.7	62.3	66.2	67.8	70.7	75.5	73.7	81.2	81.5
24.90	6.0	13.2	14.2	19.4	21.8	36.0	37.8	41.0	43.3	49.9	47.0	58.3	57.9
16.30	0.8	5.8	6.3	11.4	11.6	21.4	23.4	24.4	27.7	30.0	30.7	38.1	40.0
10.70	0.3	3.5	3.8	6.7	7.2	13.6	15.2	15.3	18.2	18.0	20.4	24.2	27.2
6.97	0.2	2.1	2.4	4.3	4.6	8.9	9.8	9.8	11.7	11.2	13.2	15.6	17.8
4.56	0.1	1.4	1.5	2.7	2.9	5.8	6.2	6.4	7.5	7.0	8.4	10.1	11.5
2.98	0.1	0.9	1.0	1.8	1.8	3.7	4.0	4.1	4.8	4.3	5.4	6.3	7.4
1.95	0.1	0.6	0.7	1.2	1.2	2.5	2.5	2.5	3.1	2.4	3.4	3.9	4.7
1.28	0.0	0.3	0.3	0.8	0.7	1.5	1.5	1.5	1.9	1.2	2.1	2.4	2.9
0.83	0.0	0.2	0.2	0.5	0.4	0.9	1.0	0.9	1.2	0.5	1.3	1.4	1.8
Grinding kinetic parameters													
A	0.258												
α	1.23												
γ	1.07												
Computed t statistic = -0.212 with 154 d.f.													
$R_2 = 0.998$													

Grinding conditions :

Feed size	: -38+25 microns
Pulp density	: 1880 kg/m ³
Pin tip velocity	: 2.56 m/s
Ball density	: 7850 kg/m ³
Ave. ball size	: 0.0036 m
Mill size	: 5 litre

Table A7.1.4. Experimental and calculated product size distributions at various levels of energy input for -100 microns natural feed using grinding conditions in Table 7.1, test no:4.

Particle Size mic.	Cumulative weight percent passing												
	Energy input levels, kWh/t												
	Feed	25		50		75		100		150		200	
	Exp.	Calc.	Exp.	Calc.	Exp.	Calc.	Exp.	Calc.	Exp.	Calc.	Exp.	Calc.	
100.00	100.0	100.0	100.0										
71.90	89.9	99.9	100.0	100.0	100.0	100.0	100.0						
52.30	80.0	99.5	99.5	99.9	100.0	99.9	100.0						
38.10	70.2	98.0	97.6	99.5	99.8	99.7	100.0	100.0	100.0				
24.90	54.7	92.8	91.1	98.0	98.3	99.0	99.7	99.8	99.9	100.0	100.0	100.0	100.0
16.30	40.4	80.6	78.2	92.8	92.0	96.7	97.0	98.6	98.9	99.9	99.8	99.9	100.0
10.70	28.6	62.6	61.5	80.7	79.0	89.7	88.5	94.2	93.6	98.8	98.0	99.7	99.4
6.97	19.7	45.2	45.0	62.8	61.9	75.5	73.4	83.5	81.4	93.2	90.8	97.1	95.5
4.56	13.2	31.4	31.2	45.0	45.0	56.8	55.8	66.2	64.4	80.5	76.8	88.0	84.8
2.98	8.1	21.6	20.4	31.3	30.6	40.3	39.3	48.1	46.8	62.9	58.9	72.1	68.1
1.95	5.5	14.5	13.6	21.0	20.6	27.3	26.8	33.1	32.5	45.1	42.3	53.6	50.6
1.28	3.3	9.2	8.5	13.2	13.2	17.3	17.5	21.7	21.5	30.3	28.8	36.8	35.2
0.83	1.9	5.5	5.2	7.8	8.2	10.3	11.0	13.3	13.7	19.5	18.7	23.9	23.3
Grinding kinetic parameters													
A	0.218												
α	1.23												
γ	1.07												
Computed t statistic = 0.135 with 126 d.f.													
$R^2 = 0.999$													

Grinding conditions :

Feed size	: -100 microns
Pulp density	: 1880 kg/m ³
Pin tip velocity	: 3.66 m/s
Ball density	: 7850 kg/m ³
Ave. ball size	: 0.0036 m
Mill size	: 5 litre

Table A7.1.5.1. Experimental and calculated product size distributions at various levels of energy input for -100 microns natural feed using grinding conditions in Table 7.1, test no:5.

Particle Size mic.	Cumulative weight percent passing												
	Energy input levels, kWh/t												
	Feed	25		50		75		100		150		200	
	Exp.	Calc.	Exp.	Calc.	Exp.	Calc.	Exp.	Calc.	Exp.	Calc.	Exp.	Calc.	
100.00	100.0												
71.90	89.9	100.0	100.0	100.0	100.0								
52.30	80.0	99.7	99.5	99.9	100.0								
38.10	70.2	98.8	97.7	99.7	99.8	100.0	100.0	100.0	100.0	100.0	100.0	100.0	100.0
24.90	54.7	93.5	91.4	98.7	98.4	99.8	99.7	99.9	99.9	99.9	100.0	99.9	100.0
16.30	40.4	82.4	78.6	95.1	92.3	98.3	97.2	99.1	99.0	99.5	99.9	99.7	100.0
10.70	28.6	64.7	62.0	84.8	79.5	92.6	88.8	95.8	93.9	97.9	98.2	98.8	99.4
6.97	19.7	47.2	45.4	66.9	62.4	79.4	74.0	86.4	81.9	92.7	91.2	95.8	95.7
4.56	13.2	32.7	31.5	47.3	45.5	59.9	56.4	68.9	65.0	79.7	77.3	86.6	85.2
2.98	8.1	21.5	20.6	32.6	30.9	41.7	39.7	49.4	47.3	60.5	59.5	69.5	68.7
1.95	5.5	13.7	13.7	22.1	20.8	28.1	27.2	33.7	32.9	42.1	42.8	49.8	51.2
1.28	3.3	8.8	8.6	14.6	13.4	18.6	17.7	22.5	21.8	28.3	29.1	33.7	35.7
0.83	1.9	5.1	5.3	9.3	8.3	11.9	11.2	14.5	13.9	18.4	18.9	21.8	23.6
Grinding kinetics parameters													
A	0.222												
α	1.23												
γ	1.07												
Computed t statistic = 0.168 with 126 d.f.													
$R^2 = 0.998$													

Grinding conditions :

Feed size	: -100 microns
Pulp density	: 1880 kg/m ³
Pin tip velocity	: 2.56 m/s
Ball density	: 3450 kg/m ³
Ave. ball size	: 0.005 m
Mill size	: 5 litre

Table A7.1.5.2. Experimental and calculated product size distributions at various levels of energy input for -53+38 microns monosize feed using grinding conditions in Table 7.1, test no:5.

Particle Size mic.	Cumulative weight percent passing										
	Energy input levels, kWh/t										
	Feed	0.35		0.72		1.06		2.12		7.51	
	Exp.	Calc.	Exp.	Calc.	Exp.	Calc.	Exp.	Calc.	Exp.	Calc.	
100.00	100.0	100.0	100.0	100.0	100.0	100.0	100.0	100.0	100.0	100.0	100.0
71.90	56.2	58.2	59.4	61.7	62.5	63.9	65.3	69.0	72.6	90.8	91.7
52.30	24.3	27.8	28.2	31.6	31.9	35.7	35.3	44.0	44.6	74.9	74.7
38.10	4.8	8.5	9.1	11.1	12.4	15.1	15.4	25.0	24.0	55.5	55.5
24.90	0.9	2.4	3.1	3.7	5.3	6.5	7.4	12.9	13.4	36.1	38.1
16.30	0.3	1.1	1.7	1.8	3.1	3.8	4.4	7.8	8.4	24.6	25.7
10.70	0.1	0.6	1.0	1.0	1.9	2.4	2.7	5.0	5.3	17.1	16.9
6.97	0.0	0.3	0.6	0.5	1.1	1.5	1.6	3.3	3.2	12.1	10.8
4.56	0.0	0.1	0.3	0.1	0.7	1.0	1.0	2.3	2.0	8.0	6.9
2.98	0.0	0.0	0.2	0.0	0.4	0.7	0.6	1.6	1.3	4.9	4.4
1.95	0.0	0.0	0.1	0.0	0.3	0.4	0.4	1.1	0.8	3.3	2.8
1.28	0.0	0.0	0.1	0.0	0.2	0.2	0.3	0.7	0.5	2.3	1.7
0.83	0.0	0.0	0.1	0.0	0.1	0.1	0.2	0.4	0.3	1.5	1.1
grinding kinetic parameters											
A	0.222										
α	1.23										
γ	1.07										
Computed t statistic = -0.053 with 128 d.f.											
$R^2 = 0.999$											

Grinding conditions :

Feed size	: -53+38 microns
Pulp density	: 1880 kg/m ³
Pin tip velocity	: 2.56 m/s
Ball density	: 3450 kg/m ³
Ave. ball size	: 0.005 m
Mill size	: 5 litre

Table A7.1.5.3. Experimental and calculated product size distributions at various levels of energy input for -38+25 microns monosize feed using grinding conditions in Table 7.1, test no:5.

Particle Size mic.	Cumulative weight percent passing										
	Energy input levels, kWh/t										
	Feed	0.35		0.67		0.99		2.48.		4.46	
	Exp.	Calc.	Exp.	Calc.	Exp.	Calc.	Exp.	Calc.	Exp.	Calc.	
100.00	100.0	100.0	100.0	100.0	100.0	100.0	100.0	100.0	100.0	100.0	100.0
71.90	93.6	95.1	94.1	93.4	94.5	94.0	94.9	96.5	96.3	96.6	97.6
52.30	73.6	75.7	74.9	75.6	76.0	77.4	77.1	81.8	81.4	85.6	86.0
38.10	35.6	36.9	37.7	38.8	39.6	42.1	41.4	49.6	49.2	60.9	57.9
24.90	6.0	8.3	8.0	10.1	9.8	12.5	11.5	19.3	19.2	30.8	28.4
16.30	0.8	2.6	2.1	4.0	3.3	5.5	4.5	9.8	9.8	17.6	16.3
10.70	0.3	1.3	1.1	2.3	1.9	3.3	2.6	5.9	6.1	11.5	10.4
6.97	0.2	0.7	0.7	1.4	1.2	2.1	1.7	3.7	3.8	7.5	6.6
4.56	0.1	0.5	0.4	0.9	0.7	1.3	1.0	2.4	2.4	4.5	4.2
2.98	0.1	0.3	0.3	0.6	0.5	0.9	0.7	1.6	1.5	3.0	2.7
1.95	0.1	0.2	0.2	0.4	0.3	0.8	0.5	1.1	1.0	2.1	1.7
1.28	0.0	0.0	0.1	0.2	0.2	0.4	0.2	0.7	0.6	1.3	1.0
0.83	0.0	0.0	0.1	0.1	0.1	0.0	0.1	0.4	0.4	0.8	0.6
Grinding kinetic parameters											
A	0.222										
α	1.23										
γ	1.07										
Computed t statistic = 0.036 with 128 d.f.											
$R^2 = 0.999$											

Grinding conditions :

Feed size	: -38+25 microns
Pulp density	: 1880 kg/m ³
Pin tip velocity	: 2.56 m/s
Ball density	: 3450 kg/m ³
Ave. ball size	: 0.005 m
Mill size	: 5 litre

Table A7.1.6. Experimental and calculated product size distributions at various levels of energy input for -100 microns natural feed using grinding conditions in Table 7.1, test no:6.

Particle Size mic.	Cumulative weight percent passing												
	Energy input levels, kWh/t												
	Feed	25		50		75		100		150		200	
	Exp.	Calc.	Exp.	Calc.	Exp.	Calc.	Exp.	Calc.	Exp.	Calc.	Exp.	Calc.	
100.00	100.0	100.0	100.0										
71.90	89.9	99.9	99.9	100.0	100.0	100.0	100.0						
52.30	80.0	99.1	99.2	99.8	99.9	99.9	100.0						
38.10	70.2	96.7	96.6	99.4	99.6	99.7	100.0	100.0	100.0	100.0	100.0	100.0	100.0
24.90	54.7	87.8	88.9	97.5	97.3	98.7	99.3	99.6	99.8	99.9	100.0	99.9	100.0
16.30	40.4	72.7	75.0	91.2	89.4	95.3	95.5	97.7	98.1	99.1	99.7	99.5	99.9
10.70	28.6	55.2	58.1	77.3	75.2	85.9	85.2	91.2	91.2	95.8	96.8	97.6	98.8
6.97	19.7	39.8	42.1	59.0	57.9	69.3	69.2	77.6	77.4	86.7	87.7	91.4	93.3
4.56	13.2	26.2	29.0	41.9	41.6	50.6	51.7	59.2	59.9	70.4	72.3	77.7	80.8
2.98	8.1	17.1	18.8	28.7	28.0	35.7	35.9	42.1	42.8	51.9	54.3	59.2	63.3
1.95	5.5	10.9	12.5	18.3	18.7	24.6	24.3	29.1	29.4	36.3	38.5	41.9	46.2
1.28	3.3	6.8	7.8	11.2	12.0	16.5	15.8	19.6	19.3	24.8	25.9	28.7	31.8
0.83	1.9	4.1	4.8	6.6	7.4	10.6	9.9	12.7	12.3	16.2	16.7	18.9	20.8
Grinding kinetic parameters													
A	0.188												
α	1.23												
γ	1.07												
Computed t statistic = -0.112 with 132 d.f.													
$R^2 = 0.999$													

Grinding conditions :

Feed size	: -100 microns
Pulp density	: 1880 kg/m ³
Pin tip velocity	: 3.66 m/s
Ball density	: 3450 kg/m ³
Ave. ball size	: 0.005 m
Mill size	: 5 litre

Table A7.1.7. Experimental and calculated product size distributions at various levels of energy input for -100 microns natural feed using grinding conditions in Table 7.1, test no:7.

Particle Size mic.	Cumulative weight percent passing												
	Energy input levels, kWh/t												
	Feed	25		50		75		100		150		200	
	Exp.	Calc.	Exp.	Calc.	Exp.	Calc.	Exp.	Calc.	Exp.	Calc.	Exp.	Calc.	
100.00	100.0	100.0	100.0										
71.90	89.9	99.9	99.9	100.0	100.0	100.0	100.0						
52.30	80.3	99.0	99.3	99.8	100.0	99.9	100.0						
38.10	70.2	97.1	96.9	99.1	99.7	99.5	100.0	100.0	100.0	100.0	100.0	100.0	100.0
24.90	54.7	90.9	89.6	96.7	97.6	98.4	99.5	99.6	99.9	99.8	100.0	99.8	100.0
16.30	40.4	77.9	76.0	89.8	90.3	94.8	96.0	97.6	98.4	99.0	99.7	99.3	100.0
10.70	28.6	60.3	59.2	76.4	76.4	86.0	86.3	91.5	92.0	96.1	97.2	97.4	99.0
6.97	19.7	43.4	43.0	58.7	59.1	70.7	70.5	79.0	78.7	88.2	88.8	92.4	94.1
4.56	13.2	30.0	29.7	41.8	42.6	52.5	53.0	61.3	61.4	73.3	73.7	81.2	82.1
2.98	8.1	20.7	19.3	29.0	28.8	37.0	36.9	44.1	44.0	55.3	55.7	64.7	64.8
1.95	5.5	14.1	12.8	19.8	19.3	25.5	25.1	30.5	30.4	39.0	39.7	47.2	47.6
1.28	3.3	9.4	8.1	13.1	12.3	17.2	16.3	20.6	20.0	26.6	26.8	32.9	32.8
0.83	1.9	6.0	4.9	8.3	7.7	11.1	10.2	13.3	12.7	17.3	17.3	21.7	21.5
Grinding kinetic parameters													
A	0.197												
α	1.23												
γ	1.07												
Computed t statistic = -0.005 with 132 d.f.													
$R^2 = 0.999$													

Grinding conditions :

Feed size	: -100 microns
Pulp density	: 1880 kg/m ³
Pin tip velocity	: 2.56 m/s
Ball density	: 7850 kg/m ³
Ave. ball size	: 0.005 m
Mill size	: 5 litre

Table A7.1.8.1. Experimental and calculated product size distributions at various levels of energy input for -100 microns natural feed using grinding conditions in Table 7.1, test no:8.

Particle Size mic.	Cumulative weight percent passing												
	Energy input levels, kWh/t												
	Feed	25		50		75		100		150		200	
	Exp.	Calc.	Exp.	Calc.	Exp.	Calc.	Exp.	Calc.	Exp.	Calc.	Exp.	Calc.	
100.00	100.0	100.0	100.0	100.0	100.0	100.0	100.0	100.0	100.0	100.0	100.0	100.0	100.0
71.90	89.9	99.7	99.8	99.9	100.0	100.0	100.0	100.0	100.0				
52.30	80.0	98.1	98.8	99.5	99.9	99.7	100.0	99.8	100.0				
38.10	70.2	94.3	95.6	98.5	99.3	99.3	99.9	99.4	100.0	100.0	100.0	100.0	100.0
24.90	54.7	83.9	86.9	94.8	96.2	97.4	98.9	98.2	99.7	99.6	100.0	99.8	100.0
16.30	40.4	69.1	72.3	85.7	87.1	91.8	93.9	94.3	97.2	97.8	99.4	98.7	99.9
10.70	28.6	52.9	55.5	70.6	72.0	80.3	82.3	85.3	88.8	92.6	95.4	95.3	98.1
6.97	19.7	38.3	39.9	53.3	54.6	63.8	65.6	70.2	73.9	81.7	84.8	87.2	91.1
4.56	13.2	26.5	27.4	38.0	38.9	46.8	48.4	52.6	56.3	65.5	68.5	72.7	77.2
2.98	8.1	17.0	17.7	26.5	26.0	33.3	33.2	37.9	39.6	48.9	50.5	55.6	59.4
1.95	5.5	11.8	11.7	18.2	17.3	23.3	22.4	26.5	27.1	34.9	35.5	40.1	42.8
1.28	3.3	7.5	7.3	12.2	11.0	15.8	14.5	18.0	17.7	24.0	23.7	27.9	29.1
0.83	1.9	4.8	4.5	7.8	6.8	10.3	9.0	11.6	11.2	15.7	15.2	18.6	18.9
Grinding kinetic parameters													
A	0.166												
α	1.23												
γ	1.07												
Computed t statistic = -0.181 with 138 d.f.													
$R^2 = 0.999$													

Grinding conditions :

Feed size	: -100 microns
Pulp density	: 1880 kg/m ³
Pin tip velocity	: 3.66 m/s
Ball density	: 7850 kg/m ³
Ave. ball size	: 0.005 m
Mill size	: 5 litre

Table A7.1.8.2. Experimental and calculated product size distributions at various levels of energy input for -53+38 microns monosize feed using grinding conditions in Table 7.1, test no:8.

Particle Size mic.	Cumulative weight percent passing												
	Energy input levels, kWh/t												
	Feed	1.45		3.63		5.82		7.27		10.90		14.54	
	Exp.	Calc.	Exp.	Calc.	Exp.	Calc.	Exp.	Calc.	Exp.	Calc.	Exp.	Calc.	
100.00	100.0	100.0	100.0	100.0	100.0	100.0	100.0	100.0	100.0	100.0	100.0	100.0	100.0
71.90	56.2	62.8	65.5	71.0	76.0	80.7	83.3	86.5	86.9	90.8	92.8	92.1	96.1
52.30	24.3	35.2	35.6	46.3	49.3	58.1	60.0	64.5	65.9	74.9	76.9	81.0	84.4
38.10	4.8	15.8	15.7	26.2	28.5	37.3	39.2	43.9	45.5	55.5	58.2	65.4	67.9
24.90	0.9	7.4	7.5	14.4	16.6	22.1	24.7	27.6	29.6	36.1	40.5	45.8	49.7
16.30	0.3	4.6	4.5	9.3	10.5	14.5	16.0	18.4	19.5	24.6	27.5	31.2	34.7
10.70	0.1	3.0	2.8	6.3	6.7	9.6	10.3	12.3	12.6	17.1	18.2	21.1	23.3
6.97	0.0	1.9	1.7	4.1	4.1	6.4	6.5	8.3	8.0	12.1	11.7	14.4	15.1
4.56	0.0	1.3	1.1	2.7	2.6	4.2	4.1	5.4	5.1	7.5	7.5	9.7	9.7
2.98	0.0	0.8	0.7	1.7	1.6	2.6	2.6	3.6	3.2	4.9	4.7	6.2	6.2
1.95	0.0	0.5	0.4	1.0	1.0	1.6	1.6	2.2	2.0	3.1	3.0	3.8	3.9
1.28	0.0	0.2	0.3	0.4	0.7	1.0	1.0	1.5	1.3	2.1	1.9	2.2	2.5
0.83	0.0	0.0	0.2	0.0	0.4	0.6	0.6	0.9	0.8	1.1	1.2	1.2	1.5
Grinding kinetic parameters													
A	0.166												
α	1.23												
γ	1.07												
Computed t statistic = -0.162 with 154 d.f.													
$R^2 = 0.999$													

Grinding conditions :

Feed size	: -53+38 microns
Pulp density	: 1880 kg/m ³
Pin tip velocity	: 3.66 m/s
Ball density	: 7850 kg/m ³
Ave. ball size	: 0.005 m
Mill size	: 5 litre

Table A7.1.8.3. Experimental and calculated product size distributions at various levels of energy input for -38+25 microns monosize feed using grinding conditions in Table 7.1, test no:8.

Particle Size mic.	Cumulative weight percent passing												
	Energy input levels, kWh/t												
	Feed	2.18		3.63		5.82		7.27.		11.50		15.99	
	Exp.	Calc.	Exp.	Calc.	Exp.	Calc.	Exp.	Calc.	Exp.	Calc.	Exp.	Calc.	
100.00	100.0	100.0	100.0	100.0	100.0	100.0	100.0	100.0	100.0	100.0	100.0	100.0	100.0
71.90	93.6	95.5	95.5	95.8	96.5	95.2	97.6	96.8	98.1	97.5	99.1	96.9	99.5
52.30	73.6	77.4	79.1	80.5	82.0	82.0	85.7	84.6	87.8	89.3	92.1	90.2	95.1
38.10	35.6	41.2	44.9	49.0	50.4	56.0	57.5	59.9	61.7	71.4	71.6	76.7	79.3
24.90	6.0	12.7	14.9	20.5	20.4	27.4	27.9	32.3	32.5	45.9	44.4	53.8	54.7
16.30	0.8	5.6	6.8	11.1	10.6	15.4	16.0	19.6	19.4	30.3	28.6	35.4	37.2
10.70	0.3	3.3	4.1	7.0	6.6	9.8	10.2	12.6	12.5	21.0	18.8	23.1	25.1
6.97	0.2	2.0	2.6	4.6	4.2	6.5	6.5	8.3	8.0	12.9	12.2	15.3	16.4
4.56	0.1	1.3	1.6	3.1	2.6	4.3	4.1	5.4	5.0	8.7	7.8	10.0	10.5
2.98	0.1	0.8	1.1	2.1	1.7	2.9	2.6	3.5	3.2	5.1	5.0	6.3	6.8
1.95	0.1	0.5	0.7	1.4	1.1	1.9	1.7	2.2	2.1	3.2	3.2	3.8	4.3
1.28	0.0	0.1	0.4	0.9	0.6	1.2	1.0	1.4	1.2	1.9	1.9	2.2	2.7
0.83	0.0	0.0	0.2	0.6	0.4	0.8	0.6	0.8	0.8	1.1	1.2	1.2	1.7
Grinding kinetic parameters													
A	0.166												
α	1.23												
γ	1.07												
Computed t statistic = -0.086 with 154 d.f.													
$R^2 = 0.999$													

Grinding conditions :

Feed size	: -38+25 microns
Pulp density	: 1880 kg/m ³
Pin tip velocity	: 3.66 m/s
Ball density	: 7850 kg/m ³
Ave. ball size	: 0.005 m
Mill size	: 5 litre

Table A7.1.9. Specific breakage rate as a function of particle size using balls of various diameters: pulp density = 1950 kg/m³, media type = steel, pin tip velocity = 3.66 m/s (Data shown in Figure 7.4).

Particle size mic.	Specific breakage rate, kWh/t ⁻¹		
	6 mm balls	3 mm balls	2 mm balls
425	0.202	-	-
300	0.279	-	-
212	0.312	-	-
150	0.319	0.090	-
106	0.233	0.113	0.068
75	0.120	0.125	0.083
53	-	0.080	0.088.
38	-	-	0.066

Table A7.1.10. Maximum breakage rate as a function of ball diameter: pulp density = 1950 kg/m³, media type = steel, pin tip velocity = 3.66 m/s (Data shown in Figure 7.5).

Ball diameter mm	Particle size mic.	Maximum breakage kWh/t ⁻¹
6	150	0.319
3	75	0.125
2	53	0.088

APPENDIX 7.2

STATISTICAL DATA FOR A LINEAR REGRESSION ANALYSIS

Multiple Regression was used to analyse the relationship between A (parameter of specific selection function) and operating parameters of the batch stirred ball mill. The programme used least squares to estimate the regression model. The model fitting results are given in Table A7.2.1.

Table A7.2.1. Model fitting results.

Independent variable	Estimate	Std. error	t-value	Sig.level
Constant	-1.857	0.378	-4.910	0.008
V	-0.473	0.123	-3.862	0.018
ρ_b	-0.146	0.053	-2.741	0.052
d	-0.832	0.133	-6.235	0.003

The low significance level for the constant term and the variables indicated that they provide useful predictive information and they should be kept in the model. Analysis of the variance statistic is given in Table A7.2.2.

Table A7.2.2. Analysis of variance for the full regression.

Source	Sum. of squares	df	Mean square	F-Ratio
V	0.0108129	1	0.0108129	14.92
ρ_b	0.0054450	1	0.0054450	7.51
d	0.0281840	1	0.0281840	38.88
Model	0.04444190	3		
R-squared (Adj.)	0.893			

The large F-ratios associated with the model were significant. The coefficient of determination (R-squared adj.) equalled 0.893.

APPENDIX 8

CONTINUOUS GRINDING RESULTS

Table A8.1. Experimental and model dimensionless residence time distribution data: mill size = 50 litres, ave. pulp density = 65.8% solids by weight, 6 mm steel balls, pin tip velocity = 2.45 m/s, pin spacing = 2.5 cm, pin diameter = 1.6 cm (data shown in Figure 8.3).

Dimensionless time θ	Normalised tracer concentration			
	Grinding time, minutes (Energy input, kWh/t)			Calculated
	3.8 (30.2)	6.1 (44.9)	8.5 (75.4)	E_{θ}
0.0000	0.0000	0.0000	0.0000	0.0000
0.0589			0.0070	0.0148
0.0616		0.0133		0.0162
0.0643	0.0134			0.0170
0.1768			0.0278	0.0444
0.1847		0.0443		0.0483
0.1929	0.0439			0.0502
0.2947			0.0600	0.0679
0.3079		0.0744		0.0730
0.3216	0.0828			0.0752
0.4125			0.0837	0.0829
0.4310		0.0898		0.0881
0.4502	0.0960			0.0896
0.5304			0.0968	0.0899
0.5542		0.0964		0.0944
0.5788	0.1027			0.0948
0.6482			0.0968	0.0907
0.6773		0.0930		0.0940
0.7074	0.0973			0.0931
0.7661			0.0899	0.0869
0.8005		0.0876		0.0889
0.8360	0.0920			0.0869
0.8840			0.0835	0.0804
0.9236		0.0783		0.0811
0.9647	0.0834			0.0781
1.0018			0.0722	0.0722
1.0468		0.0678		0.0719
1.0933	0.0728			0.0683
1.1699		0.0586		0.0624
1.1969			0.0638	0.0635
1.2219	0.0589			0.0585
1.2376			0.0563	0.0549

1.2930		0.0505		0.0532
1.3505	0.0487			0.0492
1.3554			0.0481	0.0468
1.4162		0.0431		0.0448
1.4733			0.0400	0.0395
1.4791	0.0401			0.0408
1.5393		0.0368		0.0373
1.5911			0.0332	0.0330
1.6078	0.0331			0.0335
1.6625		0.0311		0.0307
1.7090			0.0280	0.0273
1.7364	0.0262			0.0272
1.7856		0.0256		0.0251
1.8269			0.0223	0.0225
1.8650	0.0209			0.0220
1.9088		0.0217		0.0204
1.9447			0.0186	0.0184
1.9936	0.0176			0.0176
2.0319		0.0178		0.0165
2.0626			0.0156	0.0150
2.1223	0.0145			0.0141
2.1551		0.0150		0.0133
2.1805			0.0125	0.0122
2.2509	0.0118			0.0112
2.2782		0.0125		0.0106
2.2983			0.0111	0.0098
2.3795	0.0100			0.0089
2.4014		0.0105		0.0085
2.4161			0.0093	0.0079
2.5081	0.0082			0.0070
2.5245		0.0088		0.0068
2.5340			0.0071	0.0064
2.6368	0.0070			0.0055
2.6477		0.0075		0.0054
2.6519			0.0058	0.0051
2.7654	0.0059			0.0043
2.7700			0.0052	0.0041
2.7708		0.0064		0.0043
2.8876			0.0052	0.0033
2.8940	0.0050			0.0034
2.8940		0.0052		0.0034
3.0171		0.0042		0.0027
3.0226	0.0042			0.0027
3.1510	0.0034			0.0021

Table A8.2. Size distribution of batch and continuous grinding and calculated products at an energy input level of 75.4 kWh/t for the Rosin-Rammler graph: feed size(d_{50}) = 370 mic., pulp density = 61.9% solids by weight, 6 mm steel balls, pin tip velocity = 2.45 m/s, pin spacing = 2.5 cm, pin diameter = 1.6 cm (data shown in Figures 8.2 and 8.4).

Particle size mic.	Cumulative weight percent passing		
	Batch	Continuous	Calculated
18.0	95.1	89.4	83.7
16.3	-	86.3	-
13.2	86.2	78.9	76.5
5.64	49.7	47.4	52.6
4.56	41.6	40.2	45.9
3.32	31.4	30.7	35.8
2.17	20.7	20.3	23.3
1.28	11.5	11.3	12.4

Table A8.3. Calculations of product size distribution for the continuous grinding experiment using the tanks in series model.

En	C	EnxC	En _{near}	θ_{En}	E	$E_{\theta En}$	-18 mic		-13.2 mic.		-5.64 mic.		-4.56 mic.		-3.32 mic.		-2.17 mic.		-1.28 mic.	
							Y _{exp}	Y _{ical}	Y _{exp}	Y _{ical}	Y _{exp}	Y _{ical}	Y _{exp}	Y _{ical}	Y _{exp}	Y _{ical}	Y _{exp}	Y _{ical}	Y _{exp}	Y _{ical}
0.0	0.000	0.000	78.1	0.000	0.000	0.000	0.0	0.000	0.0	0.000	0.0	0.000	0.0	0.000	0.0	0.000	0.0	0.000	0.0	0.000
4.6	0.007	0.032		0.059	0.124	0.015	17.0	0.253	12.6	0.188	6.1	0.091	4.9	0.073	3.9	0.058	2.8	0.042	0.9	0.013
13.8	0.028	0.384		0.177	0.372	0.044	21.0	0.934	16.0	0.712	7.0	0.311	5.7	0.254	4.3	0.191	2.4	0.107	0.7	0.031
23.0	0.060	1.381		0.295	0.569	0.068	41.7	2.832	31.0	2.106	14.3	0.971	11.5	0.781	8.7	0.591	4.9	0.333	1.6	0.109
32.2	0.084	2.698		0.413	0.695	0.083	67.5	5.595	51.4	4.260	23.7	1.964	19.5	1.616	14.9	1.235	9.4	0.779	5.1	0.423
41.4	0.097	4.009		0.530	0.754	0.090	75.2	6.762	60.5	5.440	30.0	2.698	24.9	2.239	18.5	1.664	12.0	1.079	6.5	0.584
50.6	0.097	4.899		0.648	0.760	0.091	84.4	7.651	71.3	6.464	38.3	3.472	32.1	2.910	24.1	2.185	15.7	1.423	8.6	0.780
59.8	0.090	5.380		0.766	0.729	0.087	92.2	8.013	82.5	7.170	48.9	4.250	41.3	3.589	31.6	2.746	21.3	1.851	12.3	1.069
69.0	0.084	5.767		0.884	0.674	0.080	95.2	7.662	87.0	6.988	52.1	4.184	43.9	3.526	33.3	2.675	22.0	1.767	12.4	0.996
78.2	0.072	5.653		1.002	0.606	0.072	98.2	7.090	92.9	6.707	60.2	4.346	51.2	3.697	39.4	2.844	26.9	1.942	15.7	1.134
87.4	0.064	5.579		1.120	0.524	0.064	99.2	6.301	95.9	6.091	66.1	4.198	56.4	3.582	42.8	2.718	28.2	1.791	15.7	0.997
96.7	0.056	5.442		1.238	0.461	0.055	99.7	5.476	97.7	5.366	71.9	3.949	61.5	3.378	45.9	2.521	28.7	1.576	15.1	0.829
105.9	0.048	5.095		1.355	0.393	0.047	99.6	4.664	97.8	4.580	76.6	3.587	67.5	3.161	52.9	2.477	35.4	1.658	19.8	0.927
115.1	0.040	4.602		1.473	0.331	0.040	99.9	3.944	99.3	3.920	84.1	3.320	75.1	2.965	59.2	2.337	38.6	1.524	20.5	0.809
124.3	0.033	4.126		1.591	0.276	0.033	100.0	3.297	100.0	3.287	89.1	2.937	81.2	2.677	65.2	2.150	41.7	1.375	20.4	0.673
133.5	0.028	3.735		1.709	0.229	0.027	100.0	2.731	99.8	2.726	90.1	2.461	82.4	2.251	66.9	1.827	44.2	1.207	22.9	0.626
142.7	0.022	3.189		1.827	0.188	0.022	100.0	2.248	99.9	2.246	91.5	2.057	83.9	1.886	67.0	1.506	41.5	0.933	19.6	0.441
151.9	0.019	2.831		1.945	0.154	0.018	100.0	1.840	99.9	1.838	92.6	1.704	85.5	1.573	69.8	1.284	45.3	0.834	22.6	0.416
161.1	0.016	2.515		2.063	0.126	0.015	100.0	1.499	100.0	1.499	94.6	1.418	88.2	1.322	71.8	1.076	44.7	0.670	20.5	0.307
170.3	0.015	2.127		2.180	0.102	0.012	100.0	1.217	100.0	1.217	94.3	1.147	88.2	1.073	72.8	0.885	46.7	0.568	22.0	0.268
179.5	0.011	1.996		2.298	0.082	0.010	100.0	0.984	100.0	0.984	94.5	0.930	88.1	0.867	72.3	0.712	46.0	0.453	21.5	0.212
188.7	0.009	1.751		2.416	0.067	0.008	100.0	0.794	100.0	0.794	92.2	0.732	85.7	0.681	71.9	0.571	50.0	0.397	27.3	0.217
197.9	0.007	1.416		2.534	0.054	0.006	100.0	0.639	100.0	0.639	95.0	0.607	89.0	0.569	73.4	0.469	46.8	0.299	21.9	0.140
207.1	0.006	1.194		2.652	0.043	0.005	100.0	0.514	100.0	0.514	97.6	0.501	93.7	0.481	81.6	0.419	56.4	0.290	28.4	0.146
216.3	0.005	1.123		2.770	0.035	0.004	100.0	0.412	100.0	0.412	98.9	0.408	96.0	0.396	84.8	0.350	57.4	0.237	27.1	0.112
225.5	0.005	1.175		2.888	0.028	0.003	100.0	0.330	100.0	0.330	98.6	0.326	95.7	0.316	85.2	0.281	60.4	0.200	30.8	0.102
		78.1			8.384	1.000	Y _{cal} =83.7	Y _{cal} =76.5	Y _{cal} =52.6	Y _{cal} =45.9	Y _{cal} =35.8	Y _{cal} =23.3	Y _{cal} =12.4							

- E_n : Specific energy input at intervals (kWh/t). Batch grinding experiments were run at selected specific energy input intervals from 4.6 to 225.5 kWh/t under the same grinding conditions as used for the continuous experiment at a specific energy input level of 75.4 kWh/t (Grinding conditions for the batch grinding experiments: mill size = 5 litre, feed size (d_{50}) = 370 mic., pulp density = 61.9% solids by weight, 6 mm steel balls, pin tip velocity = 2.45 m/s, pin spacing = 2.5 cm, pin diameter = 1.6 cm).
- C : Normalised salt concentration at various specific energy input levels.
- $E_{n_{\text{mean}}}$: Mean specific energy input (kWh/t)(Eq.8.2).
- θ_{E_n} : Dimensionless specific energy input.
- E : Calculated tracer concentration using 2.5 tanks in series model (Eq.8.3).
- $E_{\theta_{E_n}}$: Normalised calculated tracer concentration using 2.5 tanks in series model.
- y_{exp} : Experimentally determined passing percentage from batch grinding experiments at given size and specific energy input level.
- y_{ical} : Calculated passing percentage for continuous grinding at given size and specific energy input = $y_{\text{exp}} \times E_{\theta_{E_n}}$.
- $Y_{\text{cal}} \sum_{i=1}^n y_{\text{ical}}$: Calculated cumulative passing percentage for continuous grinding at a given size at a specific energy input of 75.4 kWh/t.

APPENDIX 9

MILL POWER

Table A9.1. Experimental torque results using various grinding conditions and design parameters (The data were obtained from the vessels varying from 20 cm to 30 cm in diameter and 90 cm tall and 50 cm in diameter and 50 cm tall mounted on 50 litre test-rig and also from 5 litre test-rig accommodating a vessel which was 20 cm in diameter and 20 cm in height).

50 litres test rig									
s (m)	w (m)	d (m)	ρ_{eff} kg/m ³	H (m)	D (m)	V (m/s)	¹ T (Exp.) (Nm)	² TM (Cal.) (Nm)	³ STM (Cal.) (Nm)
0.025	0.016	0.006	3304	0.26	0.20	0.37	30.8	30.0	30.1
0.025	0.016	0.006	3304	0.26	0.20	0.79	35.0	31.9	32.0
0.025	0.016	0.006	3304	0.26	0.20	1.00	37.7	33.4	33.4
0.025	0.016	0.006	3304	0.26	0.20	1.47	41.1	38.0	37.9
0.025	0.016	0.006	3304	0.26	0.20	2.20	48.6	48.6	48.2
0.025	0.016	0.006	3304	0.26	0.20	2.56	52.0	55.4	54.8
0.025	0.016	0.006	3304	0.26	0.20	2.74	53.7	59.1	58.5
0.025	0.016	0.006	3304	0.46	0.20	0.37	80.5	85.0	85.4
0.025	0.016	0.006	3304	0.46	0.20	0.75	86.0	87.9	88.2
0.025	0.016	0.006	3304	0.46	0.20	1.00	91.6	91.0	91.2
0.025	0.016	0.006	3304	0.46	0.20	1.47	100.8	99.2	99.2
0.025	0.016	0.006	3304	0.46	0.20	2.20	114.5	117.9	117.3
0.025	0.016	0.006	3304	0.46	0.20	2.58	123.0	130.6	129.7
0.025	0.016	0.006	3304	0.46	0.20	2.73	126.0	136.1	135.1
0.025	0.016	0.006	3304	0.56	0.20	0.38	120.7	122.9	123.5
0.025	0.016	0.006	3304	0.56	0.20	0.73	128.1	126.2	126.7
0.025	0.016	0.006	3304	0.56	0.20	1.00	135.2	130.2	130.6
0.025	0.016	0.006	3304	0.56	0.20	1.46	147.1	139.8	139.9
0.025	0.016	0.006	3304	0.56	0.20	2.20	164.0	162.9	162.4

1 Experimental torque results

2 Calculated torque results using a torque model (Eq.9.49)

3 Calculated torque results using a semi-empirical torque model (Eq.9.54)

s	w	d	p_{eff}	H	D	V	T	TM	STM
0.025	0.016	0.006	3304	0.56	0.20	2.56	175.6	177.5	176.5
0.025	0.016	0.006	3304	0.56	0.20	2.73	183.3	185.1	184.0
0.025	0.016	0.006	3304	0.26	0.25	0.37	48.8	49.2	49.4
0.025	0.016	0.006	3304	0.26	0.25	0.74	49.6	51.7	51.9
0.025	0.016	0.006	3304	0.26	0.25	1.00	52.5	54.6	54.7
0.025	0.016	0.006	3304	0.26	0.25	1.46	56.2	61.6	61.4
0.025	0.016	0.006	3304	0.26	0.25	2.20	65.9	78.2	77.6
0.025	0.016	0.006	3304	0.26	0.25	2.57	70.6	89.0	88.1
0.025	0.016	0.006	3304	0.26	0.25	2.93	80.2	101.5	100.3
0.025	0.016	0.006	3304	0.46	0.25	0.37	141.4	136.9	137.5
0.025	0.016	0.006	3304	0.46	0.25	0.74	148.8	141.3	141.8
0.025	0.016	0.006	3304	0.46	0.25	1.00	156.9	146.4	146.8
0.025	0.016	0.006	3304	0.46	0.25	1.46	172.0	158.8	158.8
0.025	0.016	0.006	3304	0.46	0.25	2.20	197.7	187.7	187.0
0.025	0.016	0.006	3304	0.46	0.25	2.57	211.8	207.3	206.0
0.025	0.016	0.006	3304	0.46	0.25	2.93	225.0	229.4	227.5
0.025	0.016	0.006	3304	0.46	0.25	3.66	256.9	281.7	278.3
0.025	0.016	0.006	3304	0.56	0.25	0.37	185.8	197.0	197.9
0.025	0.016	0.006	3304	0.56	0.25	0.74	196.2	202.4	203.2
0.025	0.016	0.006	3304	0.56	0.25	1.00	206.8	208.6	209.2
0.025	0.016	0.006	3304	0.56	0.25	1.46	227.1	223.6	223.8
0.025	0.016	0.006	3304	0.56	0.25	2.19	259.1	258.9	258.1
0.025	0.016	0.006	3304	0.56	0.25	2.57	277.5	282.7	281.3
0.025	0.016	0.006	3304	0.56	0.25	2.93	296.9	309.6	307.4
0.025	0.016	0.006	3304	0.56	0.25	3.66	337.4	373.3	369.3
0.025	0.016	0.006	3304	0.71	0.25	0.37	307.1	307.5	308.9
0.025	0.016	0.006	3304	0.71	0.25	0.72	318.5	313.9	315.1
0.025	0.016	0.006	3304	0.71	0.25	1.00	333.5	322.2	323.2
0.025	0.016	0.006	3304	0.71	0.25	1.48	360.2	342.1	342.7
0.025	0.016	0.006	3304	0.71	0.25	2.20	406.7	386.6	385.9
0.025	0.016	0.006	3304	0.71	0.25	2.57	431.2	416.1	414.6
0.025	0.016	0.006	3304	0.71	0.25	2.93	458.4	450.3	447.8
0.025	0.016	0.006	3304	0.71	0.25	3.62	512.2	526.0	521.5

s	w	d	ρ_{eff}	H	D	V	T	TM	STM
0.025	0.016	0.006	3304	0.26	0.30	0.37	74.5	74.3	74.6
0.025	0.016	0.006	3304	0.26	0.30	0.73	80.0	77.7	78.0
0.025	0.016	0.006	3304	0.26	0.30	1.00	87.9	82.0	82.1
0.025	0.016	0.006	3304	0.26	0.30	1.47	95.1	92.2	92.1
0.025	0.016	0.006	3304	0.26	0.30	2.20	118.3	116.0	115.2
0.025	0.016	0.006	3304	0.26	0.30	2.56	129.3	131.4	130.2
0.025	0.016	0.006	3304	0.26	0.30	2.93	143.5	149.2	147.4
0.025	0.016	0.006	3304	0.26	0.30	3.67	171.7	192.7	189.7
0.025	0.016	0.006	3304	0.56	0.30	0.37	286.4	291.0	292.3
0.025	0.016	0.006	3304	0.56	0.30	0.73	295.8	298.5	299.7
0.025	0.016	0.006	3304	0.56	0.30	1.01	309.7	307.7	308.6
0.025	0.016	0.006	3304	0.56	0.30	1.47	339.3	329.8	330.0
0.025	0.016	0.006	3304	0.56	0.30	2.20	393.0	380.9	379.8
0.025	0.016	0.006	3304	0.56	0.30	2.56	421.8	414.1	412.1
0.025	0.016	0.006	3304	0.56	0.30	2.93	456.6	452.3	449.3
0.025	0.016	0.006	3304	0.56	0.30	3.67	534.9	546.0	540.4
0.025	0.016	0.006	3304	0.71	0.30	0.37	431.6	452.1	454.1
0.025	0.016	0.006	3304	0.71	0.30	0.73	446.0	461.6	463.4
0.025	0.016	0.006	3304	0.71	0.30	1.01	466.3	473.3	474.8
0.025	0.016	0.006	3304	0.71	0.30	1.47	505.0	501.2	501.9
0.025	0.016	0.006	3304	0.71	0.30	2.20	578.2	566.0	565.0
0.025	0.016	0.006	3304	0.71	0.30	2.56	615.5	608.1	605.9
0.025	0.016	0.006	3304	0.71	0.30	2.93	657.2	656.6	653.1
0.025	0.016	0.006	3304	0.26	0.50	0.37	239.9	243.8	244.9
0.025	0.016	0.006	3304	0.26	0.50	0.71	262.7	252.8	253.6
0.025	0.016	0.006	3304	0.26	0.50	1.01	286.6	265.8	266.3
0.025	0.016	0.006	3304	0.26	0.50	1.47	320.0	294.1	293.8
0.025	0.016	0.006	3304	0.26	0.50	2.21	393.0	361.2	359.0
0.025	0.016	0.006	3304	0.26	0.50	2.56	429.4	401.7	398.4
0.025	0.016	0.006	3506	0.71	0.30	0.36	447.7	479.6	481.8
0.025	0.016	0.006	3506	0.71	0.30	0.73	458.7	489.8	491.8
0.025	0.016	0.006	3506	0.71	0.30	1.01	477.6	502.2	503.8
0.025	0.016	0.006	3506	0.71	0.30	1.47	516.7	531.8	532.6

s	w	d	ρ_{eff}	H	D	V	T	TM	STM
0.025	0.016	0.006	3506	0.71	0.30	2.20	586.7	600.6	599.6
0.025	0.016	0.006	3506	0.71	0.30	2.56	626.7	645.3	643.0
0.025	0.016	0.006	3506	0.71	0.30	2.93	666.4	697.7	693.0
0.025	0.016	0.006	1042	0.71	0.30	0.37	149.2	142.6	143.2
0.025	0.016	0.006	1042	0.71	0.30	0.73	152.5	145.6	146.2
0.025	0.016	0.006	1042	0.71	0.30	1.01	161.9	149.3	149.7
0.025	0.016	0.006	1042	0.71	0.30	1.47	181.7	158.1	158.3
0.025	0.016	0.006	1042	0.71	0.30	2.20	220.0	178.5	178.2
0.025	0.016	0.006	1042	0.71	0.30	2.56	238.0	191.8	191.1
0.025	0.016	0.006	1042	0.71	0.30	2.93	258.3	207.1	206.0
0.025	0.016	0.006	840	0.71	0.30	0.37	122.2	114.9	115.5
0.025	0.016	0.006	840	0.71	0.30	0.73	125.2	117.4	117.8
0.025	0.016	0.006	840	0.71	0.30	1.01	136.2	120.3	120.7
0.025	0.016	0.006	840	0.71	0.30	1.47	152.9	127.4	127.6
0.025	0.016	0.006	840	0.71	0.30	2.20	182.6	143.9	143.6
0.025	0.016	0.006	840	0.71	0.30	2.56	197.2	154.6	154.1
0.025	0.016	0.006	840	0.71	0.30	2.93	210.4	166.9	166.0
0.050	0.016	0.006	3304	0.71	0.30	0.37	350.2	-	346.6
0.050	0.016	0.006	3304	0.71	0.30	0.73	363.0	-	353.7
0.050	0.016	0.006	3304	0.71	0.30	1.01	377.2	-	362.3
0.050	0.016	0.006	3304	0.71	0.30	1.47	401.8	-	383.0
0.050	0.016	0.006	3304	0.71	0.30	2.20	441.9	-	431.2
0.050	0.016	0.006	3304	0.71	0.30	2.56	465.8	-	462.4
0.050	0.016	0.006	3304	0.71	0.30	2.93	489.0	-	498.4
0.050	0.025	0.006	3304	0.71	0.30	0.37	399.1	-	412.5
0.050	0.025	0.006	3304	0.71	0.30	0.73	415.0	-	420.9
0.050	0.025	0.006	3304	0.71	0.30	1.01	431.6	-	431.2
0.050	0.025	0.006	3304	0.71	0.30	1.47	467.7	-	455.9
0.050	0.025	0.006	3304	0.71	0.30	2.20	521.9	-	513.2
0.050	0.025	0.006	3304	0.71	0.30	2.56	552.2	-	550.3
0.050	0.025	0.006	3304	0.71	0.30	2.93	582.9	-	593.2
0.025	0.016	0.003	3304	0.26	0.30	0.37	54.3	-	51.3
0.025	0.016	0.003	3304	0.26	0.30	0.73	56.0	-	53.6
0.025	0.016	0.003	3304	0.26	0.30	1.01	60.2	-	56.5

s	w	d	ρ_{eff}	H	D	V	T	TM	STM
0.025	0.016	0.003	3304	0.26	0.30	1.47	66.9	-	63.3
0.025	0.016	0.003	3304	0.26	0.30	2.20	78.2	-	79.2
0.025	0.016	0.003	3304	0.26	0.30	2.56	83.9	-	89.5
0.025	0.016	0.003	3304	0.26	0.30	2.93	90.9		101.4
0.025	0.016	0.003	3304	0.71	0.25	0.37	225.6		235.8
0.050	0.016	0.006	3304	0.71	0.25	0.73	234.5	-	240.7
0.050	0.016	0.006	3304	0.71	0.25	1.01	244.2	-	246.7
0.050	0.016	0.006	3304	0.71	0.25	1.47	260.8	-	261.1
0.050	0.016	0.006	3304	0.71	0.25	2.20	284.7	-	294.5
0.050	0.016	0.006	3304	0.71	0.25	2.56	298.5	-	316.2
0.050	0.016	0.006	3304	0.71	0.25	2.93	316.5	-	341.2
5 litres test rig									
s	w	d	ρ_{eff}	H	D	V	T	TM	STM
0.025	0.016	0.006	3304	0.12	0.20	0.37	7.9	8.0	8.0
0.025	0.016	0.006	3304	0.12	0.20	0.73	8.9	8.7	8.7
0.025	0.016	0.006	3304	0.12	0.20	1.01	9.9	9.6	9.6
0.025	0.016	0.006	3304	0.12	0.20	1.47	11.8	11.7	11.6
0.025	0.016	0.006	3304	0.12	0.20	2.20	15.7	16.6	16.4
0.025	0.016	0.006	3304	0.12	0.20	2.93	21.2	23.4	23.0
0.025	0.016	0.006	3052	0.12	0.20	0.37	7.3	7.4	7.4
0.025	0.016	0.006	3052	0.12	0.20	0.73	8.3	8.1	8.1
0.025	0.016	0.006	3052	0.12	0.20	1.00	9.2	8.9	8.8
0.025	0.016	0.006	3052	0.12	0.20	1.46	11.1	10.8	10.7
0.025	0.016	0.006	3052	0.12	0.20	2.20	14.5	15.3	15.1
0.025	0.016	0.006	3052	0.12	0.20	2.93	19.1	21.6	21.3
0.025	0.016	0.006	2162	0.12	0.20	0.37	5.0	5.2	5.3
0.025	0.016	0.006	2162	0.12	0.20	0.73	6.1	5.7	5.7
0.025	0.016	0.006	2162	0.12	0.20	1.00	6.8	6.3	6.3
0.025	0.016	0.006	2162	0.12	0.20	1.46	8.4	7.6	7.6
0.025	0.016	0.006	2162	0.12	0.20	2.20	11.2	10.9	10.7
0.025	0.016	0.006	2162	0.12	0.20	2.93	14.0	15.3	15.1

Table A9.2. Effect of effective density on the mill torque at various pin tip velocities (Experimental conditions : $s=0.025$ m; $w=0.016$ m; $d=0.006$ m; $H=0.71$ m; $D=0.30$ m; $E=66.0$ kWh/t. Data shown in Figures 9.4 and 9.5)

Pin tip velocity m/s	Torque, Nm			
	Effective density, kg/m^3			
	840	1042	3304	3506
0.37	122.2	149.2	431.6	447.7
0.73	125.2	152.5	446.0	458.7
1.01	136.2	161.9	466.3	477.6
1.47	152.9	181.7	505.0	516.7
2.20	182.6	220.0	578.2	586.7
2.56	197.2	238.0	615.5	626.7
2.93	210.4	258.3	657.2	666.5

Table A9.3. A typical example of experimental torque results from 50 litre stirred ball mill (Experimental conditions : $s=0.025$ m; $w=0.016$ m; $d=0.006$ m; $\rho_{eff}=3304$ kg/m^3 ; $H=0.71$ m; $D=0.30$ m; $E=66.0$ kWh/t. Data shown in Figure 9.3)

Pin tip velocity m/s	Experimental torque Nm
Start-up torque	652.0
0.10	436.0
0.21	434.3
0.37	431.6
0.73	446.0
1.01	466.3
1.47	505.0
2.20	578.2
2.56	615.5
2.93	657.2

APPENDIX 10

BATCH TEST DATA AT TWO DIFFERENT LEVELS OF ENERGY INPUT AND SOME STATISTICAL PROPERTIES OF DATA DISTRIBUTIONS

Batch grinding experiments were carried out under the same grinding conditions at two different specific levels of energy input to determine some statistical properties of the data distributions (63,65). These were: -

Mean size (d_{mean}): The mean is defined as the sum of the measurements divided by the number of measurements. It is used as an estimator of the average value of the distribution.

Standard deviation (s): It defines the sum of all the deviations from the mean. It is a measure of the spread of data.

Coefficient of variation (c): The standard deviation measures the actual amount of variation present in a set of data and it is dependent on the scale of measurement. To compare the variations in several sets of data it is desirable to use the coefficient of variation defined by the standard deviation as a percentage of the mean value.

Confidence interval (CI_{95}): It defines an interval in which lie 95 percent of the possible values.

Table A10.1. Median size of products at two different levels of energy input

Test No	Median size, mic.	
	Energy input levels, kWh/t	
	36	75
1	10.59	5.72
2	11.51	5.74
3	12.57	5.82
4	12.71	5.74
5	11.49	5.81
6	12.30	5.86
7	12.43	5.75
8	12.37	5.70
9	11.86	5.58
10	10.57	5.65
11	11.25	5.82
12	12.35	5.90
13	12.81	5.89
14	12.67	5.75
15	12.62	5.83
16	12.52	5.73
17	11.95	5.84
18	12.21	5.75
19	11.12	5.54
20	11.41	5.81
d_{mean}	11.97	5.76
s	0.703	0.095
c	5.87	1.65
Cl_{95}	$11.64 \leq d_{\text{mean}} \leq 12.29$	$5.72 \leq d_{\text{mean}} \leq 5.81$

NOMENCLATURE

Note: the symbols are also defined in the thesis. A few symbols have more than one definition due to the wide coverage of stirred ball milling.

a	Gap between the balls; exponent
B	Number of blades on impeller
B_{i1}	Cumulative breakage function
b_{ij}	Size-discretized breakage function
C	Distance of impeller from bottom
C_i	Tracer concentration at the mill exit at various times
D	Mill diameter
d	Average ball diameter
d_{50}	Median size
E	Energy input
\bar{E}	Specific energy input
E_0	Theoretical energy needed to prepare the feed
E_θ	Normalised tracer concentration
F	Drag force
F_c	Centrifugal force
F_r	Froude number
F_i^E	Initial slope of the cumulative mass fraction finer than size interval i
g	Gravitational constant
H	Load height at rest; liquid depth
H_{mill}	Hold-up of the material in the mill
J	Width of baffles
k	Size modulus of the product
k_0	Size modulus of the feed
L	Impeller diameter
M	Effective mill load; length of impeller blade
m	Distribution modulus in the Schuhmann equation
m_i	Mass fraction of the material in the mill in the i th size interval
N	Shaft rotation speed; number of tanks
N_0	Reference number
N_p	Power number
N_{Re}	Reynolds number
O	Pitch of impeller

P	Power
R	Number of baffles
r	Particle radius
S_i	Size-discretized selection function
S_i^E	Size-discretized specific selection function
s	Pin spacing
T	Torque
T_{bm}	Torque exerted on the bottom of the vessel by mass in the mill
T_{cm}	Torque exerted due to the centrifugal force of the mass on the vessel wall
T_{wm}	Torque exerted on the wall of the vessel by mass in the mill
t	Grinding time
t_{mean}	Mean residence time
t_i	Average time in interval
V	Pin tip velocity
V_c	Effective charge velocity
W	Width of impeller
w	Pin diameter
x_m	Size at which the maximum specific breakage rate occurs
Y	Cumulative fraction finer than given size
α	Exponent in the specific selection function
β	Exponent of Charles' equation that depends on the material and method of comminution
δ	Distribution modulus in the Rosin-Rammler equation
ϵ	Voids between the balls
theta	Angle of nip; dimensionless time
λ	Exponent
μ	Coefficient of friction
μ_f	Fluid viscosity
ρ_b, ρ_{media}	Ball density
ρ_{bulk}	Bulk density of the composite load
ρ_{eff}	Effective density of the mill load
ρ_f	Fluid density
ρ_p	Pulp density
ω	Angular velocity